Tectonostratigraphic Evolution and Salt Tectonic Processes of the Isthmus Saline Basin, South-eastern Gulf of Mexico: Implication for Petroleum Systems and Exploration.

by

Alejandro Salvador Ruiz-Osorio B.S., M.Sc . (Hons.)

A thesis submitted in fulfillment of the requirements of the University of London for the degree of Doctor of Philosophy

Department of Geology,

Royal Holloway University of London

September, 2016

Declaration of Authorship

I Alejandro Salvador Ruiz Osorio hereby declare that this thesis and the work presented in it is entirely my own. Where I have consulted the work of others, this is always clearly stated.

Signed:

Date: 22/ September/ 2016

Acknowledgments

I want to express my profound gratitude and respect to all those who helped me in the completion of this thesis. I would like to thank Dr. Juergen Adam for giving me the opportunity to do this challenging PhD. His supervision and sharp insightful comments and for his help and guidance throughout the project.This PhD was funded by Petroleos Mexicanos, Consejo Nacional de Ciencia y Tecnología (Conacyt) and kindly provided the seismic data for the research. Thanks to the Secretaría de Energía (Sener) for the permission to use the datasets. LandMarkTM granted the use of seismic interpretation software and Midland Valley granted the use of 2Dmove.

Professor Margaret Collinson is thanked for her advice to continue with this project.

Thanks to the members of staff and postgraduates students in the Geology department at Royal Holloway for making these years enjoyable and manageable specially, Heráclio Gutiérrez, Lucia Pérez, Azad Saeed and Dilshad Ali.

Thanks to my family, friends and Pemex colleague back in Villahermosa, Tabasco for all the help and support, my sister (Araceli, Maribel & María Luisa) my brothers (Miguel Angel, Efraín), for the support and all the fun times.

My parents (Salvador and María Luisa) for all the encouragement that they gave me since I remember and all the advice that they always repeat it in all the conversation that we usually have about life, education, and the rest. Thanks

Last but not least, to my wife Alejandra. Not a word can express my gratitude to her, for all the help and support that she gave me through these years. Throughout the duration of this thesis she has been a constant source of encouragement and always on hand when I needed a reassuring voice, and for preventing me going insane during the write-up.

To my dear boys

Diana Valeria

Alejandro Emiliano

Angel Diego

Thank you. so much

Abstract

The Isthmus Saline Basin (ISB) in the south-eastern Gulf of Mexico is part of an inverted foreland basin complex located on the Western Mexican rifted continental margin in front of the Sierra de Chiapas thrust belt. The contrasting structural architecture and a complex salt tectonic history are controlled by a combination of gravity-driven halokinetic processes, regional contractional tectonic processes and basement-involved strike-slip deformation as consequence of convergence between the Caribbean (Chortis Block) and North American plates. The aim of this research is the analysis of salt tectonic styles and kinematics of salt structures in the ISB. Regional 2D seismic lines and a 3D seismic survey have been combined with wells, outcrop data, gravity, magnetic and earthquake data from published maps to develop the first tectono-stratigraphic and kinematic analysis of the onshore Isthmus Saline Basin. Structural and stratigraphic interpretation results based on 2D and 3D seismic data provide: (1) Regional tectonic analysis, (2) insights into the salt tectonic processes and related depositional systems of the study area, and (3) basis for kinematic analysis using structurally balanced and restored cross-section. Contraction caused by the lateral movement of the Chortís block transformed the salt anticlines into tall contractional diapirs and created large intervening depocenters with up to 6 km thick. Contraction reached its peak deformation in Middle Miocene and Late Miocene times during strike-slip reactivation of basement faults due to sinistral transpression along the Sierra de Chiapas strike-slip fault system. Results of structural restoration shows that shortening varied from a minimum of 17% (7 km) to a maximum of 59% (24 km). This variation of shortening is controlled by the relationship between basement geometry and salt thickness which greatly influenced the size and style of salt structures. The reactivation of basement faults caused the development of reverse faults, thrust faults and positive flower structures which represent structural traps and new potential migration routes.

List of Contents

List of Figures

Chapter 1

Chapter 2

Figure 2.4.- Asymmetric rifting model, showing the separation between Yucatán from North America (from Pindell & Kennan, 2002)

Fig 2.5 a-b Plate tectonic reconstruction of Gulf of Mexico. Showing the rifting and drifting stages during Early Jurassic to middle Jurassic (Bathonian) (after Pindell & Dewey, 1982; Pindell, 1985).

Fig 2.5 c-d Plate tectonic reconstruction of Gulf of Mexico. Showing the rifting and drifting stages during middle Jurassic to Late Jurassic (Tjthonian) (after Pindell & Dewey, 1982; Pindell, 1985).

2.5 e-f. Plate tectonic reconstruction of Gulf of Mexico. Showing the end of drifting stage and the beginning of Pacific margin transformation since to Late Cretaceous time (after Pindell & Dewey, 1982; Pindell, 1985).

Fig 2.5 g-h. Plate tectonic reconstruction of Gulf of Mexico. showing the oblique deformation (after Pindell & Dewey, 1982; Pindell, 1985).

Fig 2.5 i-j Plate tectonic reconstruction of Gulf of Mexico showing the uplifting stage of Sierra de Chiapas and the fault thrusting caused by the movement of Chortis Block toward east. The figure 2.4j shows the present day position of Caribbean Plate (Chortis block). Red arrows represent present day motion vector of North American Plate, Cocos and Caribbean Plate (after Pindell & Dewey, 1982; Pindell, 1985).

Figure 2.6- Model proposed of the trajectory of the Chortis Block since middle Eocene (modified from Keppie & Moran-Zenteno, 2005).

Figure 2.7- Model originally proposed by Ross and Scotese (1988) and later modified by Shaaf, et al., 1995). This model support the idea of Chortis Block migrated from west to east, reaching current position. Migration period was 80 My. Additionally, this model is supported by Guzmán-Speziale & Meneses-Rocha, 2000; Pindell & Kennan, 2001; Andreani, *et al*., 2008 a,b, because during it's migration it caused exhumation of the Sierra de Chiapas fold belt and also would produce the Chiapas compression. (DeMeets, *et al,* 1994; DeMeets & Dixon, 1999; DeMeets, *et al*., 2000; Bird, *et al*. 2005).

Figure 2.8- Model proposed by Mandujano-Velázquez & Keppie, 2009). The model shows three tectonic stages of evolution of Pacific Margin. This model suggest that changes in subduction angle drove the exhumation of Sierra de Chiapas Fold belt.

Chapter 3

Figure 6.5.- Seismicity Activity in the Gulf of Mexico, Southern of Mexico and Central America (USGG National Earthquake Information Center, 2004).

Figure .6.6 Show shallow earthquake activity and the the main fault systems of Chiapas area. The black rectangle, represent the Isthmus Saline basin. The seismicity and focal mechanism are included (modified from Andreani, *et al*., 2008).

Figure.6.7 Show distribution of deep earthquake and its relationship with Isthmus Saline Basin (study area) and Chiapas fold belt provinces (modified from Andreani, *et al*.,2008).

Figure .6.8 Structural alignments interpreted from Landsat image. The black rectangle represents the study area. The pink dotted line represents the Jurassic salt boundary. The bold black line represents the transition boundary between two structural provinces.

Figure. 6.9 Main structural trends of magnetic anomalies defined by tilt derivative IMT (Data provided by PEMEX, 2012).

Fig.6.10 Delimitation of anomalous bodies and structural lineaments through tilt derivative of Bouguer anomaly (Data provided by PEMEX, 2012.). The study area is indicated in the black rectangle. Black lines define the main gravimetric trends.

Figure .6.11 Geologic Map of South-eastern of Mexico showing main structural features around the Isthmus Saline Basin. (Ortega-Gutierrez *et al*., 1992).

Figure .6.12 Structural Interpretation of the Magnetic tild derivative showing the main structural blocks of Southeastern of Mexico.

Figure .6.13 Structural Interpretation of the Gravity tilt derivative showing the main structural blocks of Southeastern of Mexico.

Figure.6.14 Interpretation of basement geometry of South-eastern of Mexico was done by the author. The black rectangle represents the research area. The structural boundaries were defined based in the combination of gravity and magnetic qualitative analysis (previous maps). ISB basin represented in black lines shows a half semi-circumference. The other half defines the Comalcalco basin represented in blue lines. The basin seems to be broken and displaced.

Figure .6.15 Interpretation of basement geometry of South-eastern of Mexico. The black rectangle represents the research area. Structural interpretation of the main fault trends was done by the author. The configuration was (modified from Jacobo-

Albarrán, *et al.,* 2003). The construction of the map is based in the combination of gravity and magnetic analysis. Colors represents depth of basement in km.

Figure .6.16 Structural map of the Isthmus Saline basin showing the orientation and geometry of salt diapirs. Some diapirs show relationship between basement faults and salt structures interpreted from gravity, magnetic, 2D seismic and wells data. The mapping was done by the author.

Figure 6.17 Structural map of the Isthmus Saline basin showing basement fault, also was map the distribution of allochthonous salt. The onshore allochthonous salt was done by Ruiz-Osorio,2017, The offshore allochthonous salt was taken from Cabrera-Gomez and Jackson (2009).

Figure 6.18 2D Seismic section and line drawing, showing the Isthmus Saline basin and part of Strike-slip Province The sketching was made by the author

Figure 6.19 2D Seismic section and line drawing, showing the Isthmus Saline basin and part of Strike-slip Province The sketching was made by the author.

Figure 6.20 2D Seismic section and line drawing, showing the Isthmus Saline basin to the NW and the beginning of the Comalcalco salt evacuation basin. The sketching was made by the author.

Figure 6.21 Shows the structural relationship between NW front of Sierra de Chiapas and Isthmus Saline Basin to illustrate the complex structural patterns that have influenced in the configuration of the Isthmus Saline Basin in a short distance. The geological modeles were done by the author.

Chapter 7

Figure 7.1 shows the location of 2D and 3D surveys used in this study.

Figure 7.2 Regional geological sections of South-eastern of Gulf of Mexico hows the location of 2D and 3D surveys used in this study.

Figure 7.3 Structural model of the SE of Mexico. The black rectangle represents the Isthmus Saline Basin.

Figure 7.4 Interpretation of TWT 2D seismic section. D3 section is oriented SW-NE of the Isthmus Saline Basin. a) seismic section; b) seismic section with interpretation; c) line drawing.

Figure 7.5 Interpretation of TWT 2D seismic section. D2 section is oriented SW-NE of the Isthmus Saline Basin. a) seismic section; b) seismic section with interpretation; c) line drawing.

Figure 7.6 Interpretation of TWT 2D seismic section. D1 section is oriented SW-NE of the Isthmus Saline Basin. a) seismic section; b) seismic section with interpretation; c) line drawing

Figure 7.7 Structural model of the Isthmus Saline Basin Interpretation of TWT 2D seismic section.

Figure 7.8 Structural model of salt withdrawal basin of Comalcalco, Reforma-Akal Uplift and its relationship with salt diapirs of ISB. Interpretation of TWT 2D seismic section.

Figure 7.9 Show a model that try to explain the structural relationships between Isthmus Saline basin and Comalcalco Basin during Middle-late Miocene.

Figure 7.10 shows location of 2D seismic section and 3D seismic surveys.

Figure 7.11 Interpretation of TWT 2D seismic section. NT-1 section is oriented NNW-SSE of the Isthmus Saline Basin. a) seismic section; b) line drawing; c) seismic section with interpretation.

Figure 7.12 Interpretation of TWT 2D seismic section. NT-2 section is oriented NNW-SSE of the Isthmus Saline Basin. a) seismic section; b) line drawing; c) seismic section with interpretation.

Figure 7.13 Interpretation of TWT 2D seismic section. NT-3 section is oriented NNW-SSE of the Isthmus Saline Basin. a) seismic section; b) line drawing; c) seismic section with interpretation.

Figure 7.14 Interpretation of TWT 2D seismic section. NT-4 section is oriented NNW-SSE of the Isthmus Saline Basin. a) seismic section; b) line drawing; c) seismic section with interpretation.

Figure 7.15 Interpretation of TWT 2D seismic section. NT-5 section is oriented NNW-SSE of the Isthmus Saline Basin. a) seismic section; b) line drawing; c) seismic section with interpretation

Figure 7.16 Interpretation of TWT 2D seismic section. NT-6 section is oriented NNW-SSE of the Isthmus Saline Basin. a) seismic section; b) line drawing; c) seismic section with interpretation.

Figure 7.17 Interpretation of TWT 2D seismic section. NT-8 section is oriented NNW-SSE of the Isthmus Saline Basin. a) seismic section; b) line drawing; c) seismic section with interpretation.

Chapter 8

List of tables

Chapter 1 Introduction

1.1 Introduction

This thesis focuses on the analysis of the tectonostratigraphic evolution and salt tectonic history of the Isthmus Saline Basin (ISB). The ISB lies at the southeastern margin of the Gulf of Mexico Basin in Mexico (Fig. 1.1). Regional 2D seismic lines and a detailed 3D seismic survey have been combined with well and outcrop data from published maps to produce the first stratigraphic and kinematic analysis of the onshore Isthmus Saline Basin (ISB), one of the most prolific hydrocarbon provinces of the Gulf of Mexico (Golzalez-García & Holguin-Quiñones,1991). The study area encompasses approximately 9,800 $km^{2,}$ located between latitudes 18° 30'N and 14°N and longitudes 97° 30' W and 90° W (Fig. 1.1).

The Isthmus Saline Basin is located in the southern of Mexico north of the Sierra de Chiapas thrust belt at the intersection between the Cocos, Caribbean and North America Plates. The principal tectonic features that border the ISB are: the Sierra de Chiapas to the South, the Yucatán Platform the east, the Veracruz Basin to the west and the Gulf of Mexico to the north. The basin fill, dated Late Jurassic to Holocene, consists of carbonates and deep water clastic sediments which represent slope and basin facies (Sosa-Patron*, et al*., 2009).

Structural and stratigraphic interpretation of 2D and 3D seismic data provide: (1) Regional tectonic analysis, (2) insights into the salt tectonic processes and related depositional systems of the study area, and (3) a good basis for kinematic analysis using structurally balanced and restored cross-sections.

The purpose of this PhD project is to (1) document the salt tectonic styles and (2) understand the evolution of salt structures in the (ISB) in the onshore sector of southeastern of Gulf of Mexico and (3) understand the role of salt tectonics in basin evolution at regional scaled. Pre-existing salt structures exert a strong influence on the tectonic style of fold belts in the Chiapas and Campeche areas (Sánchez-Montes de Oca, 1979; Meneses-Rocha, 1987) and the ISB is part of this fold belt. The role of inherited diapirs and minibasins during regional tectonic shortening in the Gulf of Mexico is still poorly understood.

An additional aim of this study is to investigate the controls of salt diapir formation and reactivation on the strata geometry in the flanks of contractional salt diapirs which represent excellent targets for HC exploration. In the vicinity of salt structures, folding and thrusting induced by salt movements has a significant influence, changing the rock properties and resulting a huge variety of hydrocarbon traps styles (Pilcher, *et al.,*2011).

It is widely accepted that salt exerts a strong influence on structural styles when acting as a contractional décollement (Letouzey, *et al*., 1995), particularly in the case of low shortening rates in convergent margin settings or gravitational failure. Even with the general characteristics of such fold-belts (e.g., large scale geometry, fold wavelength) being well described in the literature, the smaller scale structures found near salt deformation are less well constrained. This scale gap in the knowledge of these structures is mostly related to the complexity induced by pre-existing salt diapirs and minibasins and the difficulty of imaging them using the conventional seismic methods. Nevertheless, they constitute key elements due to their hydrocarbon potential.

Exploration in the ISB has focused on Tertiary siliciclastic plays since initial discoveries of San Cristobal and Ixhuatlán fields in 1906 and 1910 respectively, and culminating in the discovery of Cinco Presidentes field in 1960 (Oviedo-Perez, 1997). Only one field, Cerro Nanchital, near the southern limit of basin, produces from the Mesozoic stratigraphic succession. Elsewhere in the basin the Paleogene and Mesozoic successions have not been explored..

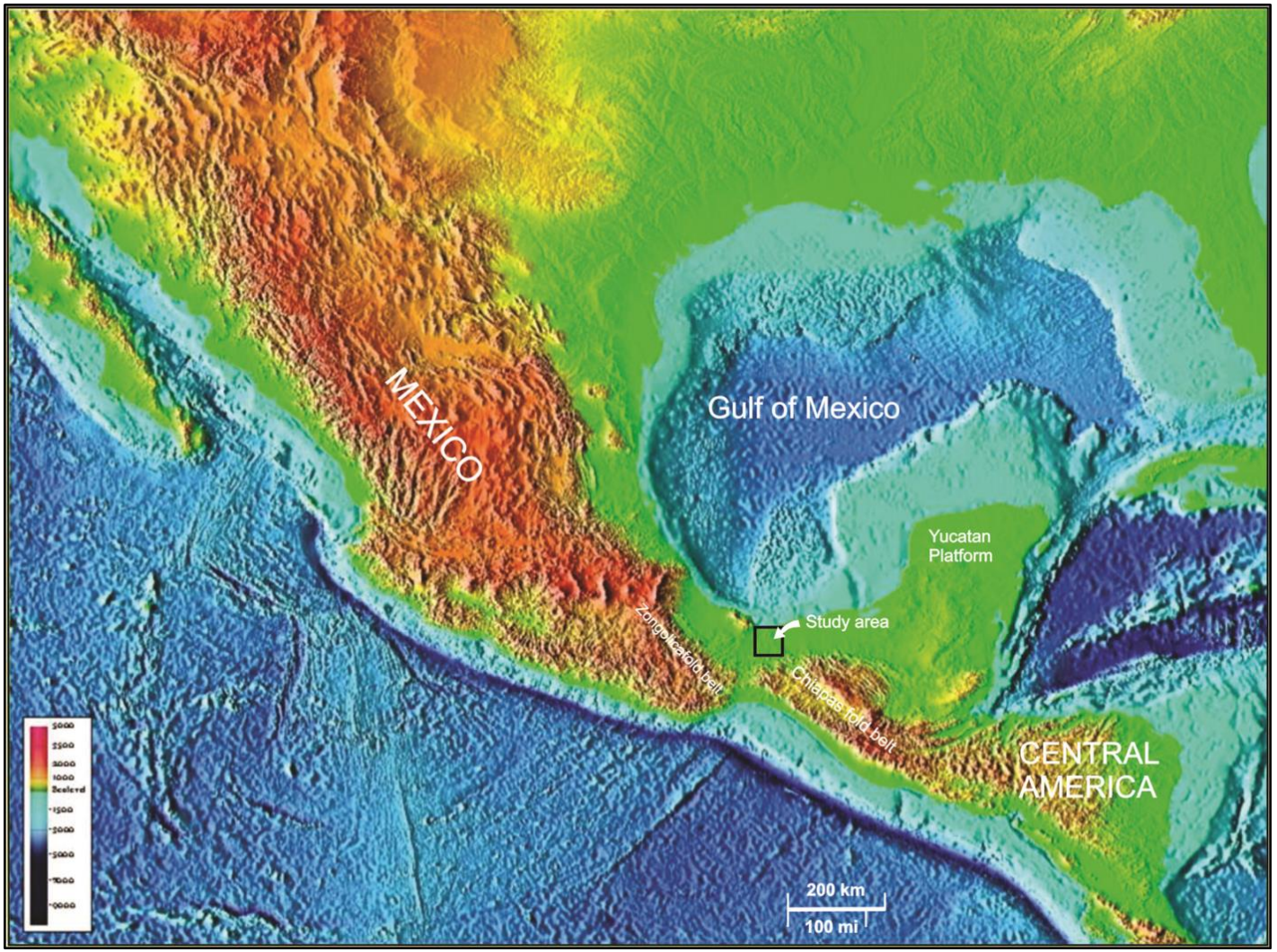

Fig.1.1 Digital elevation model of Mexico and Centro America. Black rectangle marks study area (http://glovis.usgs.gov/indexURL

1.2 The Gulf of Mexico Basin

1.2.1 Location and Exploration History

The Gulf of Mexico basin is a roughly circular structural basin approximately 1,500 km in diameter (Figs. 1.1 & 1.2). This basin is a typical rift basin characterized by basement architecture made up of grabens and half grabens, which controlled evaporites deposition. Salt was part of the post-rift thermal subsidence sequence resulting in more widespread salt layer and less basement control. (Tari, *et al*., 2003).

The Gulf of Mexico basin is bound at the east by the Florida carbonate platform and to the southeast by the Yucatan carbonate platform (Fig. 1.2). The Chiapas massif and the Maya mountains bound the southern margin of the Gulf of Mexico basin and the Sierra Madre Oriental is located along its western side (Fig. 1.2). The northern limits of the basin are the Marathon and Llano uplifts, the Ouachita orogenic belt, the Central Mississippi deformed belt and the southernmost extent of the Appalachian Mountains (Fig. 1.2).

The Gulf of Mexico basin is one of the most important petroleum provinces in the world. Hydrocarbon accumulation within southeastern Mexico results from play elements created by both passive and active margin tectonics as well as sedimentation. Conversely, play elements in the northern and northwestern Gulf of Mexico are dominantly controlled by passive-margin tectonics.

Although the largest fields in the Gulf basin are likely to have already been discovered, considerable exploration potential remains, particularly at water depths greater than 3,000 meters in the deepwater offshore (Edwards, 2001). However, onshore in the southern margin of the Gulf of Mexico Basin has produced oil and gas since the beginning of the twentieth century, mainly from the onshore and shallow offshore parts of the southern basin (Oviedo-Pérez, 1997; Mora-Oropeza, *et al*., 2001).

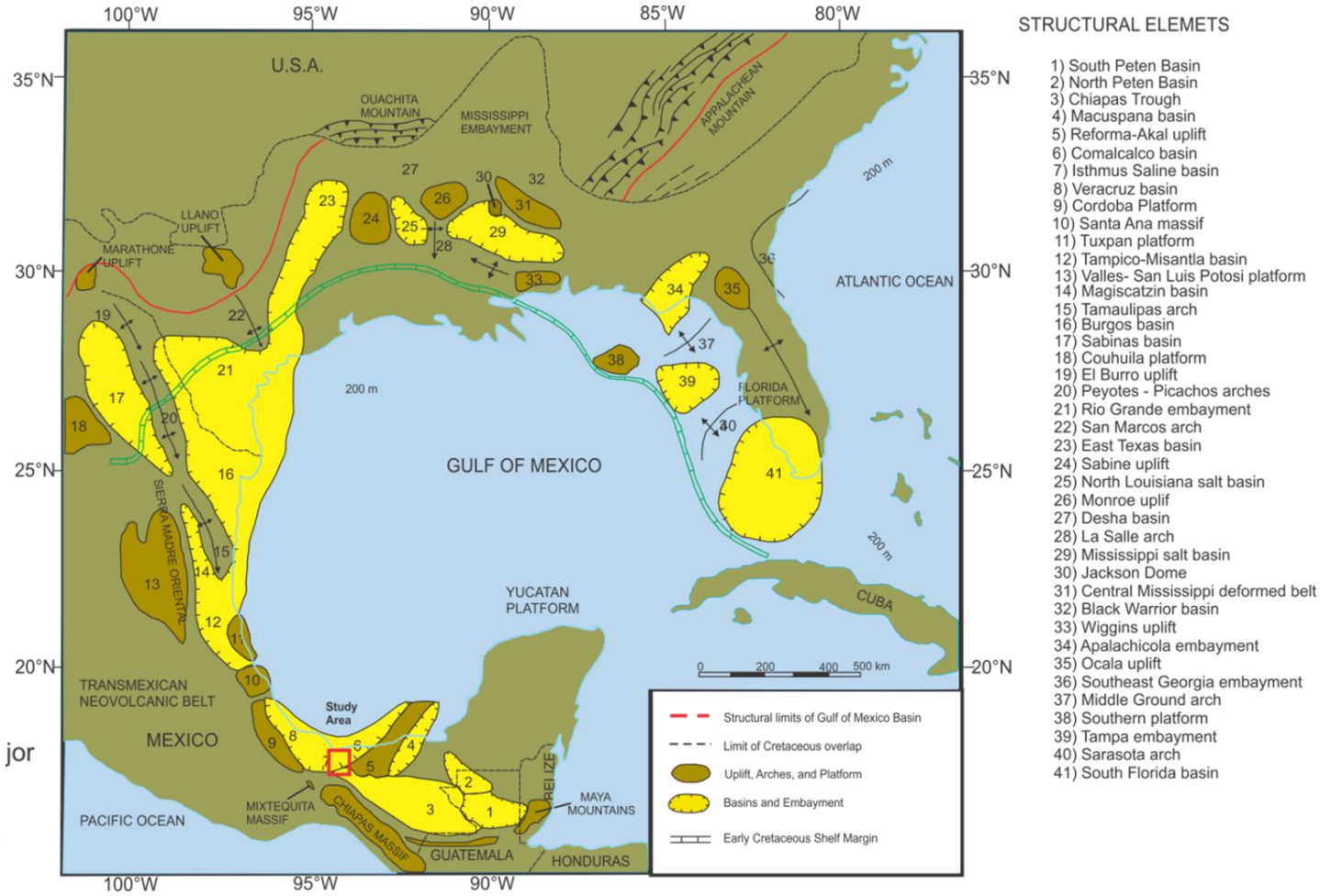

Figure 1.2 Regional structural elements and sedimentary basins surrounding the Gulf of Mexico Basin (modified from Ewing, 1991). Location of study area shown by red rectangle.

1.2.2 Geologic Setting of the Gulf of Mexico Basin

The Gulf of Mexico basin is bordered by a number of regional platforms, basement uplifts and fold belts (Fig. 1.2). The Isthmus Saline Basin is flanked by the Precambrian Chiapas Massif to the south, the Paleocene Veracruz Basin to the east and the Cretaceous Yucatán Platform to the west, a remnant of a large fragment of Precambrian crust that survived Mesozoic continental break up relatively intact (Pindell & Dewey, 1982; Fig.1.2).

The southern rim of the Gulf of Mexico (henceforth abbreviated as GoM) is formed by several Mesozoic and Cenozoic basins, which developed as a result of the separation of North and South America in early Mesozoic time (Pindell and Dewey,1982).

The Upper Triassic to Holocene sedimentary infill of the Gulf of Mexico basin rests unconformable on the pre-Triassic basement (Ewing, 1991). Few outcrops of Precambrian and Paleozoic rocks exist around the basin margins and basement rocks have only been penetrated in a limited number of wells along the basin`s margins. Depth to basement in the central part of the Gulf of Mexico basin has been estimated to be at 12 – 16 km below sea level (Sawyer et al.,1991). This basement has been interpreted to be oceanic crust and extends as far westwards of the study area (Hudec, et al., 2013, Fig. 1.3) and Sandwell et al., 1997. The inferred oceanic crust is flanked by transitional crust and extended (rifted) continental crust at the basin margins. In the Isthmus Saline Basin the basement has been interpreted as the transition between thin transitional crust and thick transitional crust characterized by various igneous, metamorphic, and older (pre-Jurassic) sedimentary rocks (Sawyer et al.,1991; Jacobo-Albarran et al., 2002; Fig.1.3). The northern and southern margins of the GoM basin are dominated by the Middle Jurassic salt section and by salt tectonics. In contrast the western margin of the GoM basin in Mexico is dominated by shale tectonics and the formation of the Mexican Ridges fold belt in the deep-water offshore (Fig.1.4)

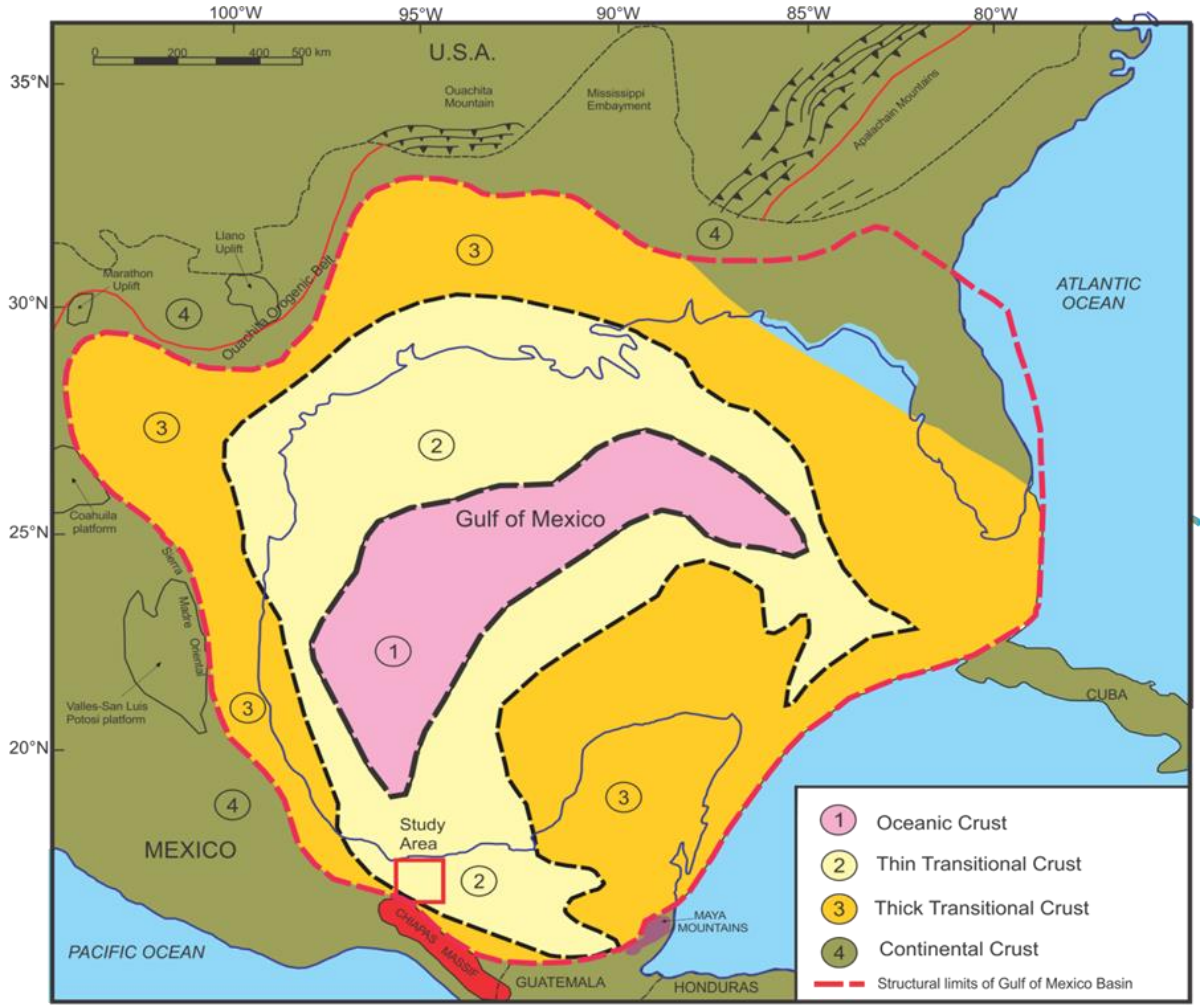

Figure 1.3 Map showing the crustal types in Gulf of Mexico. (after Sawyer, et al., 1991). Location of study area shown by red rectangle.

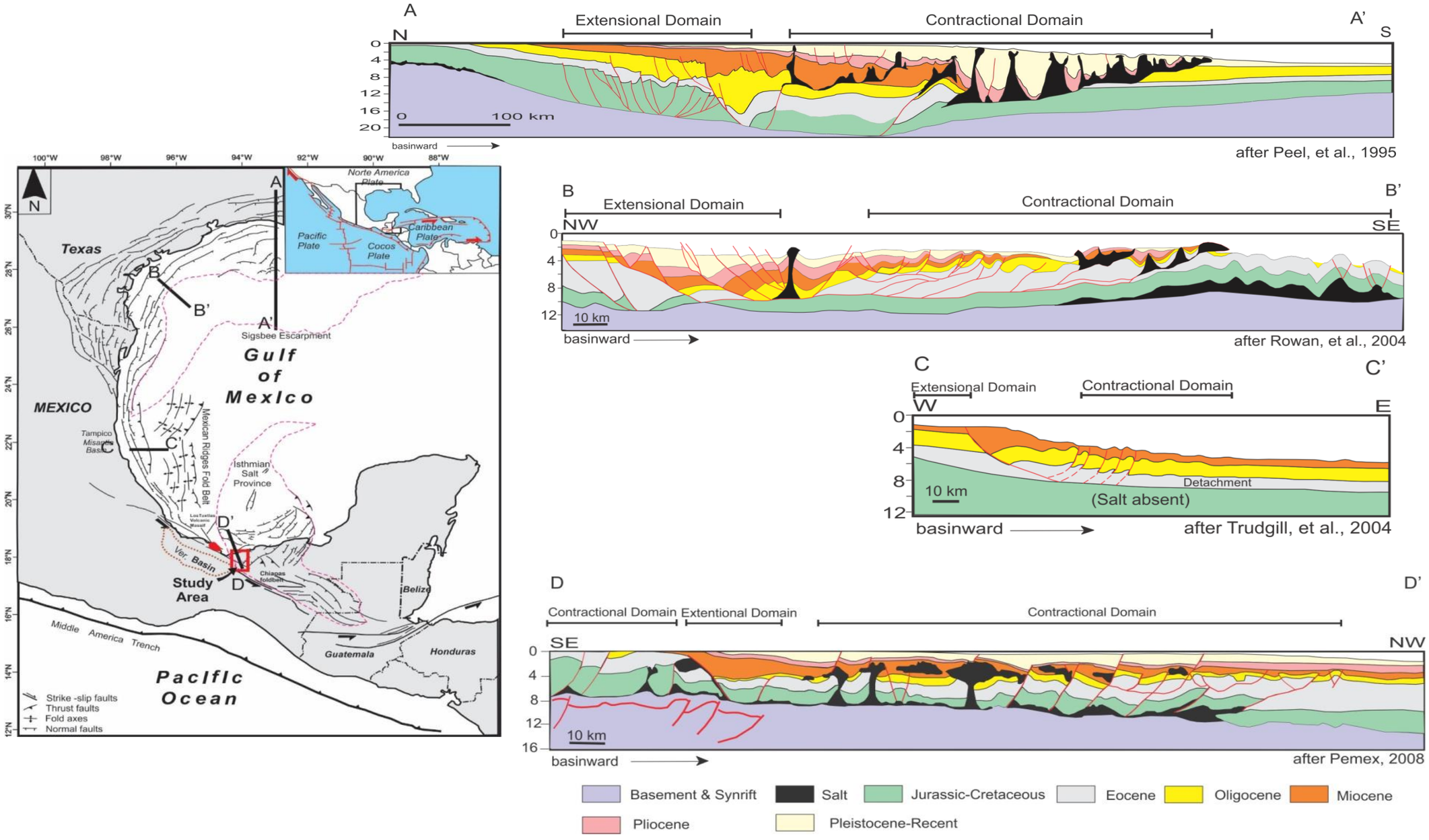

Figure 1.4. Gulf of Mexico structural overview, study area shown by red rectangle. Deformation in the north, northwest and west of the GOM is predominantly gravity driven. Conversely, deformation within the southern contains a significant component of orogenically driven deformation.Section C detaches on shale.

1.3 Research Aims

This research project focuses on the analysis of salt tectonic styles with a particular focus of salt structure and kinematic analysis in the Isthmus Saline Basin (ISB).

In this research project, I propose to establish a structural framework using regional 2D seismic lines and a 3D seismic survey, wells, outcrops data, gravity and magnetic and earthquakes data from published maps to develop the first tectono-stratigraphic and kinematic analysis of the onshore Isthmus Saline Basin. This research has five goals:

1.- Produce a map of basement architecture for the ISB

2.-Investigate the influence of basement and earthquake activity in the evolution of salt diapir evolution.

3.- Define the salt structural styles within the ISB.

4.- Perform kinematic analysis of the ISB.

5.- Suggest a structural model to explain the evolution of ISB.

1.4 Data sets

Pemex Exploration and Production, Southeastern Region in Villahermosa, Tabasco provided the geological and geophysical data for this research project. The data set consists of 1,800 km^2 of 3D PSDM seismic survey of an onshore part of the (ISB) and a set of four 2D pre-stack depth migration seismic lines of the Sierra de Chiapas. Well data and other geophysical data sets (gravity and magnetic data). I interpreted the seismic data to analyze the post-rift depositional sequences and salt structures. Additionally, formation tops, lithological and paleontological information of 8 exploration wells were provided by the Exploration Asset team. The seismic data is land information of variable quality due to the large number of obstacles encountered during the acquisition.

The seismic data were acquired in 2010 and have been recorded up to depths of 15 km.

1.5 Research Methodology

The research approach for this project is shown in figure 1.5. The research project comprises seismic interpretation, structural restoration, gravity, magnetic, earthquake data. The structural and stratigraphic interpretation of approximately 1800 km^2 of *3*D semi-regional seismic data forms the basis for tectono-stratigraphic, structural and kinematic analysis. Seismic interpretation was carried out using Landmark Graphics Decision-Space software on a Sun workstation. Three horizons were interpreted across the 3D seismic surveys. Depth maps were constructed for these surfaces. Construction and restoration of cross-sections are of critical importance in validating the structural interpretation (Hossack, 1995). The methodology will be described in detail in Chapter 6, which focuses on the restoration of cross-sections.

The integration of interpretation and restoration results will provide the boundary conditions and parameters for applied analogue experiments (e.g. salt basin geometry, extent and initial salt thickness, sediment input) to take place in the future.

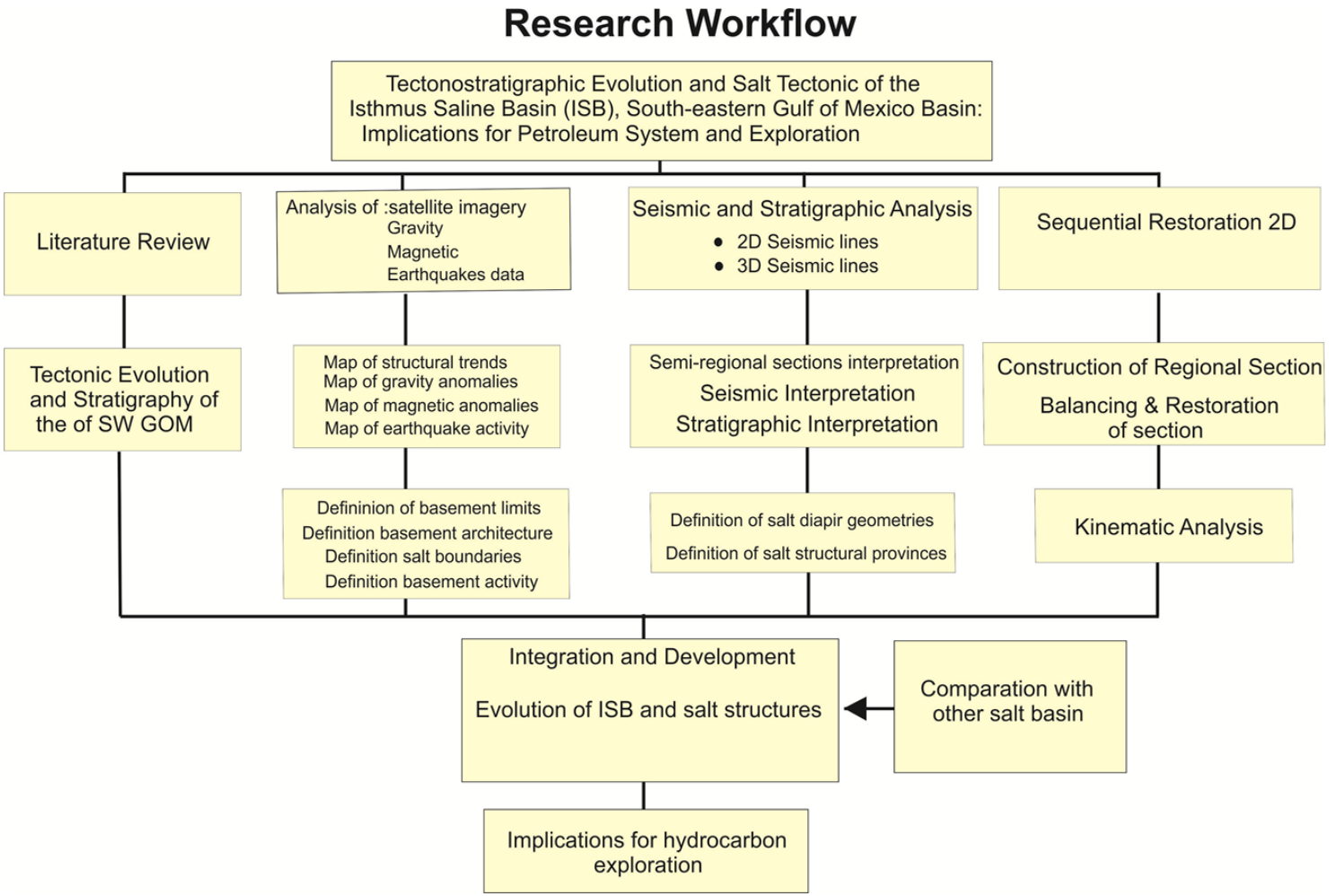

Figure 1.5 Research workflow

1.6 Thesis Outline

Chapter 1: This chapter provides a brief overview of the exploration history and the geologic setting of the Gulf of Mexico Basin and the main aims, data sets and research methodology employed during the research work

Chapter 2 & 3: Chapter 2 & 3 present an overview of the tectono-stratigraphic evolution of the southeastern of Gulf of Mexico. The tectono-stratigraphic synthesis presented in these chapters highlights the tectonic development of both the Gulf of Mexico and Caribbean basins evolution. The evolution of these basins in different stages influenced drastically the formation and evolution of the ISB.

Chapter 4: A revision and analysis of the concepts of salt tectonics with emphasis on tectonic styles of salt deformation.

Chapter 5: Presents in detail the data and methodology employed during the research work.

Chapter 6: Presents the results of analysis of gravity, magnetic and earthquake data.

Chapter 7: The chapter presents results about regional structural and stratigraphic analysis of salt tectonic processes that have controlled depositional systems and salt structures under different tectonic settings in the ISB.

Chapter 8: Presents the results of detailed analysis of local section construction and sequential restorations across Isthmus Saline Basin.

Chapter 9: Is a discussion of the results of this research.

Chapter 2 Analysis of the Tectonic Evolution of Southeastern Gulf of Mexico

1 Introduction

The Gulf of Mexico (GoM) salt basin refers collectively to all Callovian sub-basins around the Gulf of Mexico (Fig. 2.1). The Gulf of Mexico is a rifted continental margin basin that formed in the southern part of the North American plate. It has a long and complex evolution ranging from initial extension and rifting in the Late Triassic to the Present Day passive margin stage (Pindell & Dewey, 1982; Anderson & Schmidt, 1983; Pindell, 1985; Pindell, et al., 1988; Salvador, 1991; Pindell, 1994; Pindell, et al., 2000; Bird, et al. 2005) where differential sedimentary loading, gravity driven tectonics and salt tectonics dominate (Wu, et al., 1990; Weimer & Buffler, 1992; Peel, et al., 1995; Diegel, et al., 1995; Rowan, et al., 1999; Trudgill, et al. 1999; Rowan, et al., 2000; Wu & Bally, 2000, Rowan, et al., 2004). The rifting and separation of Pangea during Triassic and Early Cretaceous is evidenced by the distribution of red beds in narrow rift grabens mainly oriented with current coastline (Salvador, 1991; Godinez-Urban, et al., 2011) (Fig. 2.2). However, these rift basins, which originally trended NE-SW, rotated anticlockwise into NW-SE direction as the Yucatan block moved during Early Cretaceous time to its present day position. This chapter provides an overview of the evolution of the Gulf. This is important for understanding the structural relationship between the evolution of the Gulf of Mexico and that of the ISB.

The Isthmus Saline basin is located between the southern and western flanks of the Yucatán carbonate platform and north of the Chiapas Massif (Figure 2.1). This salt basin extends offshore into the Bay of Campeche, forming a broad basin characterized by extensive salt deposits and basin-wide comparable to the deep water northern Gulf of Mexico basin. The evolution of Southern part of the Mexican Gulf margin and the Isthmus Saline basin is characterized by a complex interplay between passive, transform, and active continental margin tectonics and sedimentation throughout Mesozoic and Cenozoic times.

The plate tectonic framework of southestern Gulf of Mexico comprises the following tectonic events:

- Continental Rifting (middle-late Triassic to early Oxfordian, Marton and Buffler, 1994; Salvador, 1987; Winker and Buffler, 1988).
- Continental break up and the initiation of oceanic spreading
- Sea floor spreading (late Callovian to Berriasian, Marton and Buffler, 1994; Pindell, 1985; Winker and Buffler,1988) and thermal subsidence (Berriasian to Albian; Coney, 1983; Goldhammer, 1999).
- Arc Collision and passive margin destruction (Cenomanian to Maastrichtian; Carfantan,1977; Quezada-Muñeton, 1987; Johnson, et al., 1999)
- Onset of Caribbean eastward motion (Chortis Block) (Paleocene to Oligocene; Coney, 1983; Carfantan, 1976 a, b; Garcia-Palomares, 1980)
- Deformation of the Chiapas fold belt (Middle Miocene to Late Miocene; Sánchez-Montes de Oca, 1978, 1986; Meneses-Rocha, 1987; Angeles, 1994; Robles, et. al., 2004).

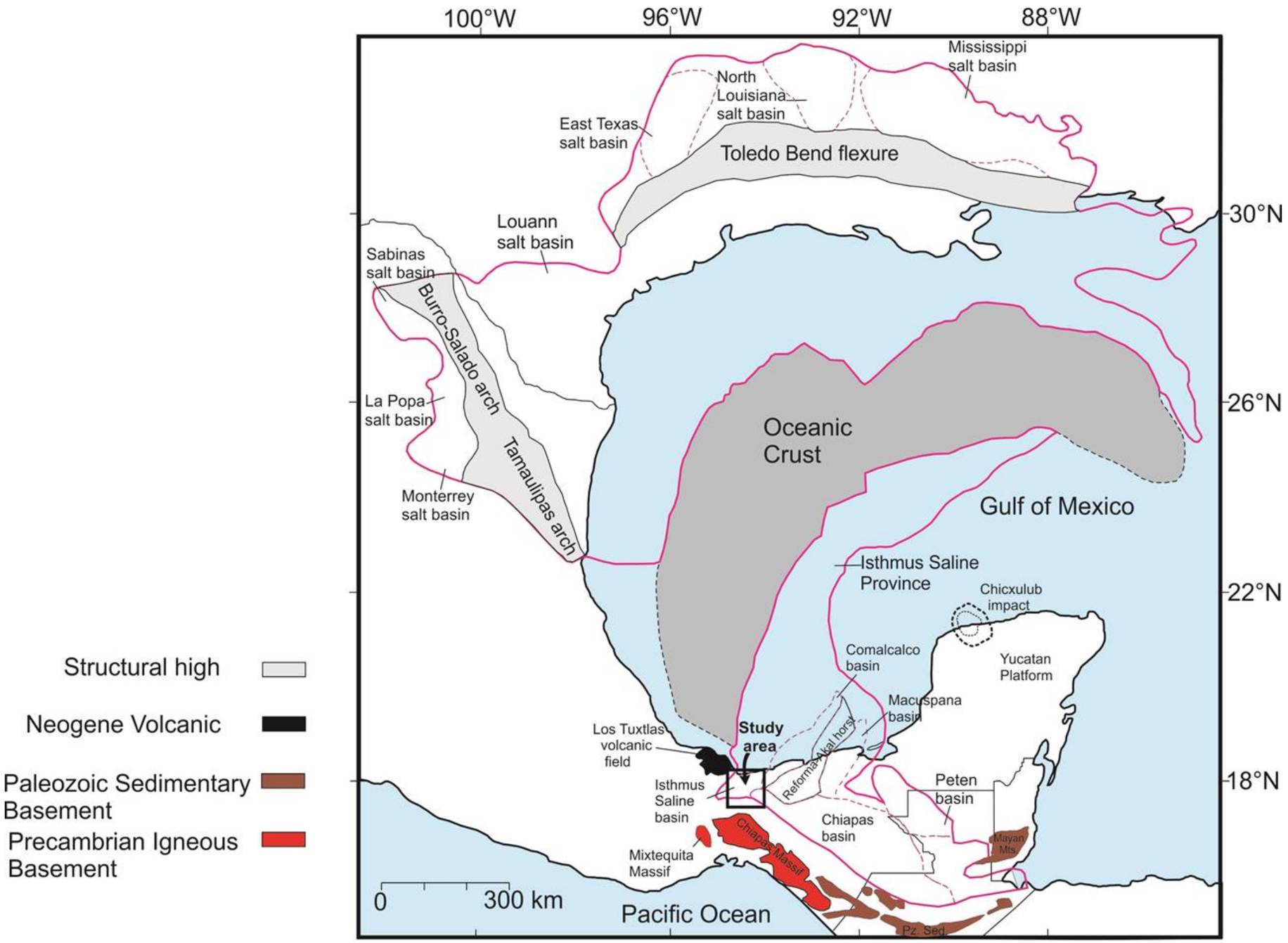

Figure 2.1- Map of Gulf of Mexico showing basins and location of the study area. Pink lines outline salt basins restricted by oceanic crust. The south-eastern salt basins are surrounded by igneous and sedimentary basement, is also shown location of the Chicxulub impact (modified from Hudec, *et al*., 2013).

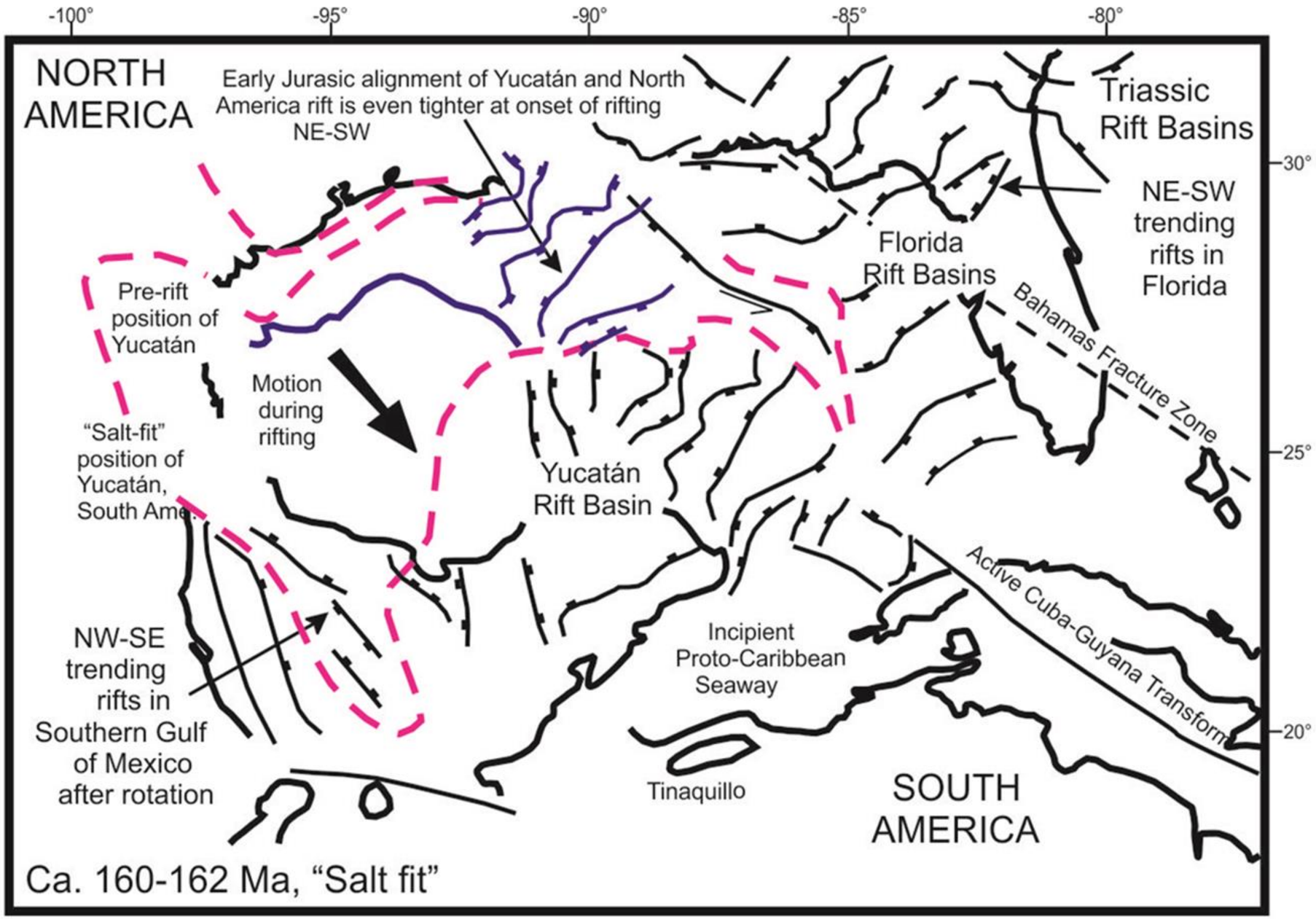

Figure 2.2 Reconstruction of Jurassic rifts in Florida and Yucatán after clockwise rotation of Yucatán. The early Jurassic rifting is shown in blue (modified from Pindell, *et al*., 2006)

2.2. Plate Tectonic Evolution of the Gulf of Mexico Basin

The Gulf of Mexico is located in the southern part of the North American Plate, adjacent to the Cocos and Caribbean Plates (Fig.2.3). Earthquake distributions define the boundaries of the North American Plate, but substantial intra-plate earthquakes have been documented (et al. 2000). According to Zoback, *et al*. (1986), DeMeets & Dixon (1999) the mid-plate stress of the North American Plate at present day is compressive, with a maximum horizontal principal stress oriented northeast to east-northeast.

The Gulf of Mexico is generally accepted to be a passive margin system with Late Jurassic oceanic crust forming the floor of the basin in its centre (Pindell & Dewey, 1982; Anderson & Smith, 1983; Pindell, 1985; Salvador, 1987; Pindell, *et al*., 1988; Salvador, 1991; Pindell, 1994; Pindell, *et al*., 2000; Bird, *et al*., 2005).

The figure 2.4, represent a structural model of the Gulf of Mexico. The model shows the separation between Yucatan from North America (from Pindell & Kennan, 2002).

Circum–Atlantic plate reconstructions for the Late Paleozoic produce a total closure in the Gulf of Mexico region (Pindell & Dewey, 1982; Anderson & Smith, 1983; Pindell, 1985; Ross & Scotese, 1988; Pindell, *et al*., 1988; Salvador, 1991; Pindell, 1994; Pindell, *et al*., 2000; Bird, *et al*., 2005). In order to improve the fit between Mid Jurassic rift-related salt provinces of the Louann salt in the northern Gulf of Mexico with the Isthmian Saline Province in the southern Gulf of Mexico, these reconstructions portray the Yucatan block between the U.S. Gulf Coast and Venezuela (Pindell & Dewey, 1982; Anderson & Schmidt, 1983; Pindell, 1985; Ross & Scotese, 1988; Pindell, et al., 1988; Salvador, 1991; Pindell, 1994; Pindell, *et al*., 2000; Bird, *et al*., 2005).

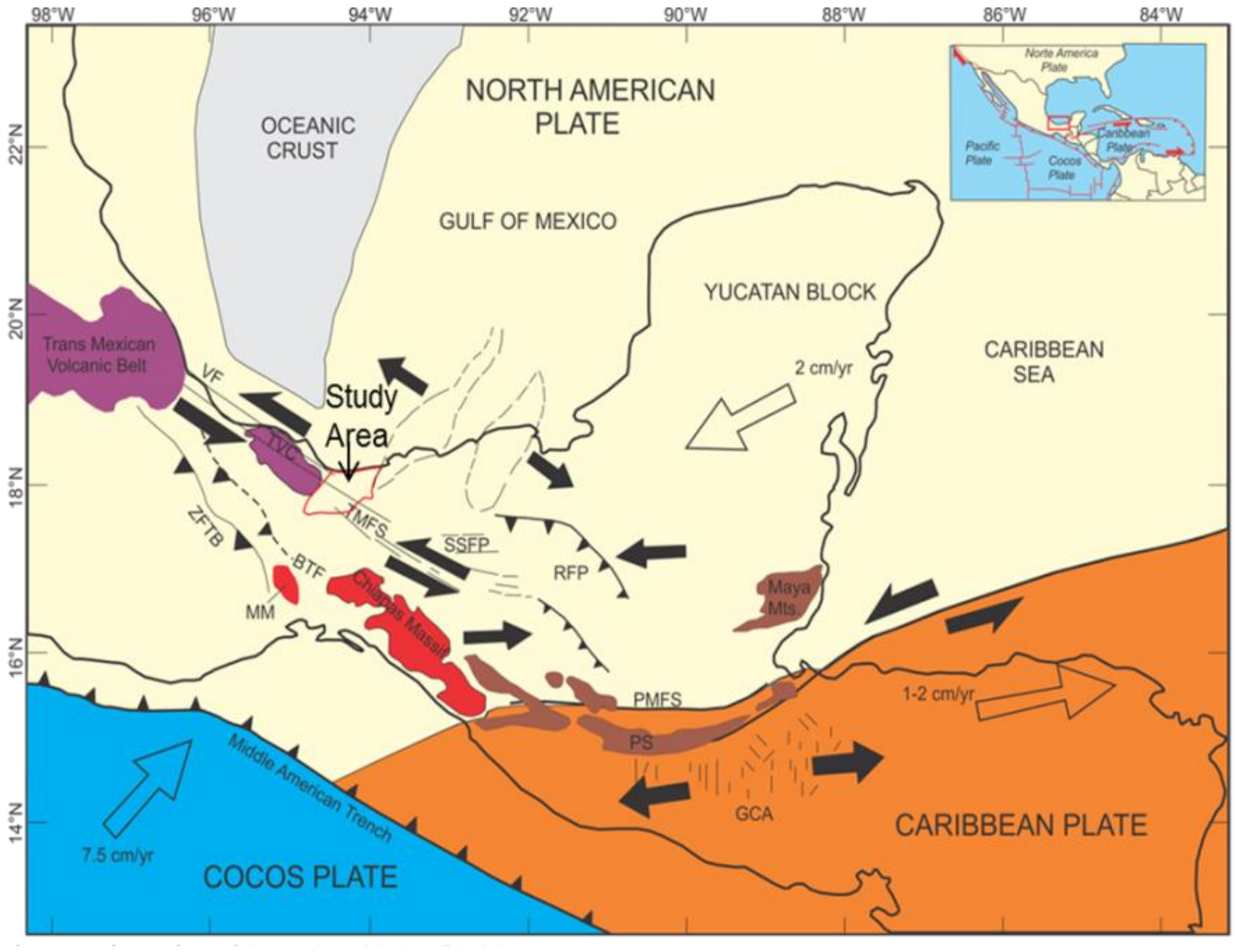

Figure 2.3 Map of southern Mexico showing Quaternary plate tectonic settings and relative plate motion. Black lines outline main faults. Black arrows represent relative motions at plate's boundaries. White arrows indicate plate movement with respect to the North American plate (De Mets, 2001). BTF- Buried Thrust Front, GCA-Grabens of Central America, MM-Mixtequita Massif, PMFS-Polochic-Motagua fault system, PS-Paleozoic Sediments, RFP- Reverse Fault Province, SSFP- Strike-slip fault province, TMFS-Tuxtla-Malpaso fault system, TVC- Tuxtla Volcanic Center, VF- Veracruz fault, ZFTB-Zongolica fold thrust belt. Modified from (Andreani*, et al.*, b. 2008).

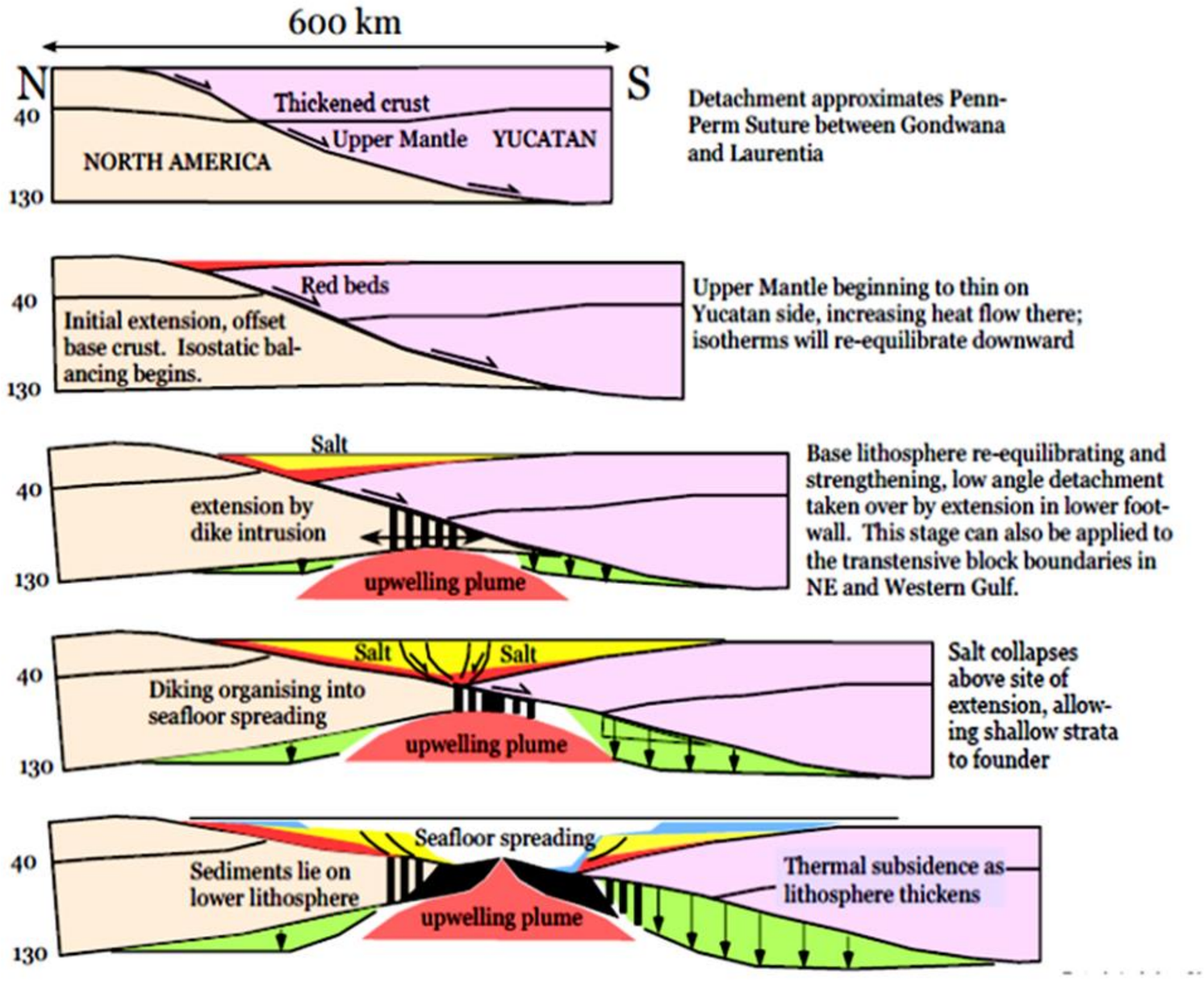

Figure 2.4. - Asymmetric rifting model, showing the separation between Yucatan from North America (from Pindell & Kennan, 2002)

2.3 Mesozoic History

2.3.1. Rifting Stage: Late Triassic to Callovian (221-163 Ma)

In the late Triassic the southern part of the North American plate was part of western Pangaea (Pindell & Dewey, 1982; Anderson & Schmidt, 1983; Pindell, 1985; Ross & Scotese, 1988; Pindell, *et al*., 1988; Salvador, 1991; Pindell, 1994; Pindell, *et al*., 2000; Bird, *et al*., 2005). At this time rifting in western Pangaea began along wide zones of intra-continental block-faulting and dike emplacement (Pindell & Dewey, 1982; Anderson & Schmidt, 1983; Pindell, 1985; Ross & Scotese, 1988; Pindell, *et al*., 1988; Salvador, 1991; Pindell, 1994; Olsen, P.E., 1997; Pindell, *et al*., 2000; Bird, *et al*., 2005, Withjack, *et al*., 2013). The initial stage of crustal stretching was the result of the separation of Pangaea into Laurasia and Gondwana. So GoM extensional tectonics is driven by a global scale tectonic event: the breakup of a supercontinent. The GoM is a small part of a big rift where the specifically South America block pulling away from North America block in a relative northwest-southeast extension (Pindell, *et al*., 2014). A mantle plume may have triggered the extensional tectonics leading towards the early breakup of Laurentia (May,1971). The rift zone coincides with a known crustal discontinuity the "Oachita-Marathon Suture", of Permian age (Bird, *et. al*., 2005). In addition, Pindell and Kennan, (2007) state that the continental margins of the Proto-Gulf of Mexico were of an asymmetric nature during the syn-rift stage, with the Yucatan Block forming the hanging wall of a low-angle detachment zone that collapsed to the southeast (Fig. 2.4).

Africa and North America began to separate in Middle Jurassic times(Fig. 2.5a) (Pindell & Dewey, 1982; Anderson & Schmidt, 1983; Pindell, 1985; Ross & Scotese, 1988; Pindell, *et al*., 1988; Salvador, 1991; Pindell, 1994; Olsen, P.E., 1997; Pindell, et al., 2000; Bird, et al., 2005). In the Gulf of Mexico, the Yucatan block progressively diverged from the southern part of the North America plate (Pindell & Dewey,1982; Anderson & Schmidt, 1983; Pindell, 1985; Ross & Scotese,1988; Pindell, et al., 1988; Salvador, 1991; Pindell,1994; Pindell, *et al*., 2000; Bird, *et al*., 2005). The resulting active rift basins were initially filled with continental red beds and volcanic rocks (Salvador, 1987; Fig. 2.5b).

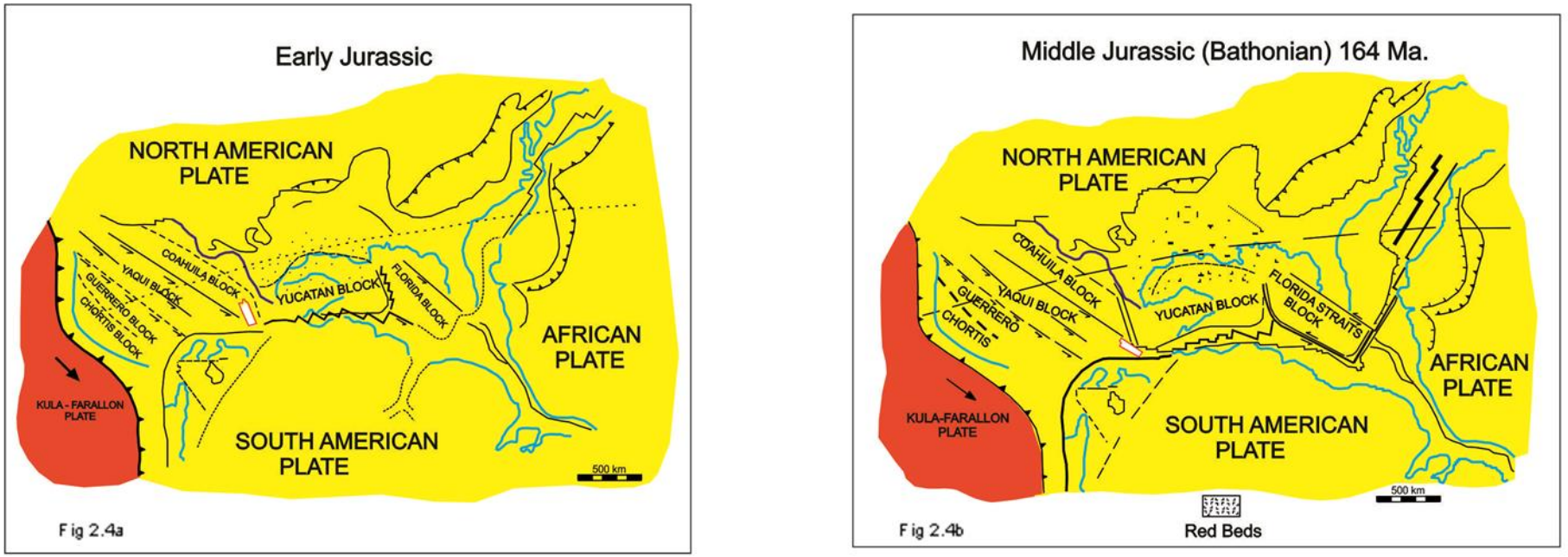

Fig 2.5 a-b Plate tectonic reconstruction of Gulf of Mexico. Showing the rifting and drifting stages during Early Jurassic to middle Jurassic (Bathonian) (after Pindell & Dewey, 1982; Pindell, 1985).

Crustal extension and thinning continued approximately until Early Oxfordian times (Pindell & Dewey, 1982; Anderson & Schmidt, 1983; Pindell, 1985; Ross & Scotese, 1988; Pindell, *et al*., 1988; Salvador, 1991; Pindell, 1994; Pindell, *et al.,*2000; Bird, *et al*., 2005). In the Gulf of Mexico, the Yucatan block progressively diverged from the southern part of the North American plate (Pindell & Dewey, 1982; Anderson & Schmidt, 1983; Pindell, 1985; Ross & Scotese, 1988; Pindell, *et a*l., 1988; Salvador, 1991; Pindell, 1994; Pindell, *et al*., 2000; Bird*, et al*., 2005).

Many publications follow current "conventional wisdom" that the first incursion of marine waters occurred in Early Callovian (Pindell & Dewey, 1982; Anderson & Schmidt, 1983; Pindell, 1985; Ross & Scotese, 1988; Pindell, *et al*., 1988; Salvador, 1991; Pindell, 1994; Pindell*, et al*., 2000; Bird, *et al*., 2005). But this age is very weakly constrained (and actually wrong, but the public data do not yet demonstrate this). Very recent work indicates that the salt age probably starts as old as Bajocian (169-170 Ma), giving a much earlier age of breakup (Olsen,1997). To the west, southeastward movement of crustal blocks of eastern Mexico prevented marine incursions into the Gulf of Mexico basin at this stage (Pindell & Dewey, 1982; Anderson & Schmidt, 1983; Pindell, 1985; Ross & Scotese, 1988; Pindell, *et al*., 1988; Salvador, 1991; Pindell, 1994; Pindell, *et al*., 2000; Bird, *et al*., 2005). During the Callovian (Fig.2.5 c), continued extension and subsidence caused intermittent marine incursions of the rift basins, which then became isolated again forming the “Louann salt basin” to the northern of Gulf of Mexico and “Isthmian salt basin” to the south (Pindell & Dewey, 1982; Anderson & Schmidt, 1983; Pindell, 1985; Rose & Scotese, 1988; Pindell, *et a*l., 1988, Salvador,1991; Pindell, 1994; Pindell, *et a*l., 2000; Bird, *et al*., 2005).

Salt deposition occurred near the end of the rifting phase and the beginning of the drifting phase in the southern and northern Gulf of Mexico. The Pacific marine waters continued its incursion across Central Mexico (Bird, et al*.,* 2005). It is important to note that rotation of Yucatan block happened after breakup of GoM and Proto Caribbean. Continental extension of the Yucatan block was accompanied by a rapid rotation of approximately 22° to 30° counter clockwise and consequent intermittent seawater flooding, which produced massive

evaporites deposition in the northern part of the Gulf of Mexico (Bird, *et al.,* 2005, Sandwell, *et al*., 2014). Due to the tectonically controlled basin morphology with lows and highs and differential subsidence rate of active grabens, the depositional salt thickness was markedly variable. Some authors have used the distribution geometry of these Jurassic evaporites deposits in order to demonstrate the counter-clockwise rotation of the Yucatan Block (Humphris, 1977, Salvador & Green, 1980). Regionally speaking, the Todos Santos Formation was contemporaneous with Isthmian Salt and Louann Deposits (Salvador, 1991a). This last statement will be further discussed in chapter 3.

During early syn-rift stage, the Oxfordian and Kimmeridgian deposits were controlled by differential subsidence of blocks of adjoining basement during overall subsidence of the margin (Meneses-Rocha, 1987). This means that, the late Jurassic interior sea was surrounded by continental shelves, ramps and platforms. The Upper Jurassic sediments evidence a marine transgression resulting from a subsiding central basin (Pindell & Dewey, 1982; Anderson & Schmidt, 1983; Pindell, 1985; Ross & Scotese, 1988; Pindell, *et al*., 1988; Salvador, 1991; Pindell, 1994; Pindell, *et al*., 2000; Bird, *et al*., 2005). As a result of the “Basin and Range” style basin architecture due to ongoing extensional tectonics of highs, the Oxfordian and Kimmeridgian sequences show changeable facies transitions and variable thicknesses.

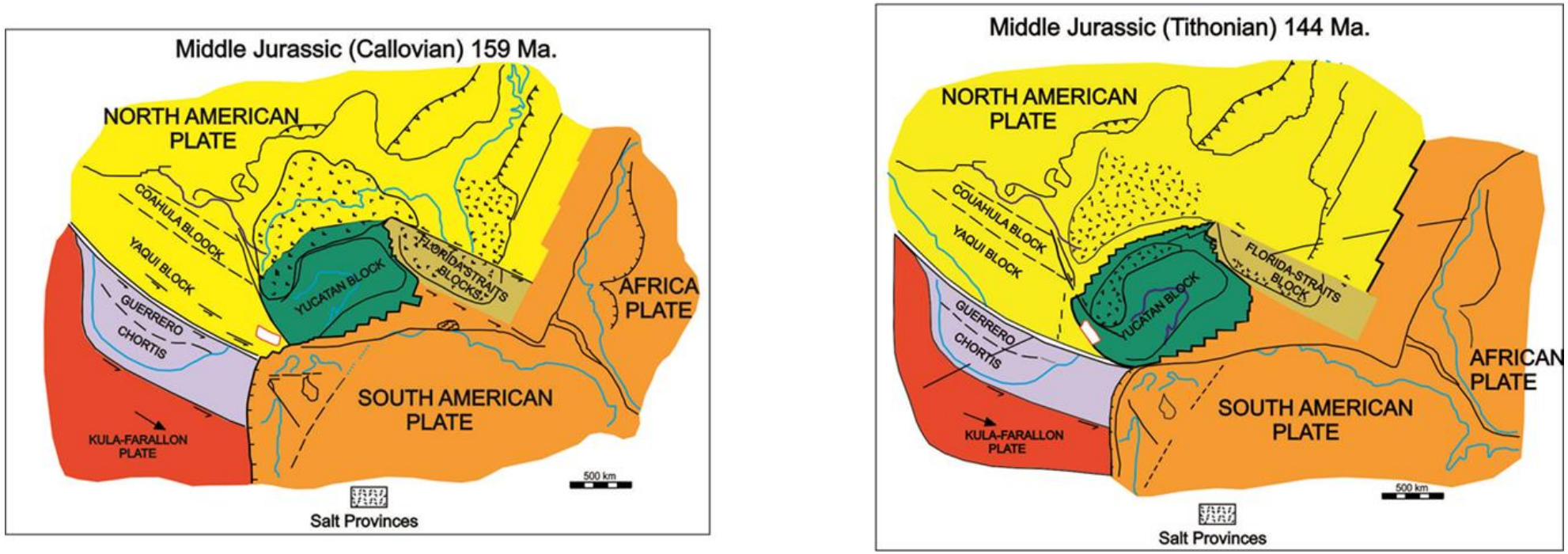

Fig 2.5 c-d Plate tectonic reconstruction of Gulf of Mexico. Showing the rifting and drifting stages during middle Jurassic to Late Jurassic (Tjthonian) (after Pindell & Dewey, 1982; Pindell, 1985).

2.3.2 Sea Floor Spreading and Drift Stage (163-140 Ma)

Salt deposition ceased when the basin dried out, followed by the deposition of undated non marine sediments (continental clastic of the Norphlet Formation) on top of salt. The timing of this drying out is poorly constrained. After an indeterminate length of time, the basin re-flooded, and marine sedimentation begin again in the form of the Smackover Formation. During this period, continental breakup occurred and oceanic spreading began in the central Gulf of Mexico (Fig. 2.5d). Sea floor spreading along the new mid-oceanic ridge separated the northern U.S Gulf Coast and Yucatan block divided the original salt basin in today's northern and southern salt provinces (Pindell & Dewey, 1982; Anderson & Schmidt, 1983; Pindell, 1985; Ross & Scotese, 1988; Pindell, *et al*., 1988; Salvador, 1991; Pindell, 1994; Pindell, *et al.,* 2000; Bird, *et al*., 2005).

The subsequent opening of the Gulf of Mexico during Jurassic time was controlled by spreading centres and transform faults, which displaced the Yucatan block southward as it rotated anticlockwise (Fig. 2.4e). Spreading centres formed in the earliest Oxfordian (Buffler and Sawyer, 1985; Pindell, 1985, Sandwell, *et al.,* 2014) and individual ridge segments were linked by left-lateral transform faults (figure Buffler and Sawyer, 1985; Pindell, 1985; Sandwell, *et a*l., 2014). In the western Gulf of Mexico N-NW to S-SE- spreading along the mid-oceanic ridge system appears to have been accommodated by a NNW striking transform boundary defined by Pindell (1985) as the Tamaulipas-Golden Lane-Chiapas Transform Fault (TGLC), or "Tehuantepec Transform" (Dickinson and Lawton, 2001), or "Western Main Transform" (Marton and Buffler, 1994). Additionally, Yucatan block spreading during ocean opening phase around 25-30 degrees, from Transform curvature in Sandwell, *et al*., 2014.

As a result the limit between oceanic and continental crust (or shear margin) is located offshore and parallel to the present day eastern coast of central Mexico.

2.3.3 Cretaceous Thermal Subsidence (140 -65 Ma)

By the Berriasian sea floor spreading ceased and the opening of the Gulf of Mexico was complete, with the Yucatán and Guerrero blocks having reached their present day position (Pindell & Dewey, 1982; Anderson & Schmidt, 1983; Pindell, 1985; Ross & Scotese, 1988; Pindell, *et al*., 1988; Salvador, 1991; Pindell, 1994; Pindel,l *et al*., 2000; Bird, *et al*., 2005). Thermal subsidence followed tectonic subsidence aafter cessation of sea floor spreading in the Gulf of Mexico in the Berriasian, in this period marine transgression was accentuated and sea water covered wide carbonate platforms with reefal conditions at their borders. As a result, extensive carbonate platforms reached a cumulative shelfal average thickness of about 2000 m (Pindell & Dewey, 1982; Anderson & Schmidt, 1983; Pindell, 1985; Ross & Scotese, 1988; Pindell, *et a*l., 1988; Salvador, 1991; Pindell, 1994; Pindell, *et al*., 2000; Bird, *et al*., 2005). Moreover, convergence between the Kula/Farallon plate and the North American plate was initiated on the Pacific margin during Maestrichtian (Fig.2.4e) (Pindell & Dewey, 1982; Anderson & Schmidt, 1983; Pindell, 1985; Ross & Scotese, 1988; Pindell, *et al*., 1988; Salvador, 1991; Pindell, 1994; Pindell, *et al*., 2000; Bird, *et a*l., 2005).

During Early and Middle Cretaceous times, the southern Gulf of Mexico was a passive margin with the presence of carbonate platforms such as Artesa-Mundo Nuevo in Tabasco, Cordoba Platform in Veracruz and Puebla states and the Yucatan platform in the Campeche, Yucatán and Quintana Roo states. Some mixed clastic-carbonate platforms had also developed, such as the platform formed in the eastern margin of Chiapas Massif. These Cretaceous carbonates, deposited in environments such as: platform margins, ramps and basinal settings (See Chapter 3 Table tectono-stratigraphic chart) have been the main petroleum reservoirs in the Mexican Gulf of Mexico.

2.3.4. Arc Collision passive margin destruction of the southern Gulf of Mexico (100 – 66 Ma)

During the Campanian, the southern continental margin of the Gulf of Mexico was affected by arc collision, which subsequently deformed the southward facing passive margin from south to north. During this stage, translation of the

Neo-Caribbean Plate (including the Great Antilles island arc system, Jamaica and Cuba) along the east along the east Yucatan margin effectively overprinted the earlier passive margin succession. The Paleo-Caribbean ocean was destroyed by subduction. The continued convergence in southeastern Yucatan margin lead to fold-thrust tectonics and foredeep clastic sedimentation. In the southern Gulf of Mexico the transition from carbonate to siliciclastic sedimentation marks the beginning of the “Laramide” deformation phase along the southern margin (Johnson, *et al*., 1999).

The southern passive margin of Yucatan began a gradual transformation into a convergent margin foredeep basin due to a major reorganization of plate motions (Fig.2.5 f). In this stage, the Caribbean Plate started migrating northward due to a polarity reversal of the subduction zone (Draper, *et al*., 1996), and began subduction distal Yucatan (proto-Caribbean) oceanic crust at a southward dipping subduction zone. By Cenomanian time, northward movement of the Caribbean plate had begun closing the gap with southern Yucatan. The load applied by the overloading arc complex caused flexural uplift of a forebulge that migrated northward across the Yucatan carbonate platform. This migration resulting in reactivation of Triassic-Jurassic basement highs and erosion of Cenomanian–late Albian shelf carbonates (Quezada, 1987; Johnson, *et al*., 1999). Carfantan (1976) called this event “Austriaca Phase”. Basement reactivation may have generated the pillowing reactivation of Callovian salt (Johnson, *et al*., 1999). The forebulge formed a broad WSW-ENE trending zone along the southern margin of Yucatan and Guatemala. Near the end of Cretaceous, a massive northward influx of flysch sediments (Sepur Formation) marks the proximity of the Caribbean Plate (further discussed in Chapter 3). Its collision and suturing with the passive margin is equivalent in time to the “Laramide Orogeny” (i.e., Late Cretaceous-Early Cenozoic). The Laramide Orogeny refers to the migration of the Sevier-Laramide orogenic system towards the Mexican side (North America Plate), as a consequence of subduction of the Farallon Plate beneath the North American plate along its western margin. According to Quezada-Muñeton (1987) the southern most expression of this deformational event in México is seen at the Sierra de Zongólica (an uplifted thrust-fold belt) and at the western end of the Sierra de Chiapas in the Middle Eocene. Conversely, Pindell and Kennan (2002) state

that the collision of the Caribbean Plate (Antilles Volcanic Arc) preceded the Laramide events in the southern flank of Yucatan block.

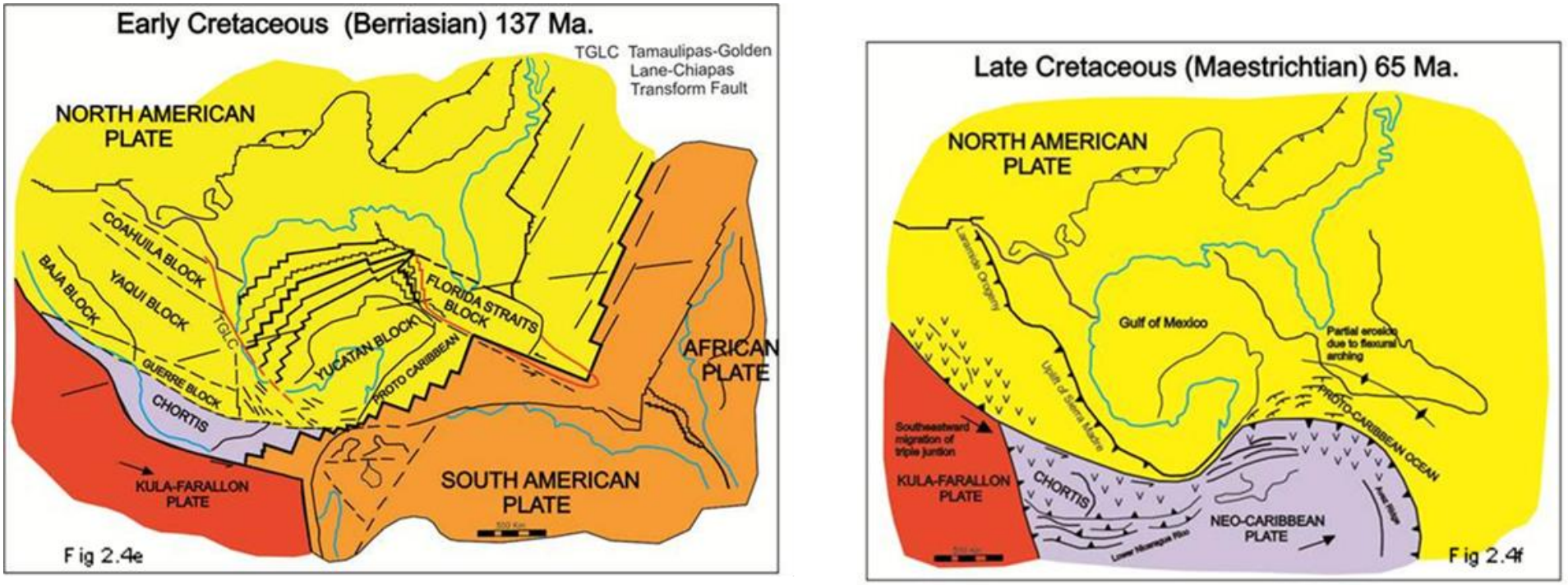

Fig 2.5 e-f. Plate tectonic reconstruction of Gulf of Mexico. Showing the end of drifting stage and the beginning of Pacific margin transformation since to Late Cretaceous time (after Pindell & Dewey, 1982; Pindell, 1985).

In their view, “Laramide” deformation in southern Mexico can be attributed to the migration of the Chortis Block during the Paleocene - Middle Eocene.

In the Maastrichtian, major collision took place between the western end of the Caribbean Plate and the southern Yucatan block. The collision was limited to the southern portion of the Yucatan block as northward movement of western Cuba was deflected north-eastward along a sinistral transform fault (the east Yucatan escarpment). The oblique passage of the trench east of Yucatan structured and destroyed the eastern pre-Maastrichtian passive margin succession there (Johnson, *et al*., 1999).

Outcrops and well information from the southern Gulf of Mexico provide evidence that the volcanic activity in western Mexico increased during Coniacian and Santonian times. The evidence of this volcanic activity is preserved in the Gulf of Mexico as the abundance of bentonite interbedded with limestone and shale (Padilla y Sanchez, 2007). During Campanian and Maastrichtian times there was an increase of the volcanoclastic deposits delivered from western Mexico to the sub-basins around the Gulf of Mexico. This event is represented by the Mendez Formation. This formation is made of a thick sequence of marls, shales and occasional of bentonite layers which are clear evidence of volcanic activity around the Gulf of Mexico at the end of Cretaceous.

2.3.5. Chicxulub Meteorite Impact (65 Ma)

The Chicxulub meteorite impact caused the formation and deposition of important breccias deposits in the surrounding basins. It is the end of Cretaceous and beginning of the Cenozoic (Grajales-Nishimura, *et. al*., 2000). However, Renne, *et al*., (2013) state a very precise age of 66.032 ± 0.058 Ma (Maastrichtian) based 40Ar/39Ar data that establish synchrony between the Cretaceous-Paleogene boundary and associated mass extinctions with the Chicxulub bolides impact.

The Yucatan peninsula in the south-eastern Mexico received the Chicxulub meteorite impact. The bolides has been calculated to be approximately 10 km wide producing a crater 180 km in diameter and 4 km deep (Hildebrand*, et al*., 1991). This catastrophic impact occurred in the northern tip of the Yucatán Peninsula, approximately 600 km away from the location of the main oil fields (Fig. 2.1). The impact caused a destabilisation of the carbonate platform edge as indicated by the more than 300 m thick succession of carbonates breccias of the Tamabra Formation, which were redeposited on the paleo-slopes and the paleo-basin floor around the southern Gulf of Mexico. Finally, an iridium rich ash fall-out was deposited on top of the breccias providing the top seal for the most important oil fields in the southern Gulf of Mexico (Hildebrand, *et al.,* 1991), such as Cantarell.

Grajales-Nishimura, *et. al.,* (2000) performed petrographic studies of the K-T breccias and stated that the oil-producing breccias and seals from the Campeche Shelf are of K-T boundary age and contain distinctive Chicxulub impact products such as shocked quartz and plagioclase. These characteristics are also similar to those observed in the outcrops of the K-T boundary in the Guayal (Tabasco State) and Bochil (Chiapas State) sections in southeastern Mexico. These impact deposits are chronologically correlative and are typically made up coarse-grained carbonate breccias covered with the K-T clay layer.

2.4. Cenozoic History

2.4.1. Oblique Orogenesis: Caribbean begins eastward motion (66-25.2 Ma)

During Late Paleocene - Middle Eocene times the old plate boundaries became inactive and new plate boundaries formed (Pindell & Dewey, 1982; Anderson & Schmidt, 1983; Pindell, 1985; Ross & Scotese, 1988; Pindell, *et a*l., 1988; Salvador, 1991; Pindell, 1994; Pindell, *et al*., 2000; Bird, *et al.*, 2005). During this stage, the suture created by the oblique collision between the Yucatan block and the Neo Caribbean Plate evolved into a sinistral transform boundary. In this way Chortis block was incorporated into the Caribbean plate. This major fault zone (the ancestral Motagua-Polochic) represents a new plate boundary between the Chortis block and the North American plate or Yucatan block (Fig. 2.4g) (Pindell & Dewey, 1982; Anderson & Schmidt, 1983; Pindell, 1985; Ross & Scotese, 1988; Pindell, *et al.,* 1988; Salvador, 1991; Pindell, 1994; Pindell, *et al*., 2000; Bird, *et al*., 2005).

Due to continued convergence along the northern Caribbean plate boundary, a narrow Paleocene - Early Eocene oblique fold-thrust belt was developed near the present location of the Motagua-Polochic fault zone (MPF in Fig.2.5g). Contractional structures were oriented WSW-ENE (Quezada-Muñeton, 1987). Associated with the Paleogene fold-thrust belt a foredeep basin accumulated up to 2000 m of finegrained clastic of the proximal Nanchital Group. Deeper marine shales of the foreland basin graded to shallow marine, non-marine (El Bosque Formation) within the Chiapas trough into 300 to 600 m thick (Quezada-Muñeton, 1987).

Subsequently to the compressive event, the region experienced a short stage of crustal relaxation, allowing diachronous growth of a Middle Eocene carbonate platform. This carbonate system was surrounded by marine, outer shelf limestone and rimmed by a high relief shelf margin with seaward facing foreslope debris aprons (Quezada-Muñeton, 1987).

In the Early to Middle Eocene time the Caribbean plate began moving eastward with respect to North American plate. Some authors eventually have

estimated that the Caribbean plate travelled approximately 1100 km eastward relative to its Late Cretaceous position (Malfait & Dikelman, 1972, Pindell & Dewey, 1982; Anderson & Schmidt, 1983; Pindell, 1985; Ross & Scotese, 1988; Pindell, *et al*., 1988; Salvador, 1991; Pindell, 1994; Pindell, *et al.,* 2000; Bird, *et al.*, 2005). Furthermore, Schaaf, *et al*., (1995) and Ferrar,i *et al.* (2007) stated that the migration of the Chortis Block along the Pacific (Acapulco Trench) was accompanied by the migration of magmatism along a large segment of the western Pacific margin. This idea is supported by the dating of the magmatic rocks that indicate a progressive migration from Puerto Vallarta in the west with ages around 100 Ma to Huatulco in the east with ages of 27 Ma (Ferrari, *et al*., 2007; sea chapter 3).

The Motagua-Polochic strike-slip fault system developed into a transform fault, connecting spreading centres within the Cayman Trough with the Pacific subduction zone. This continent-scale transform zone was dominated by sinistral transpression, which started at the end of Eocene. This age was established on the basis on the 40 ma. age of mylonites and proto-mylonites (García-Palomares, 1980; Múgica, 1987).

The Eocene-Oligocene deformation in Chiapas region was dominated by E-W synthetic sinistral strike-slip faults, some of which seem to have reactivated older normal faults (Sánchez-Montes de Oca,1986; Quezada,1987; Johnson, *et al*.,1999). Some of these faults take the form of linear, east-west striking deformation zones (Ocosingo, Tenejapa, and San Cristobal faults). The complexity and intensity of this deformation increases to the south, close to the axis of the Motagua-Polochich fault zone (Fig 2.5 g).

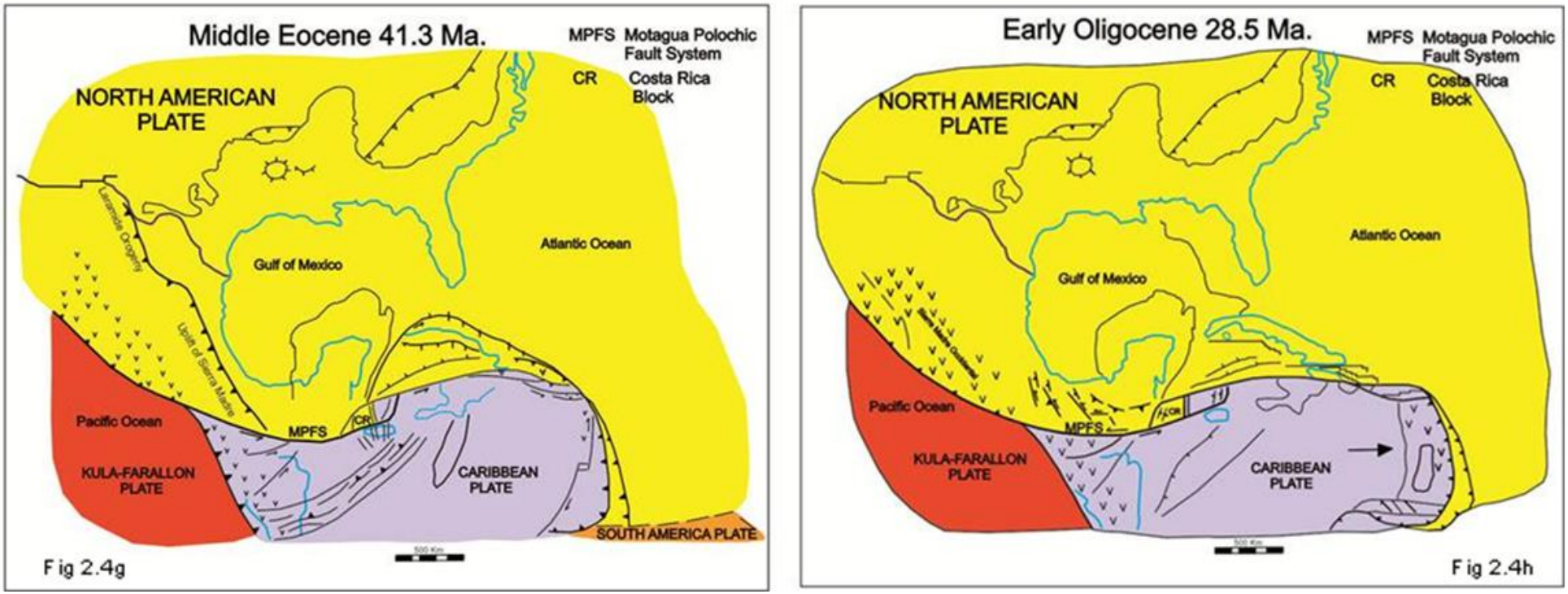

Fig 2.5 g-h. Plate tectonic reconstruction of Gulf of Mexico, showing the oblique deformation (after Pindell & Dewey, 1982; Pindell, 1985).

2.4.2. Orogenesis: Chortis block Migration (25.2 – Present Ma)

The Late Oligocene and Early Miocene represented the beginning of uplifting and deformation along the Chiapas Trough. It signalled the initial exposure of the Chiapas massif to the effects of the subduction zone along the south-western Pacific margin, and ended in a major orogenic event called the "Chiapaneca Orogeny", which developed gradually through Miocene time (Fig.2.5 h). Sánchez-Montes De Oca (1986) was the first author to propose this Middle Miocene tectonic event. He stated that this deformation implied left-lateral motion along the strike-slip faults which was resulting from the transmission of sinistral transpression from Motagua-Polochic fault system to the Sierra de Chiapas fold belt. The destabilization originated secondary faults with the same effect near the Sierra de Chiapas. Transpression combined with relative SSW movement of Yucatan block caused folding and faulting of the sedimentary sequence, resulting in SE-NW elongated anticlines, affected by reverse faults on its flanks.

The progressive eastward migration of the Chortis block controlled the northeastward motion of the Chiapas Massif. This eastward motion of the Chiapas massif and related Chiapas fold belt, driving salt mobilization and uplift, erosion and sediments transport to the north and east into the surrounding basins (Isthmus Saline, Comalcalco, Reforma and Macuspana).

This major orogenic phase continued during Middle to Late Miocene times, with compression and uplift in the Chiapas Massif. Deformation in front of Chiapas massif was facilitated by the detachment of the Mesozoic and Cenozoic sequences on the thick Callovian salt (Meneses-Rocha, 1987) Subsequently, the migration of Chortis block leave exposure the Pacific Coast to the subduction of Cocos Plate beneath North America Plate (Jonhson, *et. al*.,1999).

During Late Miocene times another north-eastward directed contractional event was triggered by the subduction of the Tehuantepec ridge, (a former oceanic transform fault composed of thickened oceanic crust) beneath south-western Mexico producing greater thrusting, uplift and erosion in south-eastern Mexico (Mandujano-Velazquez, & Keppie, 2009). This resulted in the supply of

clastic sediments to the south-eastern sub-basins of the Gulf of Mexico (Fig. 2.5 i) (Pindell & Dewey, 1982; Anderson & Schmidt, 1983; Pindell, 1985; Ross & Scotese, 1988; Pindell*, et al*., 1988; Salvador, 1991; Pindell, 1994; Johnson, *et al*., 1999; Pindell*, et al*., 2000; Bird*, et al*., 2005).

Despite the evidence of the strike-slip fault system mainly confined in the Sierra de Chiapas, some authors have questioned the kinematic evolution of the Chortis Block during the Cenozoic and consequently the formation of the Sierra de Chiapas is still not well understood. Basically, the arguments against the Chortis migration along the Pacific Margin are:

- 1.- Significant transpressive deformation must have occurred along the Pacific margin, which has not been proven (Keppie and Moran-Zenteno, 2005).
- 2.- The inconsistency between the Chortis Block displacement and the rotation of the Caribbean plate in the Eocene-Recent period.

As a result, Keppie and Morán-Zenteno, (2005) have proposed an alternative model for the Chortis Block migration. The model proposed the translation of the Caribbean plate based on a rotational pole and a change of the subduction zone since 45 Ma (Fig. 2.6)

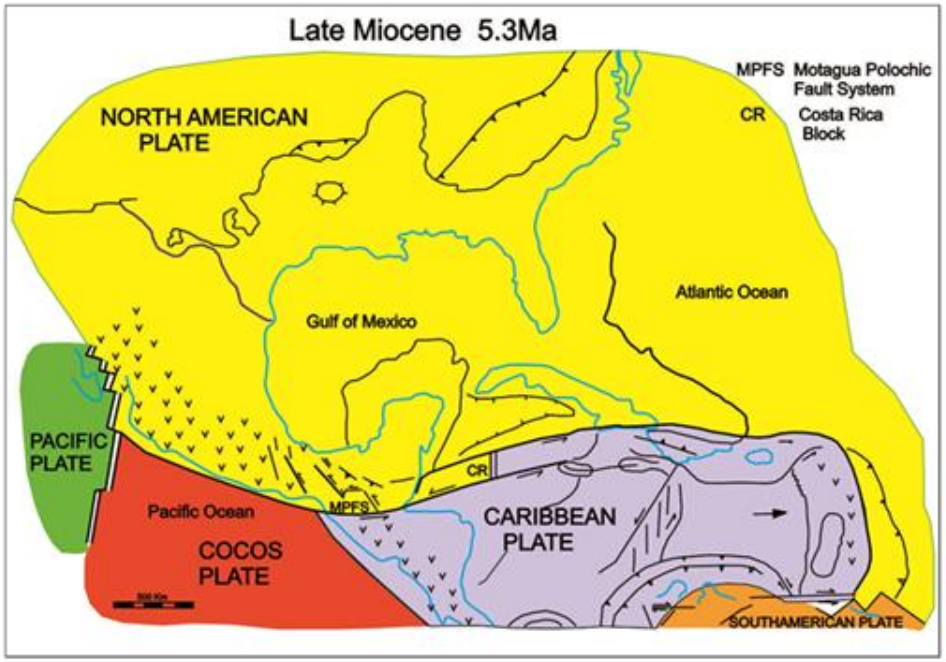

Fig 2.4i

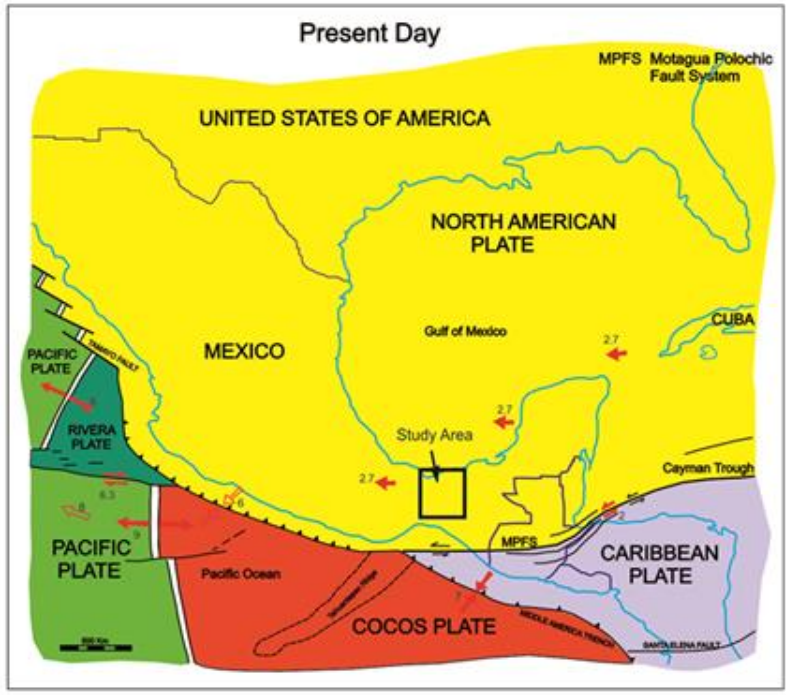

Fig 2.4j

Fig. 2.5 i-j Plate tectonic reconstruction of Gulf of Mexico showing the uplifting stage of Sierra de Chiapas and the fault thrusting caused by the movement of Chortis Block toward east. The figure 2.4j shows the present day position of Caribbean Plate (Chortis block). Red arrows represent present day motion vector of North American Plate, Cocos and Caribbean Plate (after Pindell & Dewey, 1982; Pindell, 1985).

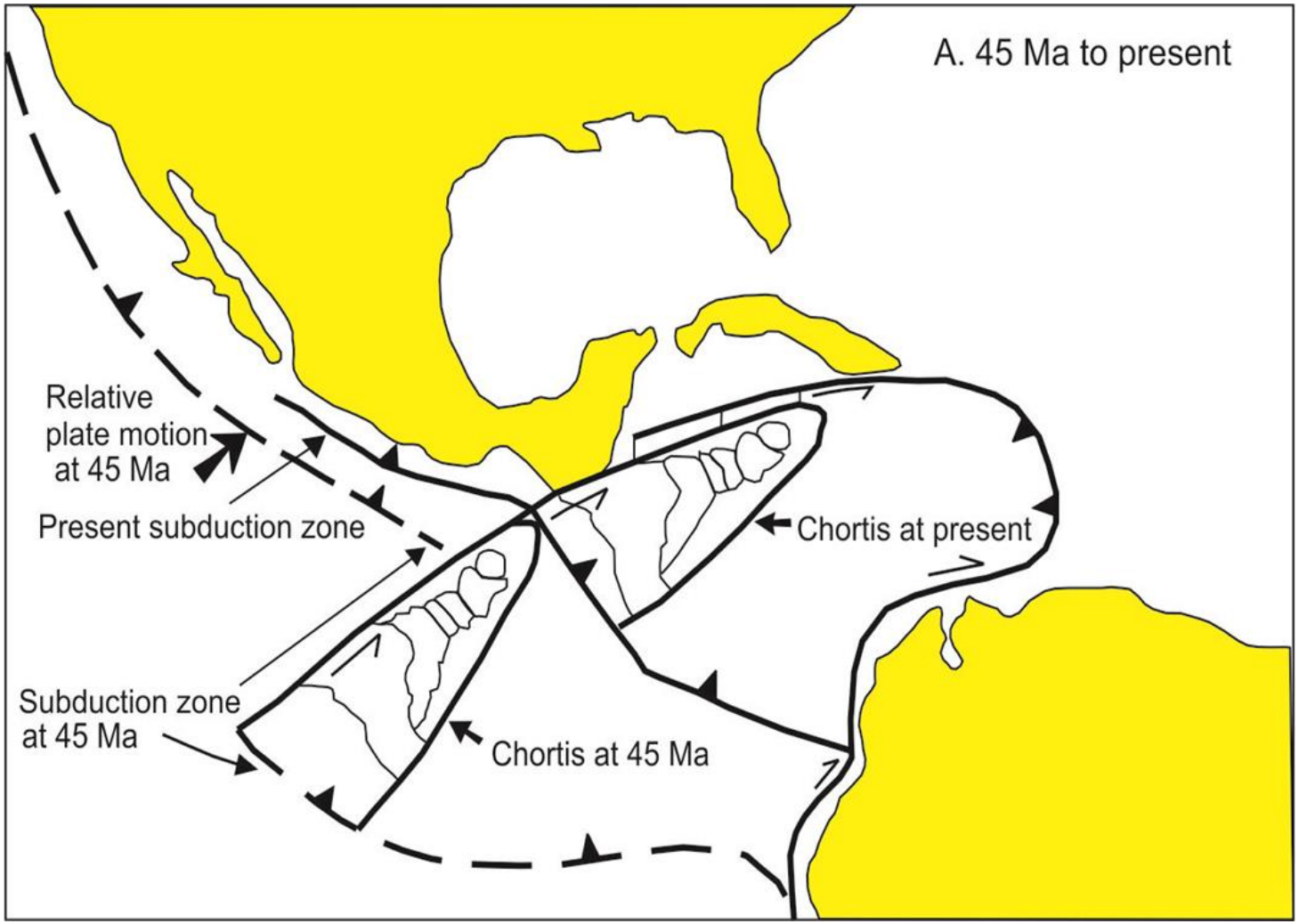

Figure 2.6- Model proposed of the trajectory of the Chortis Block since middle Eocene (modified from Keppie & Moran-Zenteno, 2005).

- There are two alternatives models for exhumation of Sierra de Chiapas. The first model emphasizes the importance of strike-slip tectonics (Guzmán-Speziale & Meneses-Rocha, 2000; Pindell & Kennan, 2001; Andreani, *et al*., 2008 a, b,) and suggests uplift of the Sierra de Chiapas may have resulted from transpressive deformation due to the change in trends of the major crustal faults that accommodate the relative motion between the North America and Caribbean plates (i.e., from the E-W directed Polochic-Motagua fault system to the NW-SE strike-slip fault system at the Sierra de Chiapas; Fig. 2.7). The second model (Mandujano-Velazquez & Keppie, 2009) suggests that the exhumation of the Sierra de Chiapas may be related to subduction of the Tehuantepec ridge system, resulting in a rapid mountain chain formation (i.e., 2-2.5 Ma), which was relatively unaffected by strike-slip deformation (Figure 2.8).

Thereafter, volcanic activity dominated Miocene-Pliocene times. Volcanic material erupted from the Tuxtla centre formed a barrier to sediments entering the Isthmus Saline basin from the west. The volcanic became the primary provenance for Pliocene sandy turbidites offshore (Robles-Nolasco, *et al*.,1998). The most recent arc volcanism in southeastern Mexico is represented by the Chiapanecan Volcanic Arc. This volcanic province is located in the central area of Chiapas State and is 150 km long NW-SE trending (Fig.2.7). It is located in the strike-slip province marked by the interaction of a triple junction trench-transform-trench of three great plates North American, Caribbean and Cocos plates, and near to the Polochic-Motagua fault system. The volcanic arc is active since the Pliocene. The youngest volcano of this magmatic arc is the Chichonal, which erupted in 1982 with an explosive Plinian-type eruption (De la Cruz-Reyna and Martin Del Pozo, 2009).

At the Present day, the North America plate continues to move west-northwestwards at rate of ~ 2.7 cm/yr (Fig.2.5j). The Caribbean plate is moving at 2.45 cm /yr to the east-southeast. (Pindell & Dewey, 1982; Anderson & Schmidt, 1983; Pindell, 1985; Zoback et al., 1986; Ross & Scotese, 1988; Pindell, *et al.,* 1988; Salvador, 1991; Pindell, 1994; Pindell, *et al.,* 2000;

DeMeets, *et al*., 1990; DeMeets, *et al* 1994; DeMeets & Dixon, 1999, DeMeets, *et al*.,2000.

.

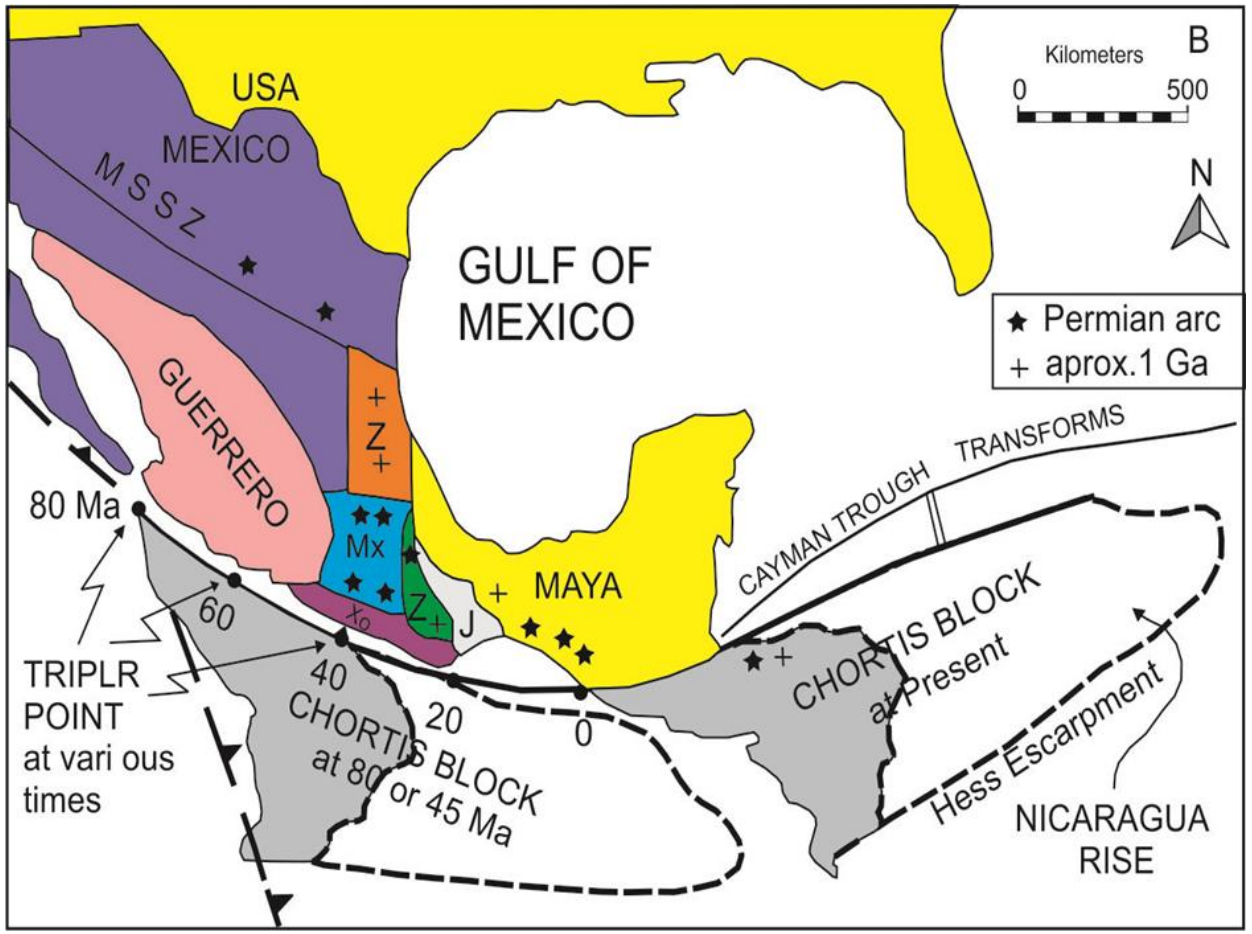

Figure 2.7- Model originally proposed by Ross and Scotese (1988) and later modified by Shaaf, et al., 1995). This model support the idea of Chortis Block migrated from west to east, reaching current position. Migration period was 80 My. Additionally, this model is supported by Guzmán-Speziale & Meneses-Rocha, 2000; Pindell & Kennan, 2001; Andreani, *et al.*, 2008 a,b. During it's migration it caused exhumation of the Sierra de Chiapas fold belt and also would produce the Chiapas compression (DeMeets, *et a*l, 1994; DeMeets & Dixon, 1999; DeMeets, *et a*l., 2000; Bird, *et al*. 2005).

Summary

1. - The opening of the Gulf Mexico comprises mainly three stages: rift (230-160 Ma), drifting (160-140 Ma) and a thermal subsidence (after 140 Ma).

2. - The post-drift stage of the Gulf of Mexico was distinguished by the development carbonate platforms around the margins of Gulf of Mexico.

3. - During the Middle-Late Cretaceous the Pacific margin started a process of destruction caused by northwards emplacement of the Caribbean Plate and a marked change in sedimentation.

4. - The end of the Mesozoic was interrupted by the Chicxulub meteorite impact. The impact caused a destabilization of the platform margins and created sediment flows, which form a significant hydrocarbon reservoir.

5. - The Cenozoic history of the southern and south-eastern Mexico is strongly influenced by the migration of the Chortis Block along the Pacific Margin of Mexico. This migration was accompanied by transpression from Early Eocene – Middle Eocene. This major orogenic phase continued during Middle to Late Miocene times, with compression and uplift in the Chiapas Massif. Subsequently, during Late Miocene the migration of Chortis block leave exposure the Pacific Coast to the subduction of Cocos Plate beneath North America Plate and caused a north-eastward directed contractional event triggered by the subduction of the Tehuantepec ridge, beneath south-western Mexico producing greater thrusting, uplift and erosion in south-eastern Mexico. Finally, at the end of Late Miocene and beginning of Pliocene intense volcanic activity dominated the supply of sediments to ISB.

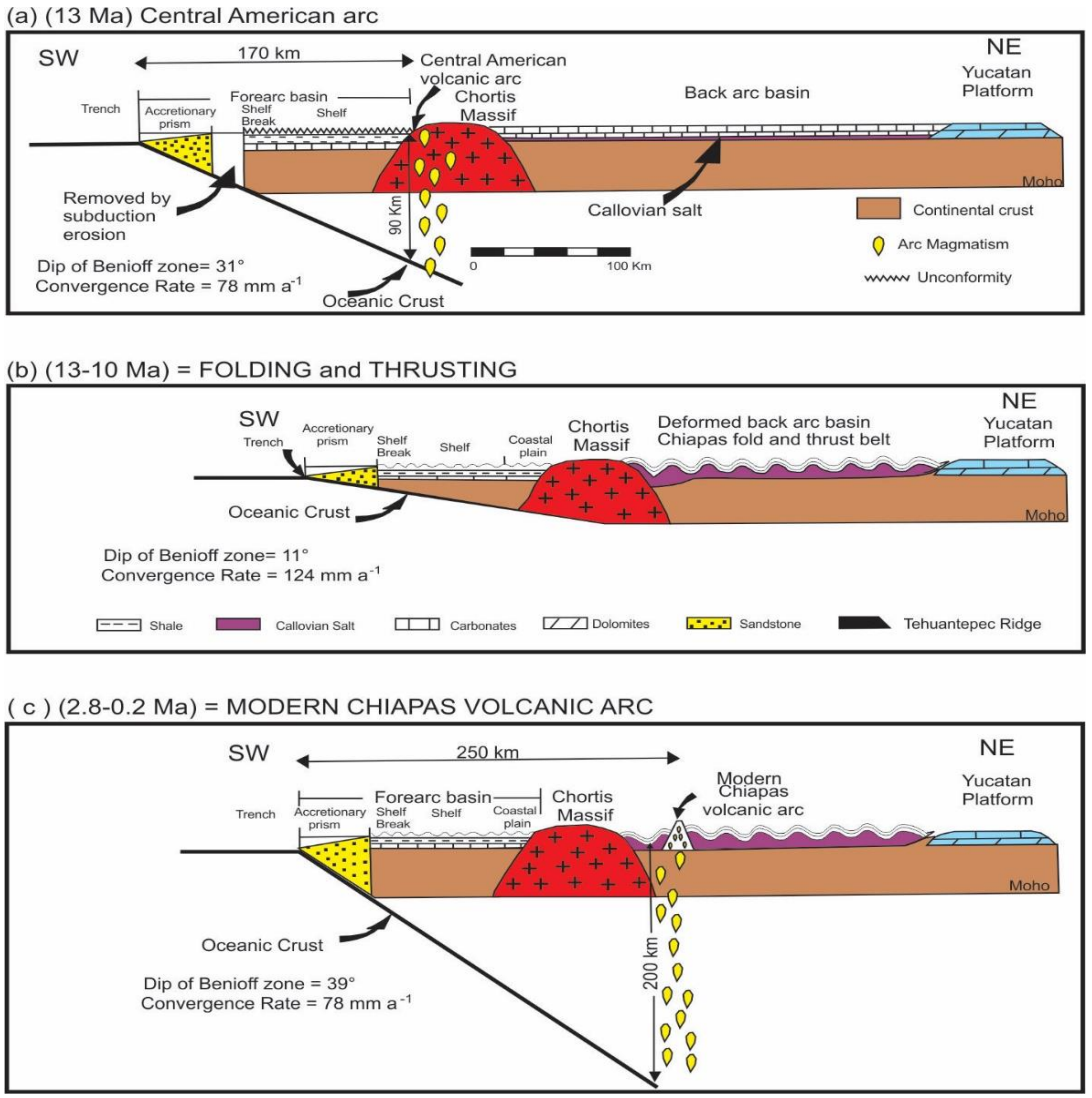

Figure 2.8- Model proposed by Mandujano-Velázquez & Keppie, 2009). The model shows three tectonic stages of evolution of Pacific Margin. This model suggests that changes in subduction angle drove the exhumation of Sierra de Chiapas Fold belt.

Chapter 3 Analysis of Regional Stratigraphy Overview: Bibliography Review

3.1 Introduction

The south-eastern margin of the Gulf of Mexico basin is characterized by a complex tectono-stratigraphic evolution. The study area is located in the transition between the passive margin of the Gulf of Mexico and the active margin on the Pacific coast. The basin evolution and its depositional environments were influenced by both plate margins. From the Triassic until early Cretaceous time the tectonic and stratigraphic evolution of the study area was dominated by events and eustasy related to the Gulf of Mexico evolution. In contrast, from the Late Cretaceous through Cenozoic the tectonic-stratigraphic evolution was dominated by convergence along the Pacific margin linked to Caribbean Plate tectonic deformation.

The depositional environment of early Mesozoic strata can be related to the regional rifting and subsequent opening of the Gulf of Mexico. Eustatically-driven, middle Jurassic to middle Cretaceous marine carbonates sequences are well developed. These sequences correlate with outcrops of the circum-Gulf margins (Goldhammer, *et al*., 1991). In Late Cretaceous time this condition ended abruptly with the onset of tectonism along the convergent Pacific margin. Thus, the later Mesozoic and Cenozoic stratigraphic development of the southern Gulf of Mexico is completely different from the evolution of the northern Gulf of Mexico margin. This chapter presents a thorough bibliographical overview of the stratigraphy of the south-eastern margin of the Gulf of Mexico (Fig.3.1).

Traditionally, the exploration targets in the Isthmus Saline Basin have been mainly turbidites and deltaic to fluvio-deltaic sediments of Neogene, and consequently, wells rarely penetrated the Paleogene succession. Thus, to establish a regional stratigraphic framework of the Cenozoic and Mesozoic basin fill it was necessary to incorporate subsurface stratigraphic data and outcrop data of the neighboring sedimentary basins to fill in stratigraphic gaps of those undrilled stratigraphic levels in the study area.

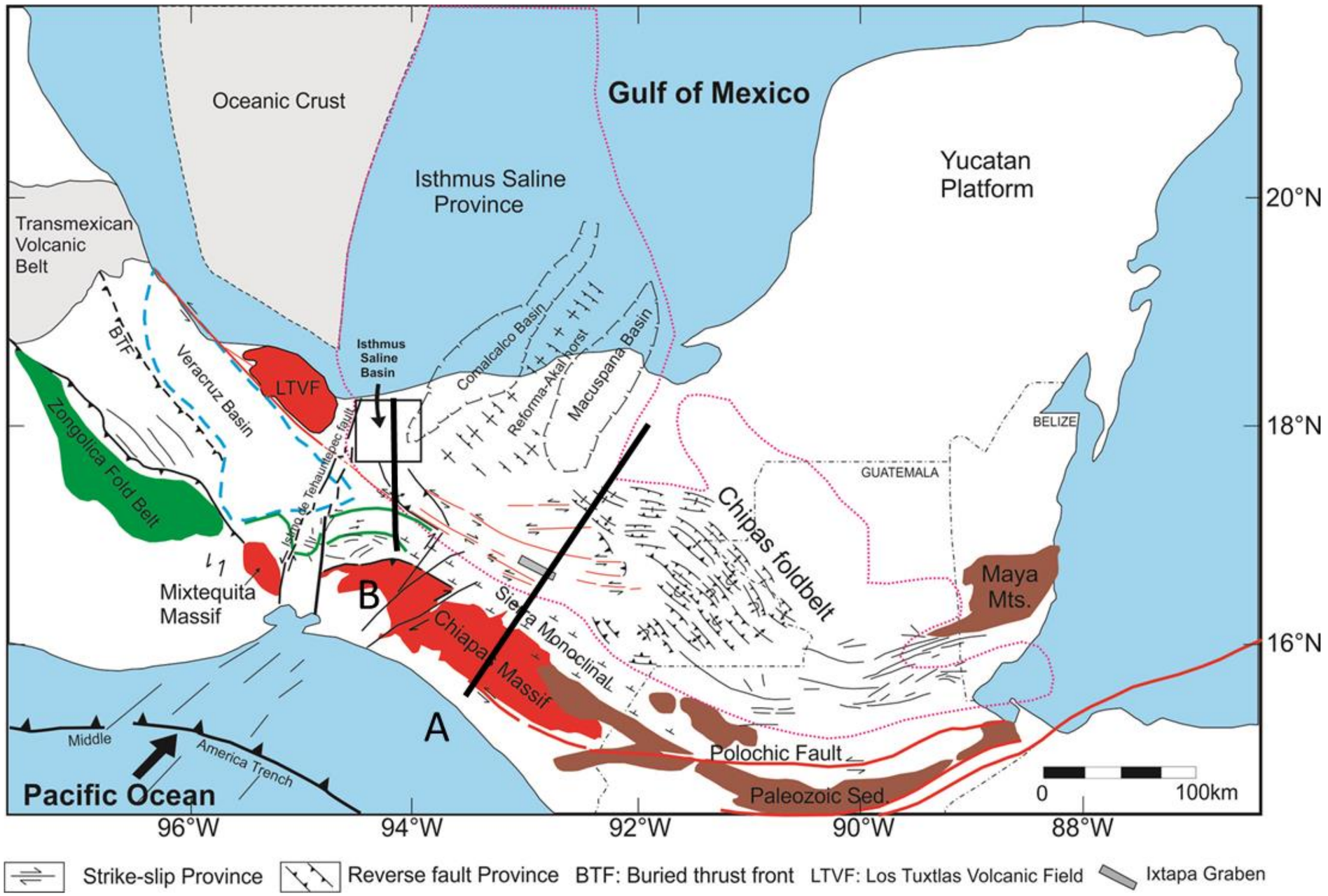

Figure 3.1 structural map of southeastern of Gulf of Mexico showing main Structural elements surrounding the study area represented by Black Square. Additionally, Istmo de Tehuantepec fault represents the western boundary of the Yucatan block. The black lines represent regional sections that show regional structural characteristics of Sierra de Chiapas and ISB (modified from Meneses-Rocha, 1987),

A

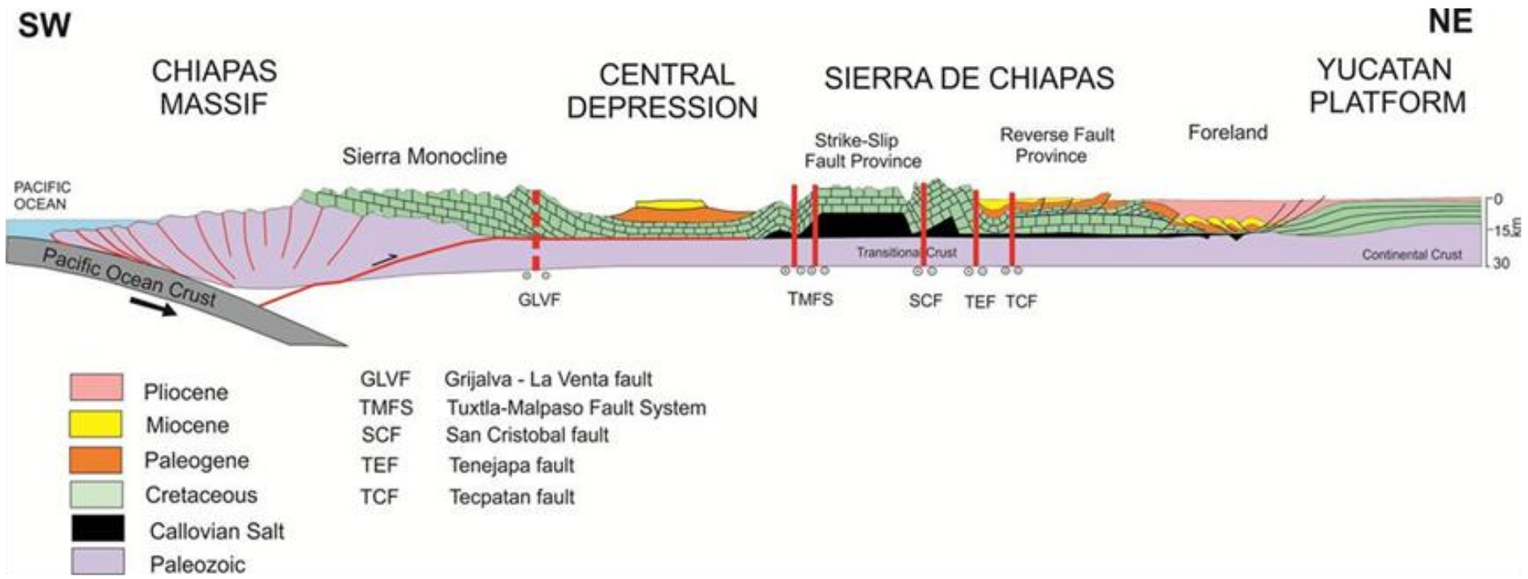

B

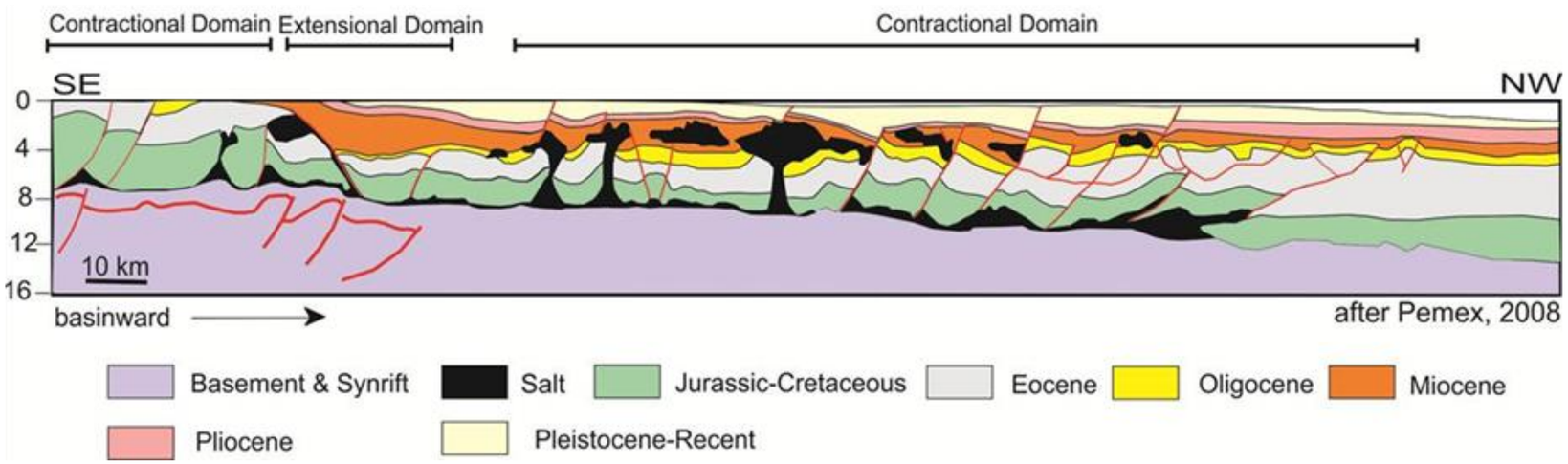

Figure 3.2 shows the structural complexity of south-eastern of Mexico. The first SW-NE schematic section, from the Pacific coast to Yucatan Platform, shows the main structural provinces of the Sierra de Chiapas (modified from Witt, et al., 2012). The second NW-SE is real depth section, shows the contractional salt structural style of NW sector of Sierra de Chiapas and the onshore and offshore salt structures of Isthmus Saline Basin (modified from PEMEX, 2009).

. Figure (3.2) is represented by two regional geological sections that show the Stratigraphy and structural style through the different structural provinces of the Sierra de Chiapas and the coastal plain where the study area is located.

The tectono-stratigraphy analysis involves six mega-sequences, which were already introduced in the chapter 2 and are represented in the Figure 3.3.

The six mega-sequences are:

(1) Syn-rift succession (middle Triassic-Kimmeridgan 230-152 Ma)
(2) Drift-related deposition (Tithonian-Berriasian 152-140 Ma)
(3) Post-drift Transgressive Succession related to Thermal Subsidence (Berriasian-Albian 140-100 Ma).
(4) Arc collision synkinematic succession (Albian-Maastrichtian 100-66Ma)
(5) Oblique collision Deposits synkinematic succession (66-25.2 Ma)
(6) Chortis block migration synkinematic succession (25.2 Ma to recent)

The first three mega-sequences record rifting, breakup and thermal subsidence of the southern Gulf of Mexico basin. All the sub-basins around the south-eastern of Gulf of Mexico margin have experienced these events to some degree. The younger mega-sequences show the transpressional events of the Chortis block emplacement along the Pacific margin during Paleogene and late Miocene as well as the subduction of Cocos plate during the last stage of Miocene and Pliocene.

The tectonic effects of these later events in the individual basin varied gradually according to their location, orientation, and geometry. Each mega-sequence will be discussed briefly in this chapter

In order, to define the geological framework in which is the study area located, it is necessary to describe the nature of the basement in southern Gulf of Mexico.

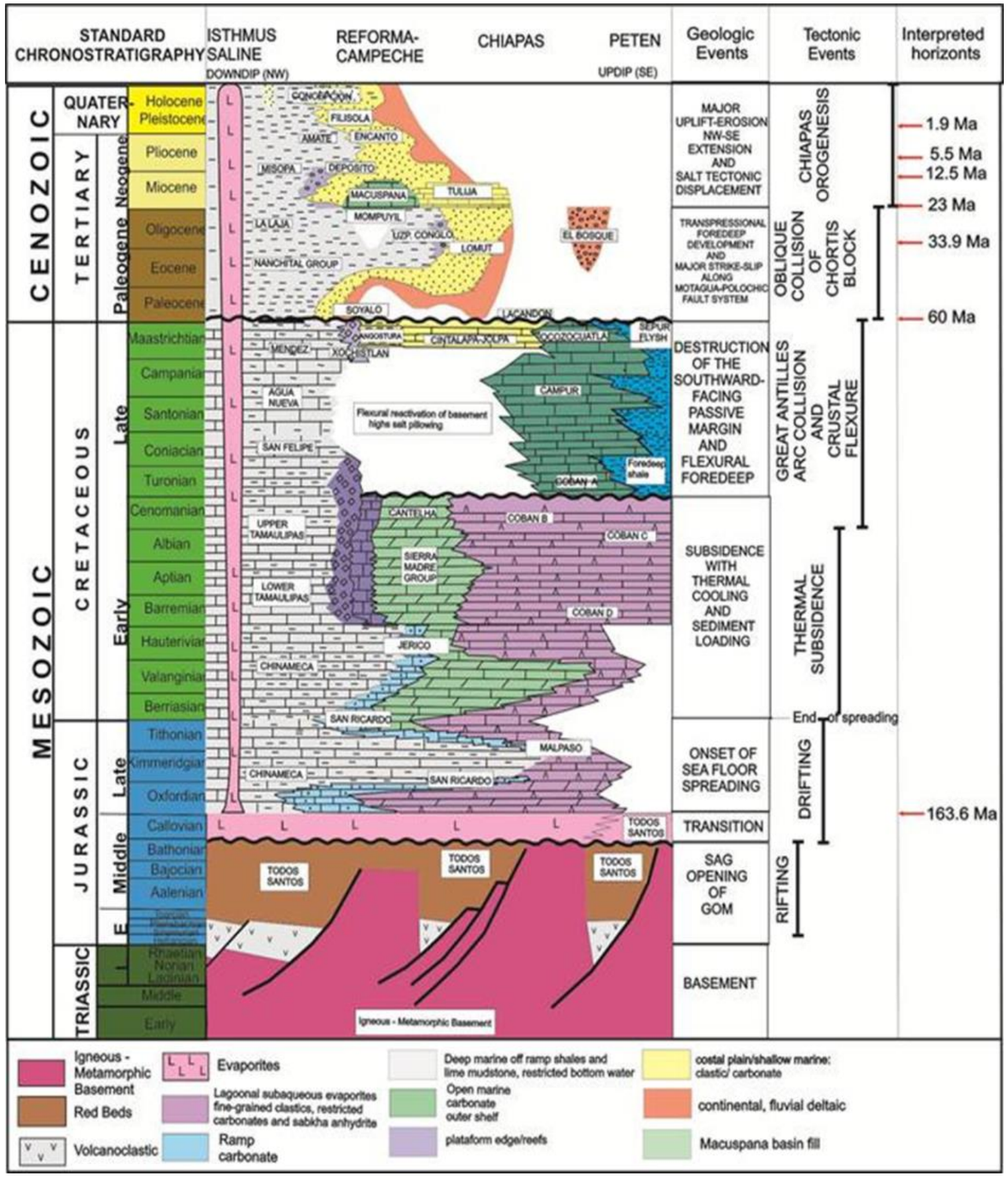

Figure 3.3 Stratigraphy of the south-eastern margin of the Gulf of Mexico (modified from Johnson, et al.,1999).

3.2 Pre- Mesozoic Basement of the Yucatan Block

The Yucatan block is considered as the remnant of a large fragment of continental crust that kept relatively intact after Mesozoic continental break up (Gose, *et al*.,1980; Buffler, *et al*.,1981; Pindell & Dewey,1982) (Figure 3.4). In the south-eastern Gulf of Mexico all the sub-basins were developed into the Yucatan block. The south limit of the Yucatan block is the Motagua-Polochic fault system, which forms the western termination of the sinistral Caribbean-North American plate boundary. The western boundary coincides with a diffuse deformation zone that divide the Tehuantepec Isthmus (Meneses-Rocha, 1987). In the southern Gulf of Mexico, the basement outcrops are characterized by at least six different tectono-stratigraphic terranes with ages ranging from Precambrian to Cretaceous (Coney, *et al*., 1980). However, the Yucatan block is constituted by two main types of basement: 1) Igneous-metamorphic basement and 2) Paleozoic sedimentary basement, which have been penetrated by wells and recognized at outcrops around the study area. The nearest basement outcrops to the Isthmus Saline Basin are represented by La Mixtequita Massif and the Chiapas Massif (Fig.3.4).

The Mixtequita Massif is composed by two different crystalline units: the Mixtequita batholiths intrusive rocks of Permian-Triassic and Jurassic age and the metamorphic Guichicovi complex of Proterozoic age (Weber, 1998).

The Chiapas Massif is a NW-SE trending crystalline basement complex, which is mainly composed of granitic and granodiorites rocks of Precambrian and Paleozoic age. Age constraints are given by pegmatite emplacement ages 866 ± 29 Ma. (Schlaepher, 1972; Sedlock, et al., 1993), and gneiss and monzonites 780± 80 and 702± 70 Ma. respectively. The Chiapas massif is locally affected by low to medium grade of metamorphism in combination with granitic intrusions of middle Paleozoic age 430± 45 Ma. (Pantoja, *et al*., 1974; López-Infanzón,1986).

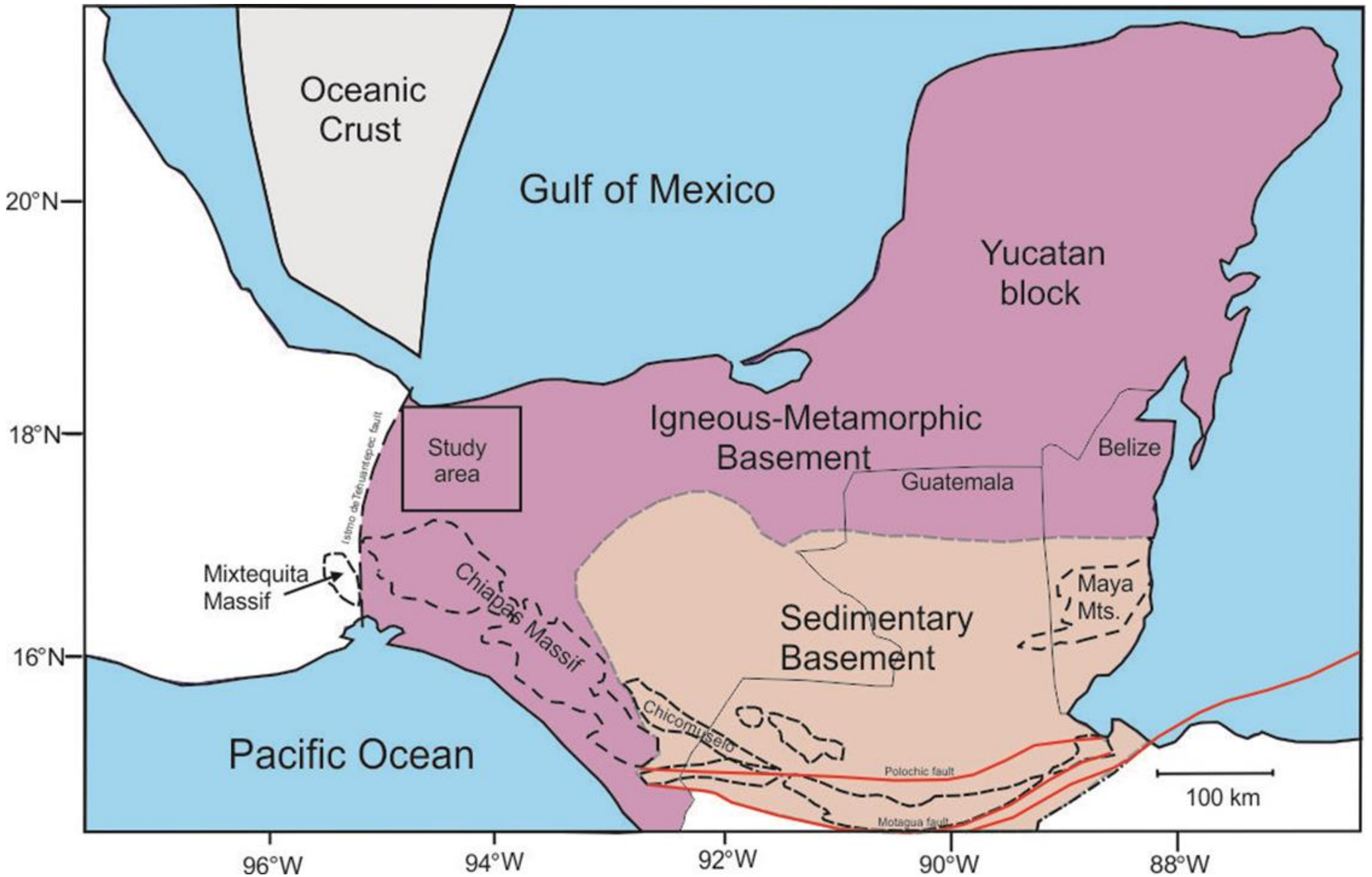

Figure. 3. 4. - Shows Yucatan block boundaries. Two types of basement have been registered by wells in south-ester of México. Dotted lines indicated basement outcrops (After Ruiz-Osorio, 2008)

Not all the intrusive rocks in the Chiapas Massif document similar ages. Burkart, et al., (1987) dated some samples as Late Cretaceous. In outcrops in the south-eastern Chicomuselo, Chiapas, northern Guatemala and west Belize, Paleozoic sedimentary rocks outcrops rest unconformable on metasedimentary rocks. The lower part of Paleozoic sedimentary succession consists of coarse sandstones and siltstones with occasional horizons of conglomerates and some locally metamorphosed shales. Hiller, *et al*., (2004) determined in the west of Villaflores, Chiapas, ages of 252 - 254 Ma, with zircon by the U-Pb method, and an age of about 243 Ma by 40 Ar /39 Ar in hornblende method for uplift and cooling of the Chiapas Massif. Hence, all this diversity of accretionary complex blocks and intrusive rocks reflect an active subduction zone beneath Yucatan block prior the late Paleozoic continental collision (Handschy, *et al*., 1987).

3.3 Mega-sequence I: Syn-rift succession (middle Triassic –Callovian 230-152 Ma)

The initial stage of crustal stretching was the result of the Gondwana plate (specifically South America and Africa) pulling away from North America in a relative northwest-southeast extension (Pindell, *et al*., 2014). The rifting stage is characterized by intense igneous activity represented by the Late Triassic Pueblo Nuevo andesitic as well extensive red beds consisting of erosional material derived from the rifted basement highs (Godinez, et al., 2009). The red beds clastic sediments filled deep rift grabens (Todos Santos Fm.). With marine ingressions during the late syn-rift stage, large volumes of evaporites formed in the basin centres simultaneously with red beds accumulating along the basin margins (Meneses-Rocha, 1987; Fig. 3.3).

3.3.1 Middle Triassic-Middle Jurassic

At the southern margin of the Gulf of Mexico the continental syn-rift deposits are represented by the Todos Santos Formation. Generally, this sedimentary sequence is characterised by diachronous ages and large thickness variations due to local supply sources and variable rift basin topography. This formation is characterized by non-marine clastic deposits represented by alluvial fans, fluvial, and lacustrine sediments (Godinez-Urban, 2009). These outcrop are extensively distributed on the western flank of the Chiapas Massif, forming up to

several hundred meter in thickness (Fig. 3.5). Red beds with 800 m thickness have been reported by Benavides (1950) at the Cerro Pelón Anticline, NW of Sierra de Chiapas. Blair (1987) reported thickness variations ranging from 250 to 1350 m in different localities in the southern Mexico. Dating red bed sequences is notoriously difficult. There is considerable uncertainty in the age assignment of the Todos Santo; the consensus in public literature is that the Todos Santos is probably of Late Triassic to Mid Jurassic age. However, Clemons (1972) argues for a much younger age (Late Jurassic to Early Cretaceous). Confusion also arises because Sinemurian to Tithonian volcanic rocks (196 ± 3 to 148 ± 6 Ma) that have been radiometrically dated have been assigned to the Todos Santos (Herrera-Soto & Estavillo-González, 1991), but this correlation appears unlikely. On the other hand, Godinez-Urban (2009) reported a red beds succession that resulted into deposition of widespread Lower Jurassic strata related to post-rift thermal subsidence in Chiapas, coeval with opening of Gulf of Mexico. The author has stated that Todos Santos Formation is composed of four lithological facies. The basal lithofacies, is called “El Diamante” and is composed of dacites of Pliensbachian-Toarcian age of (188.8 Ma.) obtained by U-Pb dating. The overlying lithofacies is called “Todos Santos” which is composed of volcanoclastic sediments deposited in lacustrine, fluvial and alluvial environments. The third sequence is composed by basaltic rocks intercalated with sediments of the Todos Santos lithofacies. The top lithological facies is made up by sandstone which contain granitic lithoclast.

In the study area, the red bed sequence is provisionally interpreted on seismic data, but its presence has not been confirmed by drilling. Based on seismic interpretation this stratigraphic level of the basin fill can be located up to depths greater than 12,000 m. In contrast, the same stratigraphic unit is outcropping at Cerro Pelón Anticline, a dome structure situated 90 km south-east of Isthmian Saline basin.

The late syn-rift stage is characterised by a thick sequence of evaporites. Non-marine clastic sediments on the basin margin gradually transition into marginal sediments and anhydrites and massive halites in the basin centre. The deposition of these marginal marine deposits represents intermittent incursions of sea water, flooding the rift grabens. These evaporites are coeval in age with

the Louann Salt Province, Minas Viejas and Isthmus Salt Province in the Gulf Mexico (Salvador, 1987) which were separated by translation of Yucatan block during the sea floor spreading.

In south-eastern Gulf of Mexico the Callovian salt is present in all sub-basins of Isthmus Saline Province (Viniegra-Osorio, 1971) (Fig 3.5). In this province, the original depositional thickness of the Callovian salt ranges from 160 to 3000 m (Angeles-Aquino, *et al*., 1996). Based on structural restoration of the northern Gulf of Mexico (Pindell, *et al*., 2014), estimated maximum thickness of 5 km of Callovian salt was deposited, on the southern margin of the USA salt basin. In the study area, allochthonous Callovian salt has been penetrated by several wells and has served as the primary detachment during deformation of the Sierra de Chiapas fold belt. It is widely distributed beneath the Sierra de Chiapas and has been drilled as far south as the Ixtapa Pull-apart Basin (Meneses-Rocha, 2001) (Fig 3.1).

3.4 Mega-sequence II: Drift Related Deposits (Tithonian-Berriasian 152-140 Ma)

This mega-sequence is characterized by a marine transgressive sedimentary record ranging from shallow marine to deep marine environments (Fig.3.6). The Oxfordian and Kimmeridgian are clastic deposit of coast zone (Zacatera Group and San Ricardo Formation), carbonates on the platforms edge (Malpaso Formation) and open marine shales and carbonate (Chinameca Formation) (Fig.3.3).

Tithonian deposits formed mostly in open marine (Sánchez-Montes de Oca, 1980). However, in some basin areas the presence of quartz-rich clastic and disseminated pyrite crystals has been interpreted as semi-restricted platform depressions under reducing conditions. It is the main source rock of the Mexican basins was deposited during this time (González-García & Holguín-Quiñones, 1992) (Fig.3.7).

The Upper Jurassic-Early Cretaceous succession of Sierra de Chiapas consist of the San Ricardo Formation, which was deposited under shallow marine conditions approximately 155 m thick. Quezada-Muñeton (1987) divided

this formation in three members: the base is represented by a calcareous member, the intermediate, is described as a marly member and the top is represented by a sandy member. The first two members were deposited during the late Jurassic and the sandy member was deposited during early Cretaceous. The calcareous member is represented by calcareous sandstones and siltstones with intercalations of oolithes, peletoidal and bioclastic packstone and grainstones the marly member is represented by siltstones, shales and marls. During late Jurassic times, the Malpaso and Chinameca formations were deposited simultaneously in the central and north sector of the Sierra de Chiapas respectively. The Malpaso Formation is represented by anhydrites and oolitic limestones grading upward into shelfal and open marine facies (Fig.3.3).

The Lower Cretaceous is represented by the sandy unit of the San Ricardo Formation. The sequence is characterized by a transgressive sequence defined by fine-sandstone with intercalation of shale and silt. The bed thickness of the sand layers ranges varies between 60 to 80 cm. The total thickness has been measured as 1300 m (Quezada-Muñeton, 1987). Only the basal succession of the formation could be dated as Berriasian, whereas in the upper sandy sequences micropaleontological material was not preserve. Further, basinward in the Isthmian Saline basin, the Kimmeridgian, Tithonian and early Cretaceous sequences are represented by Chinameca Formation that consists of basin carbonate shale deposits. This sedimentary sequence has not been drilled yet, and is very difficult to identify in seismic due to the structural complexity and limited imaging of the deep basin succession. However, the geochemical signature of the hydrocarbons exploited in the Isthmus Saline basin is the best evidence of the existence of the Upper Jurassic (Tithonian) carbonate shale.

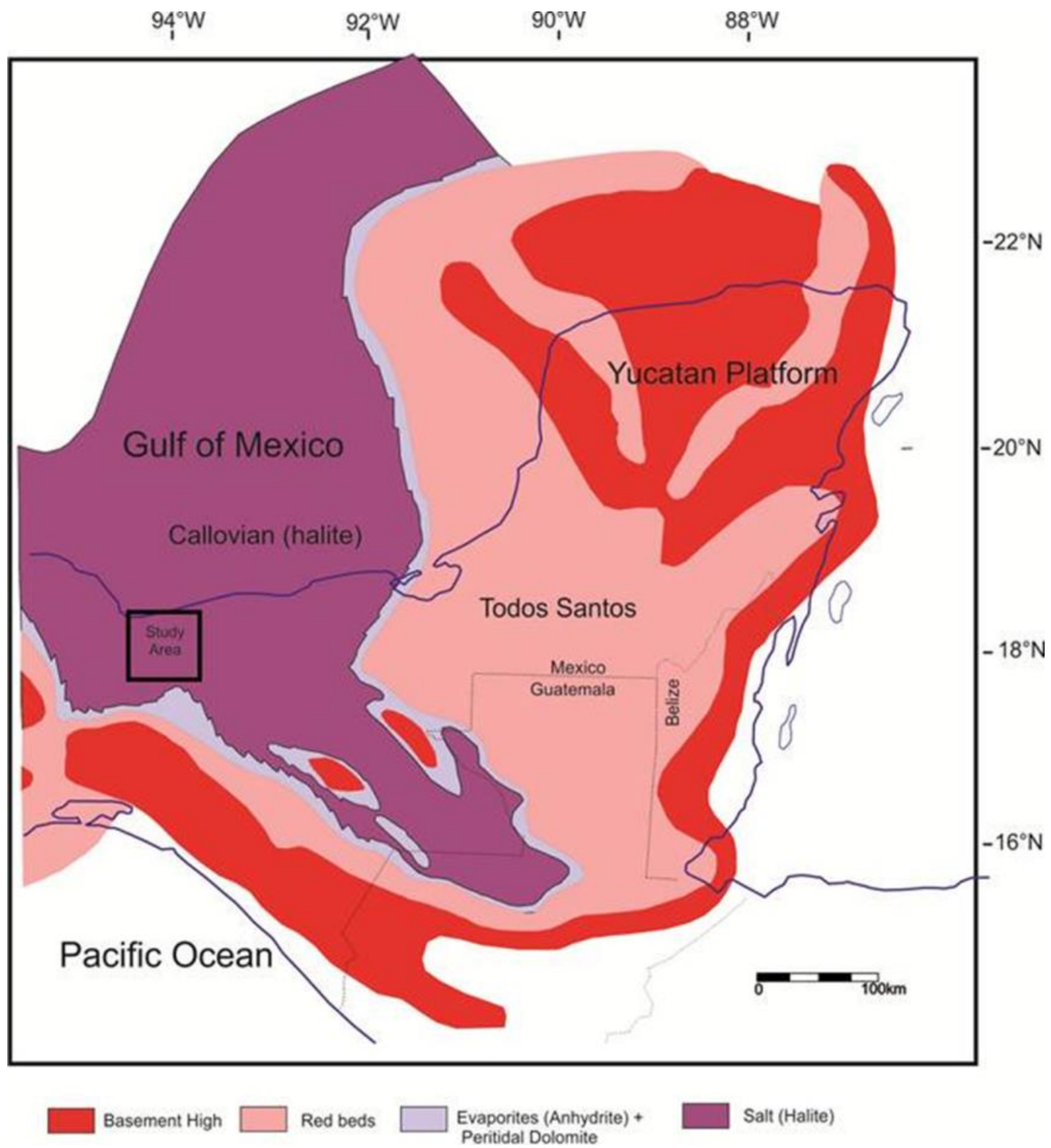

Figure 3.5 Paleogeographic distributions of salt and pre-salt sediments during of Callovian-Early Oxfordian time. (Modified from Johnson, *et al*., 1999).

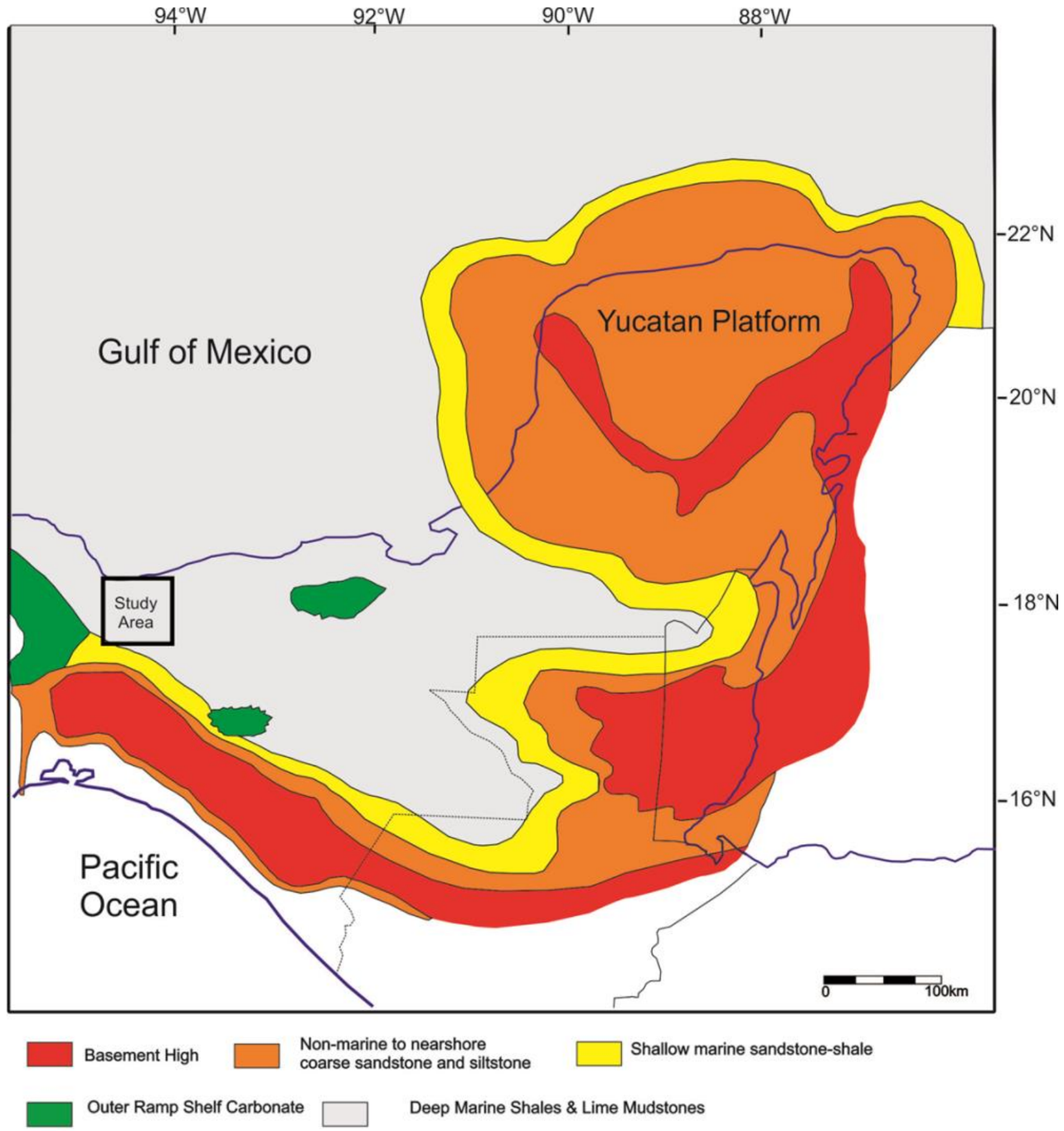

Figure 3.6 The transgressive stage of the south-eastern Gulf of Mexico (Thithonian-Portlandian age) (Modified from Johnson, *et al*., 1999).

Figure 3.7.- The Chinameca Formation consists of limestone and chert in its type locality in southern Mexico. The Chinameca Formation represents the main source rock in the region represented by breccia with abundant organic matter and ammonites. The Chinameca Formation is located at Chinameca, southern Veracruz-eastern Mexico.

3.5 Mega-sequence III: Early Post-Drift Transgressive Succession related to Cretaceous Thermal Subsidence (Berriasian- Albian 140-100 Ma)

Once the Yucatan block reached its current position with respect to North America (Angeles Aquino, et al., 1987; Sawyer, et al., 1991), basin subsidence was controlled by thermal cooling of the oceanic crust and sediment loading (Goldhammer and Johnson, 2001). In this stage, the development of extensive reefs and evaporitic platforms around the Mexican Gulf coast margins were established (Padilla y Sanchez, 2007). Contemporaneous to the build up of the carbonate platforms in the shelf areas, basinal carbonates breccias and carbonate turbidites were deposited beyond the shelf break on the platform slope and basin floor. Today, these carbonates reefs and carbonates gravity flows represent the most important reservoir in the Gulf of Mexico basin.

The Lower Cretaceous depositional environment of the Sierra de Chiapas is characterised by lateral sedimentary facies variation in the Sierra de Chiapas. The sandy facies were dominantly (San Ricardo Formation). Shallow marine conditions developed as consequence of clastic progradation from margins to the deep basin (Quezada-Muñeton, 1987). In contrast, the centre and east sector of the Sierra de Chiapas was dominated by anhydrites and dolomites of the Cobán Formation (Fig.3.8). This evaporate sequence was deposited in a restricted coastal plain environment and was laterally extensive. The evaporitic sequence reached up to 2000 m thickness due to ongoing thermal subsidence of crustal blocks and arid conditions restricted water flow favouring evaporation. The Jericó Formation represents an updip lateral facies change of the San Ricardo Formation and is characterized by quartz sandstones with red alterations typical of continental deposits (Quezada-Muñeton, 1987).

The Middle Cretaceous succession of the Sierra de Chiapas is represented by Cantelhá and Cobán formations. According to González-Alvarado (1963) the Cantelhá Formation is Albian-Cenomanian age but Rosales-Dominguez, *et al*., (1991) re-assigned an age of Cenomanian-Turonian. The Cantelhá Formation consists of dolomitized limestones, mudstones, wackstones, packstones and

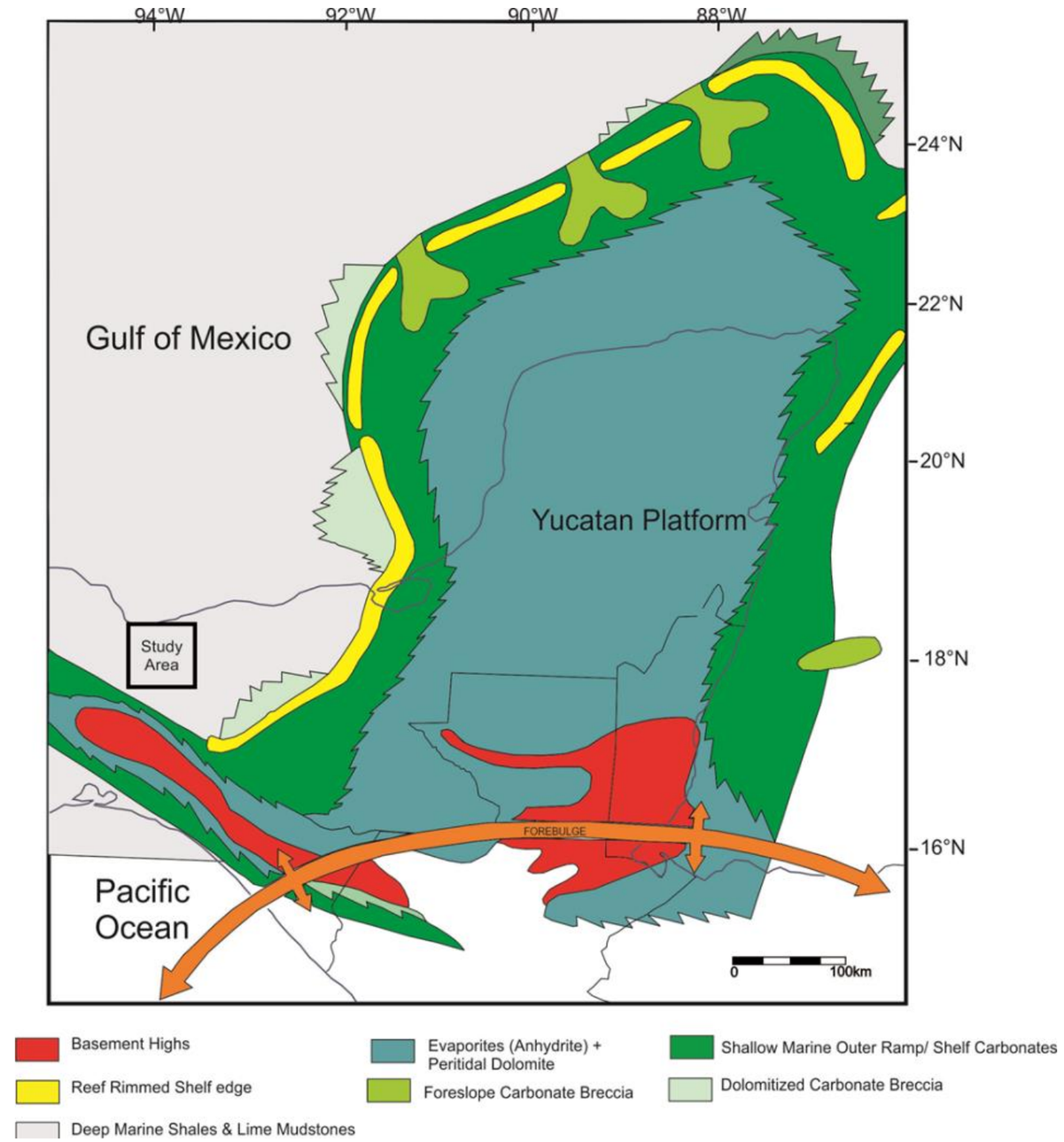

Figure. 3.8. - Paleogeographic map of Cenomanian showing the beginning of deformation in the southern margin of Yucatan platform by the proximity of the Caribbean plate (modified from Johnson, *et al*., 1999).

Dolostones with pellets, pelletoids and oolites. Quezada-Muñeton (1987), reported large thickness variation ranging from 150 m at the west and 1200 m in the east of the Sierra de Chiapas (Fig.3.9)

The Cobán Formation represents a sabkha facies and is described as a sequence consisting of anhydrite, dolostones, gypsum, mudstones, wackstones, shaly mudstones, dolomitized limestones interbedded with bentonic shale. The thickness of this formation has been reported up to 950 m (Quezada-Muñeton, 1987).

Basinward, in the study area, lower and Middle Cretaceous has not been drilled yet. However, the correlation from the Sierra de Chiapas region suggests that these stratigraphic levels are formed by the lower and upper Tamaulipas Formation which is represented by argillaceous, thin-bedded, cherty, mudstone and deep marine shales, with a total thickness of a 300 m.

Figure. 3.9 - Cantelha Formation is represented by massive carbonates platform (gray dolomites). The picture shows clearly the Tuxtla fault plane located at the Sumidero canyon in the vicinity of the city of Tuxtla Gutierrez, Chiapas. (after Sánchez-Hernández, 2013).

3.6 Mega-sequence IV: Arc Collision Synkinematic Succession (Albian-Maastrichtian 100 to 66 Ma)

This stage marks the drastic change in the sedimentary regime from south to north as consequence of destruction of stable platforms due to the proximity of the Neo Caribbean plate (Greater Antilles island arc). The southern margin of the Yucatan block was gradually transformed due to northward-directed subduction (Caribbean plate) beneath the Yucatan block (Pindell, *et al*., 2002). As a result, the carbonate and evaporitic platform sequences were buried by flysch sequences mainly in the south-eastern areas of the Yucatan block (Fig.3.10).

The initial deformation of the Yucatan block resulted in reactivation of Triassic –Jurassic basement structures. Uplift of basement highs caused erosion of the Cenomanian-late Albian reef-rimmed shelf margins, Deposition of debris aprons in the fore slope and deposition of basinal lime mudstone, shale and pelagic carbonates of the Upper Tamaulipas in the deep marine basin environments.

The Upper Cretaceous succession in the Sierra de Chiapas is represented from southeast to northwest by Ocozocuatla, Angostura, Cintalapa, Jolpabuchil, Xochitlan and Mendez Formation. The Ocozocuautla and Angostura Formations (that change to Sepur flysh towards Guatemala) were deposited along the platform in southern Sierra de Chiapas and change northward to the basinal facies of the Xochitlan and Mendez formations. In general, the distribution of these formations are controlled by the facies distribution from littoral, carbonate platform up to deep marine facies composed of shaly carbonates, calcareous shale, carbonate breccias and marls (Quezada-Muñeton, 1987; Jonhson, et al., 1999).

The Ocozocuautla Formation represented a coastal facies and is composed of fine-grains sandstones with intercalation of quartz sandstones with red alterations, shale, limestones with bioclastic fragments (Meneses-Rocha, 1985). In contrast, the Angostura Formation is mainly represented by shallow marine

carbonate composed of bioclastic grainstones, packstones of miliolids, With intercalation of breccias with fragments of reefs debris. The Cinatalapa Formation represents a shallow marine consists of wackstones, packstone with pellets and biogenic fragments, mudstones to wackstones (Meneses-Rocha, 1985). The Jolpabuchil Formation, represents a deep marine facies characterised by limited water circulation composed of wackstones, plactonic packstones with black bands and chert nodules, marls, shaly organic rich limestone and abundant bentonite (Quezada-Muñetón, 1987). Finally, the Xochitlán Formation is represented by 800 m thick sequence of calcareous breccias with gradation to sandstone. The Mendez Formation represent deep marine conditions is composed by 120 m thick marls, thin bedded gray shales, cherty lime mudstones.

The Turonian to Santonian time marked the onset of sedimentological changes in the Gulf of Mexico. In this stage, the platforms around the Gulf of Mexico drowned due to sea level rise, favouring the accumulation of deep marine limestones and shales of the Agua Nueva and San Felipe Formations (Horbury, et al., 2003).

In the Sierra de Chiapas Trough, there is no geological record of Turonian sediments, possibly resulting from uplift and erosion caused by basement uplift by basement reactivation (Johnson, et al., 1999).

During Coniacian-Santonian times volcanic eruptions in the Alisitos Arc at western Mexico supplied on abundance of bentonite in the southwestern Gulf of Mexico basins (Salvador, 1991b). Consequently, the deposits on the platforms consist of thin-bedded shaly limestones with intercalations of bentonite. The San Felipe Formation was deposited towards the basin and consists of thin bedded carbonates with a high content of siliciclastic and volcanoclastic constituents, bentonites and nodules and bands of chert. Near the end of Cretaceous time a massive northward influx of flysch (Sepur Fm.) mark the close approach of the island arc.

During Maastrichtian time (74.5 – 66.5 Ma), the major collision between the western end of the Caribbean plate (Greater Antilles island arc) and the southern Yucatan block occurred (Fig.3.10). The shelf edge at the northwest

Chiapas basin was narrowed, but between 120- 600 m of fore-slope talus breccias have been preserved. Most of the Chiapas trough was uplifted causing erosion across the Angostura carbonate shelf. The uplift of the Chiapas range was again linked to salt movement, combined with increasing contractional deformation of foreland to the east (see chapter 2).

In the study area, the upper Cretaceous succession has not been reached by drilling in the basin. However, in the Cerro Nanchital structure located to S-SW of the Isthmian Saline basin the Cretaceous succession has been penetrated and constitutes the main reservoir at a depth of 500 m. In this well, the lithology of the Upper Cretaceous consists of calcareous breccias with gradation to sandstone. Therefore, these calcareous breccias represent an excellent potential exploration target in the Isthmus Saline Basin.

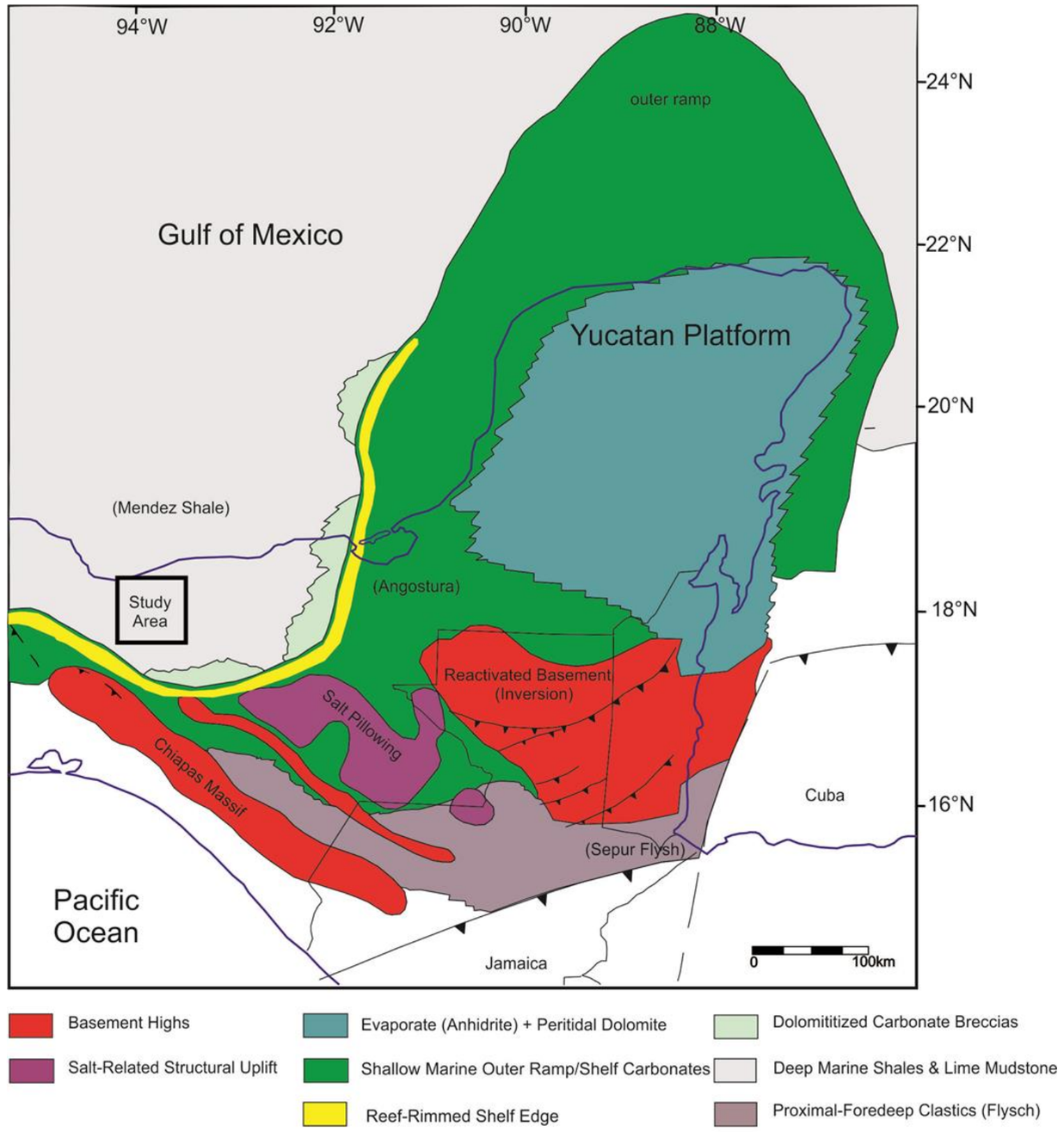

Figure. 3.10. - Paleogeographic map of Maastrichtian showing the deformation of the southern margin and a drastic change in the sedimentation from south to north due to collision of Caribbean plate with Yucatan margin (modified from Johnson, *et al*., 1999).

3.7 Mega-sequence V: Oblique Collision Deposits Synkinematic succession (66- 25.2 Ma)

During this stage, the oblique collisional suture between the Yucatan block and the Caribbean plate (Greater Antilles Island Arc) evolved into a sinistral transform boundary as the Chortis block was incorporated into the Caribbean plate. Due to continued convergence caused by the migration of the Chortis block along the southern margin of Mexico, deep-water depositional systems dominate the Cenozoic strata of the Isthmus Saline basin. Paleobathymetric data indicate that upper bathyal condition prevailed during most of the Cenozoic (Quezada-Muñetón, 1987) (Fig. 3.11).

The Sierra de Chiapas experienced a sedimentological change during the Paleocene and is represented by the Lacandon, Tenejapa and Soyalo Formations as described by Quezada-Muñetón (1987). The SW of Sierra de Chiapas area recorded an unstable period of uplifting as indicated by an angular discordance between the Paleocene flysch and Middle Cretaceous carbonates. In contrast, the Lacandon Formation represents a long-lasting carbonate platform located in the south-eastern Sierra de Chiapas. The Lancandon Formation concordantly overlies the Angostura Formation and is composed of 400 m thick bioclastic packstones, calcareous breccias and nodular bands of chert. The Tenejapa Formation represents the external platform facies and is consisting of 100 m thick of limestones with bands and nodules of pelagic chert interbedded with calcareous breccias. Finally the Soyalo Formation in the northwest Sierra de Chiapas is represented by 480 m thick flysch deposits and is characterized by greenish-gray shales with intercalations of calcareous sandstones. It represents the slope to deep-water facies. During all Cenozoic deep-water clastic deposition was prominent in the west and shallow marine deposits in the east of the Sierra de Chiapas.

In the study area the Paleocene sequences have not been penetrated yet. However, Paleocene channel deposits exposed in the Sierra de Chiapas support the assumption of continuity of debris flows and turbidite channels in the surrounding basins to the north.

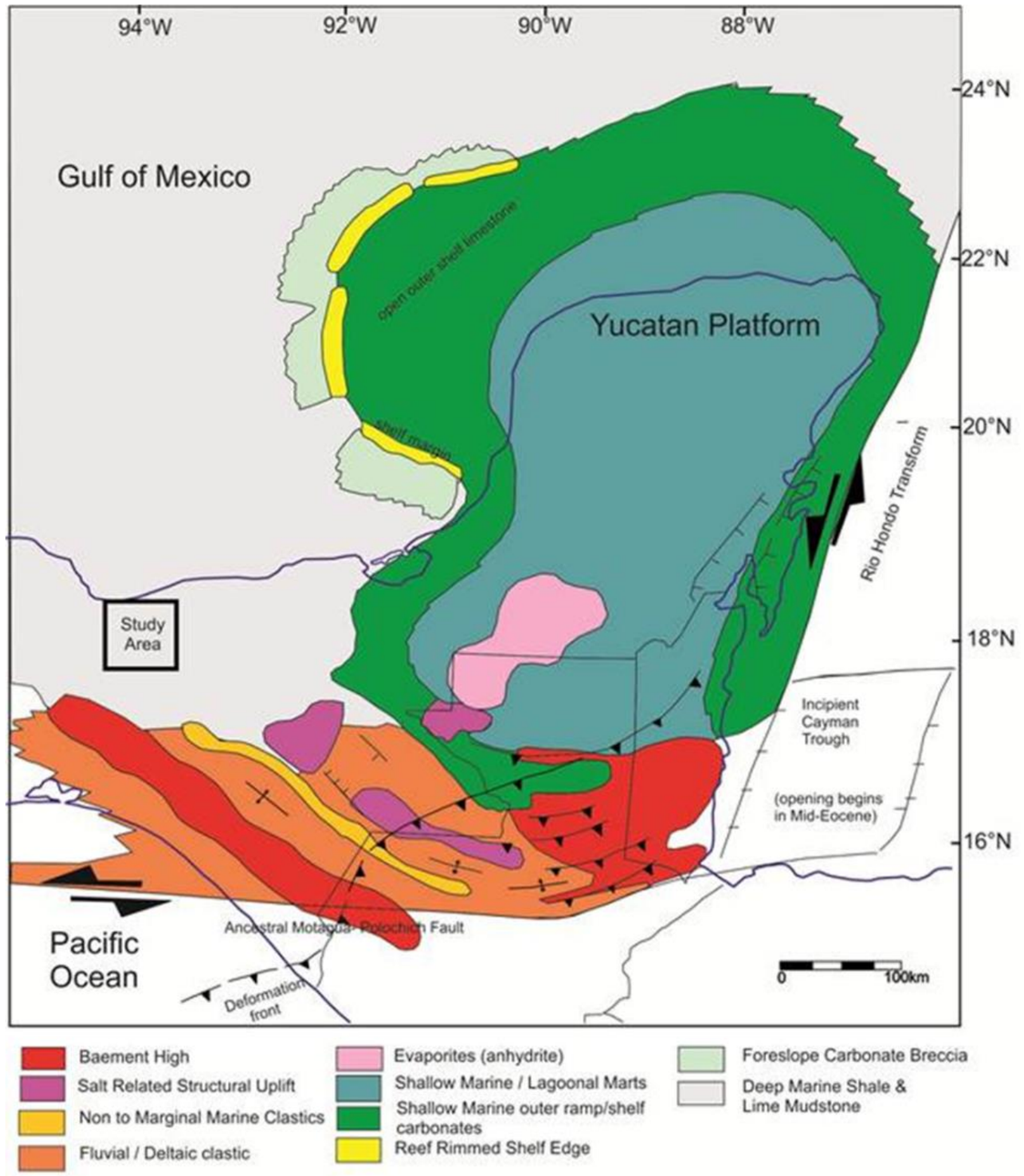

Figure. 3.11 .- Paleogeographic map of Paleocene-Eocene showing the structures related with the uplifting of the Sierra de Chiapas due to oblique collision of Chortis block (modified from Johnson, *et al*., 1999).

During Early and Middle Eocene, transpression propagated northward along the western margin of the Yucatan Block and consequently, the south-eastern Sierra de Chiapas continued to experience major lithological change. Uplift of the region caused erosion and sediment by-pass through canyons transferring sediments from platforms or rivers onshore directly to the offshore slope and the basin floor. The tectonic instability is represented up-dip by the El Bosque Formation, which is characterized by 300-800 m thick continental red beds composed of red continental conglomerates with metamorphic and igneous fragments, breccias, conglomeratic sandstones and siltstone (Mandujano-Velasquez and Vazquez-Meneses, 1996). The continental facies change laterally to shoreline sediments represented by the Lomut Formation. It consists of 900 m of sandy siltstone with interbedded bentonitic sandstones (Ham-Wong, 1979). Laterally, Uzpanapa Conglomerates with its carbonate clast represent the facies change to debris flow deposits on the continental slope (Benavidez, 1956). Basinward, up to 1800 m thick proximal Nanchital Group represents the thickening foredeep basin fill of fine-clastic sediments with grey to dark brown sandstones with intercalations of calcareous shales (Quezada-Muñeton, 1987). These are interpreted to be carbonate turbidites deposited along the slope and basin floor. Their occurrence has proven the existence of submarine slope paleo-canyons in the southern margin of the Sierra de Chiapas, north of Chiapas, Tabasco and the western margin of Yucatan Platform (Ruiz-Osorio, *et al*., 2009; Fig.3.12).

The Upper Eocene strata ranges from 200 to 350 m thickness and document an open marine facies represented by shales interbedded with thin layers of calcareous, bentonitic or sandy shales, green bentonites, mudstones and sandstones.

In the study area the Eocene sequences have been penetrated by the Ke-1 well. This well penetrated the Upper Eocene, which represent 200 m thick open marine shales and calcarous shales.

During the Oligocene the Sierra de Chiapas was strongly affected by E-W trending sinistral strike-slip faults caused by Chortis Block displacement. The stratigraphy of the Sierra de Chiapas is represented by two formations which, change laterally from carbonates to deep marine facies. In the central and

eastern part of the Sierra de Chiapas the Mompuyil Formation represents shallow marine limestones with abundant marine macrofossil and calcareous breccias and sandy shales (Quezada-Muñetón, 1987).

The La Laja Formation is composed of 1300 m thick calcareous and sandy shales interbedded with sandstone and marls (Sánchez-Rios, 1983). Basinward, the Oligocene succession is composed by open marine shaly sediments composed by bentonitic and calcareous shale with intercalations of thin beds of fine-grained sandstones and chalky mudstones.

In the study area the Oligocene sequences have been documented in the Ke-1 well. This sequence is 80 m thick with absence of different levels of the Oligocene, originated by salt intrusion and normal faulting. It is represented by open marine facies composed mainly of calcareous shales interbedded with green bentonite and thin intercalations of fine and medium grained sandstone.

Figure. 3.12. - Channelized turbidite outcrop of Lower-Middle Eocene. Sand-rich facies constitute the main fills of these channel system. The channels were formed by erosion flow (observe the person as scale). The photo was taken on the road that connects the city of Tuxtla Gutierrez, Chis. with Coatzacoalcos, Ver. (Ruiz-Osorio, 2009).

3.8 Mega-sequence VI: Chortis block Migration Synkinematic succession (25.2 Ma to recent)

Basin evolution along the southern Gulf margin marks a major orogenic deformation during middle Miocene - Upper Miocene age. The Mio-Pliocene sequence of the south-eastern Gulf of Mexico is related with the rapid uplift of Chiapas Massif and the Sierra de Chiapas exposed to the south. The uplifting of Chiapas Massif produced a massive influx of late Neogene clastic sediments toward northward prograding depocenter (Fig.3.13). The orogeny caused influx of clastic sediments but also produced volcanism, salt withdrawal, basin-scale detachment, diapirism and slope failure. All these deformation events helped to improve the quality of reservoir rock, the configuration of salts structures and by consequence the migration routes at the south-eastern Gulf of Mexico.

The Miocene deposit sequences is characterised by a strong variations of deep-water to transitional sediments associated with transpressive events occurred in the Sierra de Chiapas.

During middle Miocene the stratigraphy of the Sierra de Chiapas is represented mainly by four formations which change laterally from shallow carbonates to deep marine facies (Fig.3.3)

The Tulija Formation located in the eastern part of the Sierra de Chiapas is composed of intercalation of carbonates flows and siliciclastic bed. The central part is formed by 345 m of platform limestone. Macuspana Formation is shallow marine facies, with abundant macrofossil, calcareous breccias and sandy shales.

The north and western sector of the Sierra de Chiapas is represented by Malpaso Formation. It is represented by slope and basin floor facies (Tarango and Vázquez, 2006). It consists of conglomerates, sandstones and siltstones with fragments of metamorphic, plutonic, volcanic and sedimentary rocks. The Deposito Formation was deposited northwards beyond the shelf break, it is represented by deep marine clastic sediments composed of a thick sequence of shales and siltstones.

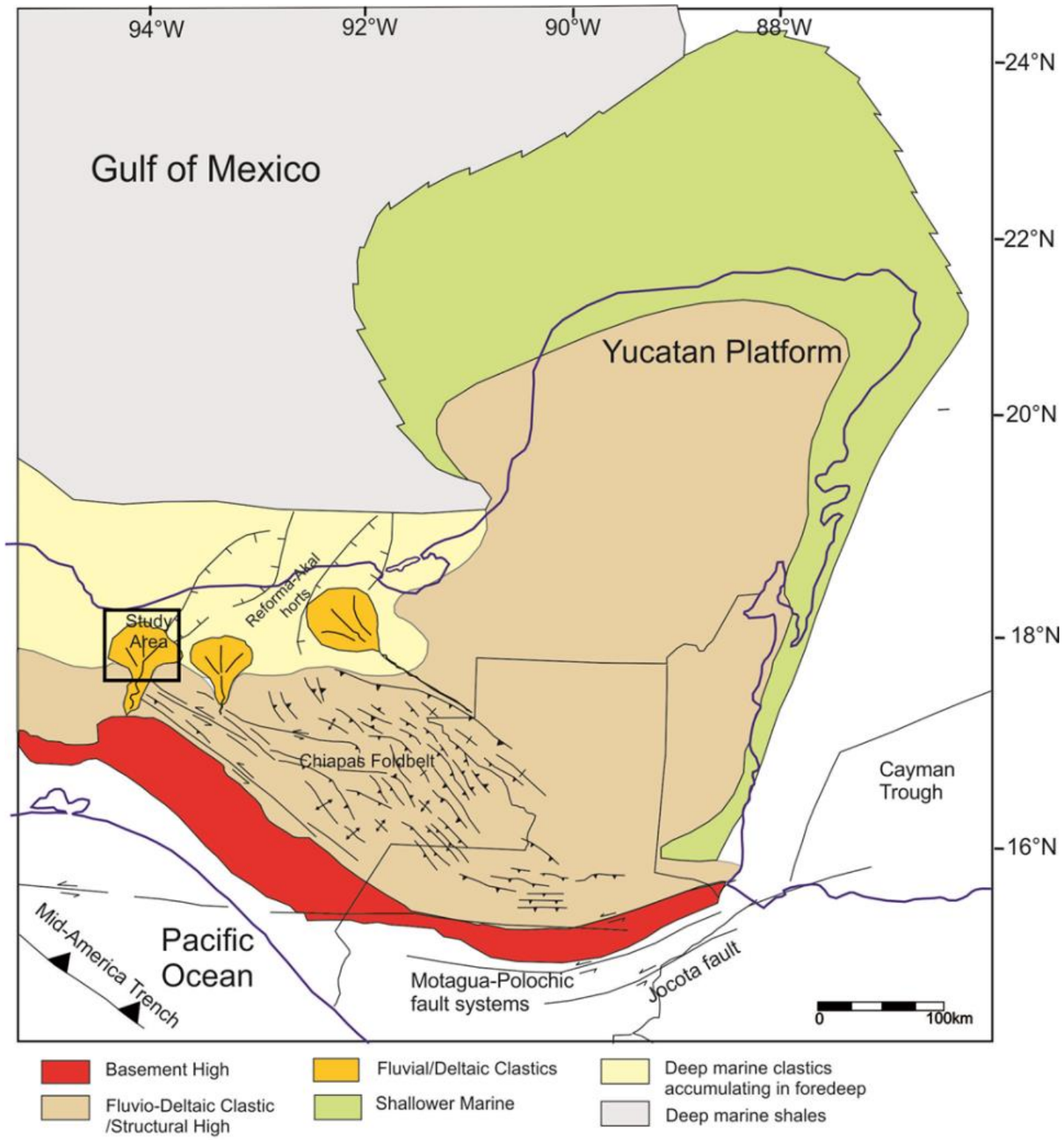

Figure. 3.13 .- Paleogeographic map of Oligocene-Miocene showing the regional uplifting of the Sierra de Chiapas due to continuous movement of Chortis block. The uplifting of the Sierra de Chiapas cause flow of gravity-driven sediments to the foreland basin (modified from Johnson, *et al*., 1999).

In the Ixtapa Graben this sequence is represented by shallow marine sediments, composed by conglomerates formed by calco-alkaline intrusive clast and shales (Meneses-Rocha, 2001). The depositational environment interpreted is braided coarse-grained delta, fed by fluvial systems that drained the uplifted Chiapas Massif. The shale has been interpreted as transgressive surface over the conglomerate succession. Meneses-Rocha (2001) states that the conglomerate could be related to a first stage of the Chiapaneca Orogeny.

The age of this formation include upper Miocene and the lower part of Pliocene. Meneses-Rocha (2001) divided the Ixtapa Formation into three sequences. The base and the middle sequences represent the Upper Miocene. These two sequences are composed by 4515 m thick of two cyclic upward coarsening sequences of alluvial debris flows at the base, alluvial channel deposits in the middle and lacustrine environments at the top.

Basinward, the Miocene sequences are represented by a deep-water sediments. The stratigraphy is composed by the Deposito, Encanto and Concepción Inferior Formations. Due to its syn-tectonic character, the thickness of these units are variable and were also controlled by salt withdrawal. The thickness variation is related to uplift of the Sierra de Chiapas and the resultant progradation of conglomerates and sandstones deposited in slope and basin floor environments which represent the Deposito Conglomerate and Nanchital Formation of the Lower Miocene. It ranges in thickness from 40 to 800 m. In contrast, the Middle Miocene is composed of shales and sands deposited in a deep water environment during Lower Miocene up the early stage of the Middle Miocene. The latest stage of the Middle Miocene and Upper Miocene is called the Encanto Formation which is characterized by shales interbedded thin sandstones. However, this formation shows notable increase of sand bodies represented by sandy shale outer fan facies, mainly composed of feldspars and quartz with less proportion of rock fragments (Ruiz-Marín, 1991). The thickness of the middle Miocene sequence is also variable, it ranges from 50 to 600 m. Finally, the upper Miocene is represented by Concepción Inferior Formation is composed by sandy turbidites composed by sandy shale interbedded with thin beds of mudstone, shale bentonite and shale. This is the most variable and thickest Miocene sequence because it ranges from 30 to 3000 m.

The Miocene in the study area is economically important because it contains the main hydrocarbon plays. The Neogene stratigraphy varies from deep-water to transitional sediments (Mora, *et. al.*, 2007). These are represented by fan slope and turbidite deposits which show features as flame structure, loading structures and both normal and inverse-graded bedding. These deep-water facies are represented as fans and channel, overbank and levee deposits. The Lower and Middle Miocene ranges in thickness from 1300 to 2100 m and consists of lithic sandstones with interbedded shale represented by outer fan facies. The Upper Miocene is divided in two main areas. Up dip, the facies are represented by shallower conditions characterized by transitional deltaic and shelf sand facies; toward the north, the environment change to slope base facies on which sandy turbidites were deposited in fans, amalgamated channels, overbanks and levee facies composed by shales with interbedded fine grained sandstones (Sosa-Patron, *et al*., 2009). In general, these deposits were controlled by minibasins produced by massive influx of clastic sediments and salt evacuation. In consequence, in many cases strata thickness diminishes above the salt diapir hinge zone and the synclines growth rapidly. Thus, whereas thickness of the Middle and Upper Miocene strata ranges from 20 to 250 m, the synclines growth in a range of 400 to 700 m. evidencing both lateral and vertical thickness and facies variations.

The Plio-Pleistocene in the Sierra de Chiapas is characterized by lacustrine and stream flood environments and volcanic rocks. The Ixtapa Graben constitutes the depocenter for sediments of the upper sequence of the Ixtapa Formation. This sequence is represented by an upward coarsening sequence consisting of siltstone at the base and sandstone and conglomerates at the top (Meneses-Rocha, 2001). The volcanic activity was significant, represented by volcanoclastic sediments, lavas, volcanic domes, ash fall, ash block and ash flow deposits of the Chiapaneca Volcanic Arc.

Basinward, the Pliocene sequences is represented by Concepción Superior and Filisola Formation, the thickness ranges from 100 to 2800 m. The Concepción Superior Formation is represented by grey shales and calcareous shales with grey sandstone, and shale bentonite deposited in a deep water environment. The Filisola Formation is composed of fossiliferous grey shales

with interbedded quartz sands. This formation has a high content of bentonite with scarce foraminifera deposited in a transitional deltaic and shelf sand facies. Finally, the Pleistocene is represented by Paraje Solo Formation, composed of greenish grey sandstones with abundant plant material, sometimes presented with interbedded conglomeratic levels, light green shales, often with molluscan fauna deposited in a deltaic plain environment influenced by river currents (Estabillo-García, *et al*., 1983).

The Lower Pliocene in the study area contains significant hydrocarbon reserves. This sequence represents the syn-tectonic and post-tectonic fills of fold and salt-controlled minibasins. During Early Pliocene the progradation advance from shelf margin toward the north-northwest. Its thickness is laterally variable, it reaches until 2500 m. additionally, the volcanic activity of Tuxtlas Volcanic Centre increased and produced an important volume of volcanoclastic deposit in the surrounding basins.

The Middle Pliocene, the southern margin of Isthmus Saline Basin is represented by shallow water facies characterized by deltaic facies which advance from south to north. Salt diapirism controlled the development of shelf and slope deposition to the northwest, controlling the distribution and development of amalgamated channels, overbanks deposits, levees and sandy facies anastomosing slope fans (Fig. 3.14).

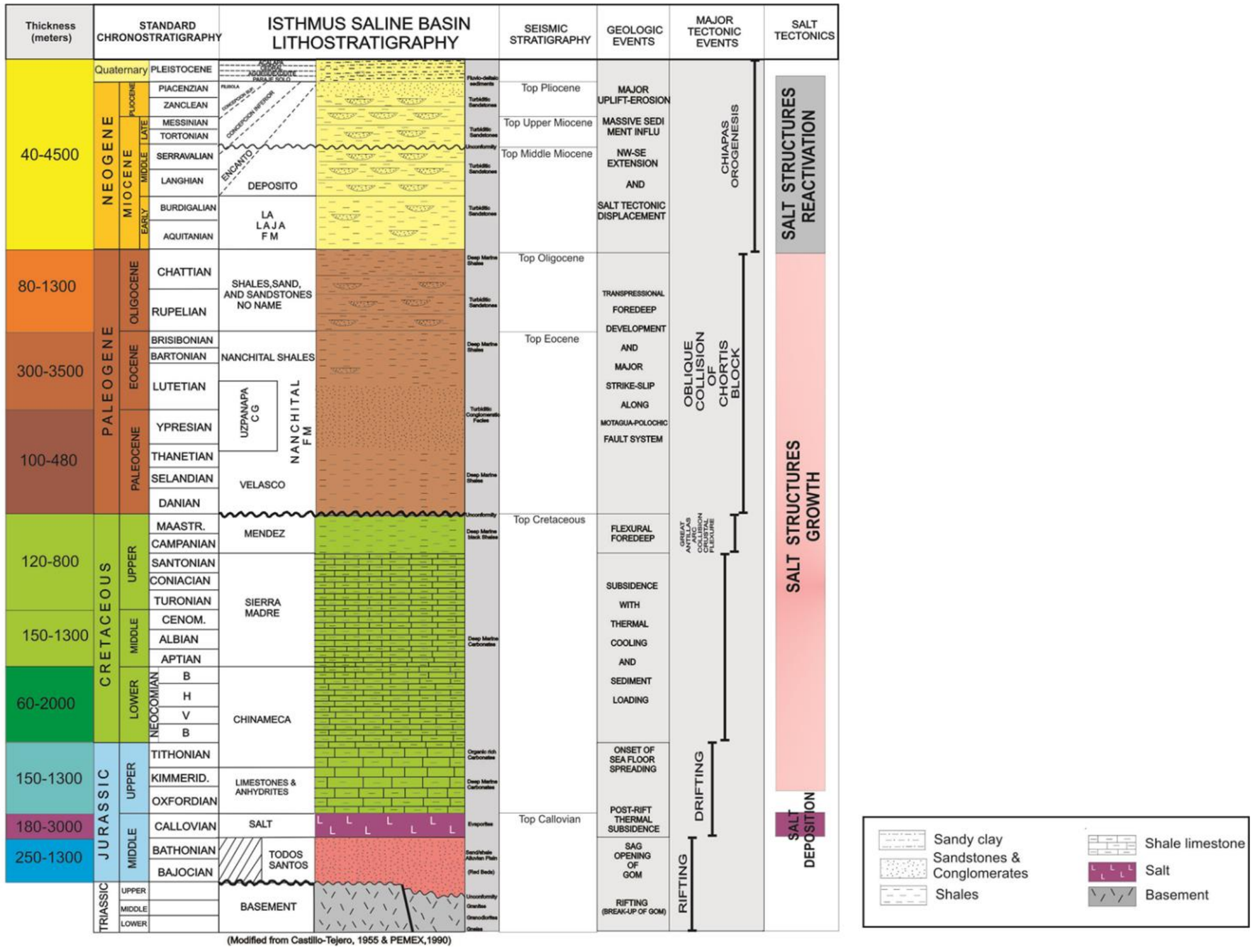

Figure. 3.14. - litostratigraphy column proposal of the Isthmus Saline Basin based on the Sierra de Chiapas outcrops and surrounding basins information (modified from Castillo-Tejero,1955; Pemex, 1990).

Summary

1.-The pre-Mesozoic basement in the south-eastern margin of Gulf of Mexico is constituted by plutonic and metamorphic Proterozoic rocks and sedimentary Paleozoic rock.

2.-.The sedimentary rocks related to the Jurassic rift stage are composed of continental red beds, evaporite deposits and volcanic rocks.

3.-The Jurassic drift mega-sequence is represented by a transgressive sequence that changed from transitional to deep marine facies. In this range of facies variations, intraplatforms depression were very important to the accumulation of source rock sediments.

4.-During the early and middle Cretaceous, the thermal subsidence stage produced a high proliferation of carbonate on wide reef platforms, thin-bedded limestones in deep marine environments and carbonate breccias along paleo-slopes, which represent the most important oil reservoirs.

5.-The proto Caribbean plate (Antilles Arc) collided with the southern margin of Chiapas and generated the erosion and destruction of the carbonate platforms. Thus, the resultant deposits in the SW Gulf of Mexico include breccias, conglomerates, sandstones, siltstones, marls and shales.

6. The Lower Eocene deformation “equivalent to Laramide event” produced a drastic change in the sedimentological facies in the Sierra de Chiapas. The lifting of the Sierra de Chiapas during the Paleocene-Eocene caused deposit of continental, transitional and debris flows and turbidites to the study area. Syn-tectonic conglomerates consist mainly of fragments of carbonate rocks of the Mesozoic platforms and lesser extent igneous and metamorphic rocks.

7. The migration of the Chortis Block to the west produced volcanism and uplift of Chiapas Massif; as a result, massive siliciclastic influx filled the Neogene basins in the SW Gulf of Mexico.

Chapter 4 Salt Tectonic-

A Review

4 Salt Tectonics – A review

4.1 Introduction

The Isthmus Saline Basin is an area of salt tectonics, characterized by a complex structural evolution and well understood salt movement history. During the past 25 years, prolific seismic imaging campaigns and advances in experimental and numerical models, structural restoration techniques and field studies (Rowan, 1995) have all contributed to a better understanding of salt tectonics. The knowledge gained through the extensive exploration of the Isthmus Saline Basin since the early 20th century can now be investigated in the light of these new concepts

For the petroleum industry, salt plays a very important role. Approximately 40% of the world's major oil and gas fields are related to salt deposits such as those found in the North Sea, Middle East and Gulf of Mexico; (Jackson and Talbot, 1994; Edgell, 1996; Fig.4.1). The interest of the oil industry in understanding the geometry and evolution of salt bodies and associated strata has led to improvements of the seismic acquisition and processing techniques through the years. For example, pre-stack depth migration has allowed better imaging of salt bodies the bases and overhangs of salt sheets and the steep flanks of many diapirs (Jones and Davison, 2014; Fig.4.2).

Physical and numerical modeling techniques have been developed for many years, but it was not until the 1980's when several researchers applied concepts of rock mechanics, modeling the overburden as brittle material. Analogue models investigating the emplacement of salt shed light into how the emplacement of these lithologies into the space generated under regional extensional stress, showing how brittle deformation is needed to thin the overburden (e.g. Vendeville and Jackson, 1992 a, b). These results triggered a change in the traditional understanding of how salt deforms.

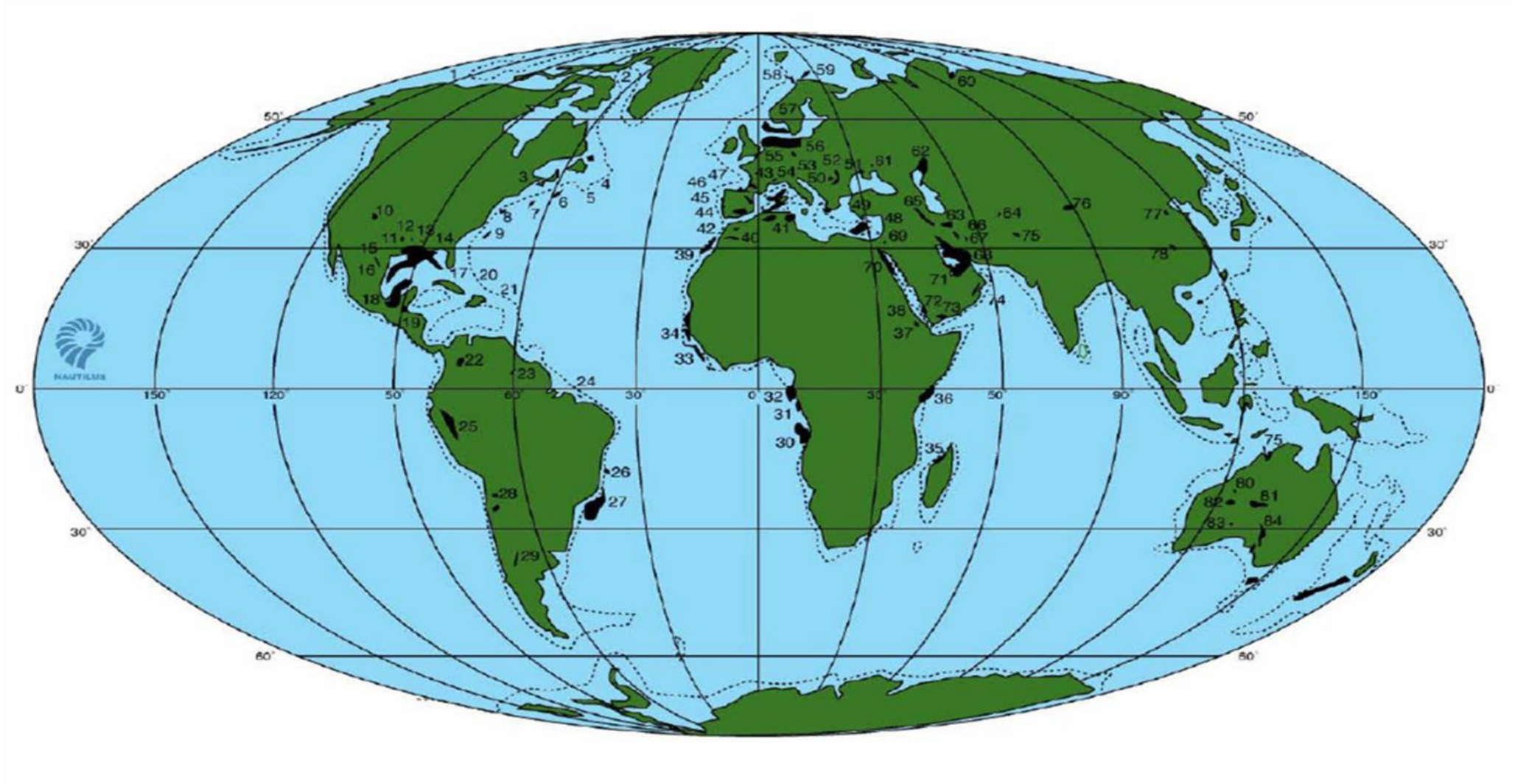

Figure. - 4.1.- Global distribution of salt basin, after Jackson & Talbot (1991); the figure was taken from Nautilus training manual. 1 Parry Islands–Central Ellesmere; 2 Sverdrup; 3 Moncton; 4 Flemish Pass; 5 Jeanne d'Arc; 6 Carson; 7 Horseshoe; 8 South Whale; 9 Sable - Georges Bank; 10 Paradox; 11 South Texas; 12 East Texas; 13 North Louisiana; 14 Mississippi; 15 Sabinas; 16-17 Gulf Coast; 18 Salina–Sigsbee; 19 PetenChiapas; 20 Cuban; 21Haitian; 23 Tarfaya; 24 Suriname; 25 Oriente–Ucayali; 26 Espirito Santo; 27 Santos; 28 Atacama; 30 Kwanza; 31 Lower Congo; 32 Gabon; 33 Guinea-Bissau; 34 Senegal-Mauritania; 35 Majunga; 36 Somali–Kenya; 37 Danakil; 38 Eritrean;39 Agadir-Essaouira; 40-41 Atlas; 42 Safi-Betic; 43Aquitaine; 44 Lusitanian; 45 Guadalquivir; 46-47 Cantabrian–West Pyrenees; 48 Levantine; 49 Ionian; 50 South Adriatic; 51 Transylvanian; 52 East Alpine; 53 Amadeus; 54 Ligurian; 55 Jura; 56-57 Zechstein; 58 Haymana–Polatli; 59 Nordkapp; 60 Tyrrhenian; 61 Carpathian; 62 Pricaspian; 63 Great Kavir–Garmsar–Qom; 64 Chu–Sarysu; 65 Iljac–Tabriz; 66 Kalut; 67 North Kerman; 68 Zagros; 69 Dead Sea; 70 Suez; 71 Emirates; 72 Yemeni; 73 Hadhramaut–South Yemen; 74 Oman–Fahud; 75 Salt Range; 76 ?; 77 Bohai Bay; 78 ?; 79 Bonaparte; 80 Canning; 81 AM Amadeus; 82 Officer; 83 CN Carnavon; 84 Flinders.

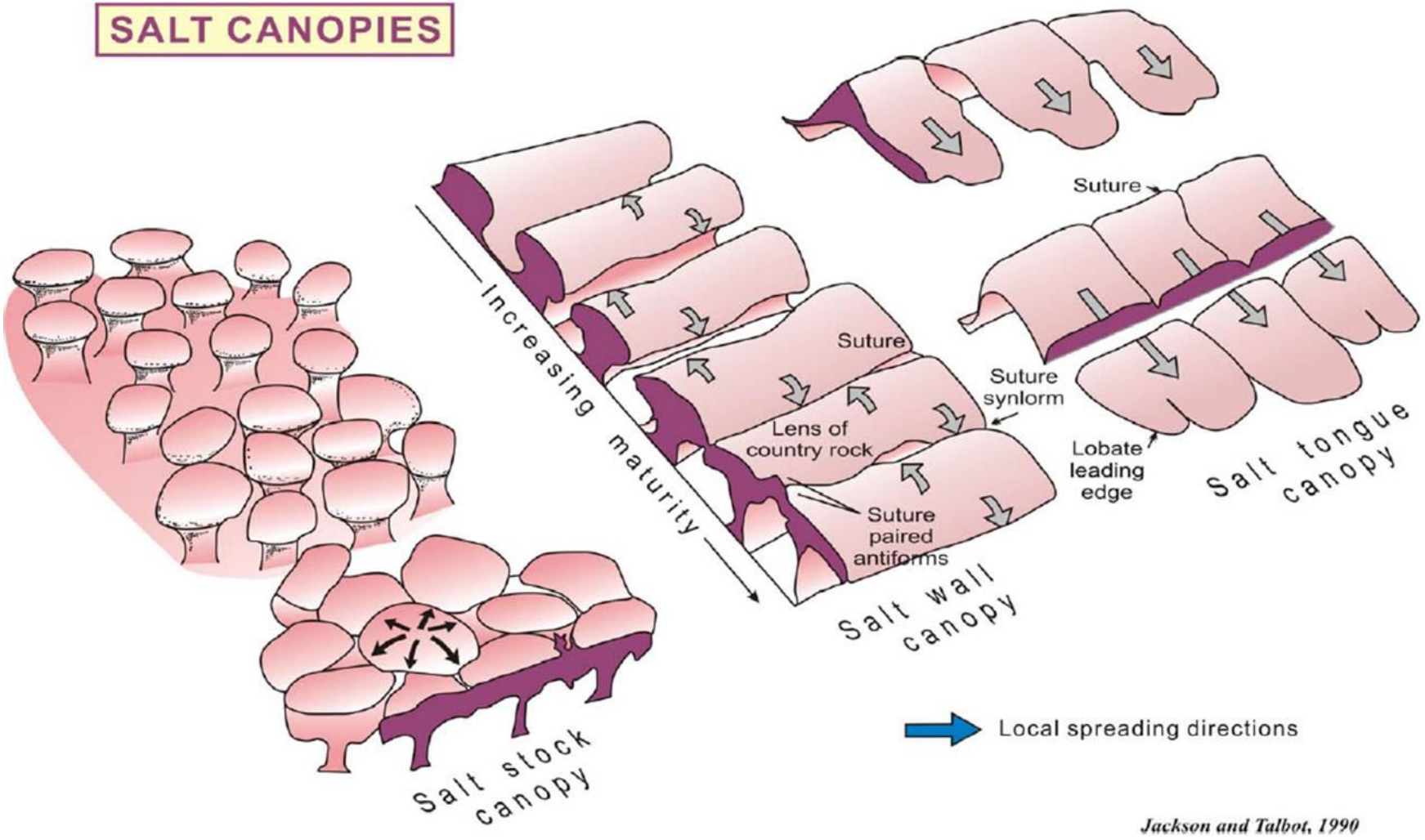

Figure 4.2 Morphology and geometry of salt canopies in related with salt maturity and its spreading directions. After Jackson and Talbot (1994).

Salt formations are usually described as composed mainly of NaCl, often alternating with anhydrite and/or mudstone. The dynamic evolution of subsurface salt bodies has an important impact on geometry of basin evolution. Salt induced changes in sedimentary patterns, uplift and thinning of overlying beds and the development of faults play a major role in the generation, migration and trapping of hydrocarbons.

4.1.1 Nomenclature used in this thesis

Here I clarify a number of structural and salt tectonics concepts used throughout this thesis. Many of these terms are defined based on the salt tectonic glossary from (Hudec and Jackson, 2011).

Pre-kinematic. Sediment sequence or sequences deposited before the start of salt flow, or other type of deformation, the pre-kinematic sedimentary interval is isopachous above local structures.

Regional (datum, elevation). Structural elevation and dip of a marker horizon, which is unaffected by local faulting, folding, or salt tectonism. The regional is a fundamental reference surface and is commonly extrapolated and interpolated for kinematic analysis.

Syn-kinematic. Sedimentary sequence deposited simultaneously with salt flow or other deformations. These sequences may show local stratigraphic thickening above differentially subsiding structures or thinning above rising structures. Generally thickness changes in syn-kinematic sequences are marked by onlaps or truncations.

Salt tectonics (Halotectonics). Large scale deformation, including halokinesis involving salt or other evaporites source layers (Trusheim, 1957; Jackson and Talbot 1986).

4.2 Mechanical Properties of Salt

Salt has characteristic physical properties different to others sedimentary rocks (table 4.1). Its complicated inner structure has produced some of the most complex salt geometries and structures, which give it a dominant role during the evolution of salt basins. Relative to most sediment, salt is:

- A viscous fluid, not a material with brittle-plastic behavior;
- Weak
- Anomalous low density
- High thermal conductivity

4.2.1 Salt Mobility and Strength

In comparison to other sedimentary rocks, salt is extremely weak and ductile under both tension and compression (Table. 4.2). When buried at depths greater than 100-200 m, salt loses porosity. Halite's density remains almost constant (in the range of 2.2 g/cc) and the salt moves as an incompressible fluid under applied stress at depths of 6-8 km (Jackson and Vendeville, 1994; Warren, 2006).

Salt deforms as a viscous material that effectively flows, in some cases at speed up to 15 m/y, such as in exposed salt glaciers of Iran (Talbot, *et al.*, 2000). Subsurface salt flow is closely related to the combination of Poiseuille flow and Couette flow, in which the viscous material is sheared due to lateral translation of the overburden (Davison, *et al*., 1996).

Viscosity is a measure of fluid's resistance to flow, the ratio of shear stress to the rate of shear strain. Salt located between layers of others sedimentary rheologies acts as a weak detachment.

Physical properties

Salt-seismic velocity	4500 ms^{-1}
Salt-viscosity	10^{14}-10^{19}Pas
Salt-density	2100 - 2200 Kg^{-3}- can decrease with depth/increase temperature
Salt-thermal conductivity	6.0 W/m K (surface), 4 W/ m K (@ 130ºC)
Salt-melting point	800ºC
Salt-permeability	10^{-20} m^2
Salt-rate of solubility	East Flower Graben Banks - 10,700 -21,700m^3per annum
Anhydrite-density	2980 kgm^{-3}
Anhydrite-seismic velocity	6500 ms^{-1}
K rich salts (Carnalite)-Viscosity	10^8 Pas

Table 4.1 Main mechanical features of salt, after Davison, *et al* (1996a)

Type of flow	Strain rate s^{-1}	Velocity Mm/a	Velocity
Lava flow	10^{-5}- 10^{-4}	$5x10^{-12}$- $3x10^{-13}$	1 - 60 km/hr
Ice glacier	10^{-10}- $5x10^{-8}$	$3x10^{-5}$- $2x10^{7}$	1 - 60 m/day
Salt glacier	10^{-11}- $2x10^{-9}$	$2x10^{3}$- $2x10^{6}$	10 - 100 km/Ma
Mantle currents	10^{-14}- 10^{-15}	10 - 10^{3}	1 - 5 m/day
Salt tongue spreading (< 30 Km wide)	$8x10^{-15}$- 10^{-11}	2 - 20	2 - 20 km/Ma
Salt tongue spreading (> 30 km wide)	$3x10^{-6}$- 10^{-15}	0.5 - 3	0.5 - 3 km/Ma
Salt diapir rise	$2x10^{-16}$-$8x10^{-11}$	10^{-2}- 2	10 m - 2 km/Ma

Table 4.2 Representative strain and flow rate parameters in salt compared with other tectonic settings (after Jackson and Vendeville, 1994).

Salt rock deforms by intra and inter-crystalline processes (e.g. pressure solution and solid-state creep processes) with an effective viscosity of between 10^{14} and 10^{19} Pa.S (Urai, *et al*., 1986; Van Keken, *et al*., 1993; Nalpas and Burun, 1993, Vendeville et al., 1995; Weijermars et al., 1993). In the Iranian salt viscosity measured as 10^{13} to 10^{16} Pa.S. These variations in the viscosity are closely related to water content and salt temperature (Fig. 4.3). Additionally, there are other physical factors that can influence salt viscosity, such as; its position in the diapir and the grain size (Davison, *et al*., 1996a). The intensity of salt flow and recrystallization can in part depend on the levels of impurity. Intergranular pressure-solution is most rapid on grain boundaries between grains of different mineralogy. In contrast, grain boundary heal is more likely to occur between halite-halite grain contacts and has the potential to heal and resist compressional forces (Urai, *et a*l., 1986). The capacity of salt to heal itself explains its ability to serve as an effective seal, except if grains of distinctive mineralogy are intersected by the fault plane (Warren, 2006).

Wet salt, which deforms by solution-transfer creep, is hundreds of times weaker that dry salt, which deforms by dissolution creep (Urai, *et al.,* 1986). The minute quantities of water caught up as inclusions or between grains of salt have a profound effect on strength.

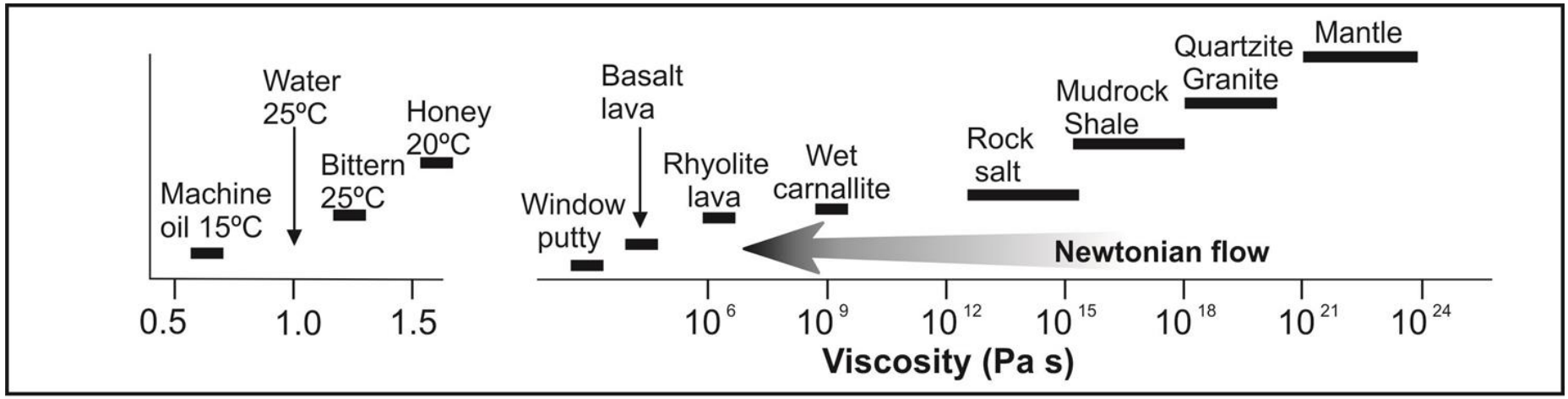

Figure 4.3 Range of viscosity values in different materials (after Warren, 2006).

4.2.2 Density

Salt has a relatively constant density of approximately 2200 kg/m^3. Increased temperature at depth can cause a slight decrease in halite density as a result of thermal expansion (Fig. 4.4). In contrast, the behaviour of shale and sandstone during burial compaction generates progressive loss of porosity and consequently higher density and strength (Jackson and Talbot, 1986; Warren, 2006). Figure 4.4 shows salt is denser than surrounding strata when it is near the surface, but is less dense than siliciclastic rocks at burial depths in excess of 700-900 m. During salt basin evolution, this inversion point is known as the “critical depth” and occurs at different depths dependent upon the lithology and conditions within particular basins.

4.2.3 Buoyancy

Gravitational instability and buoyancy forces can result in halokinesis and diapir rise. The term “buoyancy” and “pressure head” are frequently used to describe the driving forces of a mobile salt layer (Jackson and Talbot, 1986; Jackson and Vendeville, 1992a, b; 1994; Jackson and Talbot, 1994).

The “buoyancy” is defined as an upwards force due to density contrast. The term “pressure head” is an idea developed by hydrologist. The pressure head is a measure of pressure at a fixed depth relative to sea level. Specifically, it is the height to which water would rise in a static well connected to the aquifer. So, the pressure head surface defines the potential. The dip of the surface defines the potential gradient. If the aquifer is dipping, the potential gradient may not be the in the same direction as the pressure gradient. If the water is not flowing through a permeable aquifer, it means there is no potential gradient (the pressure head is the same at all point). The same concept may be extended to salt as fluid, although we could never measure the head by drilling wells and letting salt flow up the well.

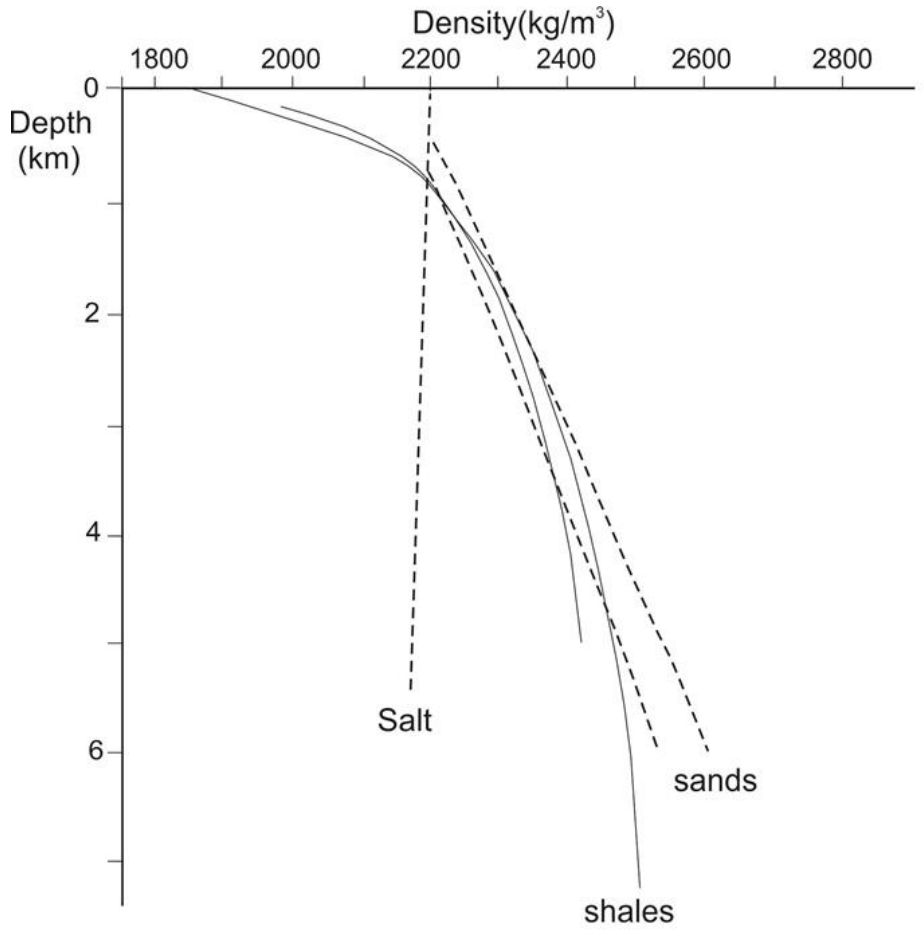

Figure 4.4 Comparison chart among bulk density and depth in salt and related with terrigenous clastic in the Gulf of Mexico basin (from Jackson and Talbot, 1991).

In ancient Greece the great mathematician Archimedes, was the first to apply mathematics to physical phenomena and explain the “Principles of Buoyancy”, which postulate that: “Any solid lighter than a fluid will, if placed in the fluid, be so far immersed that the weight of the solid will be equal to the weight of the fluid displaced.”

Any body sinking in a liquid will experience an upwards forces, acting through the centre of gravity of the replaced fluid, equal to the weight of the displaced fluid. If the body is of lower density than the fluid, the upward force will be identical to its weight, and the body will stay afloat. This fundamental idea led, with some slight variations, to more complicated definitions that accommodate the systems that have been traditionally used to model a loaded salt layer (Fig.4.5).

If halite is considered as a liquid layer, loaded with a solid object of lower density (the overburden), Archimedes’ Principle applies. The overburden is “buoyed up” with a force equal to the weight of the displaced mobile salt layer (Fig.4.5a). If a mobile layer is loaded with an object of greater density. The upwards buoyancy force will be less than the weight of the overload and, space permitting; the higher density object will sink into the mobile layer.

In a geological setting the space required for free ascension of the underlying mobile layer, and thus the sinking of the object, may be restricted. The object / mobile-layer interface can progressively undergo greater pressures as the object increases in weigh, regardless of the object’s density. Under these conditions, the mobile layer becomes similar to the hydraulic fluid in a piston system. This referred to as a “pressurised fluid” (Fig. 4.5b). Based on this pressurized fluid model, Vendeville and Jackson (1992a) concluded that salt should be considered as a pressurized liquid and that differential fluid pressure is the main controlling factor of salt flow. Furthermore, Jackson (1995), describe, the historical development of ideas on salt tectonics. He showed that the early models were based on models in which both the salt and the sediment overburden are represented as fluids (“the fluid era”).

a) Unconstrained solid supported by a liquid

b) Constrained solid supported by a liquid

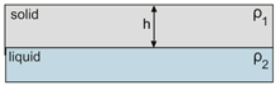

c) Solid supported by a liquid
(Rayleigh - Taylor instability)

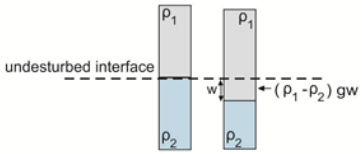

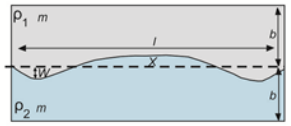

ρ=*density*
h=*thickness*
b=*level of the solid sinks in the liquid*
g=*aceleration due to gravity*
η=*viscocity*
w=*displacemt of liquid interface*
x=*volume of displacement/upwelling*

Buoyancy and carapace Rheology, after Turcotte ans Shubert (1982).

if $\rho_1 < \rho_2$, and the system is in isostatic equilibrium, the upward force at the base of the solid equals:

$$F = \rho_2 * gh$$

This is equal to the displaces fluid:

$$F = \rho_2 * gh$$

Therefore

$$\rho_1 * h = \rho_2 * gh$$

Regardless of density contrast the upward force at the base of the solid equals;

$$F = \rho_1 * gh$$

The system no longer need be in isostatic equilibrium.

A liquid / liquid interface will distort and fluid motion will occur. The density contrast between the fluids controls whether the distortion are retarded or amplified.

The force at the base of the distortion:

$$F = (\rho_1 - \rho_2)\, gw$$

if $\rho_1 < \rho_2$, $F<0$

The force works in the opposite direction to gravity. The interface will experience an upward force and the distortion is retarded.

if $\rho_1 > \rho_2$, $F>0$

The force works in the same direction as gravity. The interface is dispalced further downward and the distortion is amplified. The higher density sinks.

if $\rho_1 > \rho_2$ the system is unstable and amplified displacements distort the fluid-fluid interface.

The rate of growth (ta) is dependent upon the density contrast, the viscosity and the layer thickness (at low amplitudes):

$$ta = 13.04m / (\rho_1 - \rho_2)gb$$

The lower the density contrast the more viscous the fluid, the longer the instability takes to grow.

Figure 4.5 Bouyancy and carapace Rheology, after Turcotte and Schubert (1982).

A denser fluid overlying a less-dense fluid will sink down into it by Raleigh-Taylor overturn (e.g. Turcotte and Schubert, 1982), as shown in fig. 4.5c. While this approach was able to replicate some features of natural salt tectonics, the representation of the overburden by a fluid is geologically unreasonable. Recognizing this, later model addressed the cover as a brittle material such as sand (“the brittle era”).

4.2.4 Pressure effects

When an evaporitic sequence is loaded by the overlying sediments, the pressure of the salt increase. The intrusion of salt through fragile sedimentary layers occurs when the pressure of the salt exceeds the strength of the overlying sediments. Figure 4.6 shows in a case when the fluid (salt) has less density than the overlying sediments (Jackson and Vendeville, 1994). When the overlying sedimentary sequences are thin, it may be weak enough for salt to break through it. Conversely, thicker sequences are likely to resist the upward pressure exerted by the salt. The thickness of the sediments required to resist the upward pressure of a certain thickness of salt is defined as the “piercement threshold” (Jackson and Vendeville, 1994; Fig. 4.6). Thinning of the sedimentary sequence overlying a salt layer below the piercement threshold, for example by erosion, may allow a salt diapir to rise, piercing the overburden (Fig. 4.6b). Active piercement can also occur in situations where the roof is thinned by extension or erosion (Fig.4.6c).

Vendeville and Jackson (1992a) have defined the set of conditions required for salt evacuation and diapirism. These are (1) an open space near the surface must exist for the salt to move into; (2) the overlying sedimentary sequence must be thin and weak enough to allow salt to overcome overburden strength; (3) tectonic processes that help to create fractures or spaces where salt can flow; (4) flow is a result of salt’s passive reaction to external forces.

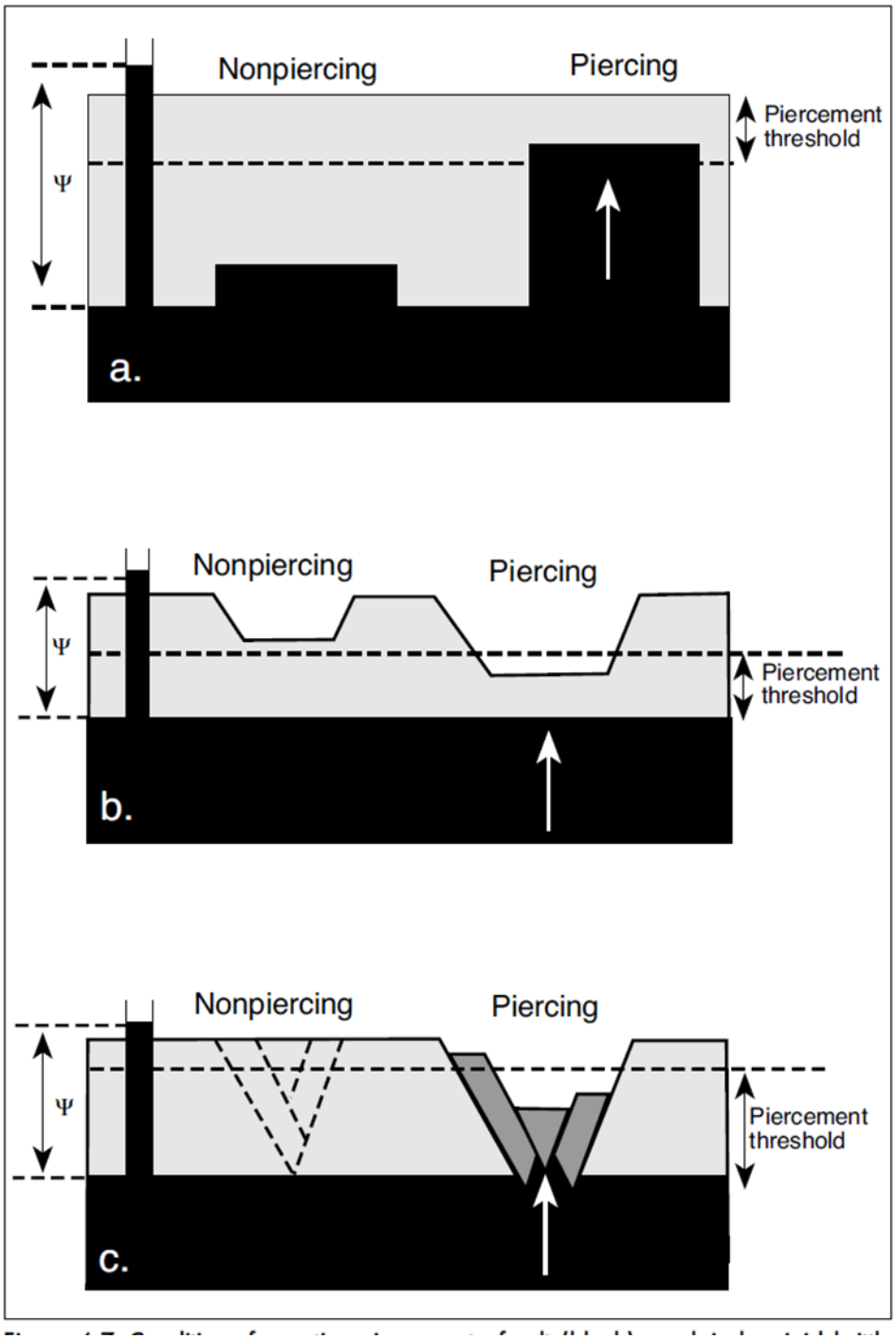

Figure 4.6 Requirements for active piercement of salt (black) superimposed by an inflexible fragile overload (grey) (after Jackson and Vendeville, 1994).

4.2.5 Thermal effects

Halite has unique thermal properties compared to other common lithologies. In particular, the thermal conductivity of salt is much higher than that of other minerals and sedimentary formations (Fig. 4.7). Thermal conductivity of halite decreases with temperature, so that salt at the depth 5 km has a third the conductivity of salt at shallow depths (Davison, *et al*., 1996).

Whit increasing burial, halite expands due to temperature and contracts due to the pressure to which it is subjected (Jackson and Talbot, 1994); in the thermal expansion is greater than the pressure-induced contraction.

As a result, thermally induced convective flow is possible in a salt layer thicker than 2.9 km and subjected to a geothermal gradient of 30°C per km. (Talbot, 1978).

The unusually high thermal conductivity of salt (Fig.4.7) has a big impact on chemical dissolution and precipitation, hydrocarbon maturity and fluid flow. Salt is highly conductive, and transmits heat more efficiently by conduction than by convection. Heat may also be transmitted rapidly by convection of pore fluids in rocks adjacent to salt (Talbot, 1978).

Grain size plays a major role in controlling salt strength. When grain sizes are in the range of 1 to 2 cm both pressure solution and dislocation creep becomes powerful deformation mechanisms (Van Keken, *et al*. 1993). Salt is an anisotropic material difficulting the seismic imaging of sediments underneath salt layers.

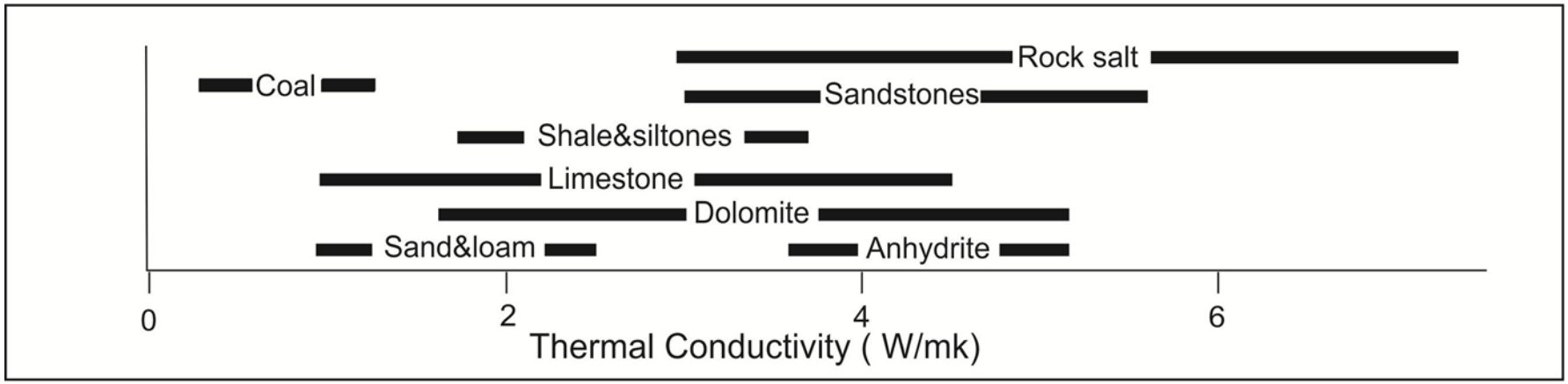

Figure 4.7 Thermal conductivity ranges of different geological materials (after Warren, 2006)

Another physical characteristic of salt is that it has a very low permeability compared with other sedimentary rocks. Nevertheless, it can be fractured in a brittle mode at high strain rates as occur in Sergipe-Alagoas Basin, Brazil (Davison, *et al*., 1996a)

4.2.6 Patterns of salt flow

The behaviour of salt, when its flows are observed over long geological times, can be described as that of an incompressible fluid (Davison, *et a*l., 1996a). Davison, *et al*. (1996a) differentiated five types of salt flow (Fig. 4.8):

Poiseuille flow (channel flow): takes place when the overburden pressure of sediment drives lateral flow within an unconfined layer. As a result of friction between the salt and the overlying and underlying sediments, the greatest flow, occurs in the centre of the salt layer (Fig.4.8a)

Couette flow (shear flow): this type of flow occurs when the viscous material is sheared due to lateral translation of the overburden (Fig. 4.8.b). As a result, the salt is dragged in direction of sliding. Generally, the salt flow as a mixture of both Poiseuille flow and Couette flow 4.8c as shown.

Multi-layer flow: In this is case, flow is a combination of both Poiseuille flow and Couette flow (Fig.4.8.c). It occurs in cases when sedimentary layers are interbedded within the salt sequence and, as a result, the resistance between rigid surfaces will reduce the rate of lateral flow (Fig.4.8 d).

Overburden Drag: Occurs when salt is pulled down-slope as a result of extensional or contractional stresses. It is an exceptional condition of Couette flow (Fig.4.8 f).

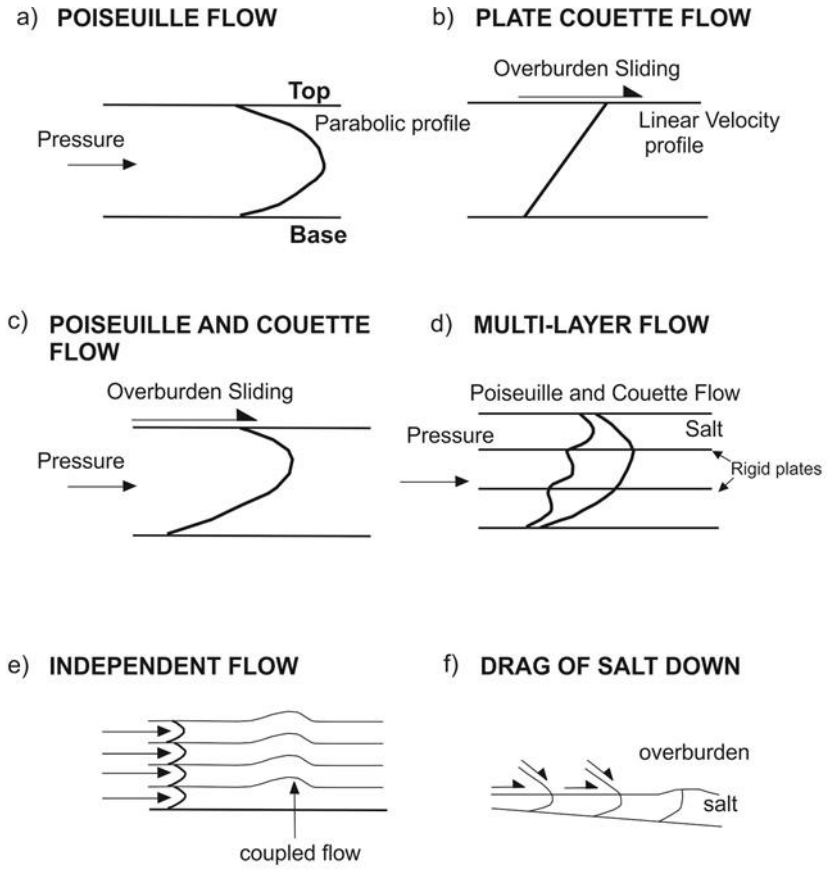

Figure 4.8 Diagrammatic models of salt flow. (a) Poiseuille flow (channel flow) in an alone thick layer. (b) Plate Couette (shear flow) Produced by overburden sliding. (c) Combination of Poiseuille and Couette flow. (d) Poiseuille and Couette flow in a multi-layer of equivalent thickness. (e) Layers react together during movement perpendicular to layering. (f) Drag of salt down to a detachment horizon to produce a thicker salt (after Davison, *et al*., 1996a).

4.3 Cause & control factors of salt flow

The formation of salt structures is close linked with external forces resulting from for example regional extension, regional contraction, and differential loading. The main mechanisms controlling salt deformation on a large scale are differential loading, buoyancy, and dissolution (Jackson and Talbot, 1986, Jackson & Vendeville, 1994, Davison, *et al,* 1996a, Waltham, 1997; Stewart and Clark, 1999).

Three main factors control the formation and movement of salt. These are: (1) pressure inside salt layer, (2) friction of overload and (3) independent features of salt deformation and flow (e.g. rates of regional shortening, extension and sedimentary propagation and aggradation) (Jackson & Vendeville, 1994).

Jackson & Vendeville (1994) amalgamated these three factors into three proportions: V/B, P/B, and P/V, where, V represents the salt viscosity, P represents the salt pressure, and B is the vertical resistance imposed by the overburden. The ratios between these parameters provide insights into the development, geometry and flow of diapirs. The first ratio, (V/B), relates the strength of the salt and overburden. The thinner the overburden the higher ratio and therefore the salt may extend and fault the overlying sequence. The second ratio, (P/B) defines whether a diapir can break through its overlying overburden. If the ratio is high, salt may break the resistance of the overburden. The third ratio, (P/V), illustrates the likelihood of diapirs emerging on the surface. A high ratio evidences rapid extrusion, whereas a low ratio results of an increase viscous drag and therefore delayed diapir rise.

4.3.1 Differential Loading

Differential loading of salt results from lateral pressure change as a consequence of variations in thickness and / or density of the overburden (Jackson and Talbot, 1986, Jackson & Vendeville, 1994, Ge, *et al*., 1997). G, *et al*. (1997) demonstrated through a series of scaled physical models the importance of progradation for salt tectonics and the development of allochthonous sheets. As part of experiments, they analyzed two end groups excluding regional extension and contraction factors. In the first set of models, a flat contact exists between salt and basement (Figure 4.9), whereas in the second group of models basement is characterized by a series of faulted blocks (Figure 4.10).

The results of the first model showed a basin-propagating salt weld below the prograding sediment wedge. Incomplete evacuation left salt pillows as residual highs, but no diapiric salt structures were formed. In contrast, progradation over a salt layer underlain by basement steps, begun with the formation of an extensive anticline along each basement step. Later, the core of which was later filled with salt. The salt within the anticline's core then started actively piercing the fold's crest. This was followed by passive diapir growth and local sourcing of allochthonous salt sheets. The repetition of this deformation cycle over each basement resulted in a structure in which the age amplitude, complexity and maturity of salt-related structure decrease basinward (Fig. 4.10).

Ge, *et al*. (1997) showed that huge landward-dipping (counter-regional) pseudo-faults can emerge entirely by salt expulsion rather than regional extension. Their model shows that progradation alone can generate salt anticlines that mature into salt walls, stocks, glaciers or linked, multi-tiered complexes of evacuated sheets and salt welds. The progradation sedimentary wedge expels salt basinward regardless of the density relationship between salt and sediments as described by Jackson and Vendeville (1994) for the Gulf of Mexico.

Based on the previously described models, it appears that there is a close relationship between underlying basement geometry and the formation and evolution of salt diapirs and allochthonous salt sheets. Salt may flow under both

regional extension and sediment progradation. Thin or thick skinned extension is likely the main mechanism for triggering diapirism in deeply buried salt bodies, while progradation is the main driving mechanism of salt located near the surface. When a salt dome reaches the level of neutral buoyancy, whether below or above the surface, gravity spreading becomes the most important mechanism of salt flow. This occurs for example, in salt glaciers (Jackson and Talbot, 1986).

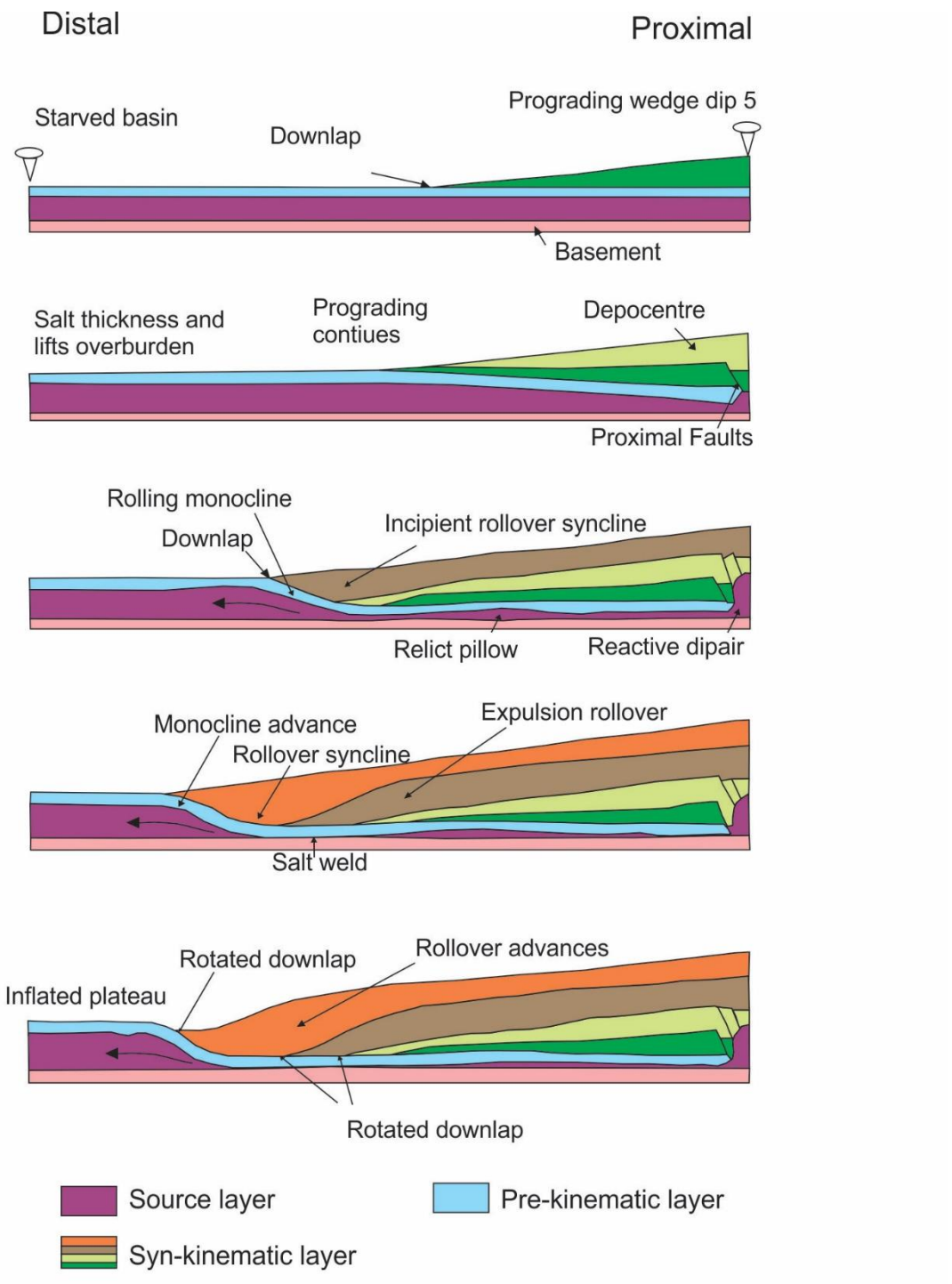

Figure 4.9 the evolution of a prograding wedge above a tabular salt layer, after Ge, *et al*., (1997)

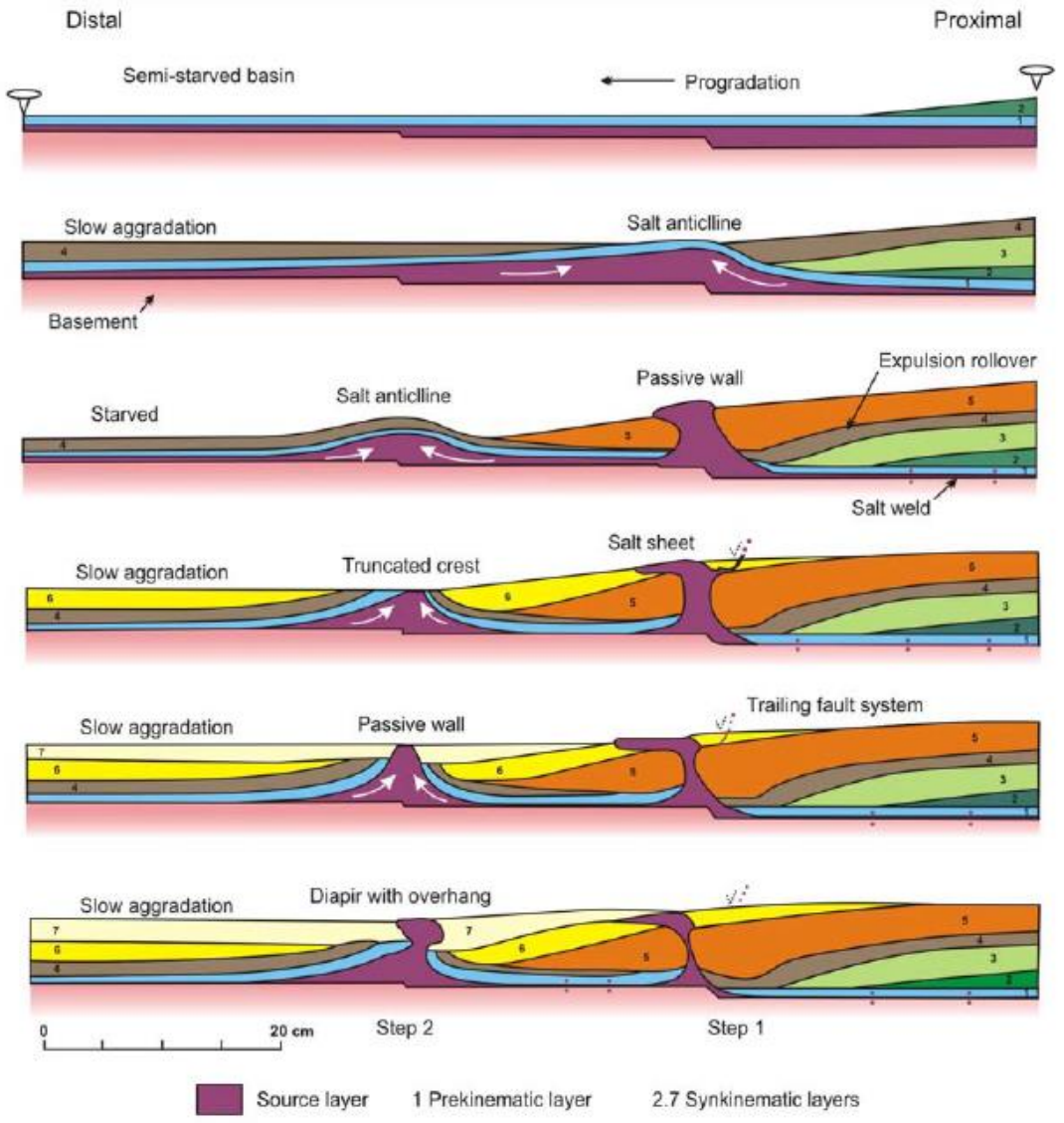

Figure 4. 10 Diapirs above basement steps during down dip salt migration . After Ge, *et a*l, (1997).

Salt's propensity to flow means that diapirs, initially formed by early progradation of a wedge of continental shelf or platform sediment, can be later reactivated or overprinted during extensional or compressional episodes. Differential loading is more efficient when the overburden is formed by carbonates rather than clastic sediments; carbonates are heavier than clastic since the onset of deposition (Jackson and Vendeville, 1994).

Figure 4.11 illustrates how dry and wet salt is much weaker than other sedimentary rocks, except for extremely shallow uncompacted shale (Jackson and Vendeville, 1994).

4.3.2 Salt Dissolution

Various authors have proposed that some salt structures have been produced by salt dissolution (e.g. Jenyon, 1984, 1986, 1988; Mart & Ross 1987, Clark, *et al*., 1999, Cartwright, *et al*., 2001). However, physical models and field examples have evidenced that these depressions are generally created by extension (Vendeville & Jackson, 1992a, 1992b). The role of salt dissolution has not been considered in most modern studies, but it is probably significant.

Ge & Jackson (1998) carried out a series of sandbox experiments to investigate the impact of salt dissolution on salt structures. They used a sequence of dry sand to simulate the overlying sequences and transparent polymer as an analogue for salt layers. Dissolution was recreated by the removal of polymer holes in the base of the salt sequence. I present a brief summary below:

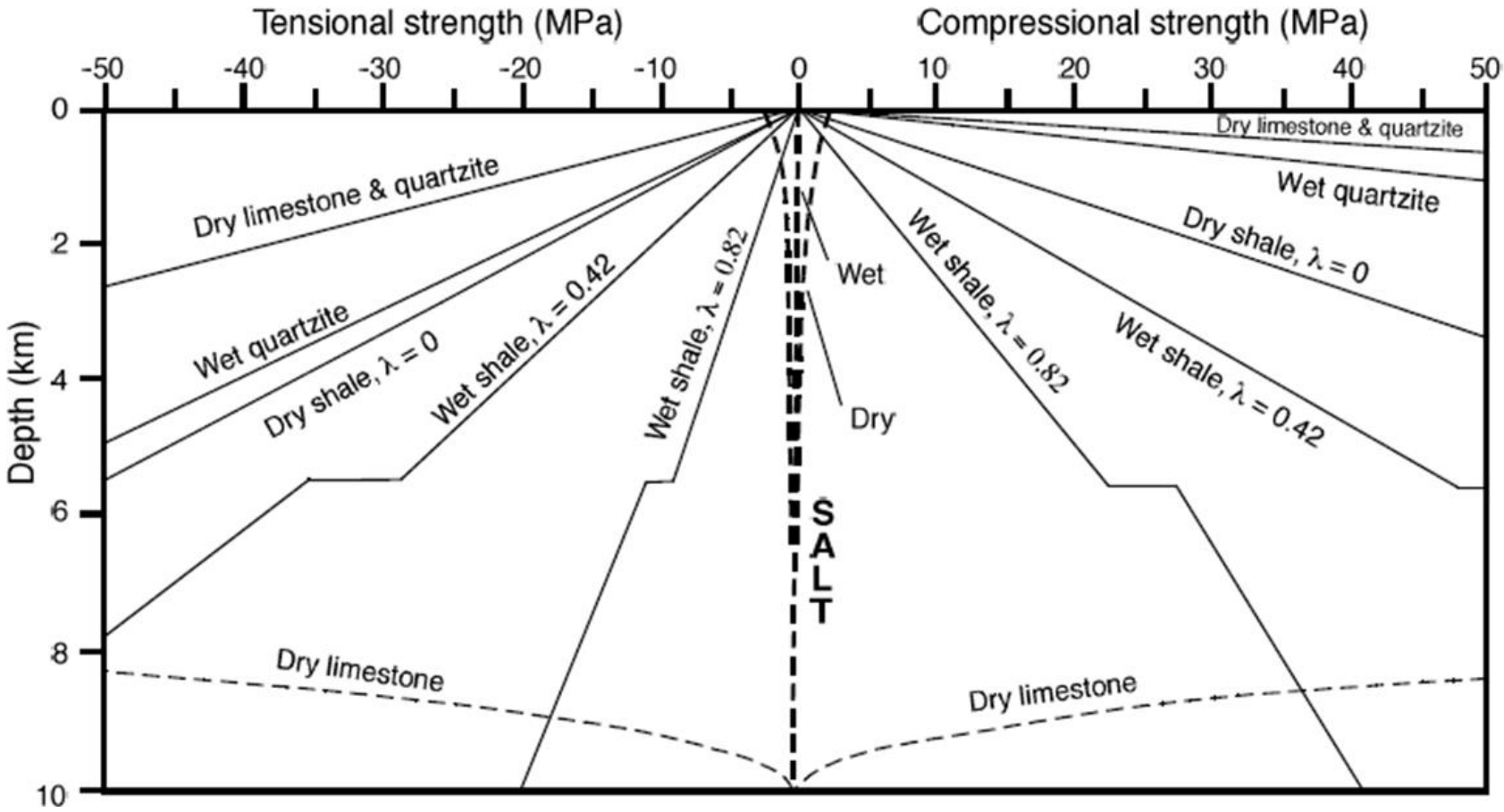

Figure 4.11 A plot differentiation of creep and frictional strengths of dry salt with equivalent strengths of dry and wet sedimentary rocks. Creep strength is the deviatory stress required to drive salt flow at a representative strain rate of 10 -14 s-1. Pore pressure coefficient is the ratio of pore pressure to lithostatic pressure: 0 for dry rocks, 0.42 for hydrostatically pressure strata and 0.82 for overpressure strata. In contrast, wet salt is so weak that its creep curve plots virtually on the central axis. (After Jackson and Vendeville, 1994).

The removal of salt resulted in the development of a syncline with a box geometry enclosed by a curved monocline.

- When a diapir walls is removed, it creates a depression. The trough is represented by internal contractional zone and external zone is characterized by extensional faults.
- The overlying sequence shows a series of stepped faults with a convex-up geometric profile.
- Reducing the size of the diapir or its dissolution is unlikely. For this phenomenon to take place, simultaneously.

Studies in the North Sea Central Graben area propose that the dissolution of Zechstein evaporites played a significant role (Clark*, et al*., 1999; Stewart, *et al*., 1999; Cartwright, *et al*., 2001). Accounting for the loss of almost 50% of the salt layer (Bishop, *et al*., 1996, Hossack, 1995). In Delaware Basin of Texas and New Mexico, it has been found that salt dissolution, reaching a value up to 50%, results from the activity of artesian groundwater (Jackson & Talbot, 1986). Salt dissolution has been reported on Cape Breton Island (Alsop, *et al*., 1996); and salt karst features have been observed in Yemen (Davison, *et al*., 1996 b).

The process of salt dissolution has three main consequences: (1) the formation of a cap rock crust (Clark, *et al.,* 1999), (2) the removal of large amounts of halite and (3) the formation of anhydrite. Salt dissolution occurs as a result of fresh or marine water mobilization through sediments during the first stage of salt deposition or around external salt structures (Warren, 1997). In addition, the compaction process and drying up of underground rocks ejects pore water and may contribute to driving ascending flow.

Salt dissolution has been studied in a regional basin level. The studies have suggested four principal mechanisms for salt dissolution (Fig.4.12). (Warren, 1997, Cartwright, *et al*., 2001):

1. Dissolution of the top of the salt dome due to the migration of under-saturated fluids.
2. Dissolution of the salt dome base due to the migration of fluids coming from sediment.

3. Dissolution of the salt mass due to the migration of fluid along the bottom and the side walls of the body of salt.
4. Dissolution of the salt body due to fluid migration producing compaction between evaporitic sequences interbedded with terrigenous sequences.

4.4 Halokinetic salt structures

4.4.1 Diapir Up growth

There are two mechanisms, which can explain the up growth of diapirs after their formation. These are downbuilding and upbuilding (Fig.4.13), (Jackson and Talbot, 1994). In downbuilding, the diapir increases in relief relative to the source layer, but the diapir top surface does not increases in relief come closer to the sediment surface. In upbuilding, the diapir increases in relief. The salt source layer remains at constant depth below the sedimentary surface, and the crest rises towards the surface.

The style of sedimentation associated with salt tectonism can be broken down into three groups: pre-kinematic, syn-kinematic and post-kinematic (Jackson & Talbot, 1994; Fig.4.14). Usually salt structures pass through three stages of growth: the pillow stage, the diapir stage and the post-diapir stage (Jackson & Talbot, 1994). These correspond to the evolution of salt structures described by Trusheim (1960). The pillow stage is characterized by the thinning of sediments over the crest of the pillow, and thickening into the adjacent primary peripheral sink. Depositional facies are affected by pillow growth, with higher energy facies developing over the crest. In the diapir stage, the salt body pierces the overburden. As the pillow withdraws to form diapirs, secondary peripheral sinks may develop close to the diapir, and inside the earlier primary peripheral sinks. Turtle structures, may also form during this time. During the post diapir, stage the diapir only continues to grow by thinning its lower trunk or by complete detachment from the mother salt.

4.5 Salt-related Depocenter and Minibasin Evolution

A salt-withdrawal minibasin is defined as “a syn-kinematic basin subsiding into relatively thick, allochthonous or autochthonous salt” (Jackson and Talbot, 1991. As their name implies, minibasins are much smaller than sedimentary basins, typically only a few tens of kilometers in diameter. However, they can subside several orders of magnitude faster than most crustal basins (up to 10 km/m.y. over short periods; Worrall and Snelson, 1989)

.

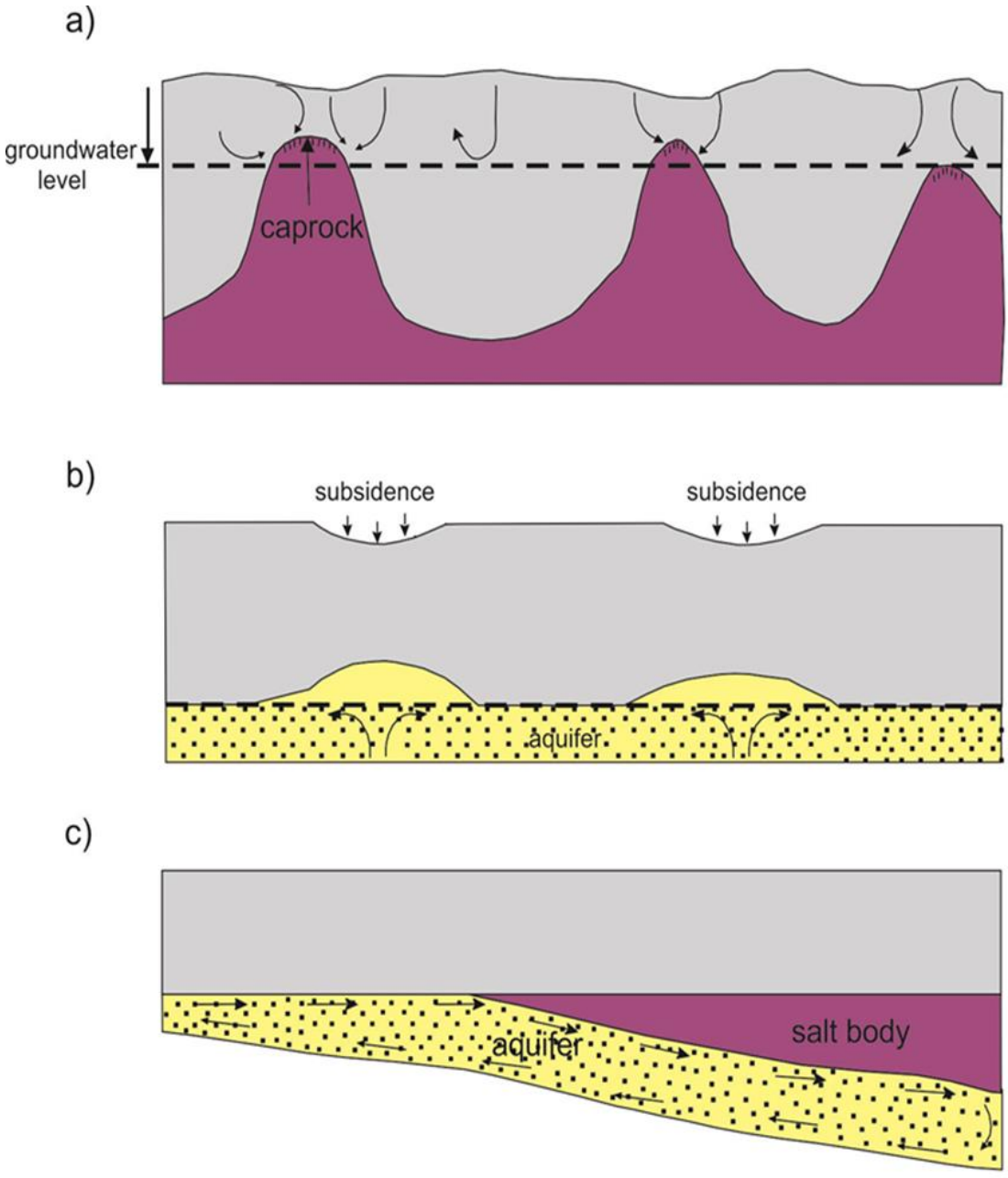

Figure 4.12 Different kinds of salt dissolution. (a) overlying dissolution consequential of ground-water penetration. (b) overlying dissolution, resulting from ground-water flow along sub-salt aquifer, and (c) Lateral dissolution, consequential from circulating along the lateral margin of the salt body after Cartwrigh (et al., 1999)

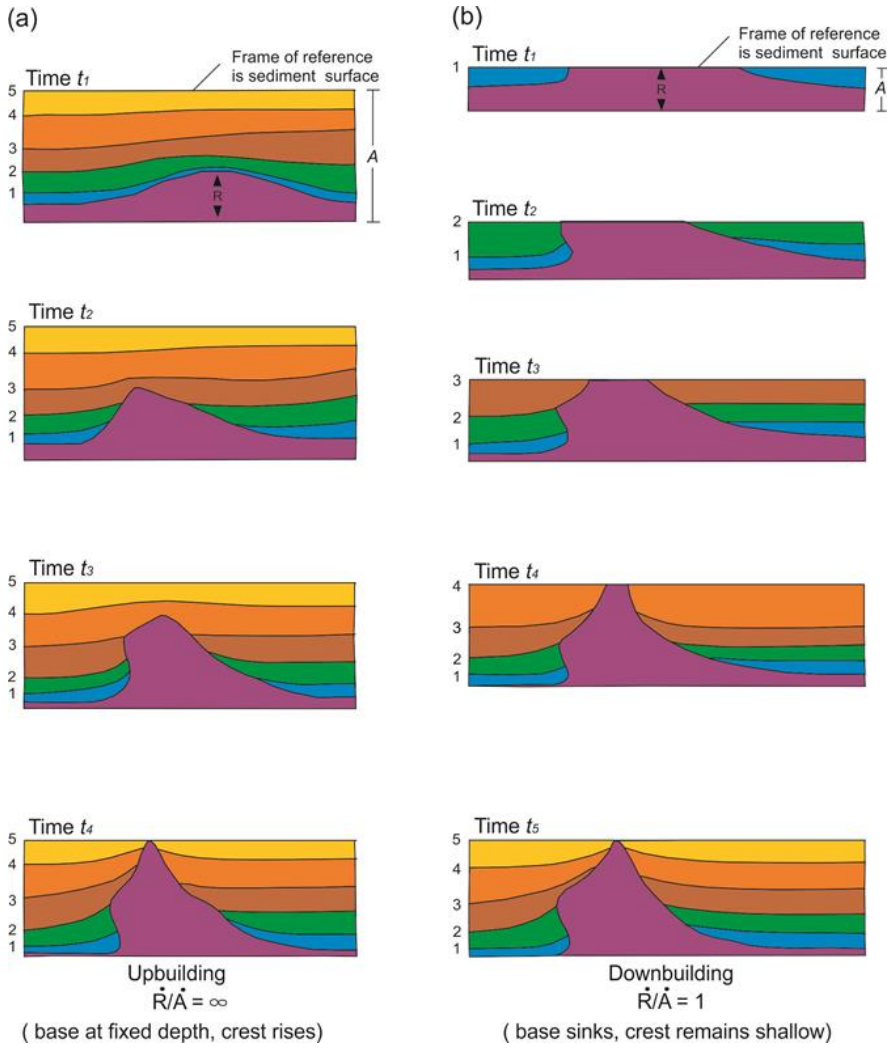

Figure 4.13 Two different modes of diapir growth downbuilding and up-building (after Jackson and Talbot 1986)

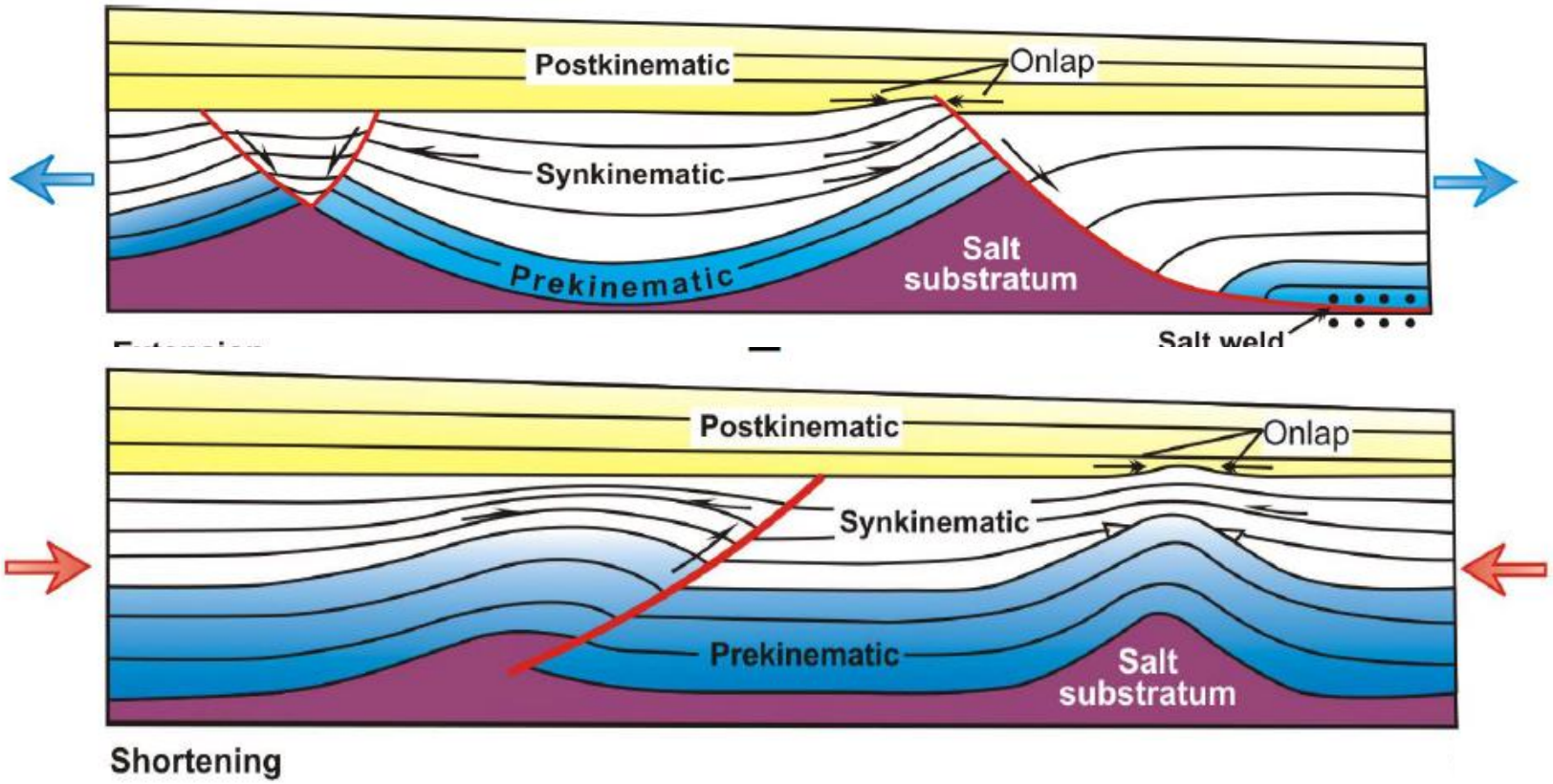

Fig.4.14 Synkinematic strata geometry in a) extensional and b) contractional setting (after Jackson and Talbot, (1994).

Subsidence rates of >1 km/m.y. can be sustained for several million years and have produced late Pliocene-Pleistocene minibasins up to 8 km thick. Salt expelled from beneath a minibasin wells up around the minibasin margin, forming a network of salt walls or massifs that partly or completely surround the minibasin.

The study of minibasins is not recent; Barton (1933) and Trusheim (1960) supplied a method for their analysis. Minibasins have been reported in many Mesozoic salt basins worldwide subsiding into relative thick, allochthonous or autochthonous salt (Hudec, *et al*., 2009). The best studied minibasins are located on the continental slope of the northern Gulf of Mexico, where minibasin depocenter have been observed sinking into thick allochthonous salt sheets (Bouma*, et al.,* 1978; Humphris, 1978, Humphris Jr, 1979; Bouma, 1982; Diegel, *et al.,* 1995; Prather*, et al.,* 1998; Rowan and Weimer, 1998; Beaubouef and Friedmann, 2000; Winker and Booth, 2000).

Minibasins undergo rapid sinking when sediments are denser than the underlying salt (density-driving subsidence). The final stage of minibasin evolution is achieved when it is welded to its base. The type of welding, depends on the geometry of the salt basin on which a particular minibasin was developed (planar base salt or into a funnel-shape feeder for a salt sheet) (Hudec and Jackson, 2011). After the basin welds, the core of the basin can no longer subside, so it remains high while its flanks continue to subside, leading to formation of an inverted (turtle) minibasin.

The discovery of giant oil fields in the margins of minibasins on the north of Gulf of Mexico slope have aroused great exploration interest (e.g., Holman and Robertson, 1994; Sawyer, *et al*., 2007). Turbid currents entering a minibasin may pond, overrun the barrier at the downslope end of the minibasin, or exit through a canyon along cut through the downslope barrier (e.g., Badalini et al., 2000; Beaubouef and Friedmann, 2000; Toniolo, *et al*., 2006a, 2006b).

Conversely, in Isthmus Saline Basin most of the discovery oil fields are located at crest of contractional diapirs. The development of salt anticlines into tall contractional diapirs created large intervening depocenter with up to 6 km of siliciclastic sediment thick.

In the ISB has been identified minibasins subsiding into relative welding, allochthonous salt and also subsiding over autochthonous salt located over Middle Miocene unconformity. In the last years, the interest of minibasin exploration has caused great expectative in the Isthmus Saline Basin focused on the stratigraphic margin of minibasins.

Most studies have focused on the stratigraphic aspects of minibasin evolution rather than the subsidence mechanisms for creating accommodation space. Hudec, *et al*., (2009) recognized six minibasin subsidence modes, which I summarize below (Fig. 4.15).

- Density-driven subsidence, the vertical stacking of sediments result in the faster sinking of depocenter than its thinner surrounding. The minibasin end sinking stage until the bottom of depocenter touches the base of salt, forming a weld.
- Diapir shortening, is represented by thrust fault within minibasin and strong lateral shift in depocenter during the contractional stage.
- During extensional processes, stretching of the entire salt structure. Extensional diapir collapse forms a minibasin above the salt regardless of the density of any sedimentary roof present.
- Decay of salt topography. In the course of establishing an allochthonous, salt sheet a salt bulge is generated on the surface. The bulge is developed by upward movement of the salt and, like a viscous fountain, spreads by gravity to drive sheet advance. When the salt source is exhausted, the salt bulge rapidly decays by gravity spreading. The salt sheet develops a bathymetric low which allows for the accommodation of sediments, forming a minibasin, which will subside regardless of sediment density.
- Sedimentary topographic loading, when sediments prograde over salt body, sediments laterally adjoin air and water, which are invariably much less dense. This differential loading causes the sedimentary wedge to subside, creating space for more sediment. Salt expelled from beneath the subsiding wedge may create a dynamically supported bulge in front of the wedge tip. The process continues until a minibasin welds onto the base of the salt body.

- Subsalt deformation affecting the base of salt may produce relief at the top of the salt due to subsalt normal faulting (e.g., Vendeville, *et al*, 1995; Schulz-Ela and Jackson, 1996). This type of minibasin is most common above autochthonous salt in basement-faulted terrenes, which control subsalt deformation, the sediment fill and the initiation of minibasin.formation. However, some minibasin overlies subsalt synclines, suggesting that down warping of the salt sheet initiated them.

4.6 Allochthonous salt structures

When salt moves away from its original source (the authochthonous), it is know as Allochthonous. Allochthonous salt sheets are sub-horizontal bodies of allochthonous salt that has moved above sediments that are younger than the salt source layer. The emplacement of most salt sub-horizontal diapirs starts either in the hanging wall of thrust faults or as extrusion from the top or rising diapirs. Salt sheets move in four patterns: (1) extrusive advance, (2) open-toed advance, (3) thrust advance, and (4) salt-wing intrusion (Hudec and Jackson, 2006; Fig. 4.16). These processes are characterized by the geometry and thickness of the ceiling above the advancing sheet. Models for salt-sheet advanced will be summarized below:

• Extrusive advance- occurs when salt flows and extends from a passive diapir feeder quicker than sedimentation, erosion, and dissolution can contain it (Talbot and Jarvis, 1984; Talbot, 1998). The advance of extrusive salt diapirs is a result of gravity spreading. Therefore, the process of extrusion closely related with the rate of sediment aggradation. If no sedimentation exist then salt will simply expand horizontally deposit, then salt will expand horizontally. This means, oscillation in the salt advance rate and sediment-aggradation rates can impulse salt sheet to climb up through ramps and flats. The allocthonous salt connects salt sheet diapirs, which may join to create salt canopies. Once the salt canopies are buried, salt canopy can advance only by thrusting close their borders.

• Open-toed sheet advance- the sheet is extrusive at its toe but is partly buried by a roof strong enough to modify the underlying salt flow. The roof

resists salt flow. Conversely, salt flow exerts traction on the base of the roof, which may be pulled apart by extension or crumpled against buttresses.

- Thrust advance- the salt diapir and its roof continue to move through a thrust fault plane. This process of advances is driven by gravity or by regional shortening. Salt geometry in an overthrusting salt diapir represents the edge of thrust, contrary to the sedimentation flow-influenced shapes of extrusive and open-toed sheet.

- Salt wing intrusion- occurs when a wedge of salt is emplaced into a thin pre-existing salt layer that shares a boundary with the diapir, although this is less common. The salt roof is uplifted as a detached anticline as result of contraction. The shortening cause folds to detach on the shallow evaporites, which become filled by the salt wings. The uplifting motive to onlap or erosion of roof strata. It is possible that these actions can occur several times during the growth of salt sheets to produce salt-sheet derivates. Three derivates are common: plug-fed extrusions, plug-fed thrusts, and source-fed thrusts. The description of these salt structures is based mainly on the shape of the feeder structure and how salt moves forward (Hudec and Jackson, 2006

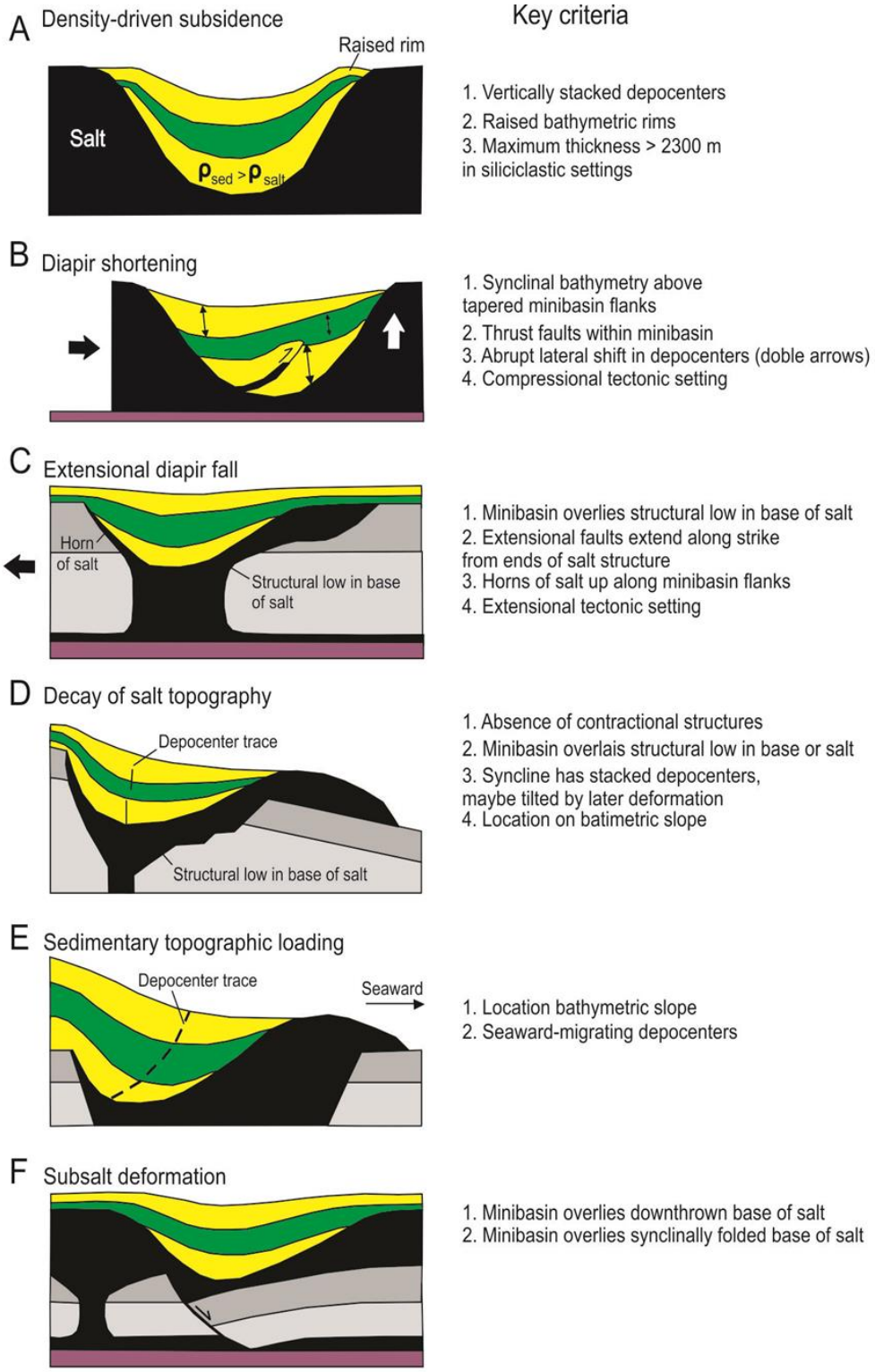

Figure 4.15 minibasin-sinking models and criteria used to discriminate between them (after Hudec, *et al.,* 2009)

4.7 Salt structures related to Regional Extension

Extensional tectonic regimes are more common in active rift basins and the external platform and upper slope of passive margins (Tankard and Balkwill, 1989; Jackson and Vendeville, 1994). Several specialized studies have proposed that regional extension is one of the main causes for salt deformation and evolution of salt domes. In the absence of precursor salt diapirs, the main control on the extensional structural style is salt thickness (Hudec and Jackson, 2007). When salt is present in thin layers, it usually works as a detachment surface, rather than generate diapirs or evacuation basins. Conversely, where salt is thick, diapir and evacuation salt basins are likely to develop (Hudec and Jackson, 2007).

Extensional tectonics can be described as either thick-skinned where the basement and sedimentary cover is involved, or thin-skinned where just sedimentary cover is affected. Extensional tectonics are established when σ1 is vertical and perpendicular to σ3 which is the minimum horizontal and less than the lithostatic stress. The geometric control exerted by the basement and the position of the

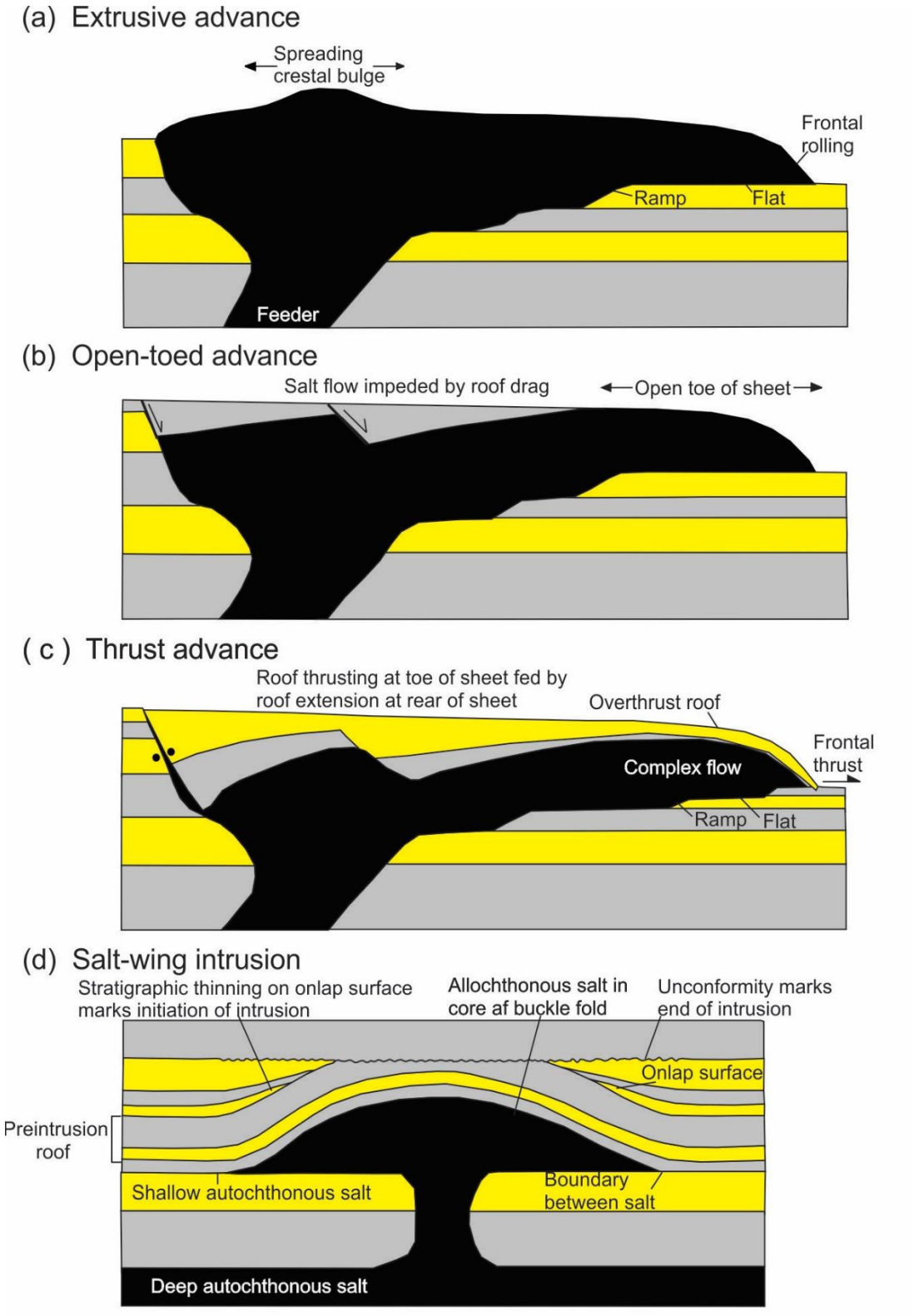

Figure 4.16 Schematic models that show four different ways of salt-sheet advance. (Modified from Hudec & Jackson (2006)

Salt have resulted in a classification based on the salt's position and age with respect to crustal sediments as: pre-rift salt, syn-rift salt and post-rift salt.

4.7.1 Thin-skinned extension

Vendeville and Jackson (1992a) described how regional extension and faulting of dense sedimentary sequence overlying a salt layer plays an important role in the growth of salt diapirs. Under regional extension, diapirs break through the overlying sequences in three different styles: reactively, actively and passively (Fig. 4.17; Vendeville and Jackson, 1992a; Jackson, *et al*., 1994a).

Reactive diapirism begins with the formation of a graben or half graben. A reactive diapir breaks through by filling the gap generated during the divergence of overburden blocks. During block divergence, salt comes near the surface under a subsiding thin-skinned graben. The continued extension may lead to the development of a salt diapir, in cases when the overlay is expanded by at least 20% (Jackson and Vendeville, 1994; Fig. 4.17 c). During salt uprising at the top, new faults are generated. Each fault cuts the overlying sedimentary sequence in minor blocks. The rate of sedimentation and the amount of divergence are the main controls on reactive diapirism. Rapid divergence and reduced speed of sedimentation result in a reduction of diapir room and formation of reactive diapir. Conversely, if divergence is reduced and there is an increased sedimentation, diapirism will be inhibited due to the thickening of the overlying sedimentary sequence and development of new structures such as growth faulting and salt rollers-sharp crested low diapirs (Jackson & Vendeville, 1994). In summary extensional faulting is a successful mechanism for starting diapirism, regardless of the former overlying sedimentary sequence thickness, type of lithology or density (Vendeville and Jackson, 1992a, b). Whenever the regional divergence ceases, reactive diapirism will also end.

Active diapirism, takes place when the pressure at the diapiric crest allows lifting and pushing the thin overlying sedimentary sequence, generating the rotation and dispersing the remains of its roof while dragging up adjoining strata. The diapir requires powerful intrusion to remove the roof of sediment on top of salt, which is relatively thin. The roof must be attenuated, by at least 20% of the entire thickness of the overlaying diapir border (Jackson, *et al*., 1994b).

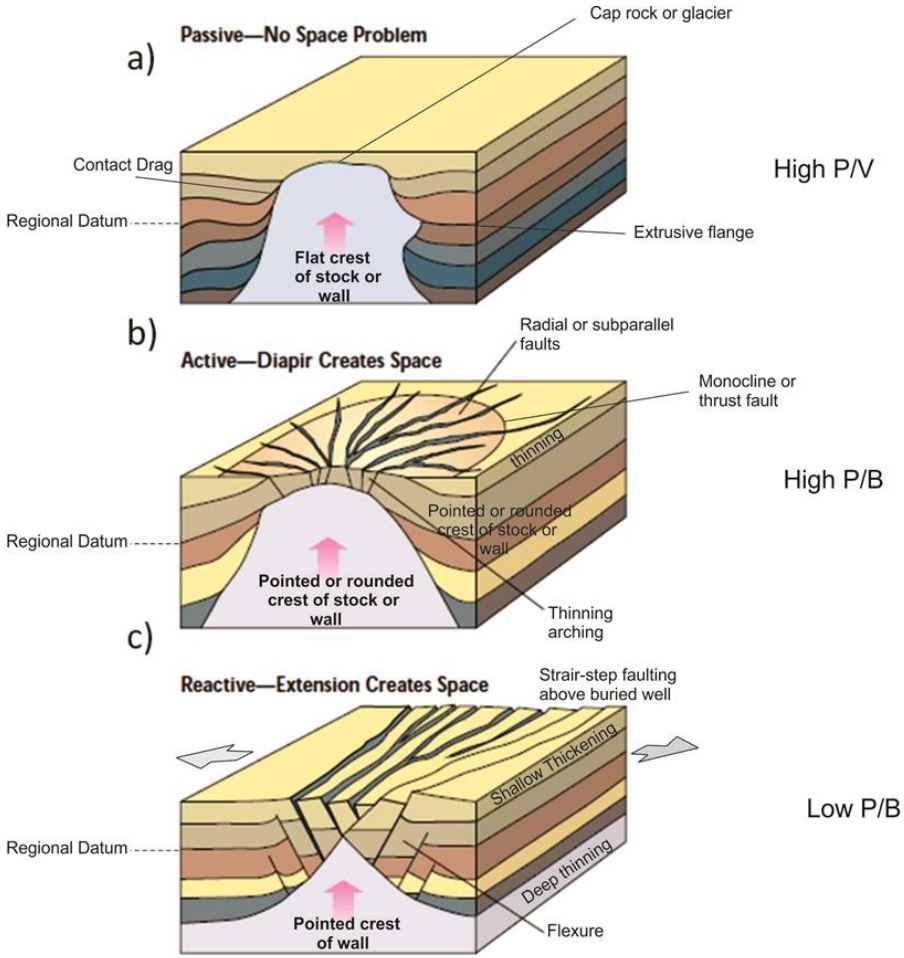

Figure 4.17 Piercement modes for diapirs (grey) and their characteristics structures. Regional datum (dashed line) is the base of stippled layer. P, V and B refer to stresses due to salt pressure, salt viscosity and overburden strength, respectively (after Jackson, *et al*., 1994).

This generally happens when divergence and reactive growth is much faster than sedimentation and is controlled mainly by salt viscosity (Jackson and Vendeville, 1994; Fig.4.17b)

When a diapir or salt wall forms and moves upwards towards the earth's surface it becomes a passive diapir, usually edged by salt allochthonous. Its edges extend and fall down under the weight of the expelled salt mass. The diapir grows taller by downbuilding during continuous sedimentation without any faulting or thickness changes. If the salt supply is subsequently, exhausted gravity spreading may cause the diapir to collapse (Vendeville and Jackson, 1992b). When the raising of salt is not vertical restricted during the passive phase, there is no need for the rotation, faulting or movement of flanking strata as is the case during active diapirism. When the source of salt is exhausted, diapirs stop growing and a burial process begins as a result of the high rate of sedimentation. The geometry of passive diapirs is closely related with the rate of salt flow and sedimentation (Fig. 4.17a).

The succession reactive-active-passive can be changed by modification of the speed of divergence, reduction of the salt source layer or alteration in sedimentation variations. This means that diapirs can follow various evolution paths (Jackson, *et al*., 1994).

Jackson and Vendeville (1994) conducted a series of analogue experiments, proposing four different mechanisms for the formation of diapirs (Fig.4.18).

The initial experiment, (Fig. 4.18a), simulates both basement and sedimentary sequence to be spread out separately over and beneath the salt layer. The depression in the overburden triggered a salt diapir, while the deep basement through acts as a basin for the salt, causing the overlying to fold into a gentle syncline. In the second experiment (Fig. 4.18b), the evaporite layer is deposited over a basement fault and beneath in part separated pre-rift overlay. This resulted in draping of the pre-rift cover monoclinally over the syn-rift normal fault. Stretching of the outer arc of the monoclinal drape created a depression in the overburden, which started a diapir. The third model (Fig. 4.18c), is

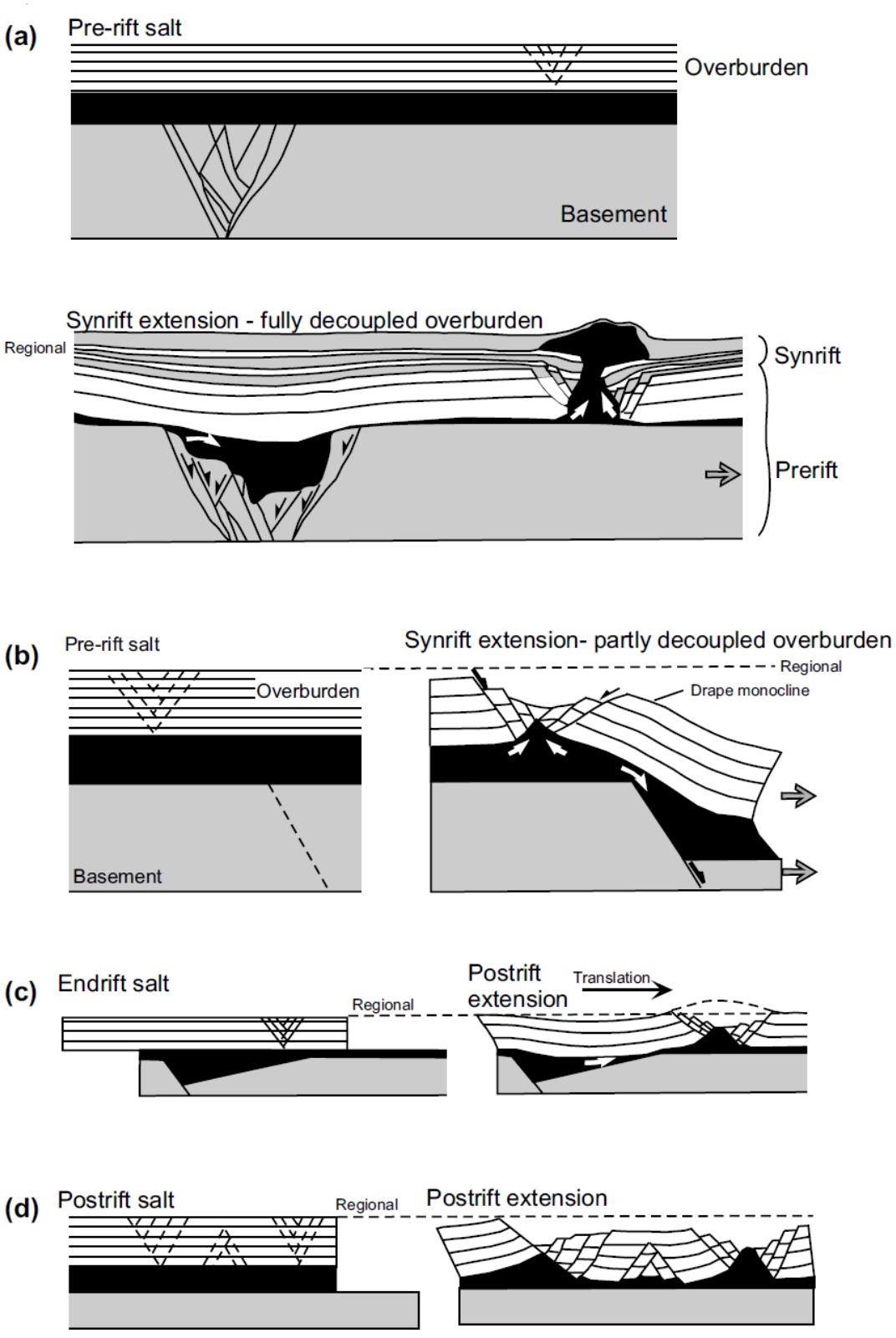

Figure 4.18 Thin skin extensions as a trigger mechanism for diapirism. After Jackson and Vendeville (1994).

represented by a half graben which is characterized by a depression for the evaporite layer, salt accumulates during rifting by filling depressions on the faulted surface. Extension of the overburden mainly by gravity spreading without any deformation in the basement leads to movement of the overburden basin-wards and deformation into a series of broad wavelength buckle folds. The salt flows to fill in the graben and the overburden subsides over the thick part of the half graben. The last stage of the experiment (Fig. 4.18d) shows how the overlying sedimentary sequence spreads out without basement faulting control. Diapir will grow to fill up the space generated by the depression development.

The importance of understanding salt diapir evolution for exploration is summarized below (Vendeville & Jackson, 1992a):

- The initial reactive phase is associated with a regional fault system
- The reactive phase may be accompanied by increased sediment accommodation space above the diapir.
- Beds will be truncated by the salt or pinched out abruptly when adjacent to the salt during the active phase. The zone of steep dips adjacent to the salt can be relatively narrow.
- Beds will thin more gradually over the salt during the passive phase and the zone of step dips adjacent to the salt can be relatively wide.
- Unlinked, crestal collapse faulting due to flexing above the salt is often more common during the passive phase.

4.7.2 Thick-skinned extension

Strictly, thick-skinned extension refers to the stretching of the entire column, including the basement and the sedimentary sequence. For the purpose of salt tectonics, "thick skinned extension" is taken to mean any situation in which the strata below the ductile salt layer experience extension, regardless of whether these include the crystalline basement. Several studies explain how basement faulting controls the initiation of diapirism (Parker and McDowell, 1955; Vendeville, 1991; Koyi, 1991; Richard, 1991; Withjack and Callaway, 2000). Parker and McDowell (1955) considered that, basement faults with less displacement than the thickness of salt layer could form monoclinal structure in

the upper block due to faulting. Laboratory experiments show that the viscous material moved from the bottom to areas of lower pressure on the upper block. Figure (4.19) shows different stages of evolution of salt diapirs due to faulting of the basement.

Basement faults have impact the sedimentary sequences above the detachment layer in two different ways: by length of line balance and by local tilt. As basement extends through divergent faulting, the surface above basement must also spread out (Fig. 4.19).

Consequently, both basement and overburden faults may be displaced but connected to the detachment surface of salt. With continued extension of the basement, the detachment surface will be offset by basement fault, connecting directly to the surface of salt (Koyi, *et al*., 1993; Jackson and Vendeville, 1994; Stewart, *et al*., 1996 and 1997, Withjack and Callaway, 2000).

The impact caused by the continued divergence of the basement generates the progressive rotation and inclination of the detachment surface as well as sedimentary cover, in some cases leading to gravity sliding (Withjack and Callaway, 2000).

Koyi, *et al*., (1993) investigated the parameters that control the structural relationship between the basement and sedimentary cover when a detachment layer is present. The boundary conditions studied include basement fault slip vector, basement fault dip, fault slip rate; evaporitic layer thickness, proportion of salt layer thickness to basement fault displacement, and proportion of salt layer thickness to cover thickness.

Withjack and Callaway (2000) demonstrated that high angle basement faults reduce the width of the deformation zone within the overburden and the distance between the deformation zone and the tip of the basement faults (Fig.4.19). They also found that, the effect of basement faulting in the fragile overlying uplifted blocks results in the formation of a depression.

4.8 Salt structures related with Regional Contraction

Contractional salt tectonics is related to convergent processes (including transpression), inverted rift basins and the lower slope of passive margins (Letouzey*, et al*., 1995; Rowan, *et al*., 2004). In convergent regimes, hundreds of kilometer of shortening can be accumulated at plate boundaries. In deepwater fold belts within passive margins shortening is typically limited to a few tens of kilometers (Rowan et al., 2004; Fig.4.20). Shortening requires either the minimum principal stress (σ3) or the intermediate principal stress (σ2) to be vertical. The first causes shortening while the second results in transpression.

Regional shortening can be either thin-skinned (involving the cover) only or thick-skinned (involving the basement). Faults formed during thick skinned shortening tend to be characterized by higher dip angle than those formed as a result of thin-skinned deformation or a combination of both. There is a big structural contrast between the style of fold and thrust belt underlain by a salt décollement layer and not underlain by a salt layer (Fig.4.21), (Letouzey, *et al*., 1995; Rowan, *et al*., 2004). These contrasts can be synthesized as follows under the presence of a salt detachment layer (Davis and Engelder, 1985; Jackson & Talbot, 1986, 1994):

- In a contractional system folding is more common than thrusting
- There is no preferential vergence of folds and thrusts.
- Low angle cross-sectional taper wedges result in extremely broad fold and thrust belts.

Contraction (shortening) can initiate diapirism. When shortening occurs above a salt décollement, simple detachment folds typically form. If the overburden is eroded and/or weakened by faulting, salt may break through to the surface (Sans & Koyi, 2001). Any further upward movement of salt will result in an allochthonous salt sheet (Hudec & Jackson, 2006). In contrast, if the overload sequence is not affected by erosion piercement is generally prevented.

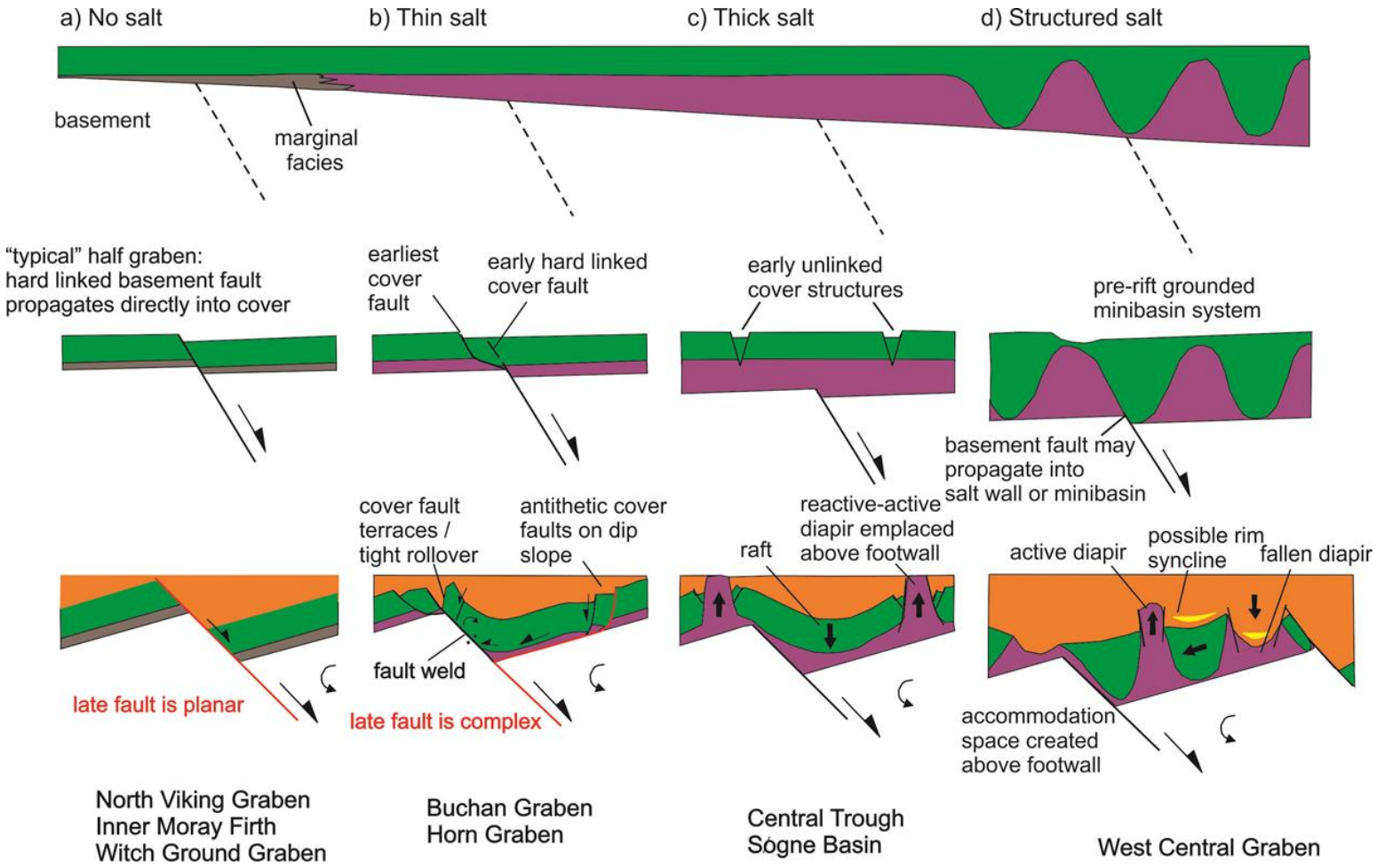

Figure 4.19 Thick skin extensions on halokinesis a trigger mechanism of salt structures. After Stewart (1999).

Letouzey, *et al*. (1995) analyzed, through laboratory experiments, three styles of compressional salt tectonics (Fig.4.22):

- shortening at the toe of prograding and gravity-gliding systems (thin-skinned)
- thin-skinned deformation found in fold and thrust belts
- Intracratonic inverted basins with basement involvement (thick-skinned)

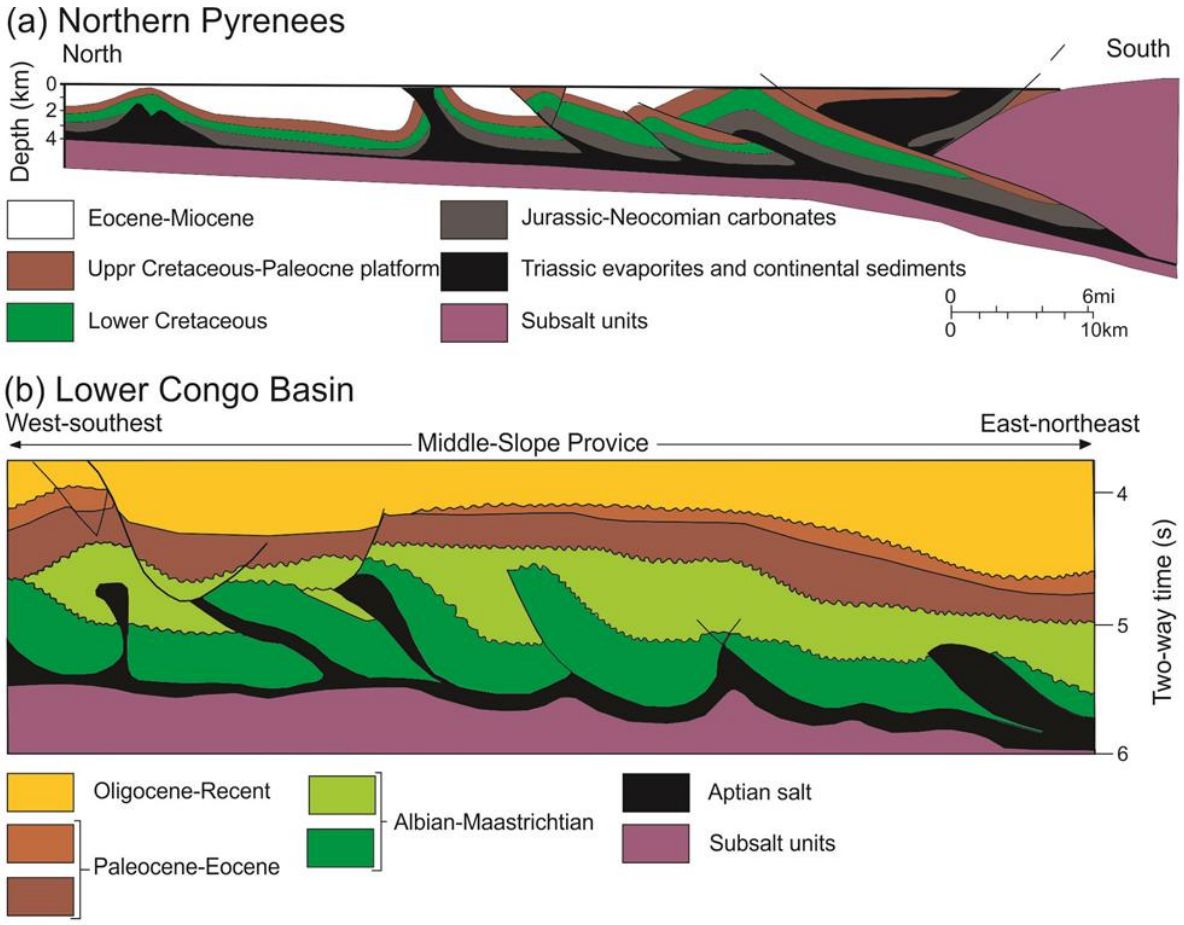

Figure 4. 20 Salt compressional structures in orogenic belts and passive margins (a) overcharged salt, squeezed compressional diapirs and fold diapirs at the north of Pyrenees (Hayward and Graham, 1989); (b) thrust and anticline diapirs squeezed in the lower slope in the passive margin of Angola (Cramez and Jackson, 2000)..

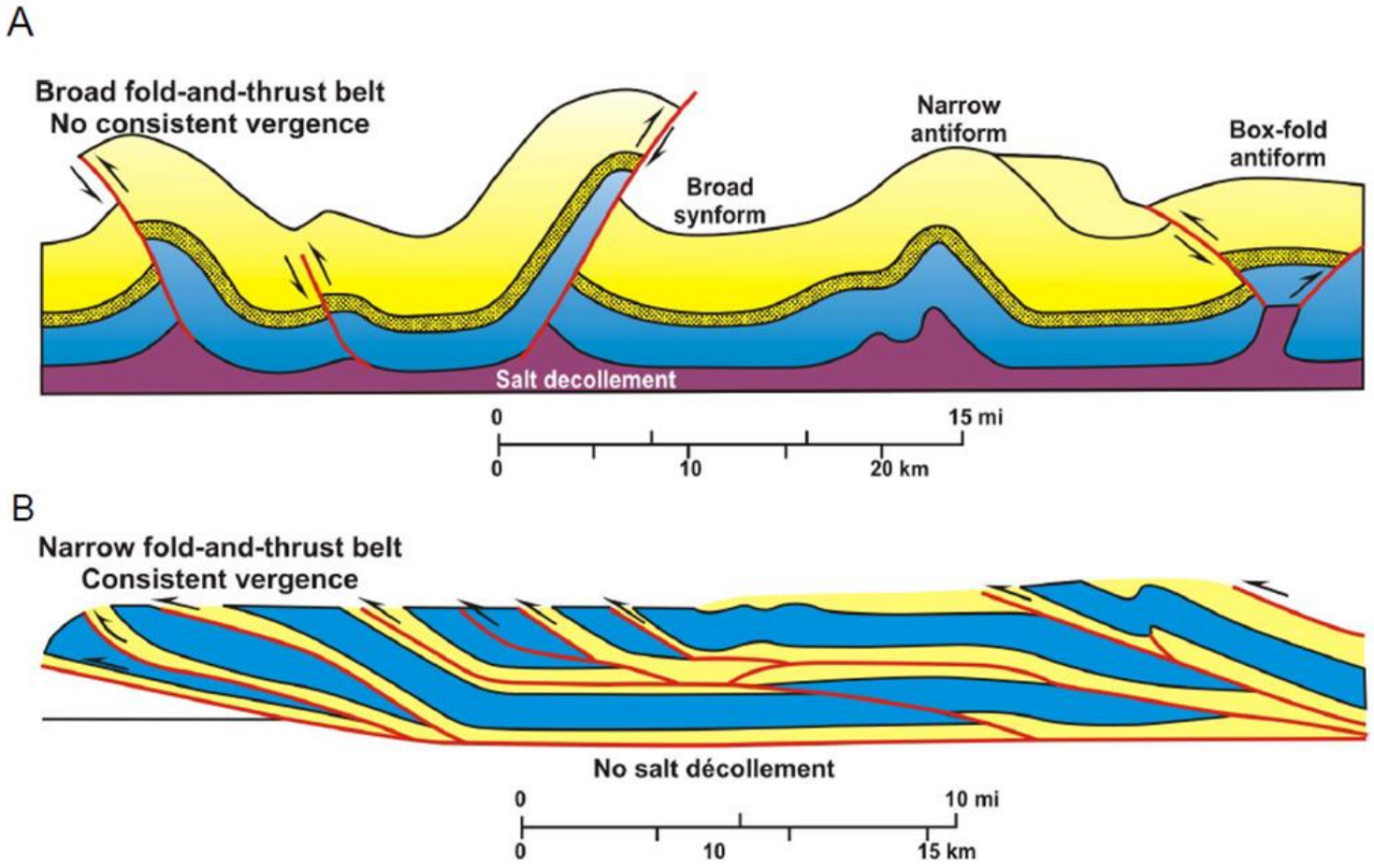

Figure 4.21 Comparison between structural styles in folds and thrust belt underlain by (A) salt, (B) not underlain by salt. After Jackson and Talbot (1994).

These studies demonstrated that the presence of salt exerts a crucial influence in the in style and in the development of contractional structures. Furthermore, they demonstrated that the structural configuration of fold belts, as well as the propagation of deformation and deformation style is intrinsically linked to the weak salt décollement and the friction coefficient along the detachment (Colleta, *et al*., 1991; Calassou et al., 1993).

Several experiments have shown that surface detachments associated with a lower basal friction coefficient often result in low angles deformation or lower coulomb wedge taper angles and thinner cross section. These features are manifested in the easy propagation of the deformation into the basin, creating wide folds and thrust belts (Davis, *et al*., 1983). This style of thrusting over a salt layer is observed in many basins such as the Jura Mountains in France and Switzerland (Philippe, 1994) and the Zagros in Iran (Farhoudi, 1978) where the deep Precambrian age Hormuz Salt acted as a décollement.

Jackson and Vendeville (1994) discard regional compression in fold and thrust belts as a mechanism for salt diapirs initiation. They suggest these types of salt structures form in divergent systems before the onset of shortening. Sand box experiments carried out by Vendeville (1991) showed that buckling of the overlying could not generate diapirs. Salt could diapirically escape from anticline cores if (a) the anticlinal top was eroded or thinned as a result of local divergence and (b) the anticlinal crest was thinned and pressurized as adjoining synclines grounded onto the basement and blocked lateral escape of salt. He concludes that thrusting is a more likely mechanism for diapir formation than buckling.

4.9 Summary

The properties of salt are unique. There are forces acting on salt that contribute to its ability to flow, as well as mechanical properties that restrict salt's flow.

Salt properties drastically influence the type of deformation. The very low friction coefficient of salt layers and weakness of salt induces a symmetric stress system. This results in the development of pop-up structures rather than asymmetric thrust faults.

The structural style in fold belts with or without salt décollement surface is substantially different.

Shortening and extensional collapse may occur above salt or overpressure shale detachment sequences.

Salt is the main detachment level between the folded cover rocks and the underlying faulted basement (in the ISB). However, thin and thick skinned deformation controls the formation and geometry of structures.

Whether a particular region has undergone extension or shortening will determine the resulting structures.

Structural styles on extensional deformation are linked with down dip contraction through a small deformed transitional zone.

There are many types of salt structures including diapirs, sheets, pillows, and glaciers.

The morphology and geometry of salt diapirs can follow different evolutionary paths through time.

Salt sheets geometry is dependent on the mechanism of salt advances.

Several mechanisms may lead to minibasin subsidence. Each mechanism produces a different pattern of facies in particular to each type of minibasin. Minibasin subsidence depends on the tectonic environment, regional bathymetry, and sedimentation rate.

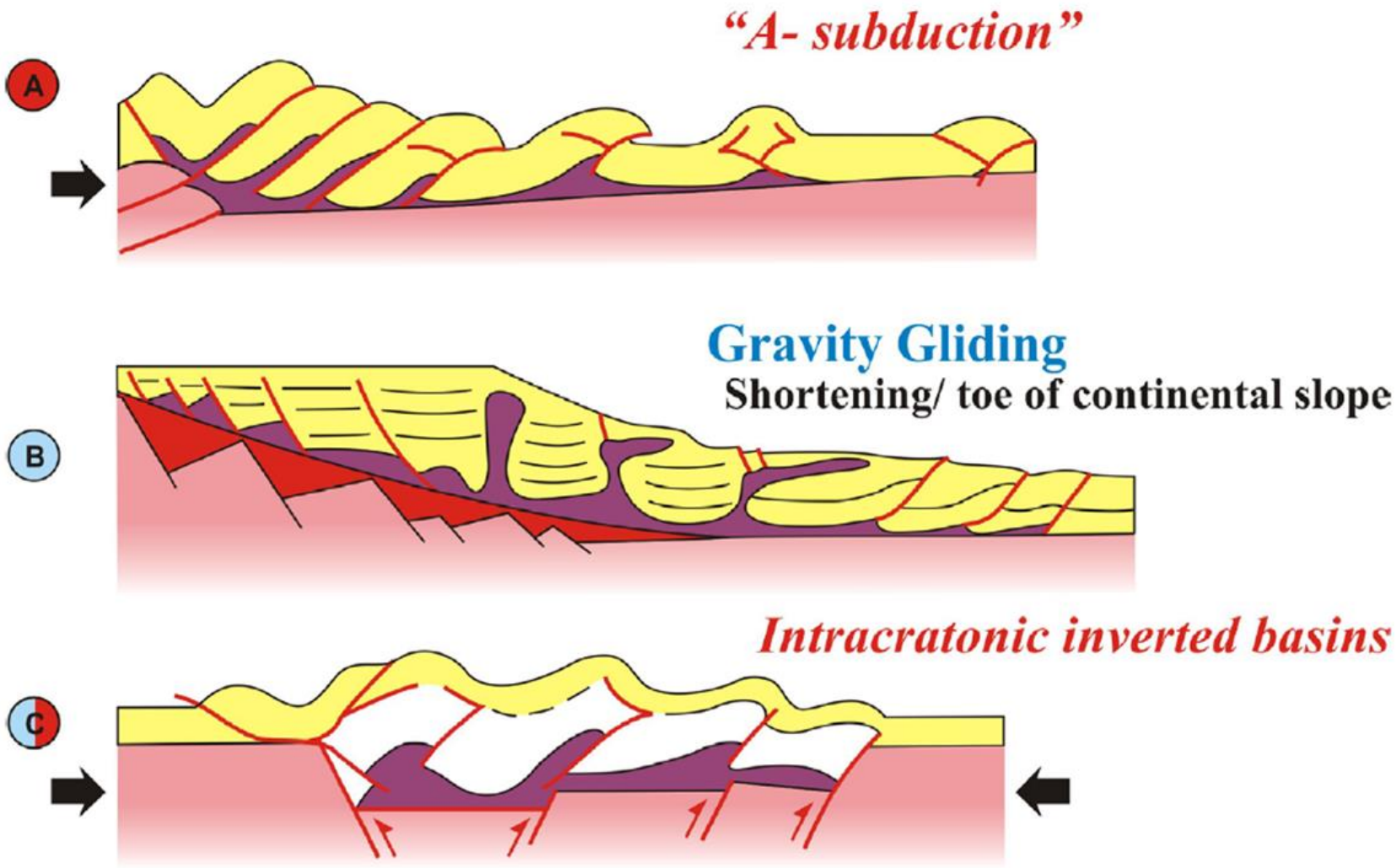

Figure 4.22 Thin skinned deformations in front of fold and thrust belt. A) Shortening in the upper fold belt, B) Gravity gliding related to shortening at the toe of continental slope. C) Inverted Intracratonic basin. After Letouzey, *et al*. (1995).

Chapter 5 Data and Methods

5.1 Introduction: The Dataset

This study is based on the analysis of 3D seismic data and integration of 2D seismic images from Isthmus Saline Basin (Figure 5.1).

Petroleos Mexicanos provided a series of datasets, consisting of:

2D and *3D* seismic surveys, covering approximately 2479 km^2

Approximately 800 km of regional, semi-regional and detail *2D* seismic lines images

15 composite well logs with paleontological control;

Gravity and Magnetic surveys, over the region

The following sections briefly sum up this data, before discussing the complication associated with the interpretation of salt-structures using subsurface data, and the process of seismic interpretation used in this research.

5.2 Seismic Data

5.2.1 3D Seismic Data

The two 3D seismic datasets available to this research was supplied by Pemex-Exploration and Production and cover mature salt diapir area with their associated deep-seated structures. The seismic surveys cover a range of structural settings from both the West and East of Isthmus Saline Basin.

Table 5-1 describe the survey size, line spacing, sample rate and seismic processing format of the 3D seismic volumes used during the interpretation process.

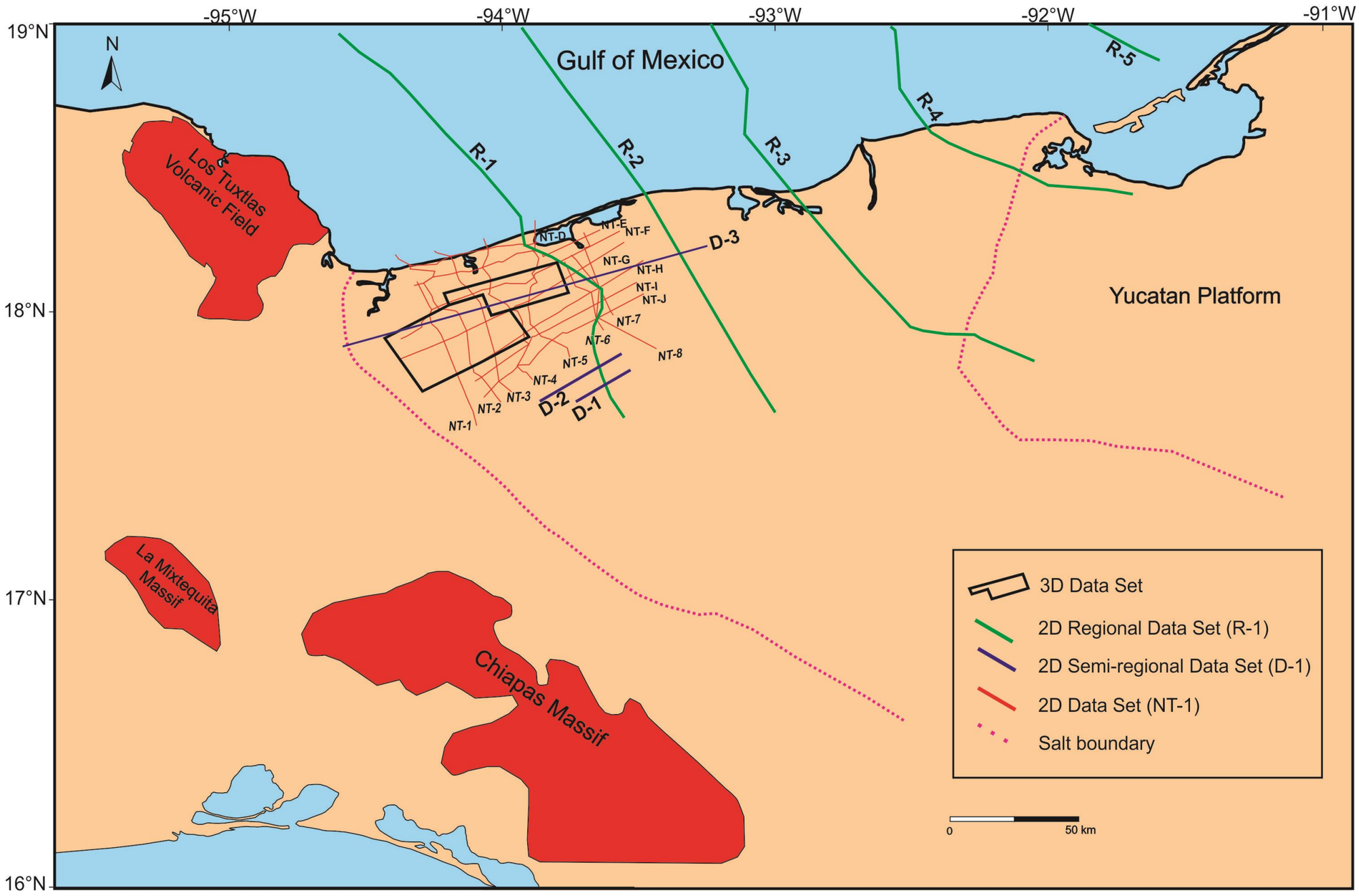

Figure 5.1 Distribution of 3D and 2D seismic data.

Survey	Size	Line Spacing (XLN/ILN)	Sample Rate	Seismic type available	Vintage (acquired/processed)	Format used for Interpretation
Cabritos	923 km^2	25 * 25	4 ms	PSDM Beam	2006/2011	PSDM
Tepetate	1556 km^2	25 * 25	4 ms	PSDM Beam	2011/2012	PSDM

Table 5-1 3D Seismic Survey Details

5.2.2 What do the survey shows?

The Tepetate 3D survey located in the west of Isthmus Saline Basin cover salt thrust fault structure surrounded by large depocentres.

The Cabritos 3D seismic survey highlighting five mature-morphology salt diapirs with small dimension depocentres.

Overall analysis of seismic surveys was done using detailed geological sketches in order to define the geometry of the salt diapirs, which have undergone different stage of deformation. Despite 3D seismic surveys is still challenging to understand salt deformation. Hence, seismic correlation during interpretation stage was difficult.

5.2.3 2D Seismic Data

Approximately 800 km of regional 2D time migration seismic images was available to this study (Table 5.2). This data was used to establish the regional tectonic framework and to gain a further understanding within Isthmus Saline Basin not covered by 3D survey data. These three sets of 2D seismic data helped to define boundaries between contractional and extensional domains. The interpretation was based on geological sketches, with the purpose to relate the position of salt diapir with the basement. The quality of the seismic data is good on Cenozic sequence but chaotic at the dipiar flanks.

Map Reference (Figure 5.1)	Name of Line	No. well used by section
NT' s sections Dip lines (trending approximately)	NW-SE	
1	NT-1	8
2	NT-2	17
3	NT-3	13
4	NT-4	21
5	NT-5	23
6	NT-6	2
7	NT-7	2
8	NT-8	3
NT' s sections Strike lines (trending approximately)	NE-SW	
D	NT-D	8
E	NT-E	8
F	NT-F	12
G	NT-G	4
H	NT-H	2
I	NT-I	3
J	NT-J	9

Table 5-2 Regional 2D Seismic lines and 165.wells used in the research.

5.3 Well Data

During the construction of the NT s sections, 110 well logs composites were compiled to establish a stratigraphic and depositional environment correlation (Fig. 5.2). The Isthmus Saline Basin is a Tertiary basin, which has stratigraphic and paleontological control available for the seismic correlation. The Neogene stratigraphy varies from deep-water to transitional sediments associated with compressional-extensional salt-related tectonics. The first exploration well was drilled in 1907 targeted at Late Miocene and Pliocene sands overlying salt diapirs. Mainly, the production of hydrocarbons in the basin is associated with Late Miocene

- Pliocene turbidites and wave dominated sand delta deposited above salt diapirs. Most recently, a successful well was drilled beneath salt canopies opening up new areas of opportunity for exploration. Due to this scarcity of Paleogene data, the identification of seismic horizons was often accomplished by correlating with regional sections.

5.4 Gravity and Magnetic Data

This research involves the interpretation of magnetic and gravimetric data of Southeastern Mexico. The analysis take into account the surface geology, analysis of seismicity, seismic and subsurface data available to delimit blocks of the basement at the regional level. Regional and semi-regional gravity and magnetic dataset was available to this study. Regional isostatic gravity and total-intensity magnetic data was compilated from Hudec*, et al*., (2013) as well as the PEMEX-potential methods dataset. CAASA company recorded the PEMEX-potential methods dataset in 1982. To date, gravity and magnetic data have been of limited use in identifying structural boundaries in the southern of Gulf of Mexico.

5.5 Earthquake Data

Database compilation found on the Internet Geological Survey (USGS), the National Seismological Service, the site of Civil Protection of the State of Chiapas and publications. Guzman-Speziale (1989) performed and catalogue "One Hundred years of seismicity in Mexico" of the Institute of Geophysics of the UNAM (1999). With the data obtained database containing the date, the position of earthquake, latitude, longitude, depth and magnitude. Approximately, 3200 earthquakes were collected from 1900 to 2002. For interpretation, were constructed a series of maps, showing the location and earthquakes depths.

5.6 Seismic Data Quality

5.6.1 3D Seismic Data Quality

The quality of the 3D seismic datasets varies significantly. All seismic data, show considerable degradation of imaging with depth, which represent a big problem for interpretation. Additionally, the data set have the further problem of significant image

degradation proximal to near vertical salt structures. Examples sections are shows in (Figure 5, 3).

While each of the seismic surveys used by this research successfully images the Paleogene to Recent interval, the quality of the seismic image varies significantly.

The Mesozoic section in the surveys is less clear, and the volumes exhibit the greatest degradation of seismic image with the Mesozoic interval.

The seismic image reaches up to 15 km; however, the pre-Jurassic salt interval is almost acoustically transparent in the Isthmus Saline Basin. Whilst real reflectors are occasionally imaged, these remain relatively weak in character and are often swamped by multiples and artefacts. As a result, discerning the geometry and lateral extent of pre-Jurassic salt reflectors is extremely difficult, and it has not proved possible to tie around a pre-Jurassic salt horizon in any of the areas examined by this research.

The depth to which the boundary between the pre-Jurassic and Callovian salt intervals has been buried in the Isthmus Saline Basin prevents clear imaging of this horizon in any of the seismic surveys examined by the study. Thus, the evolution of the mobile Callovian salt layer cannot be directly interpreted, and must be inferred from the deformation and syn-kinematic evolution of the post-salt overburden

5.6.2 Regional 2D Seismic Data Quality

The regional 2D seismic lines available to this research in image vary significantly in their quality. The lines are varying quality, and the difference acquisition and processing parameter of each survey offers a different quality of image with respect to the deeper (Fig. 5.4). Seismic sections used in this project were acquired with shallow objectives, so the deep part is not very clear. Therefore, due to the significant depths to the Callovian salt in the deep basin, exploration activity has conventionally focused on shallower intervals. As a result, most seismic section are optimised for the imaging of relatively shallow structures, and complicated, costly,

processing methods such as pre-stack time migration rarely incorporate data from greater than time 3-5 second (TWT).

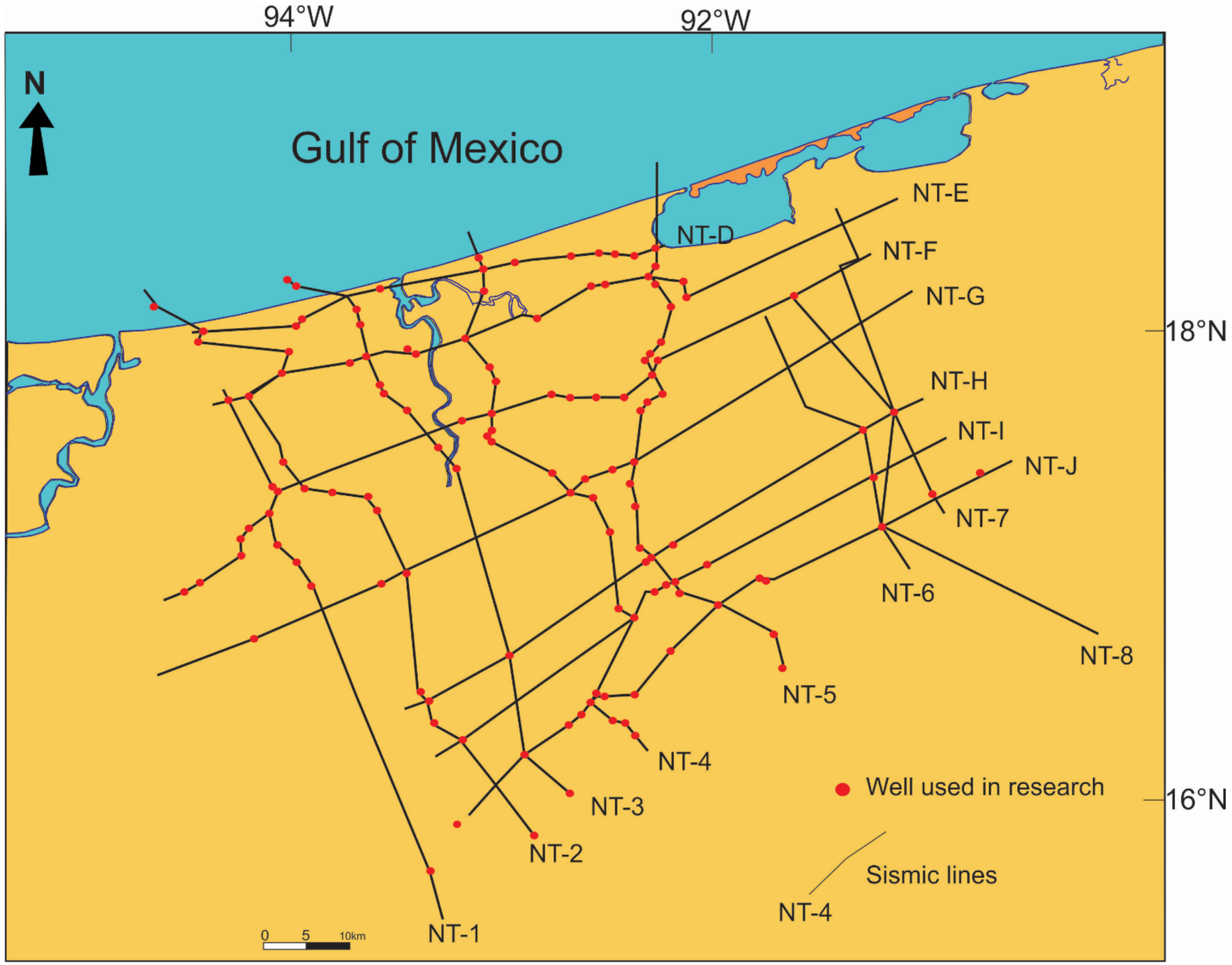

Figure 5.2 Location of well used for seismic correlation.

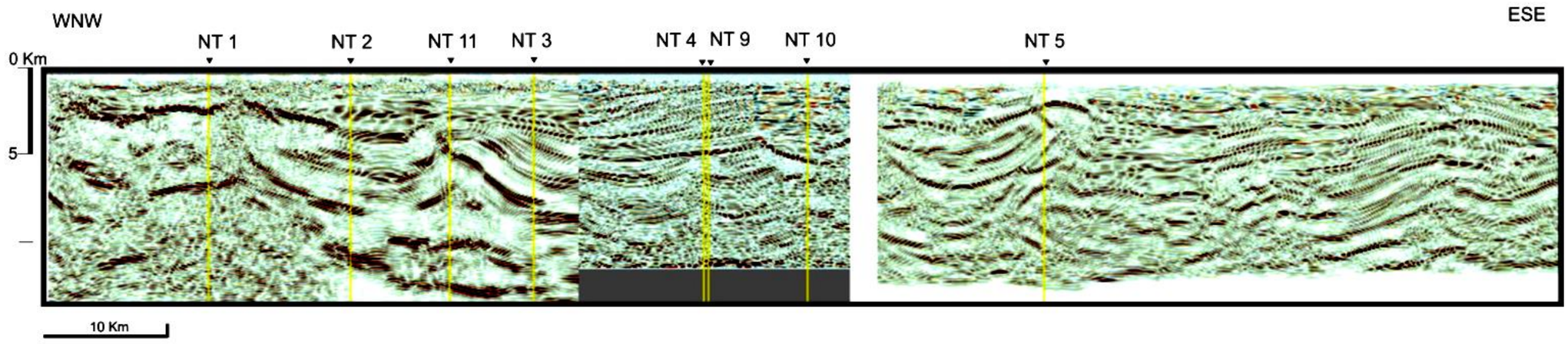

Figure 5.3 Random sections of the Tepetate and Cabritos seismic cubes. Typical quality of the 3D seismic dataset.

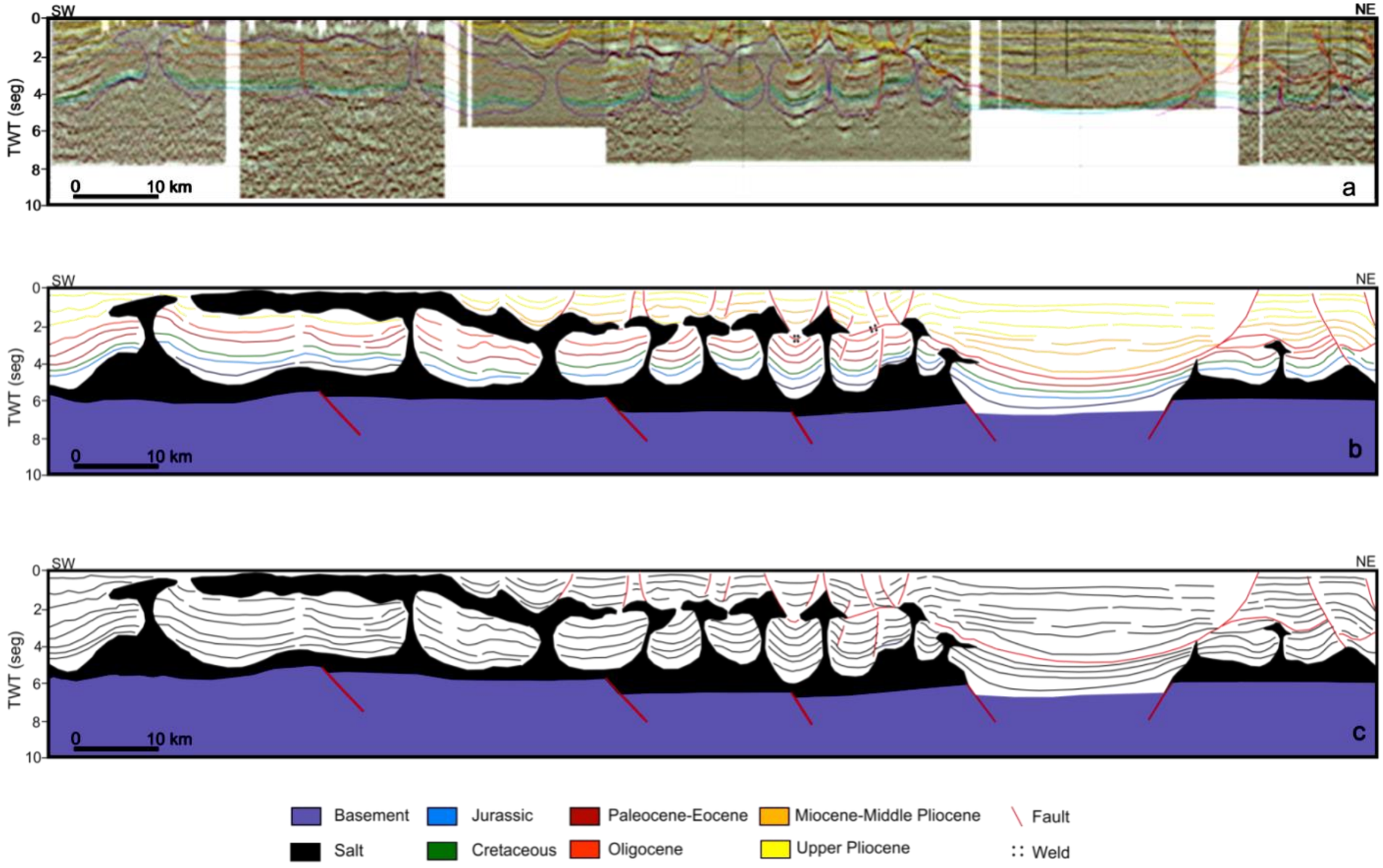

Figure 5.4 Typical qualities of the 2D seismic datasets.

5.7 Interpreting Salt Structures using 3D Seismic Data

5.7.1 Data Clarity

A number of difficulties arise from using subsurface seismic data to interpret salt structure. In addition to the relatively coarse imaging of real structure by seismic data, the physical nature of salt, coupled with the complex, steep-sided, structures arising though salt migration can significantly degrade the local seismic image. This degradation of imaging ability is due to a combination factors:

- Complex lateral and vertical velocity model variations due to the presence of salt;
- Steeply dipping post-salt strata;
- Intense fracturing and faulting of the post-salt overburden;
- Subtle lateral syn-kinematic lithological variation within the sequence;
- A complex salt sediment interface geometry
- Shallow gas acoustic “shadows”, which is commonly associated with Isthmus Saline salt diapirs.

Additionally, due to the significant depths to the Mesozoic carbonates more than 7000 m in Isthmus Saline Basin, exploration activity has conventionally focused on shallow intervals. As a result, most seismic surveys are optimised for the imaging of relatively shallow structures. Hence, processing methods such as pre-stack depth migration (in the 3D seismic) rarely incorporate data from depths greater than 4000m.

5.8 Seismic interpretation method

The interpretation of horizons from the Tertiary sequences was selected for interpretation based stratigraphic control and one or more of the following criteria:

- They are unconformities, hence may represent pulses of diapiric growth.

- They onlap onto unconformities, and hence may define diapir shape at that time.
- They may contain channels, which may help to determine stratigraphic traps.
- They are high amplitude reflectors, hence are readily correlated, and often display well-defined fault patterns.
- They horizon correlate with existing picks of marker defined by biostratigraphy.

5.9 Construction and Restoration Methodologies

5.9.1 Section Construction and Restoration Workflow

The workflow used during the restoration of the salt structures derived from the interpretation of four seismic lines is shown in (Fig. 5.5). The workflow was iterative with adjustments made at various stages during the restoration process due to incorrect stratigraphic correlations or identified errors and inaccuracies during the decompaction routine.

5.9.2 Regional elevation

One of the key concepts used in section balancing is the idea of regional elevation. This is the level to which a key bed will return in the undeformed state and is an essential component of area-balanced calculations (Hossack, 1995). Regional levels and paleo-bathymetries were estimated by palaeontological control of several wells around the study area for any particular time.

The up-dip direction of cross-sections was assumed to be towards the southwest and southeast and into the basin. The exact values of the slope on these regional surfaces may have varied according to the position of the platform edge at any particular time. However, the position in which the sections are located and the paleobathymetric setting in which most of the geological events took place were developed in slope facies, except for the Middle Pliocene surface that was developed in platform facies.

5.9.3 Pin Lines and Loose Lines

Traditionally, the dip and elevation of reference beds are projected inwards from the foreland in thrust belt restorations or from the footwall into the hanging wall in extensional restorations. Regional elevation is a powerful tool to decide the style of deformation because reference beds are raised above regional elevation during contraction and lowered below regional elevation during extension (Hossack, 1995). Regional pin lines were located at the ends of the sections where there was no apparent deformation in this case NW and NE.

In contractional domains, the regional pin-lines were located towards the basinward (northward) termination of the individual sections. If an extension section were modelled, the pin-line would have been located in the footwall of extensional faults.

5.9.4 Restoration Algorithms

No agreement exist in the literature about the best restoration method for sediments associated with salt structures. Two methods are generally available in restoration programs: flexural slip and inclined simple shear. The former is used in contractional thrust belts so that constant bed lengths are retained in constant-area deformations. Extensional fault restorations techniques usually use inclined simple methods, where bed lengths are not maintained constant (Hossack, 1995).

The restoration algorithms for the reconstruction of both fault surfaces and hanging wall structures were chosen from those available in Midland Valley's 2D Move program (Midland Valley, 2013). The inclined simple shear algorithm, which was used for the restoration of hanging walls above the listric, faults where the structural styles are dominated by extension and salt withdrawal.

Flexural slip unfolding algorithm often used in contractional domains was used for the restoration of detached folds in the deepwater fold belts. This line-length unfolding algorithm maintains bed thickness variations (Midland Valley, 2013).

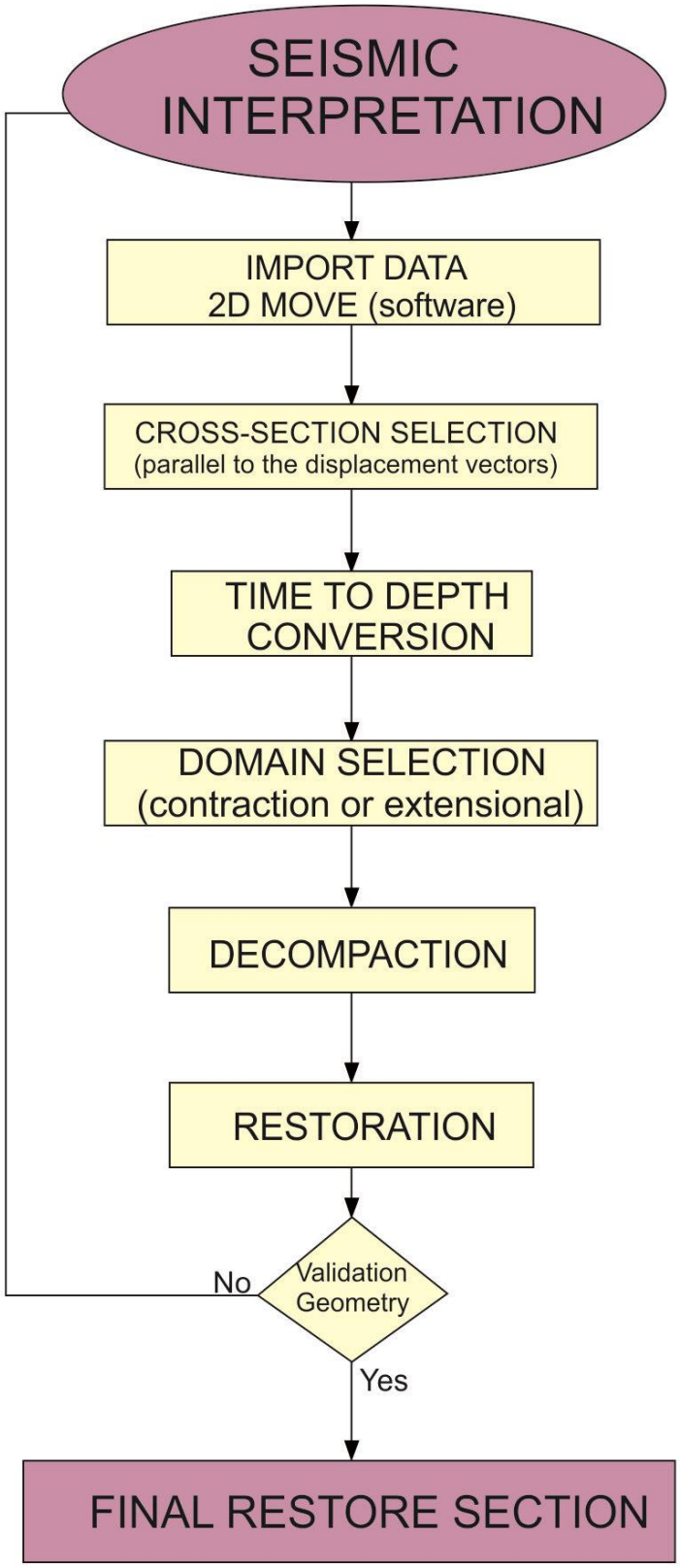

Figure 5.5 Methodology and workflow of balance cross sections.

5.9.5 Decompaction and Isostatic Compensation

Decompaction calculations remove the progressive volumetric changes due to loss of porosity with increasing depth of burial through geological time. After each stage of structural restoration, cross-section thickness was modified to

compensate for the change in sedimentary compaction caused by the layer that was stripped off. The amount of vertical expansion of any sequence at a given location is a function of its lithology (porosity) and the change in overburden thickness (Rowan, 1993). In 2DMove, the decompaction algorithm assumes that the reduction in porosity with depth is exponential (Midland Valley, 2013).

Porosity values and decompaction parameters were taken from internal reports on similar stratigraphic units in the Southeastern part of the Mexico basin (PEP-IMP, 1999). During restoration, the flexural isostasy algorithm (Midland Valley, 2013) was used to account for isostatic changes caused by the sediment loading. The value for the 'load crustal density' of 2680 kgm^{-3} was taken from an average of the South Gulf of Mexico sedimentary section (PEP-IMP, 1999).

5.9.6 Errors and Limitations in Section Construction and Restoration

For decades, section balancing has been used to test the viability and admissibility of geological interpretations (Dahlstrom, 1969; Elliott, 1983). Interpretations that cannot be restored satisfactorily are regarded to be erroneous and should be reconsidered until they can be successfully balanced.

Errors may be introduced both in the construction and restoration stages of section balancing through inaccurate depth conversion of the seismic data when seismic data is in time (i.e. lack of calibrated well data) and porosity values used in the decompaction algorithms (lack of well data) as well as errors in the initial seismic interpretations (Rowan, 1993).

The principal limitations on the precision and validity of balanced cross-sections are inherent in both section construction and restoration (Rowan, 1993). Errors may be introduced if:

1. - The cross-section being balanced is not parallel to the tectonic transport direction Cross-sections should always be constructed parallel to the direction of tectonic transport in order to limit the inaccuracies introduced by the movement of material in and out of the cross-sectional plane.

2. - Multiphase movement along faults is not recognised (i.e. there are no associated growth strata).

3. - There is movement of ductile material such as overpressure shales in and out of the plane of the section, (i.e. area of the section will not be preserved).

4.- There are problems defining the stratigraphic template and regional levels through time particularly paleobatimetry and topographic variations through time.

5. - Incorrect velocities are applied during depth conversion as well as errors due to problems with the porosities used for decompaction.

6. - Erosional events and unconformities where unknown amounts of section have been removed are not well known.

The restoration algorithms applied are geometrically or kinematically unsuitable to restore the deformation processes.

Sediments can undergo lateral compactation, which is effectively invisible because it creates no seismically visible structure.

All of the above factors will generate uncertainties in the processes of section construction and restoration. In general, these limitations are difficult to quantify but must always be borne in mind when assessing the results of section construction and restoration. However, it may be argued that a balanced and restorable cross-section is better than an unbalanced cross-section.

5.10 Summary

The seismic data was registered up to 15 km; however, the pre-Jurassic interval is acoustically transparent in the Isthmus Saline Basin.

Three 2D seismic datasets used in this research vary significantly in their quality. This change in the quality depend on the acquisition and processing parameters used in each survey. The 2D seismic used in this study was designed for shallow targets so deep part is unclear.

Chapter 6 Gravity, Magnetic and Seismicity

6.1 Introduction

In the last two decades, the southern Gulf of Mexico has been surveyed with widely space two-dimension seismic data and in some specific areas with three dimensions pre-stack depth migrated seismic data that have permitted imaged some salt structure features in deep Jurassic basins. However, the structural complexity that exists in the Isthmian Saline Basin and neighbouring structural domains is such that are not clearly defined by reflection seismic pre-salt structures and salt depositional boundaries. The intense deformation and salt diapirs rejuvenation have constrained the interpretation and the understanding of this basin.

However the structural configuration of the crystalline basement has not been analysed in more detail but it forms the basis for our understanding of the evolution of salt basins and related salt structures which it is a high priority in the oil industry.

This chapter will integrate and analyze the gravity, magnetic and seismicity data of the Isthmus Saline Basin in order to access the basement architecture and its influence on salt thickness.

The presented analysis of the regional tectonic structures and basement structural domain of south-eastern Mexico and in particular the basement architecture of the ISB integrates results from gravity and magnetic data, earthquakes epicenter locations, satellite images, lithologies description of wells and outcrops,

Additionally, all these analysis will help to have a better idea how the basement have controlled salt development and how it have influenced the generation, migration and trapping of hydrocarbons which are of great importance in petroleum system knowledge of this basin.

6.2 Establishing the architecture of the Isthmus Saline Basin

The Isthmian Salt Province (Viniegra-Osorio, 1971; Garrison and Martin, 1973) is divided in several offshore and onshore sub-basins (Fig. 2.1). The Isthmus Saline sub-basin that is the main subject of this research is an onshore sub-basin and it is bordered to the south by the NW flanks of Chiapas Fold Belt. Prior to this study, this sub-basin has not been structurally analysed in detail, due to the problems of seismic imaging of the deeper basin strata as consequence of the 6 km thick Tertiary sedimentary sequences as well as the complex salt diapirs and salt sheet and lack of depth stratigraphic well control.

6.2.1 Main structural elements that control and constrain Isthmus Saline Basin

Isthmus Saline Basin is surrounded by important structural elements which have influenced the tectono-sedimentary and salt tectonic evolution of the ISB to a greater or lesser degree (Jannette, et al., 2003). Figure 6.1 including the:

Veracruz basin

Los Tuxtlas volcanic field

NW Chiapas fold belt in the front of the “Sierra de Chiapas”

In the intersection of these structural elements there is another NE-SW trending geological feature that is not physically visible. Meneses-Rocha (1985) has called this geological feature as Istmo de Tehuantepec fault, which has been defined by a trend of earthquakes epicentres. It will briefly describe in order to have an overview and characteristics of these provinces and set the relationship with Isthmus Saline Basin.

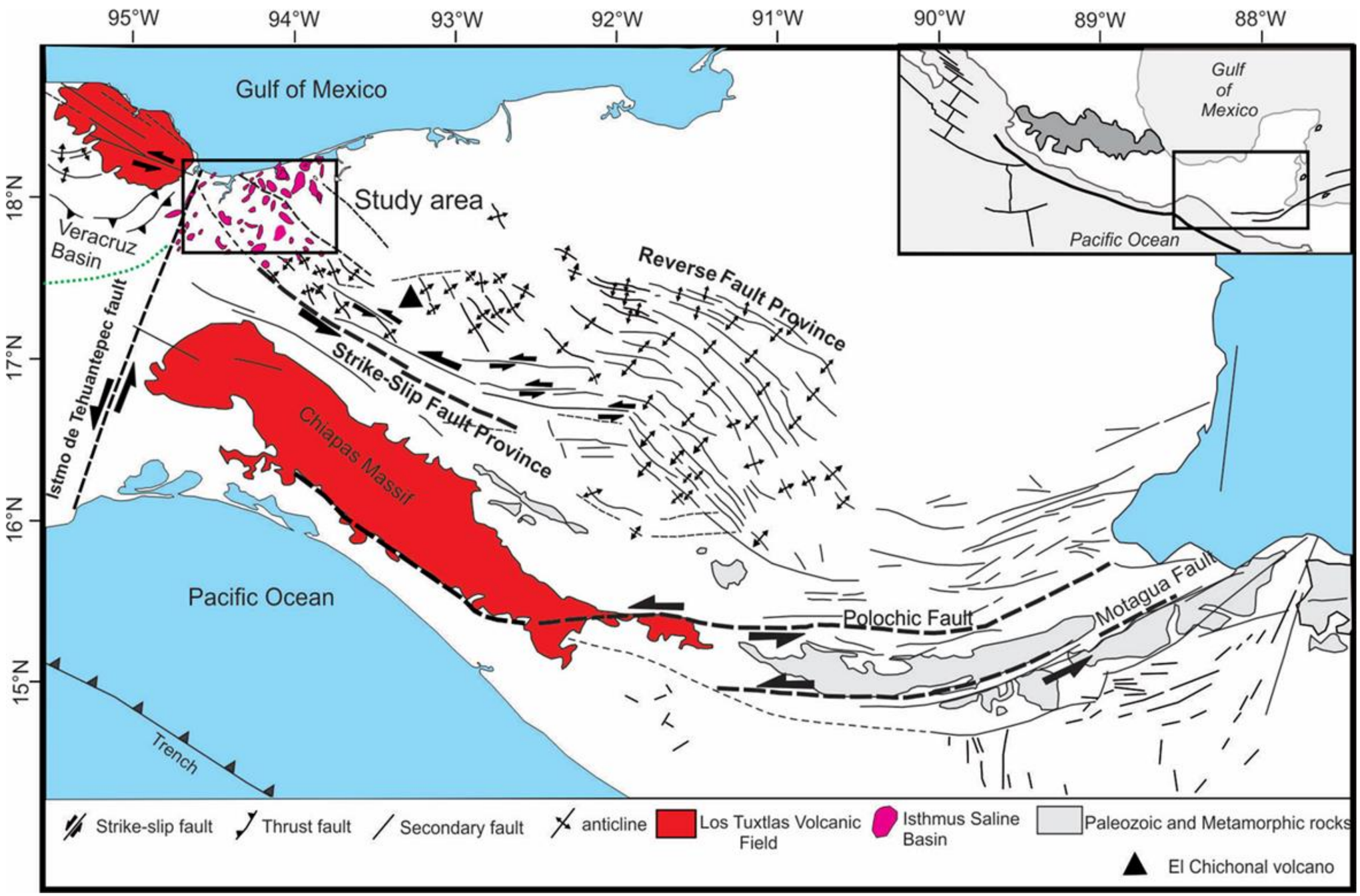

Figure 6.1 Main structural elements that constrain ISB marked with black rectangle. Strike-slip and Reverse Fault Province are represented by only anticlines. The black triangle indicates the location of the Chichonal volcano (modified from Andreani, *et al*., 2008

6.2.2 Los Tuxtlas Volcanic Field

The Los Tuxtlas volcanic field is a NNW-SSE trending belt of alkaline mafic volcanic field parallel the Gulf of Mexico coast and is located to the WNW of Isthmus Saline Basin (Andreani, *et al.,* 2008) (Fig. 6.2). The volcanic activity has been dated between 8-7 M.y. (Nelson and González-Caver, 1992; Jacobo-Albarran, 1997) and still active. Related Middle and Upper Miocene volcanic deposits have been reported as part of sedimentary basin fill of the Veracruz and Isthmus Saline basin, respectively (Jannette*, et al*., 2003). The Los Tuxtlas volcanic field is affected by NW-SE strike-slip faults but the principal fault is associated to E-W oriented secondary fault, interpreted as synthetic Riedel shears (Tchalenco, 1970). The strike-slip faulting has been interpreted to be a left-lateral based on stream offsets evidence and fault slip (Andreani et al., 2008).

6.2.3 The Chiapas Fold Belt "Sierra de Chiapas"

The Chiapas fold belt front extends from the Isthmus of Tehuantepec to the Mexico-Guatemala border (Fig.6.2). The fold belt consists mainly of Mesozoic carbonates and Paleogene siliciclastic sequences, and is limited to the south by the Chiapas Massif. The fold belt of Chiapas has been divided in two provinces: strike-slip and reverse fault tectonic provinces by Guzman-Speziale and Meneses-Rocha (2000) (Fig. 6.2). The strike-slip province borders the Isthmus Saline Basin which will be described with the purpose of linking the kinematics of surface with subsurface deformation in the Isthmus Saline Basin.

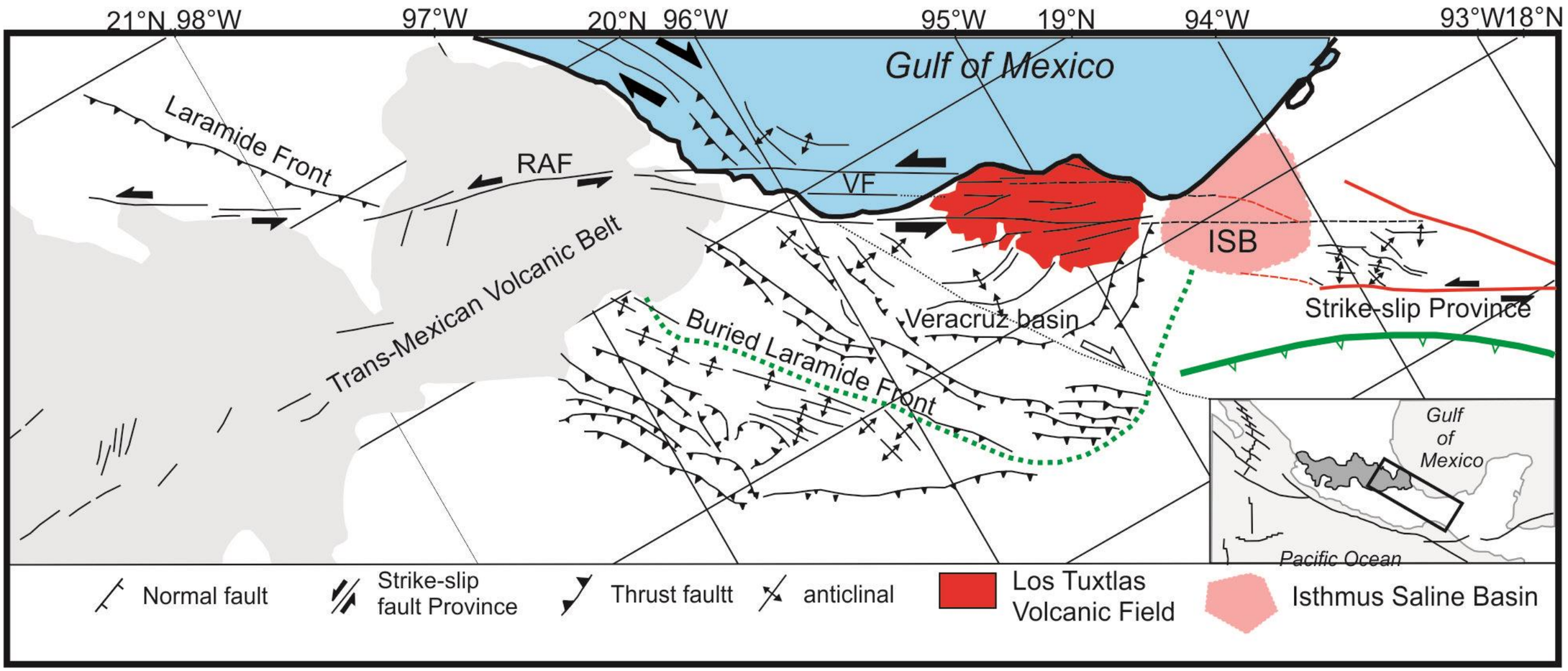

Figure 6.2 The Los Tuxtlas volcanic centre is a NNW-SSE trending belt of alkaline mafic volcanic field parallel the Gulf of Mexico coast. The Isthmus Saline Basin is represented in pink polygon. Veracruz basin is located to the south, oriented NW-SE. (modified from Andreani, *et al*., 2008).

Strike-slip fault province

The strike-slip fault province is characterized by series of structural highs and lows and by stretching zones separated by left-lateral strike-slip faults (Sanchez-Montes de Oca, 1979; Meneses-Rocha, 1985; Guzman-Speziale and Meneses-Rocha, 2000). The uplifted blocks are represented by NW-trending *en echelon* recumbent anticline structures formed by Cretaceous and Paleogene sequences. Structural lows and related basins with up to 5000m of Cenozoic sediments are located in divergent fault system or where releasing double bend is developed with up to 5000m Cenozoic sediments (Andreani *et al*, 2008). In the strike-slip province, the stretching areas are represented by El Chichonal volcano and Navenchauc, Huitepec volcanoes. The first is emplaced in the Chapultenango half graben (Garcia-Palomo et al, 2004) and the second and third volcano is emplaced in Ixtapa graben (Meneses-Rocha, 2001). The strike slip faults have different orientation along of all provinces. The western sector, which limits Isthmus Saline Basin, is characterized by NW-SE trend faults; the central sector is represented by E-W trending faults and terminates to the east in a horst tail array with NW-SE faults (Fig.6.2).

Reverse fault province

The reverse fault province is a structural trend forming the middle leg of a very lazy Z (Fig.6.2). It is formed by a series of narrow anticlines where the intervening synclines are generally missing. The age of the folding and faulting is post-Middle Miocene, because beds of this age form the youngest strata in the folds (Meneses-Rocha, 2001). Fan and box-shaped folds, or asymmetric anticlines without a general trend of vergence are present in this province. Meneses Rocha (1991) considers that in the stratigraphy of reverse fault province the Middle Jurassic and the Lower and mid-Cretaceous strata contain incompetent rocks (dolomite and anhydrite) that produce two potential detachment horizons at the level of Middle Jurassic salt deposits and along the Lower and mid-Cretaceous evaporites.

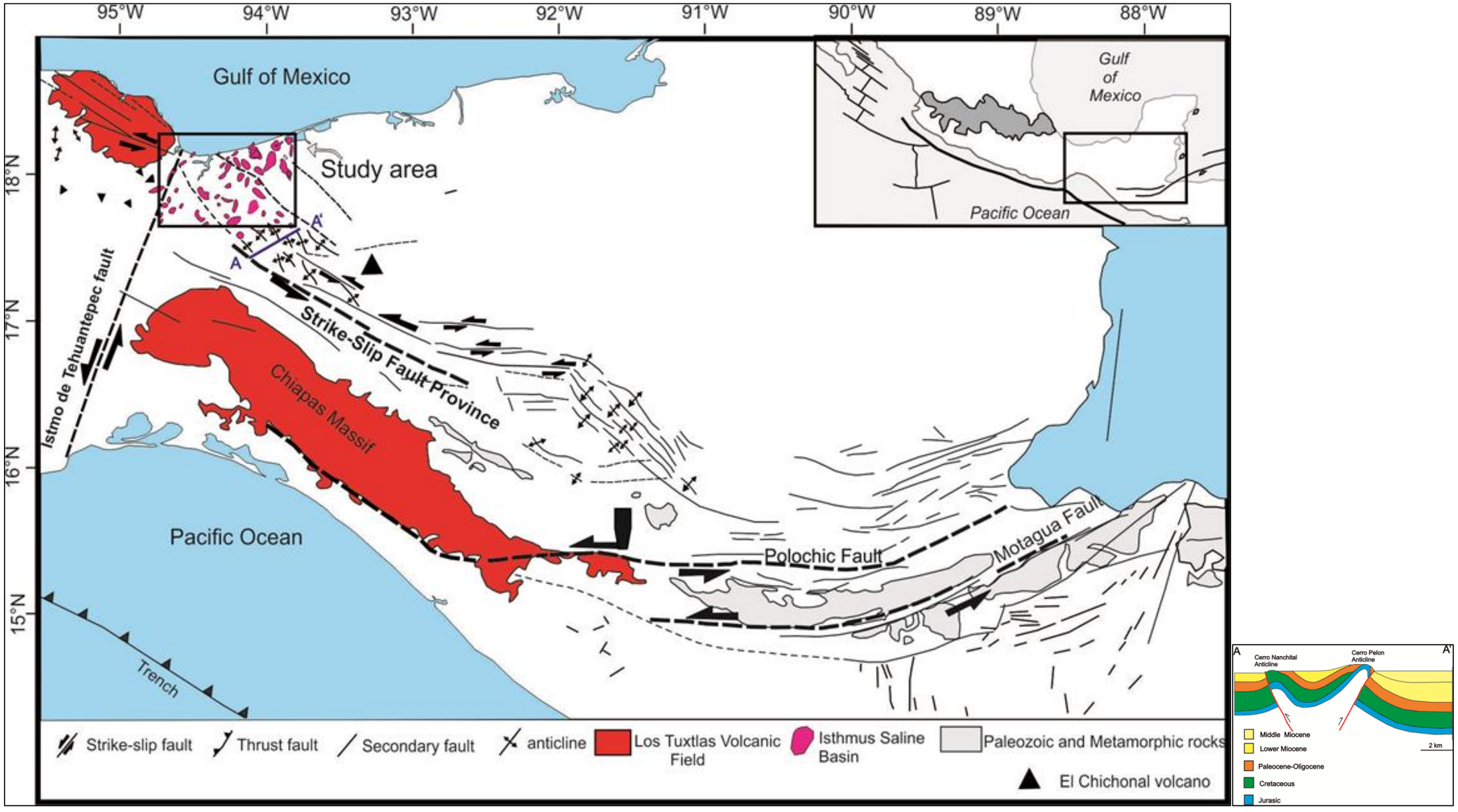

Figure 6.3 represent the Strike-slip Province and it relationship with ISB. The section A-A' shows a sketch of divergent fault system (modified from Andreani, *et al.*, 2008).

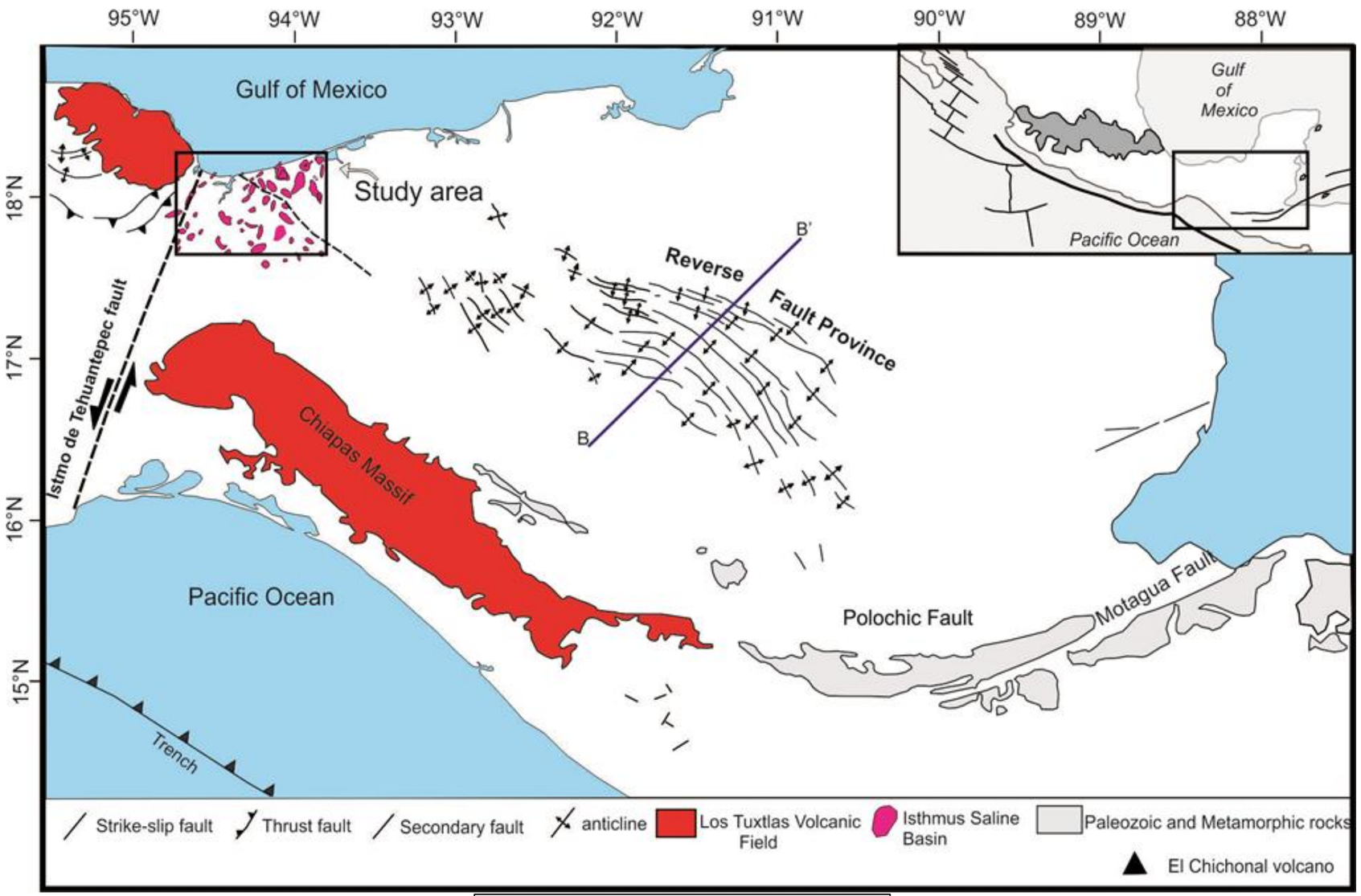

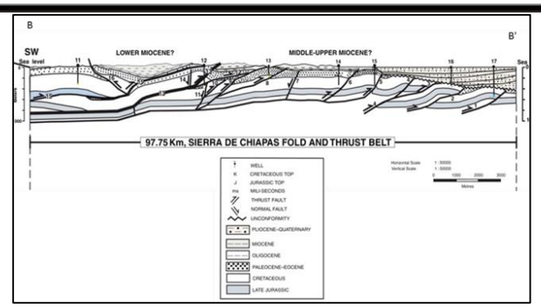

Figure 6.4 the map shows the area considered as Reverse Fault Province. The line of section B-B' shows the structural style that characterize the reverse fault province (the map was modified from Andreani, *et al*., 2008; and the section was modified from Mandujano and Keppie, 2009).

6.3 Seismicity Activity in the Gulf of Mexico

Earthquakes are the release of energy along faults in the earth's crust; their presence indicates large active structures affecting the basement of a basin. The Gulf of Mexico has been considered traditionally as a passive margin and practically aseismic (Fig. 6.5). Nonetheless, in the northern Gulf of Mexico, some infrequent earthquakes of moderate magnitude have taken place along the continental margins and offshore coasts of Louisiana and Mississippi of magnitude that not exceed *Mw* 5.8. (Suárez and López, 2015). Frohlich (1982) interpreted this events based in the resulting focal depth of 15 km near the base of the crust as an accumulation of stresses due to the warping of the lithosphere under the load of the sediment pile. In the offshore area, three earthquakes with magnitudes *Mw* 4.6, *Mw* 5.2 and *Mw* 5.8 took place in a region of intense hydrocarbon production and exploration (Nettles, 2006). Gangopadhyay and Sen (2008) in base on a mechanical model explained this phenomenon as resulting from shear stress build-up in the salt deposits. The researcher argued that tabular and Allochthonous salt deposits are strong enough to produce brittle failure under the appropriate conditions.

In contrast, the south-eastern Gulf of Mexico, there is showing a wide seismic zone with earthquakes depths between 10 and 298 km that has been mainly linked to Cocos Plate subduction a volcanic activity. In the south-eastern Gulf of Mexico earthquakes with magnitudes as large as *Mw* 6.4 have been recorded close to the study area recorded close to the study area (Guzmán-Speziale & Meneses-Rocha, 2000; Andreani, *et al.,* 2008; Suárez and López, 2015).

Therefore, the earthquake activity that have occurred in the southeastern Gulf of Mexico represent one the biggest difference between the northern Gulf of Mexico and its counterpart to the south which is reflected in the tectonic activity and complexity of the geologic structures.

The seismicity in the Southeast of Mexico has been recorded in two mains areas: Isthmus of Tehuantepec and in the Chiapas Fold Belt (Fig 6.6).

).

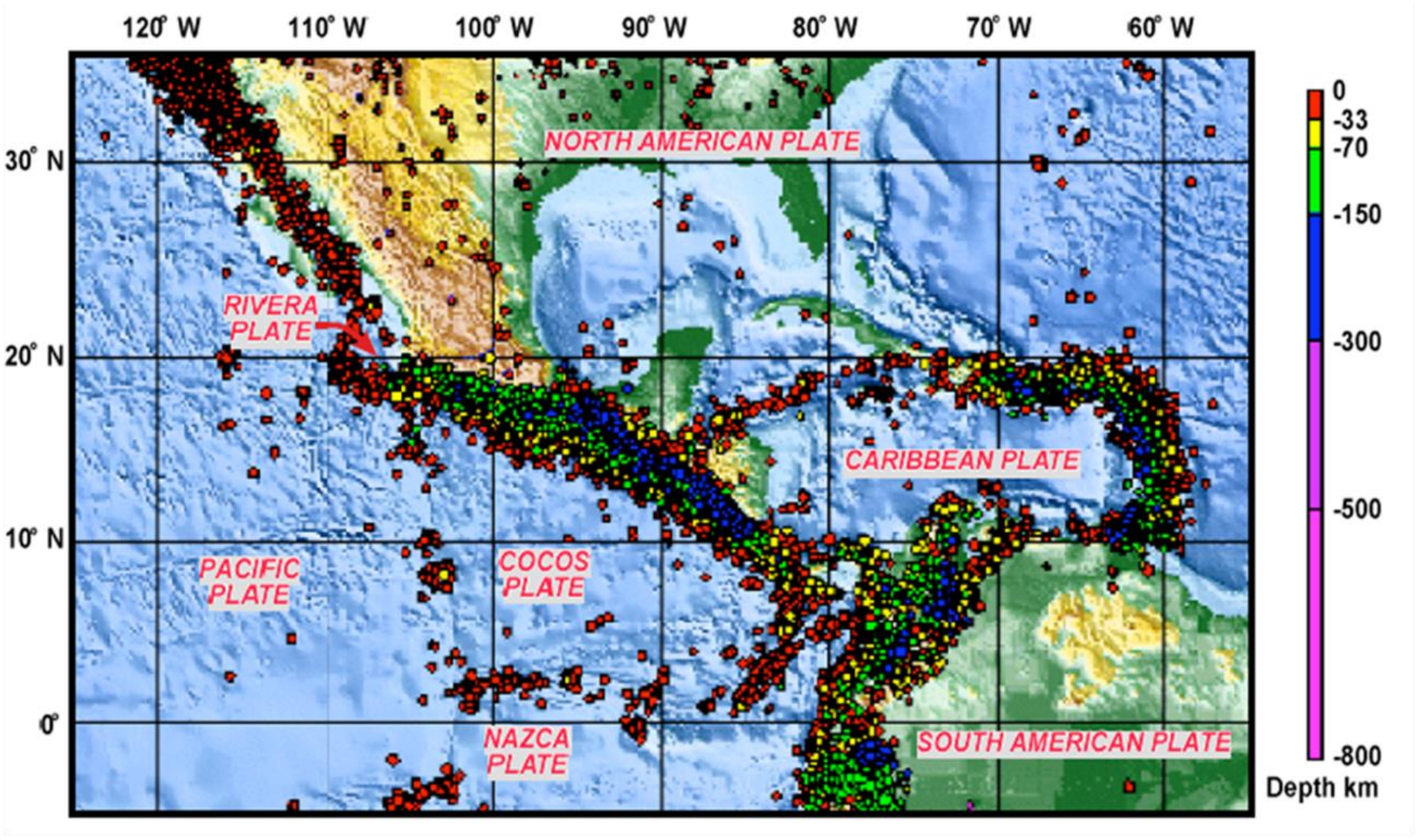

Figure 6.5. - Seismicity Activity in the Gulf of Mexico, Southern of Mexico and Central America (USGG National Earthquake Information Centre, 2004)

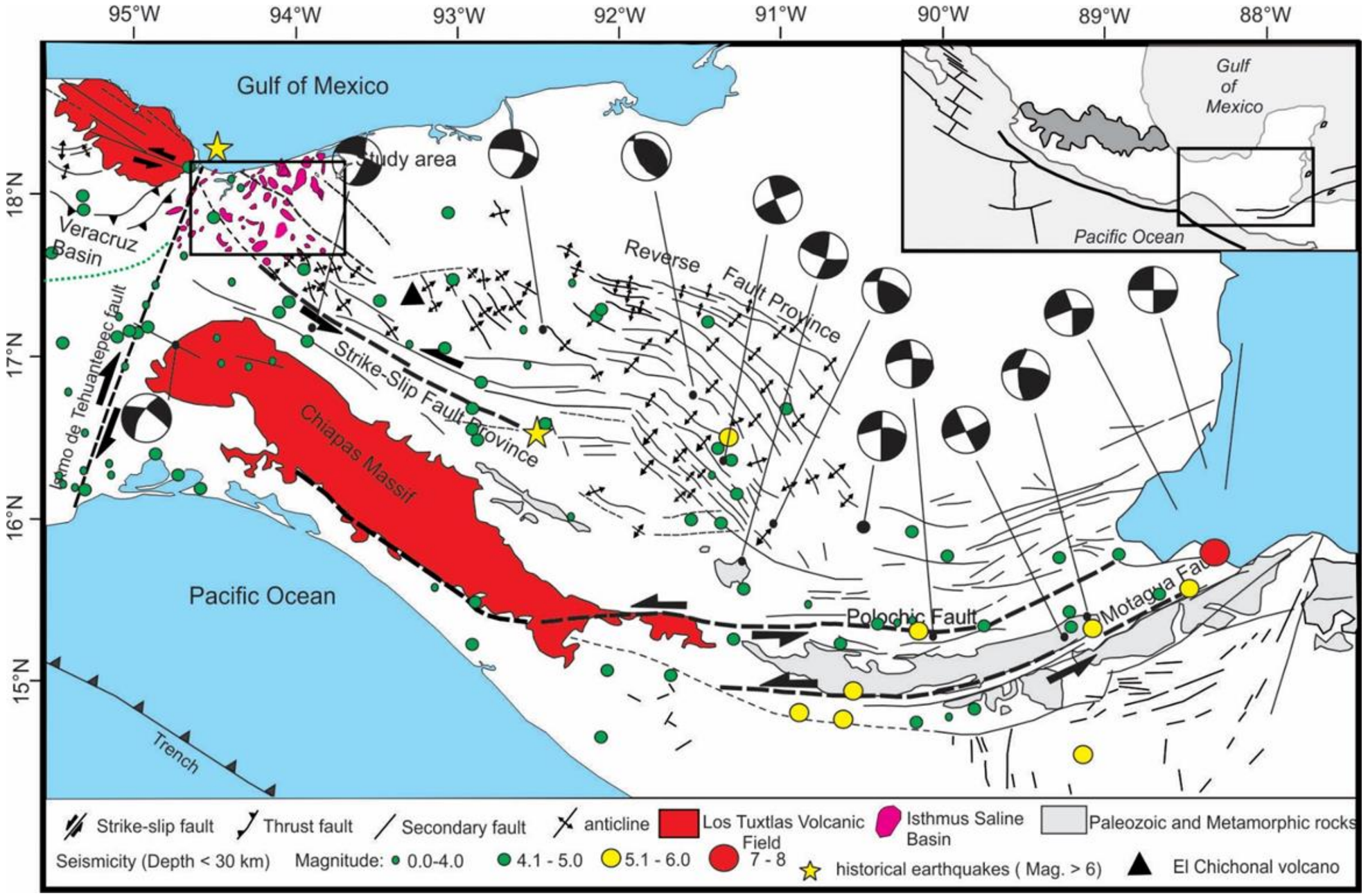

Figure 6.6 Show shallow earthquake activity and the main fault systems of Chiapas area. The black rectangle, represent the Isthmus Saline basin. The seismicity and focal mechanism are included (modified from Andreani, *et al.*, 2008).

6.3.1Isthmus of Tehuantepec Seismicity

The Isthmus of Tehuantepec is an area with high seismic activity and is considered as a large stress concentration zone (Suárez, 2000). In this area, shallow and deep seismic activity have been recorded Suárez and López (2015) established, despite the great concentration of earthquakes the individual events are not large enough to generate reliable focal mechanism to give information about the tectonic origin of this seismicity. Nevertheless, the Isthmus of Tehuantepec is the most active zone of intraplate seismicity in Mexico (Suárez and López, 2015)

In 1959 and 1973, two strong earthquakes of (Ms 6.4) and (Ms 5.3) took place, the first in the town of Jaltipan, Verecruz and the second near to coast of the city of Veracruz. Suárez (2000) postulated that both seismic events are related to reverse faulting allowing at a high angle with the axes of maximum compression oriented northwest-southeast. However, a remarkable feature of these two earthquakes is that the focal depths determined were 27 and 22 km deep, respectively. However, these depths contradict the interpretation, because the depth of the earthquakes are very unusual to be considered intraplate earthquakes so these events of high seismic magnitude are not related with the pacific subduction zones due to slab in the area is over 150 km (Andreani, *et al.*, 2008).

6.3.2 Chiapas Fold belt Seismicity

In contrast to the Isthmus of Tehuantepec, the seismicity of the strike-slip fault province is characterized by moderate-size shallow events (Andreani, et al., 2008). Available fault-plane solution data show left-lateral strike-slip mechanisms (Guzmán-Speziale, et al., 1989; Guzmán-Speziale & Meneses-Rocha, 2000). The largest earthquake event in Chiapas of Ms 7.8 (Figueroa, 1963) took place in 1902, followed by a least twenty moderate aftershocks. The destructions occurred in the Rio de Chiapas valley inside a 100 km long and ~25 km wide zone oriented NW-SE.

The Reverse fault province is characterized by shallow seismicity. However, the quantity of events in this area is lower than within the strike-slip province. Guzmán-Speziale & Meneses-Rocha (2000), found one fault-plane solution in the Harvard Global CMT catalogue, which was related with reverse fault mechanism (Fig. 6.6).

6.4 Interpretation of Seismicity in Isthmus Saline Basin

The Isthmus Saline Basin is located between the Isthmus of Tehuantepec and the Chiapas strike-slip province. The SE of Mexico is characterized by high intra-plate seismic activity caused by the convergence of the Cocos, Caribbean and North America Plates. The available earthquakes data (Servicio Sismologico Nacional, 1997) were classified by depth into shallow events less than 30 km deep and deeper events with over 30 km depth. Subsequently, the two groups were plotted on the regional tectonic maps in order to identified active structural trends and fault sets in the basement (Figs.6.6 and 6.7).

The figures 6.6 shows the location of earthquakes with depths less than 30 km. Shallow epicentres are mainly linked to the Motagua-Polochic fault system as well as strike-slip province of the Chiapas fold belt. The NW-SE seismicity trend shows continuity toward the Isthmus Saline basin where the seismicity is significantly attenuates. The seismicity trend extend to the nearby the Los Tuxtlas Volcanic field and Veracruz basin where some earthquakes took place. In the same NW direction but slightly offset an Ms > 6 offshore earthquake was registered, which indicates seismic activity on the basement level extends into the onshore area. The seismicity pattern in these provinces show a sinistral strike-slip, which could be interpreted as transverse fault segmenting the Chiapas basement and possibly the Isthmus Saline basin.

In the Reverse Fault Province, shallow seismic activity has been observed. The seismicity pattern follows anticlines trends and focal mechanism confirms left lateral displacement (Guzman-Speziale and Meneses-Rocha, 2000).

Toward the W of the strike-slip trend, in the Isthmus of Tehuantepec area, a NE-SW shallow earthquakes alignment has moderate intensity, however, in the

Isthmus Saline basin area the seismicity weakens or disappears. The shallow seismicity pattern in the WNW area of the Sierra de Chiapas and the Isthmus Saline basin document two main structural domains. A domain of NW-SE trending basement faults has been repeatedly reactivated as left-lateral fault. These reactivated basement faults, are inherited the Mesozoic rift stage and subsequent rotation of the Yucatan block, and probably controlled both deposition of Jurassic salt and the migration of hydrocarbon of the Isthmus Saline basin during Middle Eocene–Miocene contractional deformation of the Sierra de Chiapas. In contrast, the presence of NE-SW-trending left strike-slip faults in the Falla del Istmo de Tehuantepec suggest that some convergence between the Cocos and North America plates is accommodated by lateral movement of crust blocks along the Sierra de Chiapas by strike-slip faults as well as by crustal shortening along thrust faults in the south-eastern Mexico (Guzman-Speziale and Meneses-Rocha, 2000). This system has not been well described previously; because it is obscured by the dominant NW-SE trending structural features of the Sierra de Chiapas fold a thrust belt. However, petrophysical well data analysis has shown an excellent NE-SW fractures system on the youngest geological sequences.

Figure 6.7 shows the seismicity pattern of the deep earthquakes over 50 km depth, which are linked to the seismicity along the subduction interface. Earthquakes related to subduction have a parallel orientation with the Pacific coastline and are mainly concentrated in the area of the Isthmus of Tehuantepec and the Chiapas massif. Very few earthquakes epicentres occur north of the main southern border fault. However, some epicentres are linked with the fold and thrust developed in the Strike-slip province. Very few deep earthquakes are located underneath the Isthmus Saline Basin and in Reverse Fault Province. This distribution of deep epicentres shows that the influence of subduction in the Southeast of Mexico is limited by the main fault of the strike-slip province and just a few deep earthquakes that overstep this boundary are related with the NW-trending recumbent anticline structures of the strike-slip province.

6.5 Regional fault trends on Landsat images

Figure 6.8 shows the result of the integration of regional faults systems mapped on Landsat satellite images around different structural provinces. The map shows two main structural fault patterns in order to highlight their significance in the deformation of Sierra de Chiapas.

One prominent structural trend represented shows changes in fault trends from NW-SE to E-W and subsequently NW-SE (in black lines in Fig.6.8). These systematic changes of fault trend reflect the transition between the strike-slip and reverse-fault province. The rose diagrams show the main structural trend in the south-east of Gulf of Mexico. In study area represented with the black rectangle, the lineaments are obscure by the coastal plain; however a slight topographic relief demonstrates the continuity of NW-SE structural trend affecting the salt diapir zone.

The NE-SW fault system is less prevalent (represented in red lines in Fig.6.8). However, there is evidence that this system displaces the NW-SE system. The E-W strike-slip fault system is obscured by intrusive igneous and volcanic rocks of the Arco Volcanico Chiapaneco complex (Damon and Montesion, 1978; Capaul, 1987). Nixon (1982) argues that volcanism in this area is related to the subduction of different ages and different subduction angles and suggests that the interaction of the Cocos Plate, the Caribbean and North America form a complex and extensive tectonism related to the Chichonal volcanism. This volcanic activity has been dated as 2.17 ±0.94 Ma to recent (Jacobo-Albarran, *et a*l., 2003).

Shallow seismicity along the Isthmus Saline Basin, strike-slip provinces and reverse fault province is a direct evidence of NW-SE active basement, which is not completely straight, it shows lateral offset in the seismicity pattern from strike-slip province to the Isthmus Saline basin and Veracruz basin. The seismicity alignments are interrupted through the Isthmus Saline Basin.

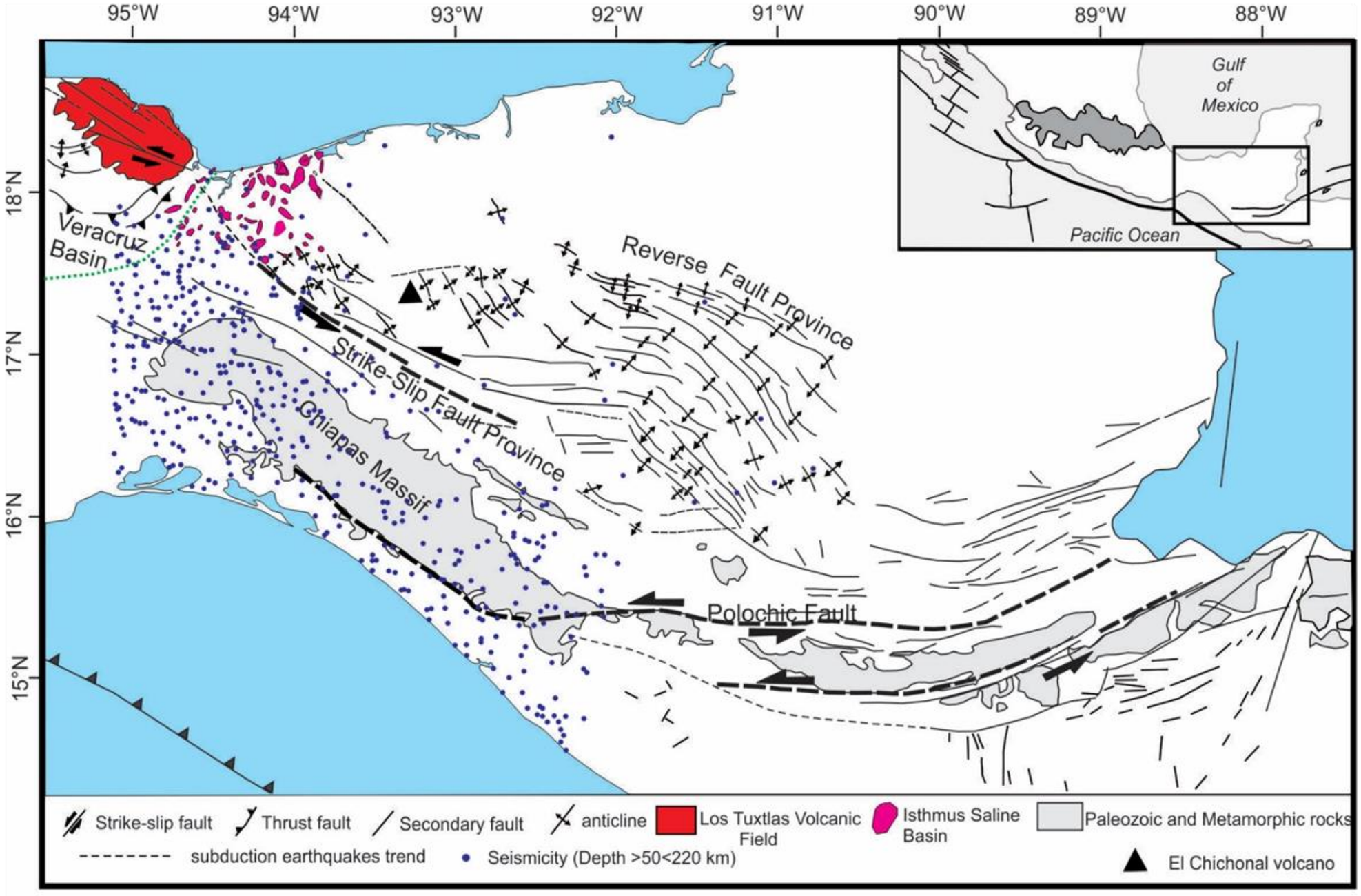

Figure.6.7 Show distribution of deep earthquake and its relationship with Isthmus Saline Basin (study area) and Chiapas fold belt provinces (modified from Andreani, *et al*., 2008).

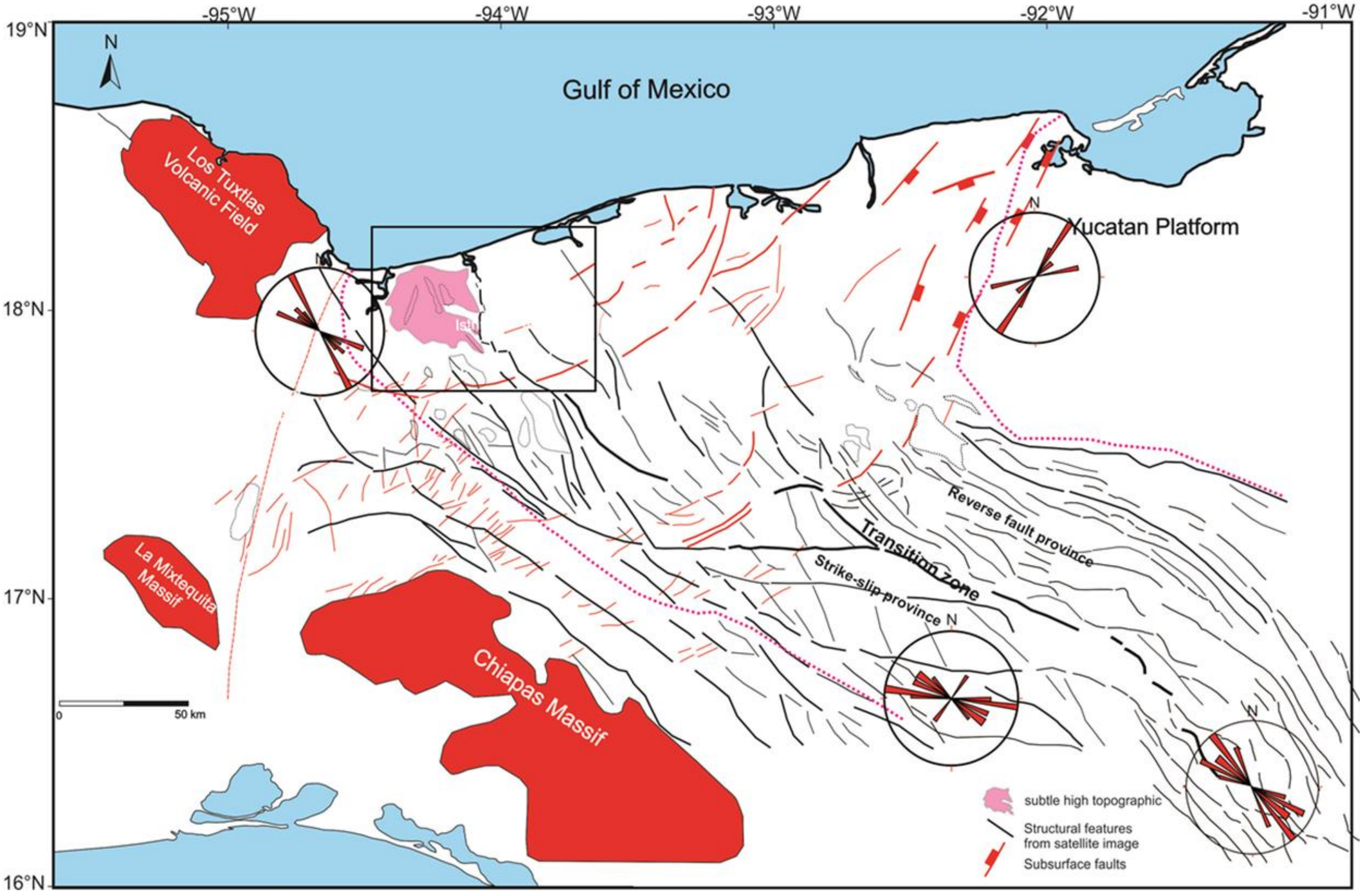

Figure .6.8 Structural alignments interpreted from Landsat image. The black rectangle represents the study area. The pink dotted line represents the Jurassic salt boundary. The bold black line represents the transition boundary between two structural provinces.

Additionally, a series neotectonic observations shows that the NW-SE fault system is active and has played an important role in the salt tectonics of Isthmus Saline basin. These geological events (neotectonic data) include recent volcanic activity of Chichonal volcano, hydrothermal activity with high concentrations of salt in the fluids, the collapse of the land surface in the Choapas Village and offshore earthquake of Ms > 6 suggest that NW-SE are strike-slip active in the Isthmus Saline Basin.

The NE-SW strike-slip system intersects and displaces the NW-SE fault system. The high concentration of shallow and deep earthquakes in the Istmo de Tehuantepec area indicates the intersection of the two fault systems. This interception point may represent the boundary between the transitional and continental crust? The intersection between these two strike-slip fault systems probably has played an important role on salt tectonics evolution of salt structure in recent time in the Isthmus Saline basin. However, the low earthquake activity in the study area may be due to the loss of continuity of the structural trend NW-SE. which is represented by a huge subsiding of the basement

6.6 Qualitative Analysis of Potential Field Data

The structural limits and architecture of the Isthmus Saline basin have not yet been defined due to their structural complexity. So far, the relationship between basement architecture and sedimentary sequences is unknown. Therefore, the interpretation of potential data, e.g. magnetic and gravity maps is an excellent tool to support structural models that help to define the basement geometry and its controls on salt structures and sedimentary sequences. Consequently, in order to understand the geometry of the basement and blocks boundaries, published maps by Hudec, *et al.*, (2013) of Total Magnetic Intensity (IMT) and Bouguer anomaly (Gravity) and Tilt derivative of IMT and Tilt derivative of Bouguer anomaly (from PEMEX, 2012) were interpreted qualitatively (Fig. 6.9 and Fig.6.10 respectively).

Magnetic and gravity derivatives can be likened to seismic attributes as they can help define the physical properties of the source structure causing the anomaly (Verduzco, *et al*., 2004). This contribution looks at the *tilt derivative*, first reported in 1994. The combination of the tilt derivative and its *total horizontal derivative* are highly suitable for mapping shallow basement structure and different density bodies as that they have distinct advantages over many conventional derivatives (Verduzco, *et al*., 2004). In addition, it has been necessary to use all the tectonic and structural information for comparison with the interpretation so far available from shallow and deep earthquake seismicity.

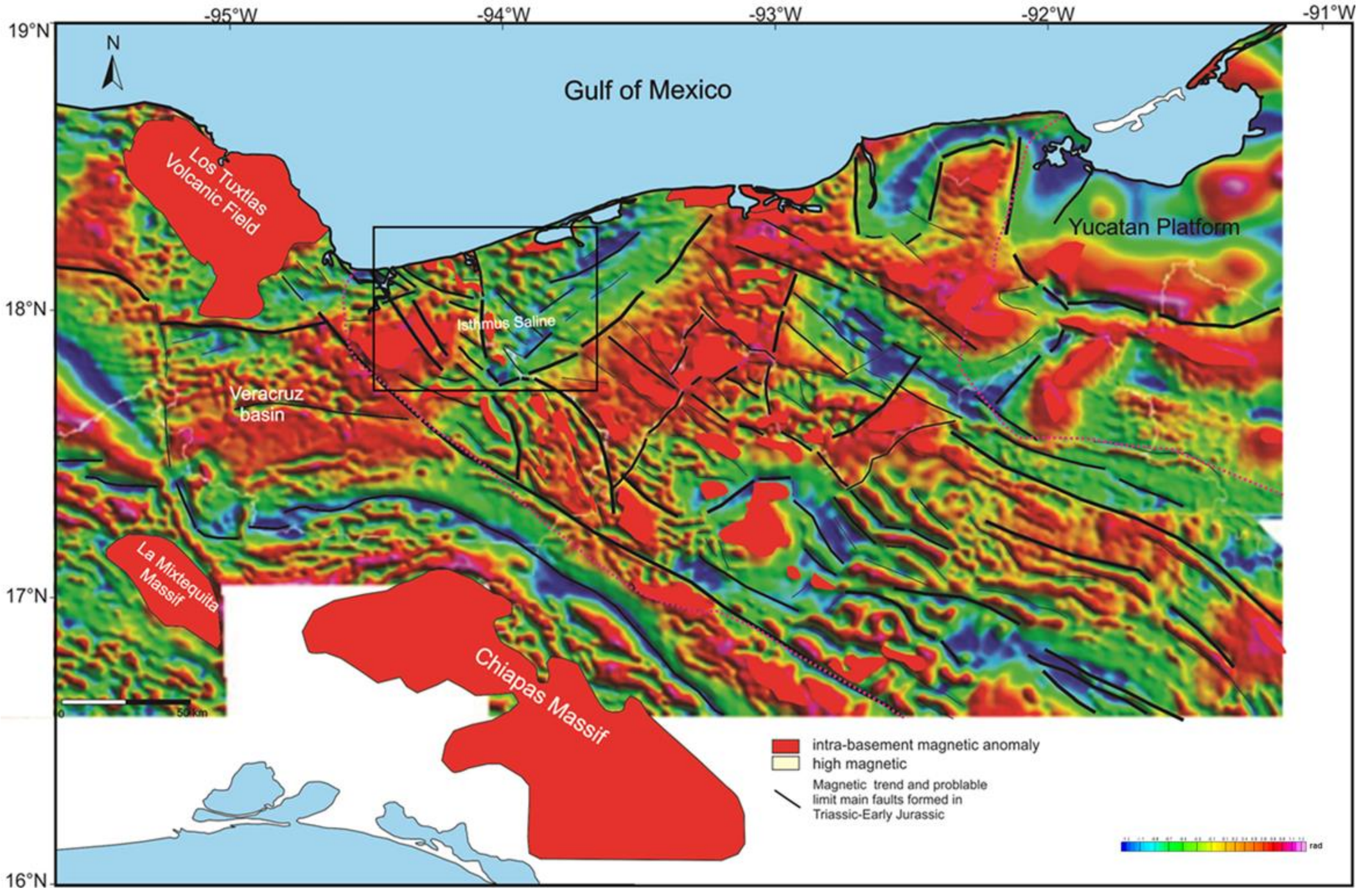

Figure 6.9 Main structural trends of magnetic anomalies defined by tilt derivative IMT (Data provided by PEMEX, 2012).

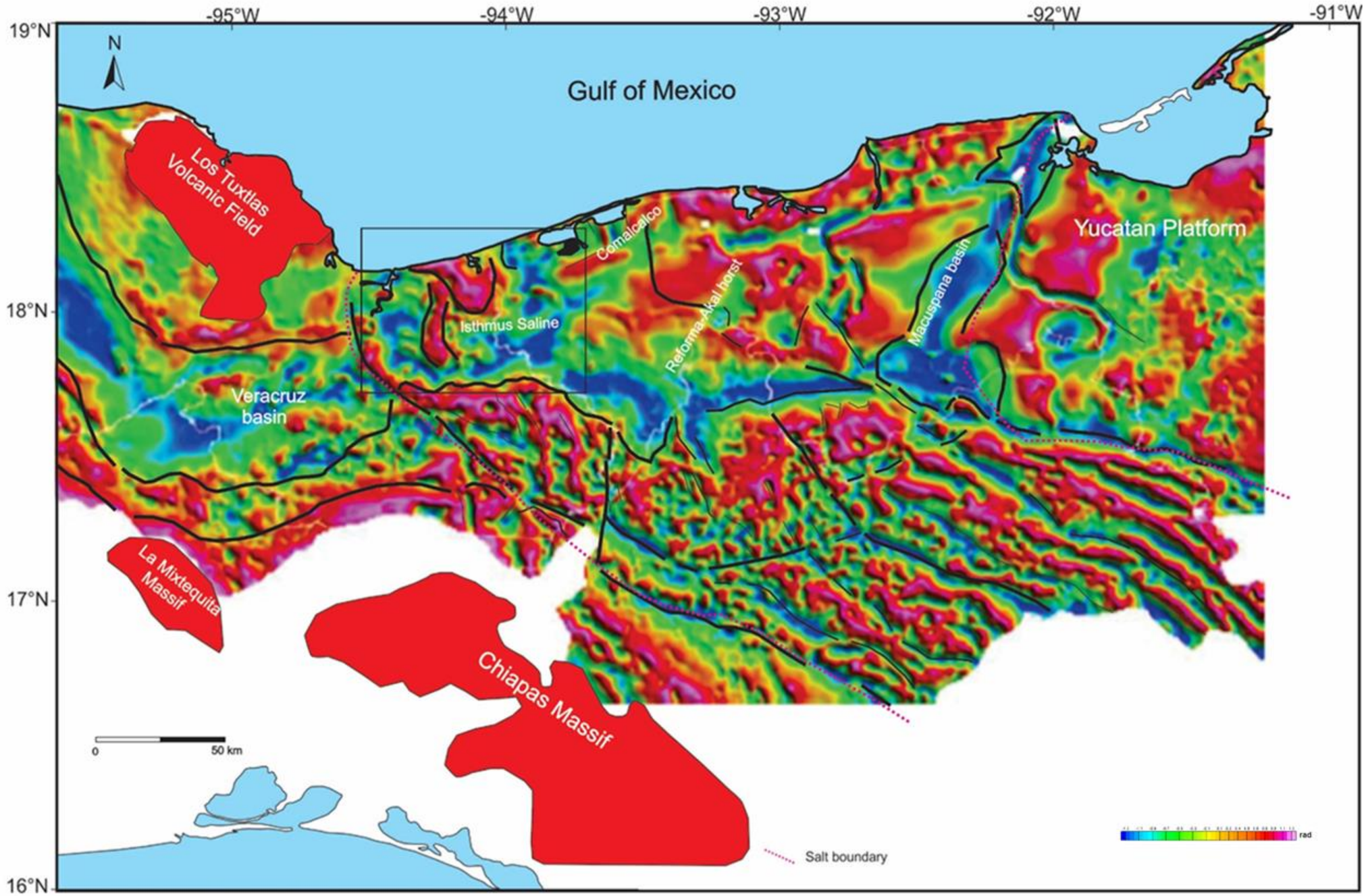

Fig.6.10 Delimitation of anomalous bodies and structural lineaments through tilt derivative of Bouguer anomaly (Data provided by PEMEX, 2012). The study area is indicated in the black rectangle. Black lines define the main gravimetric trends.

Before the description of the interpretation it is necessary, to define briefly both gravimetric and magnetometric theoretical concepts.

The gravimetric method is a tool to measure the lateral density contrast between one area to another generating a gravimetric anomaly (Sheriff, 1978). This anomaly may be caused by one or more geological structures such as folds, faults, unconformities, igneous intrusions, salt domes. This structure may be close to the surface or deeper in the subsurface. If the mass is deep then, the amplitude of the anomaly will be smaller and more extensive. Therefore, during the interpretation the size of the anomaly, the density contrast and depth must be considered (Sheriff, 1978).

The magnetometric method defines the anomalies caused by magnetic susceptibility contrasts due to the content of ferromagnesian minerals in rocks (Sheriff, 1978). Commonly intrusive and extrusive rocks can be defined when they affect the sedimentary sequences.

The gravimetric and magnetic analysis considered a regional structure framework of southeastern of Mexico. In order to establish geological-geophysical correlation between the main gravimetric anomalies and strike-slip faults was integrated a surface geology map to relate anomaly versus geology (Figure 6.11).

6.6.1 Regional Magnetic Interpretation

The susceptibility magnetic contrast as well as the magnetic gradient obtained by the IMT and TILT derivative of IMT data allowed makes a subdivision of the Southeast basin. The subdivision represent individual block basement with particular magnetic properties each one. The South-eastern basin was divided in five main structural blocks, which present a different structural pattern in the basement (Fig. 6.12).

Magnetic block anomalies, are located in the Chiapas Massif, La Mixtequita Massif and the Los Tuxtlas Volcanic field, which are characterized by intrusive

igneous and volcanic rocks, it could serve as a reference with well defined magnetic anomalies of geological features.

Block 1 is located in the south and is characterized by NW-SE magnetic alignments which are geologically linked with the southern sector of Strike-slip Province and Reverse Fault Province of Chiapas Fold Belt. This block is characterized by having magnetically anomalous bodies oriented NW-SE parallel to the main trend that marks the edge of the basin (Fig.6.12). The anomalous bodies are long and narrow. In the north of this block is a feature with high values of magnetic susceptibility displayed in yellow and red colour which correlate with Santa Fé intrusive igneous and volcanic rocks with high magnetic susceptibility. Additionally, this block shows small high magnetic anomalies (red colour anomalies) which has been related with sub-lithospheric intra-basement magmas bodies associated with active faults (Pindell, 2014, Jacobo-Albarran & Valencia-Islas, 2000).

Block 2 is located at northeast margin of the SE Mexico. It shows a change in the direction of the magnetic boundaries to NE-SW. This magnetic alignment is geologically related to the Macuspana Basin, which is a Cenozoic basin. This structural block is limited by magnetic anomaly oriented NE-SW, which is related with intrusive igneous rocks reported in the Cobo-301 well (Pemex, 1983).

Block 3, is located at central part of the SE Mexico, this block is bound by magnetic alignments oriented NW-SE and NE-SW. The block shows broad distribution and high magnetic anomaly represented in yellow colour, which could be related with intra-basement magnetic anomalies, oriented NW-SE. This magnetic block correlates geologically with the Reforma-Akal horst that represents the main Mesozoic oil block (Fig. 6.12).

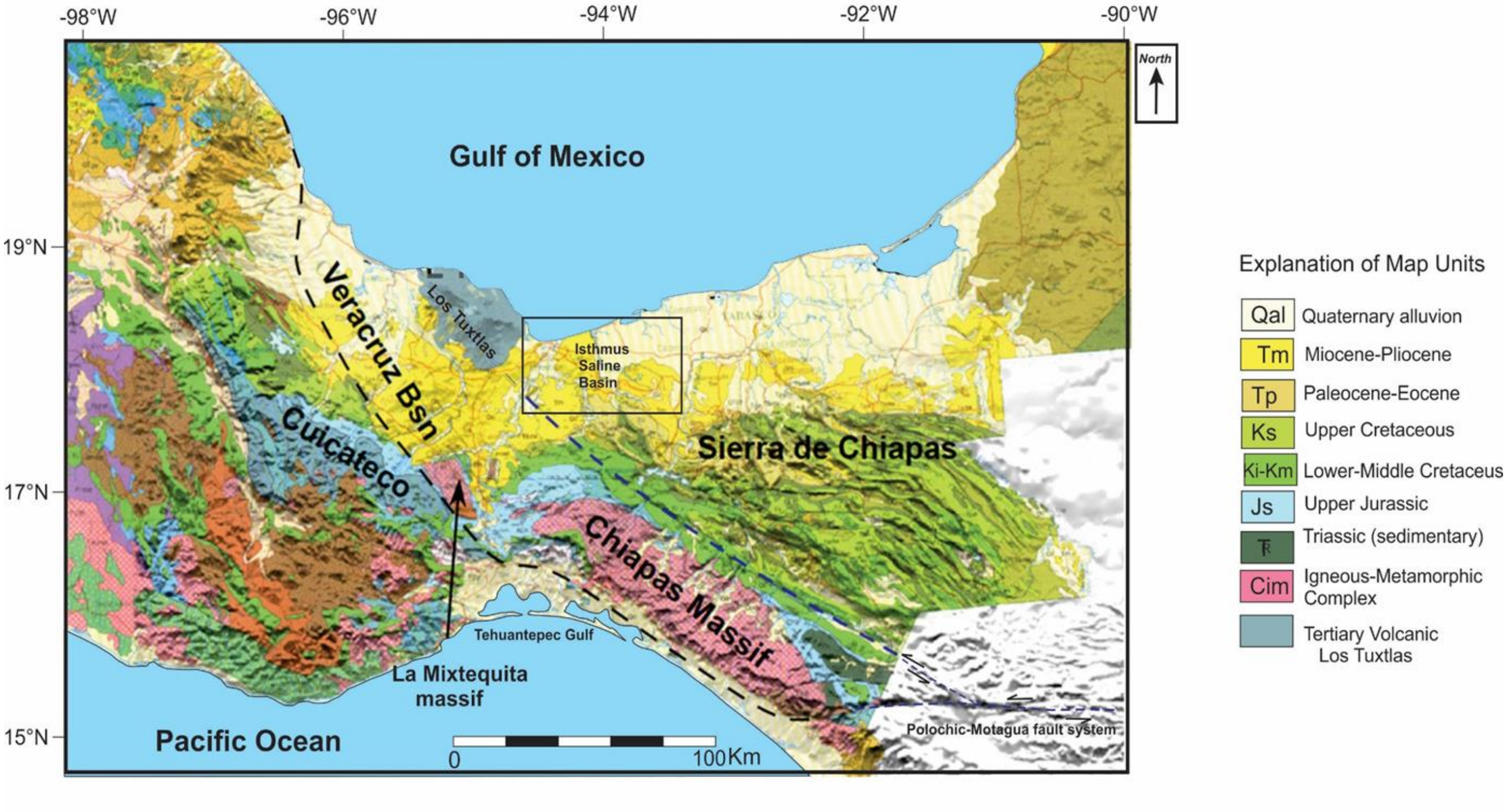

Figure .6.11 Geologic Map of South-eastern of Mexico showing main structural features around the Isthmus Saline Basin. (Ortega-Gutierrez, *et al*., 1992)

Block 4 is located on the SW margin of the SE Mexico basin. The block is limited by NW-SE slightly bent magnetic boundaries. This magnetic block is geologically related with NW boundary of the Strike-slip Province and shows high magnetic anomalies, which correlate with intra-basement magnetic anomaly (Fig 6.12).

. Block 5, is located at NW margin of the SE of Mexico basin, it represent the Isthmus Saline basin area. This block has two main structural trends. The first is characterised by a NW-SE anomaly trend, which is limited to the south by a NE-SW magnetic alignment but internally divided in small blocks by NW-SE magnetic alignment. This fragmented block has a high magnetic anomaly as well as intra-basement magnetic anomalies related to high of basement with high values of magnetic susceptibility. The second area is represented mainly by a combination of small block with NW-SE orientation and NE-SW magnetic alignment. This area is characterized by low magnetic susceptibility which can be interpreted as a deep block; meanwhile, the west side shows an anomaly pattern that could be interpreted as stepped blocks.

The NW-SE magnetic anomalies alignments of the Isthmus Saline basin could be correlated with block 4, but the magnetic alignment of block 4 show a NE displacement with respect to block 5 (Fig.6.12)

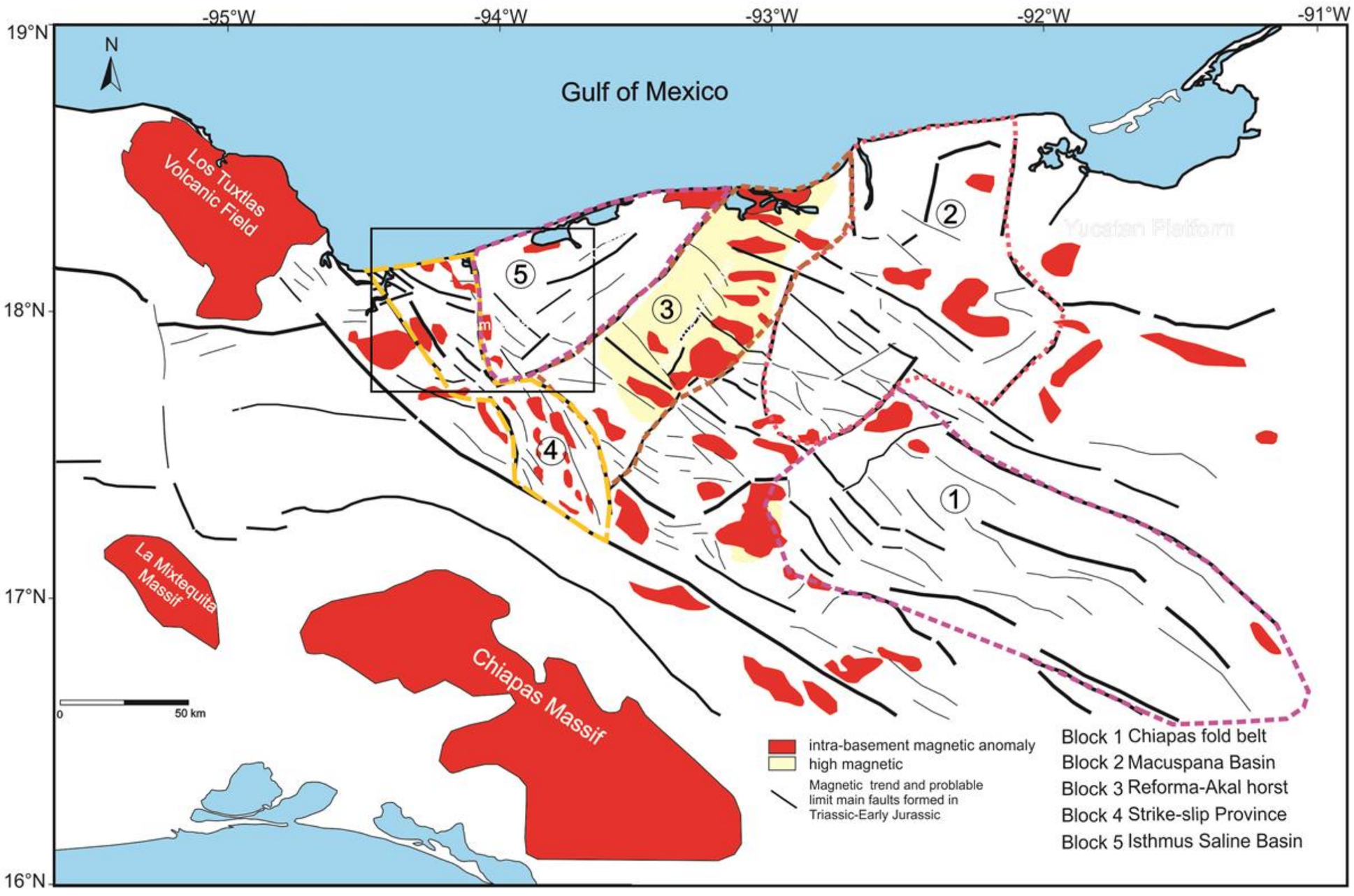

Figure .6.12 Structural Interpretation of the Magnetic tild derivative showing the main structural blocks of Southeastern of Mexico.

6.6.2 Regional Gravimetric Interpretation

The gravimetric method is useful to define density contrasts caused by folds, faults, unconformities, igneous intrusion, salt domes, shale domes (Sheriff and Geldart,1995). Additionally, it provides information on areas with large thickness of Cenozoic sediments. Consequently, this contrast between structural elements and thickness variations allows identification of subsidence caused by tectonic activity in basement blocks.

The analysis and interpretation of the Bouguer and tilt derivative of Bouguer (gravity filter) data along Southeast of Mexico defined gravity trends and negative gravity anomalies, which are related with low density material as salt and shale domes. In contrast, positive gravity anomalies will be related with high density rocks (Fig 6.13).

The tilt derivative gravity map was divided in five structural blocks in based on dimensions of anomalies patterns. The high and low gravity anomalies were correlated with structural geological features defined from stratigraphic control.

Block 1 is located in the Chiapas fold belt. It is represented by NW-SE high gravity anomalies, which has the characteristic to be large and narrow features. The low gravity anomalies are few and relatively thin. It has the same pattern than the anomaly trend. This block is related high density rocks, represented by platform carbonates. The gravity anomaly could represent salt core fold-thrust structures probably controlled by deep faults basement. The positive gravity anomaly represents the Santa Fé intrusive igneous and volcanic rocks (Fig. 6.13).

Block 2, is located at southwest margin of the strike-slip province, is represented mainly by NW-SE high gravity anomalies and very few low gravity anomalies. These anomalies has the characteristic to be small, narrow and with some degree of rotation. These anomalies are interpreted as high density rocks characterised by dense carbonates and fold-thrust structure probably are controlled by the basement with little influence of salt (Fig.6.13).

Block 3 is located at NE margin of the basin. It is represented by NE-SW large and wide low gravity anomaly. This anomaly is related with the Macuspana basin, which is characterised by 5000m depth basin filled with Neogene shales and sand rocks (Fig.6.13).

Block 4 is located at the centre of the basin. It is represented by NW-SE and E-W high gravity anomalies. Toward the south of this block is characterized by a series of E-W large and wide low gravity anomalies, which probably represent deep salt structures or the boundary of fault between the platform and slope. Meanwhile, toward the north high gravity anomalies, are characterized by large and a wide amplitude anomaly. These gravity anomalies are believed to be related with relatively shallow Mesozoic structures cored by deep salt (Fig.6.13).

Block 5, is located at NW of the basin. It is represented by two main patterns of low gravity anomalies. The first pattern is formed by five small low gravity anomalies with variable orientation. This low anomaly is linked to deep salt diapirs, which are part of the east sector of Isthmus Saline Basin. The second pattern is related with a large and wide low gravity anomaly that is located in the WNW sector of Isthmus Saline Basin. This low anomaly pattern is related with a shallow salt canopy that has been drilled by exploration wells (Fig. 6.13).

The Isthmus Saline basin is limited to the west by Veracruz basin. The Veracruz basin is represented by wide and large low gravity anomaly. The Veracruz basin is characterised by 5000 m of Paleogene and Neogene sediments. The northern and southern of the Veracruz basin is limited by large and wide high gravity anomalies represented by high density volcanic and igneous rocks (Fig.6.13).

The gravity and magnetic analysis of Isthmus Saline and Veracruz basin have allowed establishing narrow structural boundary between these basins.

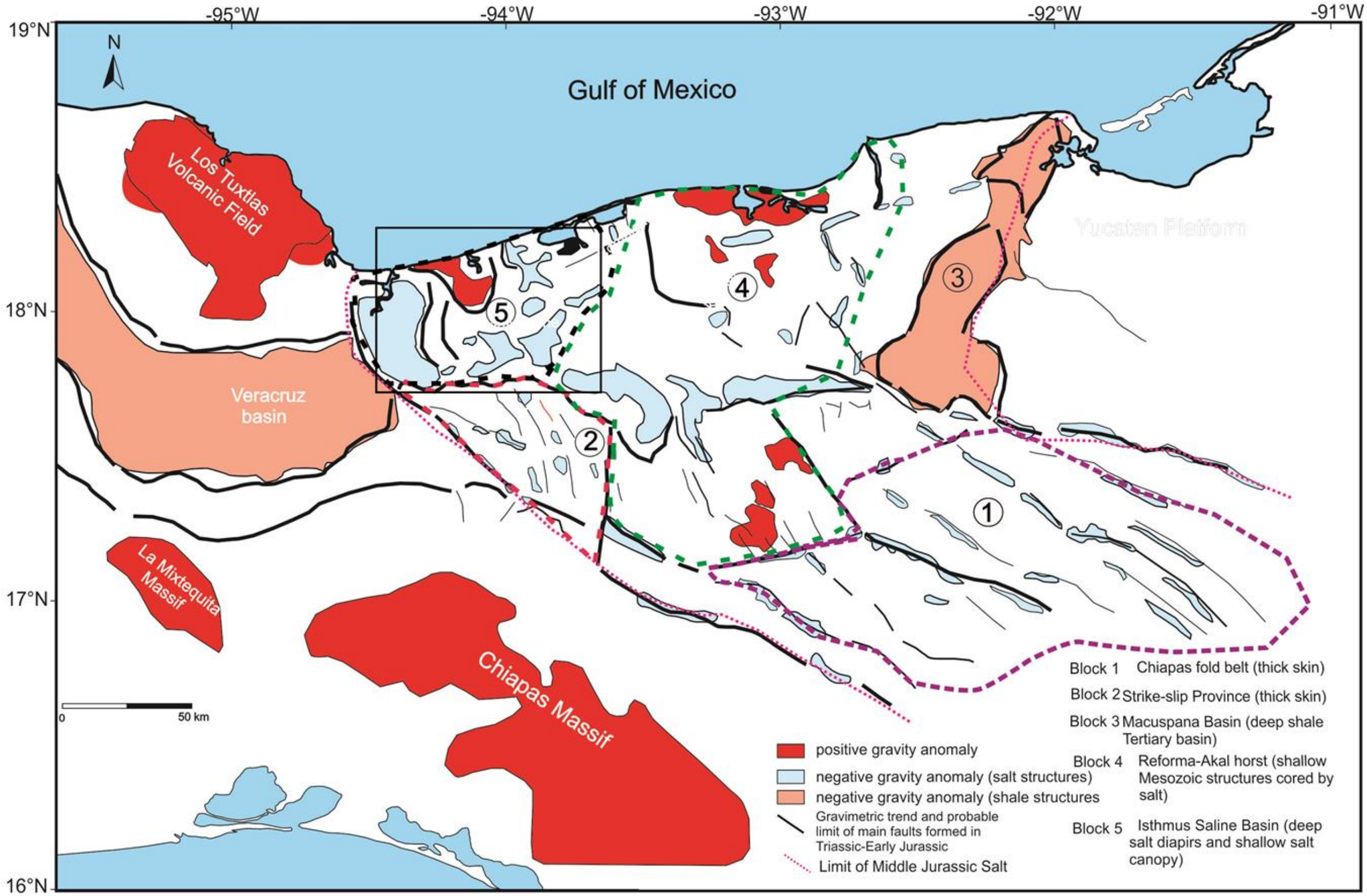

Figure .6.13 Structural Interpretation of the Gravity tilt derivative showing the main structural blocks of Southeastern of Mexico.

6.7 Basement Architecture

So far, the basement geometry has not been important to understand the relationship between the geologic setting, development and architecture of salt structure.

In this research I analysed and interpreted the structural lineaments from Landsat satellite images, the distribution o 2D seismic data to define the basement geometry and the distribution of salt structures in the Isthmus Saline basin.

The complexity of the fault system arrangement basement of ISB makes difficult to establish a dominant structural pattern. Meneses-Rocha (1987) has emphasized the significance of “northwest-southeast” trending strike-slip faults as a weakness and structural anomaly in the geological history of the southern Gulf of Mexico. However, only the south-eastern part of the basin maintains that structural trend (Fig.6.14). The boundary between the south-eastern and northern area of the basin is marked by a NE-SW lineament, which coincides with the extensional zone represented by volcanic and intrusive igneous rocks of Santa Fe - Chichonal volcanic complex. Toward the north of Santa Fe – Chichonal volcanic complex, the NW-SE Triassic - Early Jurassic fault system lost the structural continuity because it is dislocated by a northeast-trending tear fault, represented as NE-SW normal faults (represented in blue lines) during the Neogene. The figure 6.15 shows a structural map of the complex basement architecture and the structural interpretation of South-east of Mexico modified from Jacobo-Albarran, et al (2003). The red colours represent the position of Chiapas Massif and blue represent the geometry of deep structure of the basement, which are main centre of hydrocarbon generation of South-east of Mexico. Additionally the volcanic centre activity show the position of weakness zone where the Neogene intrusive and volcanic rocks were emplaced. However, the light blue colour (figure 6.15) shows how the ISB represent a semi-circular graben bisected by left strike-slip fault, which was controlled by the strike-slip fault system oriented NW-SE. The basement tends to become shallow towards the east.

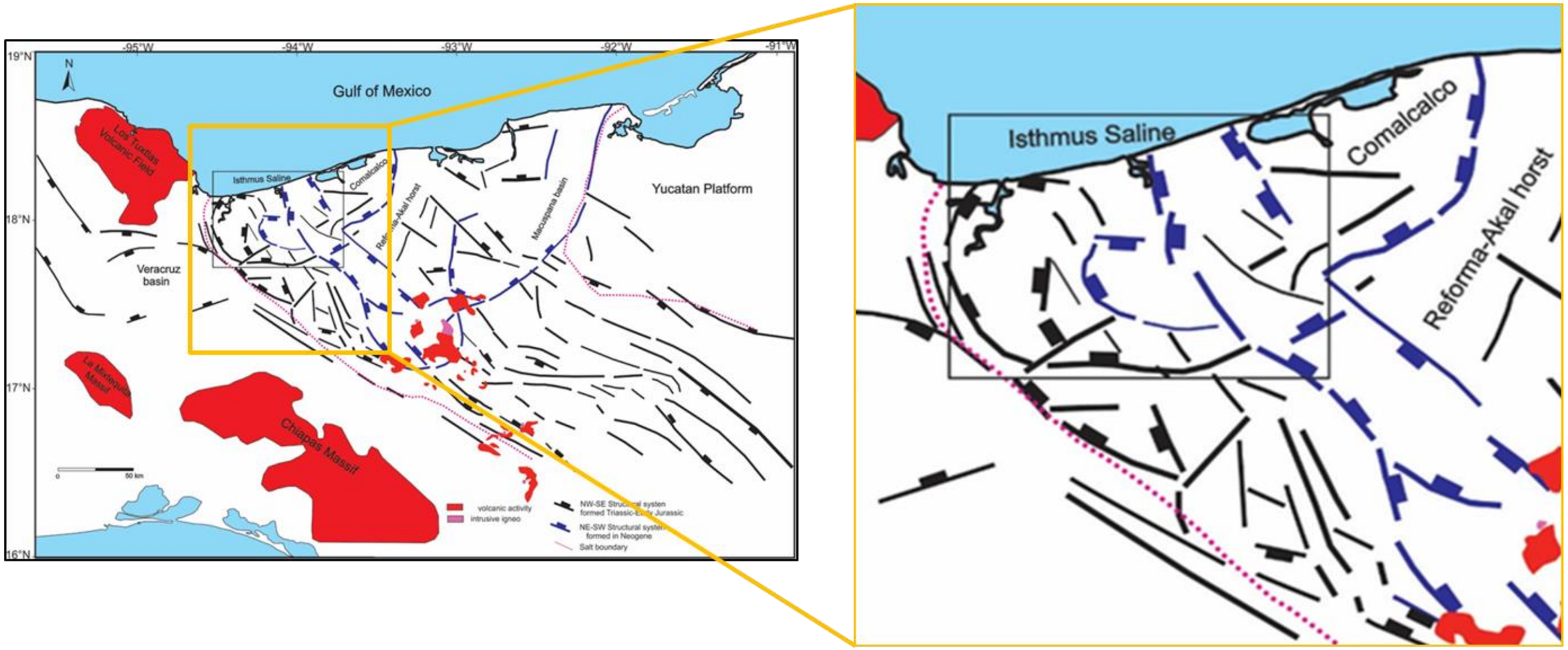

Figure .6.14 Interpretation of basement geometry of South-eastern of Mexico was done by the author. The black rectangle represents the research area. The structural boundaries were defined based in the combination of gravity and magnetic qualitative analysis (previous maps). ISB basin represented in black lines shows a half semi-circumference. The other half defines the Comalcalco basin represented in blue lines. The basin seems to be broken and displaced.

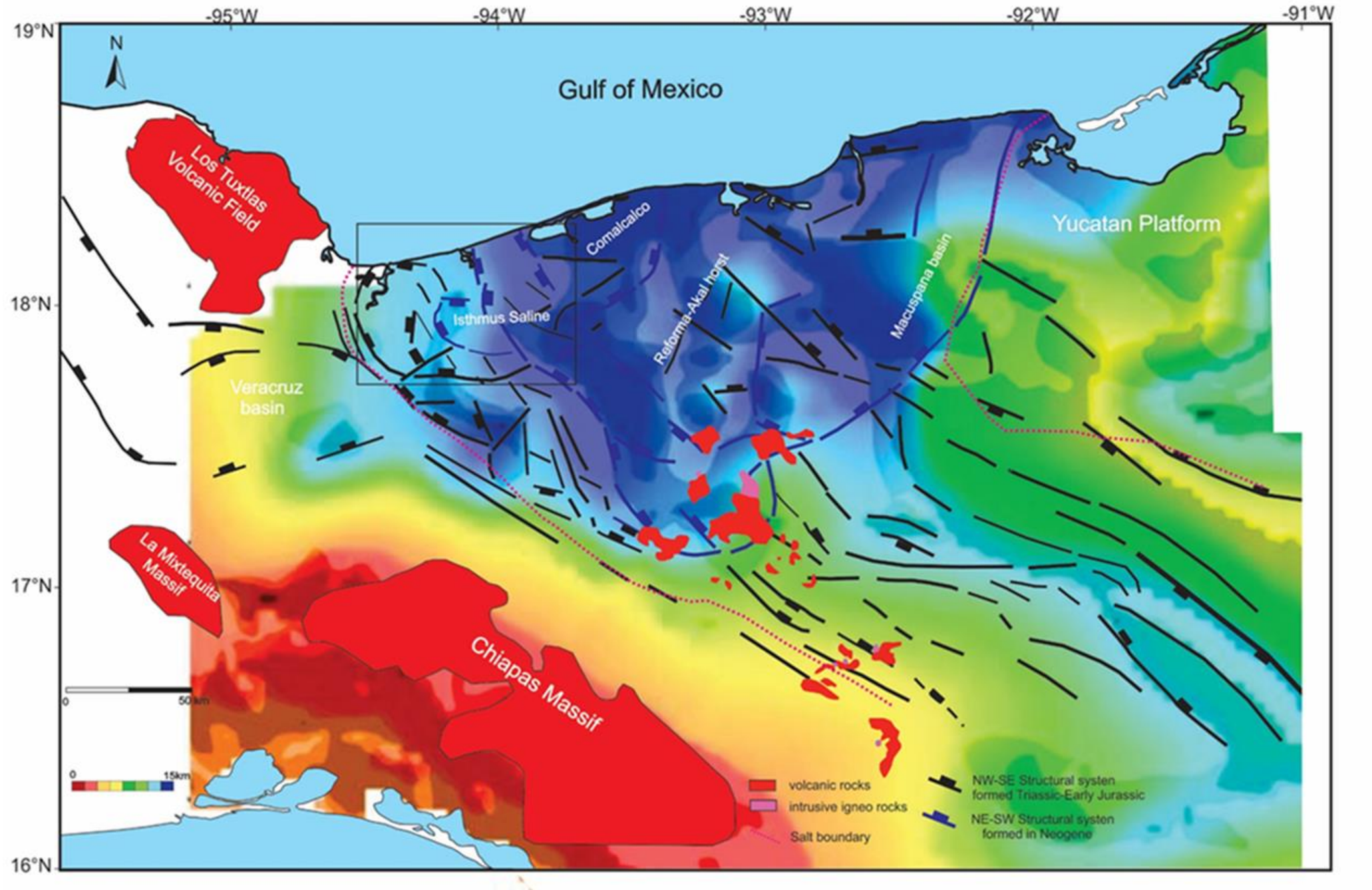

Figure .6.15 Interpretation of basement geometry of South-eastern of Mexico. The black rectangle represents the research area. .Structural interpretation of the main fault trends was done by the author. The configuration was (modified from Jacobo- Albarrán, *et al.,* 2003). The construction of the map is based in the combination of gravity and magnetic analysis. Colours represent depth of basement in km.

6.7.1 Isthmus Saline Basin Configuration

Salt diapir distribution in the Isthmus Saline basin was controlled by gravity and magnetic data, 2D seismic lines and well data.

The semi-circular configuration of ISB basement shows the differential sinking from West to East and South to North of basement. There are magnetic and structural evidence of inversion within the ISB (Fig.6.16).This type of structures is common in intracratonic basins (Letouzey et al., 1995). However, the Isthmus Saline basin is part of a passive margin that has been shortened obliquely as result of convergence of Chortis Block and North America Plate. The Isthmus Saline basin was reactivated by NW-SE left strike-slip shortening, which transformed the salt anticlines into tall contractional diapirs and salt thrust created large intervening depocenter with up to 6 km thick sediment.

Salt structures in the study area display a pattern in the location, orientation and maturity (pillow, piercement and salt canopy) of the salt structures (Fig. 6 16). The faults that delineate the Isthmus Saline basin show a semi-concentric pattern. In the central area of the basin to the north, has been defined by high density gravity element and a magnetic block that has been interpreted as a high basement. The south of the basin is bounded by an E-W fault that represents the NW tip of strike-slip province. Toward the west, the boundaries of the Isthmus Saline basin and Veracruz basin are poorly defined. However through the potential methods it was possible define a fault to the NW. toward the E the deep of the ISB graben increase stepwise from west to east. In the east, the basin shows sinistral strike-slip faults that divide the basin forming the Comalcalco basin to the east; in this zone the depth is more abrupt.

The salt structure orientation in the ISB is represented by elongated diapirs sub-parallel to the faults at the west sector of the basin. The centre part basin show salt structures elongated to the NW-SE and comprise walls and salt core thrust. Toward the east the salt structures are bigger, elongated with different orientation. and comprises pillows, diapirs and walls.

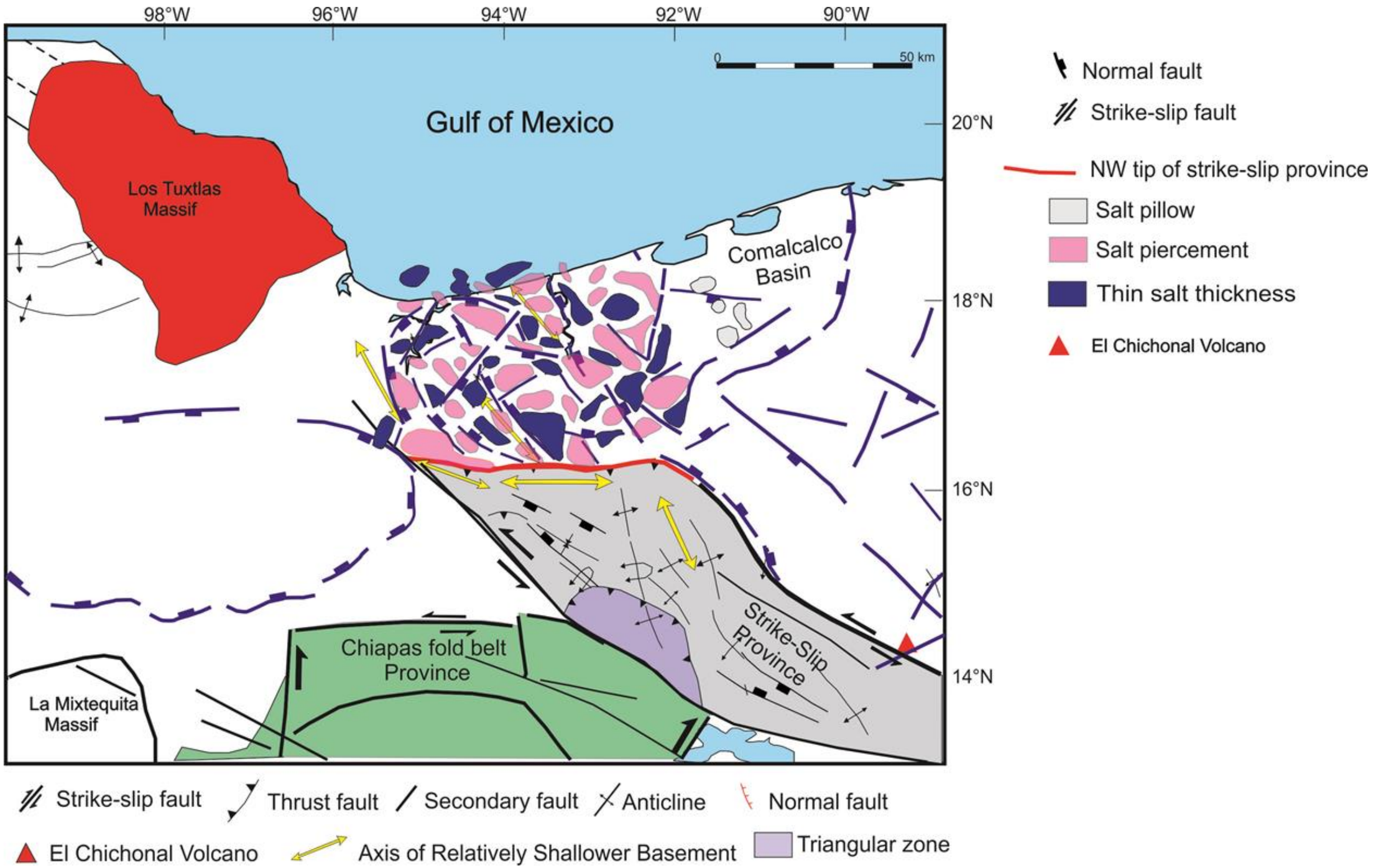

Figure .6.16 Structural map of the Isthmus Saline basin showing the orientation and geometry of salt diapirs. Some diapirs show relationship between basement faults and salt structures interpreted from gravity, magnetic, 2D seismic and wells data. The mapping was done by author.

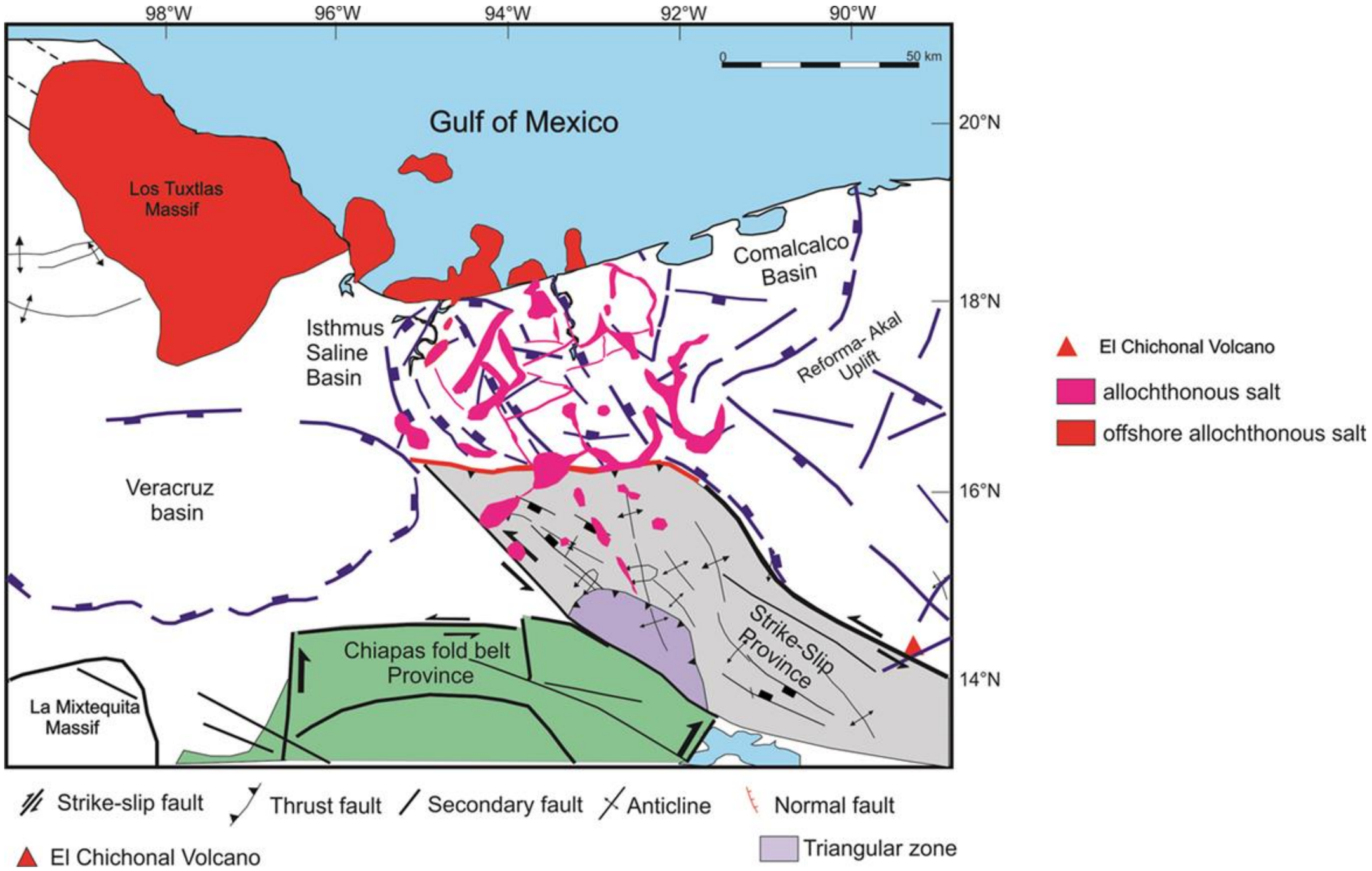

Fig.6.17 Structural map of the Isthmus Saline basin showing basement fault also was mapped the distribution of allochthonous salt. The offshore allochthonous salt was taken from Cabrera-Gomez and Jackson, (2009),.

The allochthonous salt distribution in ISB shows two main orientations (Fig.6.17). The first, is oriented NW-SE, represented by thin elongated diapirs almost parallel to the faults of the basin and small individual allochthonous salt bodies. The second, is oriented NE-SW, this allochthonous salt sheets are located to the west of the basin and tend to be more continuous and almost 2000m thick. The offshore allochthonous salt was integrated from the work done by Cabrera-Gomez, et al., 2009 with the purpose of knowing the continuity and distribution of allochthonous salt.

Due to the new PEMEX regulations on the use of the information, it will not be possible to show all the seismic information. Although, the seismic sections used show a very poor quality image was possible to sketch models that could give an idea about the structural geology of the ISB and its surroundings.

The figures 6.18, 6.19 and 6.20 exhibit the seismic sections and their respective sketches that allowed proposed geological models of the ISB. The fifteen seismic sections also exhibit other deformation style; unfortunately this cannot be shown for lack of permits. The seismic section allowed interpret basement shortened together with salt and overburden. Secondly, to the south of Isthmus Saline basin, in the Strike-slip Province there are transpressive structures that evidence thick skin deformation caused by strike-slip faulting. The Figure 6.21, .illustrate four sections located the north flank Chiapas Fold Belt, and the south flank Strike-slip Province and their relationship with Isthmus Saline basin. The interpretation of four geological models oriented NW –SE allow to demonstrate that the south-east of Mexico and specifically the research area is under the influence of a complex mixture of different tectonic processes

Section A, oriented N-S is located in the western part of the Isthmus Saline Basin and north flank of Chiapas Fold Belt. The section shows evidence of thick-.skin deformation. The orogenic driving shortening resulted in the formation of inverted roller structures to the south, while to the ISB the structures are represented by salt thrusting and extrusion through the different stratigraphic levels and evacuation of allochthonous salt during Upper Miocene.

Section B, oriented NW-SE is located in the southern flank of the Strike-slip Province. The geological model shows evidence of thick-skin deformation, resulting in thrusting and back-thrust structures to the south. Northward, the structures are related with shortening, represented by core anticlines and salt thrusting toward the ISB during Upper Miocene.

Section C, oriented NW-SE is located in the southern flank of the Strike-slip Province. The geological model shows evidence of thick-skin deformation resulting in thrusting and back-thrusting to the south. Toward north the shortening structures are represented by salt diapirs squeezed, salt core anticlines and salt thrusting in ISB during Middle Miocene.

Section D, oriented NW-SE is located to the south of Comalcalco Basin. The geological model shows evidence of thin-skin deformation. This section shows evidence of gravity driven extension during Eocene. The extesional stage is represented by salt-roller to the south. The contractional deformation is evidenced by reactivation of salt anticlines; salt diapir squeezed and salt folding in the ISB during the Upper Miocene.

All these geological features represented in the geological models fit with a geodynamic model where the role of compression caused by orogenic tectonic processes and gravitational tectonics are controlling the geometry, orientation and maturity of salt tectonics in Isthmus Saline basin. In this particular case the importance of its role appears to have varied considerably from place to place and in different time.

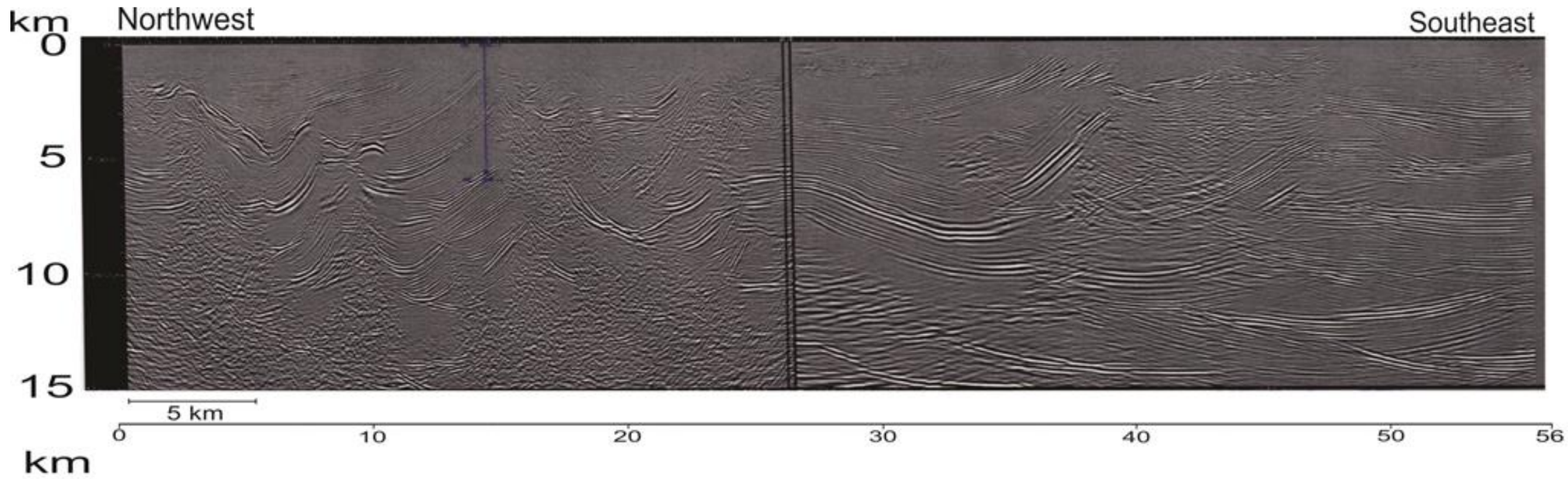

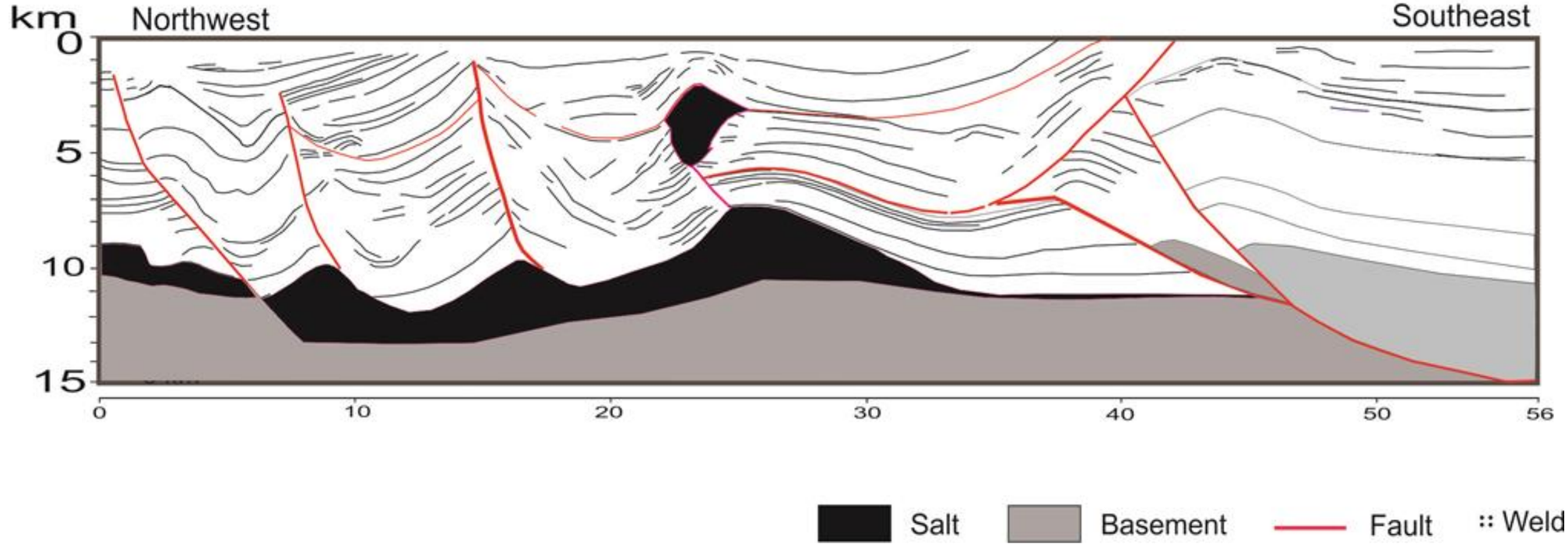

Figure .6.18 2D Seismic section and line drawing, showing the Isthmus Saline basin and part of Strike-slip Province the sketching was made by the author

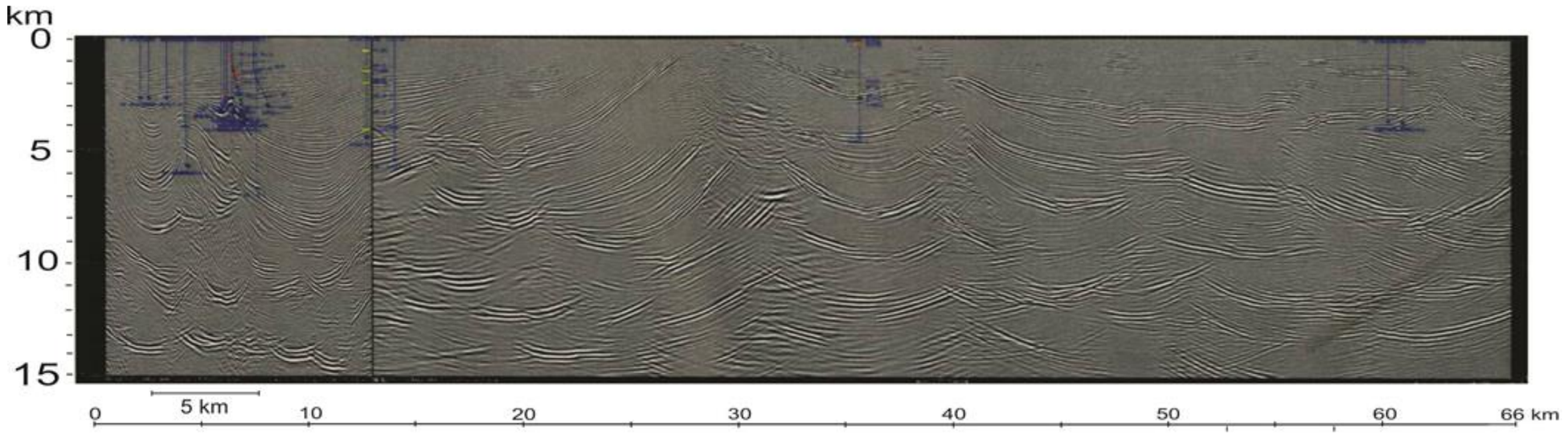

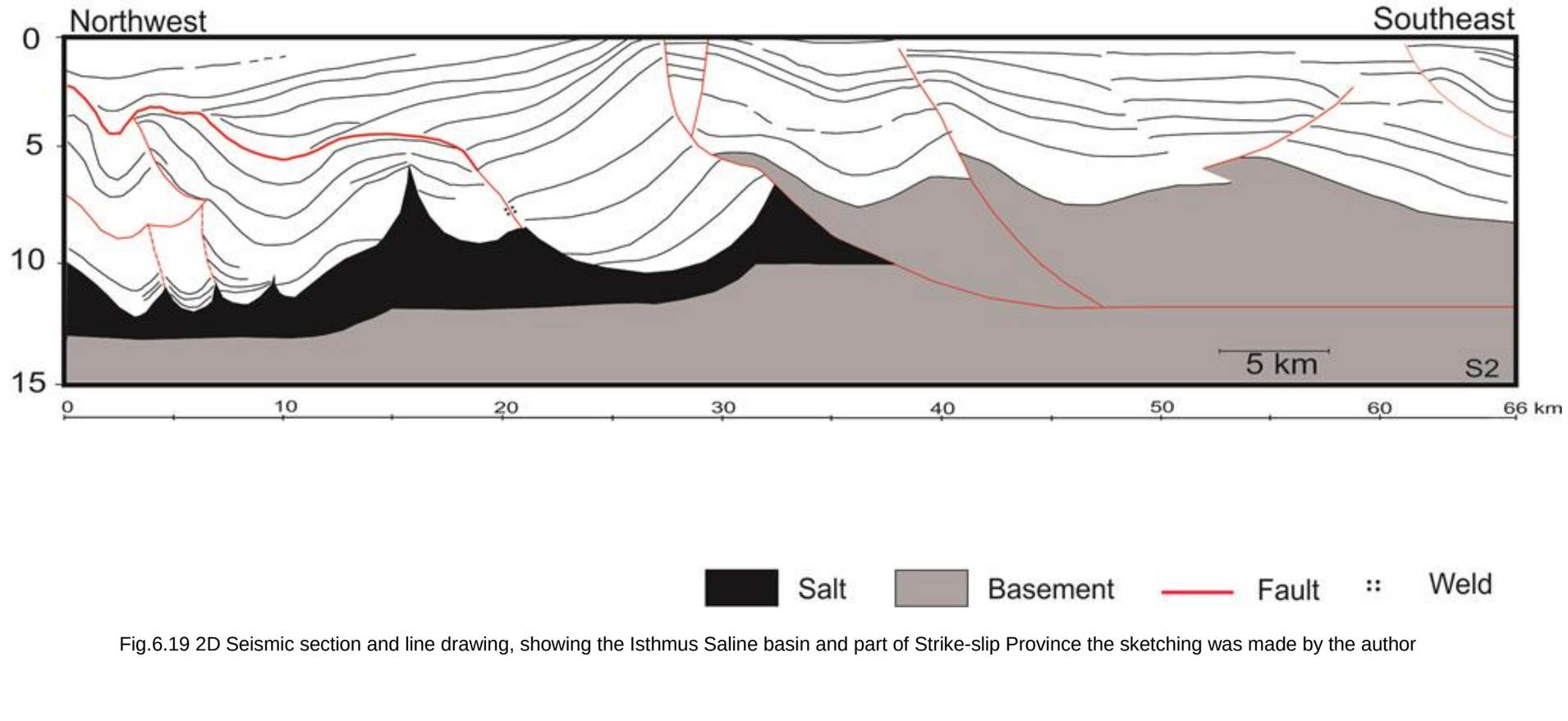

Fig.6.19 2D Seismic section and line drawing, showing the Isthmus Saline basin and part of Strike-slip Province the sketching was made by the author

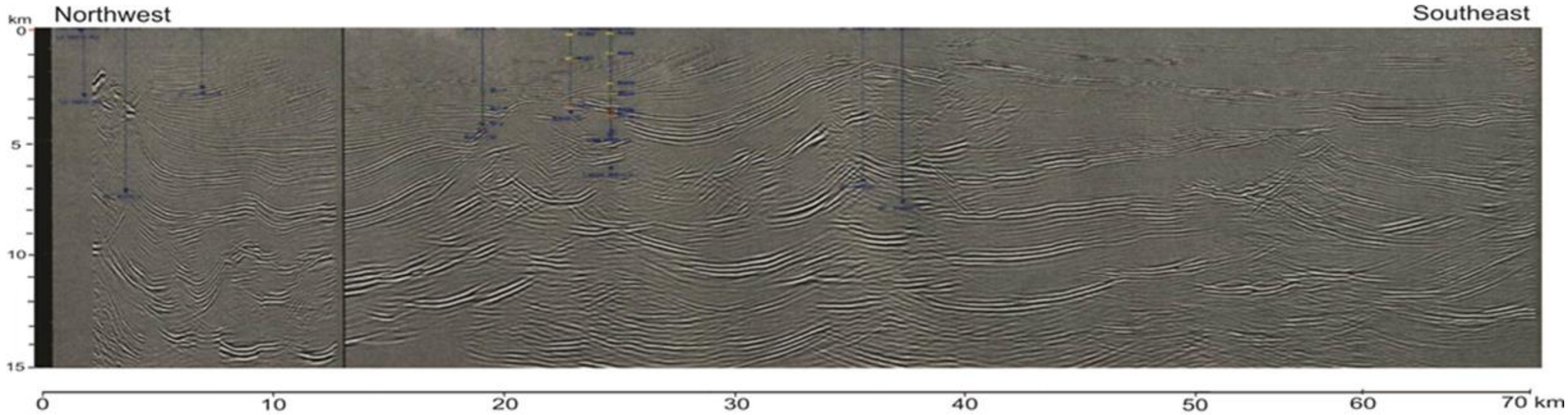

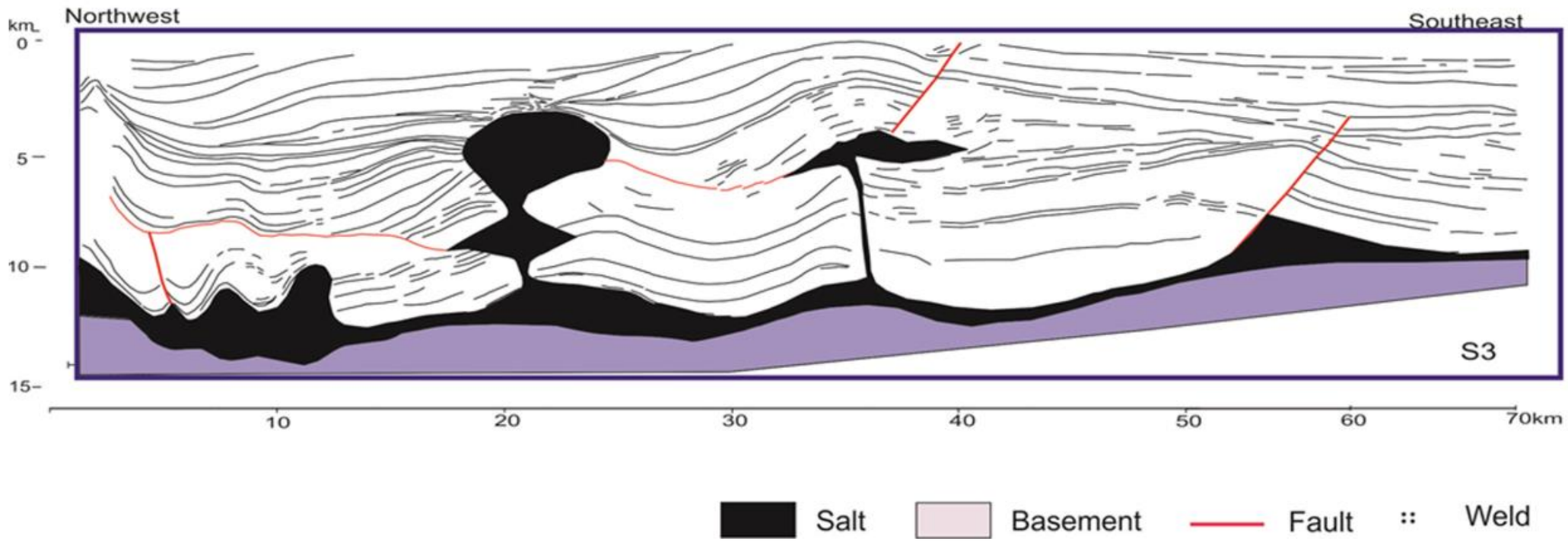

Figure 6.20 2D Seismic section and line drawing, showing the Isthmus Saline basin to the NW and the beginning of the Comalcalco salt evacuation basin. The sketching was made by the author

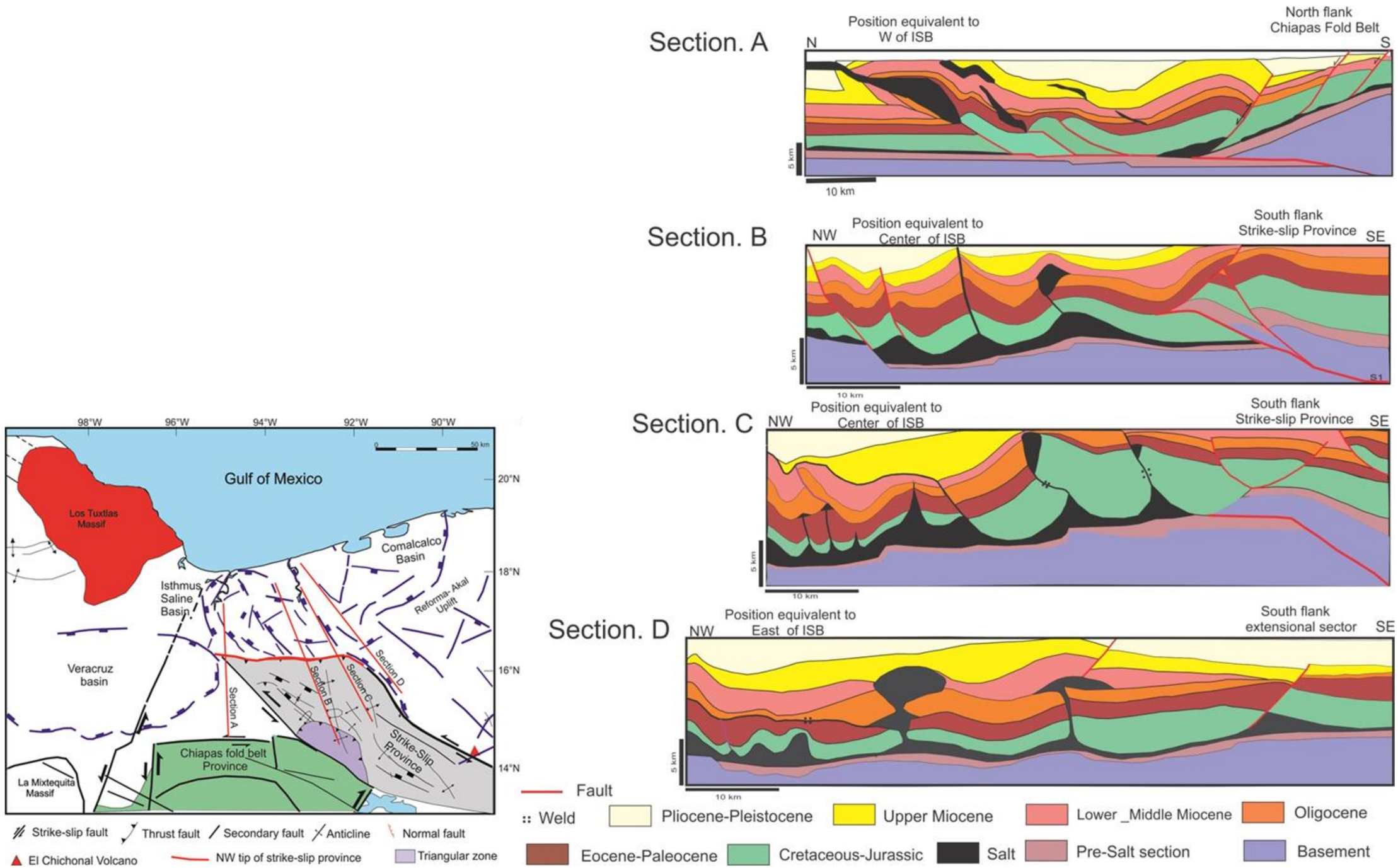

Fig.6.21 shows the structural relationship between NW front of Sierra de Chiapas and Isthmus Saline Basin to illustrate the complex structural patterns that have influenced in the configuration of the Isthmus Saline Basin in a short distance. The geological models were done by the author.

6.8 Summary

The earthquake activity of south-eastern of Gulf of Mexico is very different from the passive margin of the north of Gulf of Mexico.

Earthquake activity defines two main areas that constrain the Isthmus Saline Basin: the Istmo de Tehuantepec Fault Zone that is oriented NE-SW and the Strike-slip fault province oriented NW-SE.

The shallow earthquakes events recorded in the Motagua-Polochich and Strike-slip fault system indicate left lateral strike-slip events. Between these two systems faults the Reverse Fault Province acts as a fault step between Motagua-Polochic and Strike-slip Fault System.

The NW-SE seismicity trend of Motagua-Polochic and Strike-slip Province continues toward the Isthmus Saline basin where transpressive structures are represented by squeezed salt diapirs and thrusted salt-cored anticlines. However, the presence of seismicity is significantly attenuated.

The distributions of deep earthquakes, which are related with subduction events, mark a structural boundary. This structural limit coincides with the main fault of the Strike-slip Province oriented NW-SE (Malpaso Fault).

The interpretation of Landsat image shows three fracture systems, which coincides with the main seismicity trends.

1. - The first fracture system is oriented NW-SE, exist in the Reverse Fault Province and then continue to the NW front of Sierra de Chiapas. It represents the fracture system produced by reactivation of the basement blocks (horse and grabens) which evidence recent activity seismicity produced by the sinistral strike-slip.

2. - The second fracture system is oriented W-E, is represented in the Strike-slip Province, This fracture system is related with Polochic-Motagua fault system, which is seismically active.

3. - The third fracture system, is oriented NE-SW is the most recent fault system. This fracture system is related with the seismicity produced by the subduction. This fracture system was generated by the contraction which move or break the NW-SE fracture system.

The combination of the gravity and magnetic tilt derivative has resulted highly suitable for mapping shallow basement structure and different density bodies originated by salt and shale sediments.

The magnetic analysis allows defining the architecture of the South-eastern Gulf of Mexico. The basin has been divided in five blocks that were defined in base of own magnetic properties.

The Isthmus Saline basin is a combination of thick skinned deformation in front of a thrust belt and an inverted extensional basin driving by oblique contraction.

The structural configuration of the basement in the Isthmus Saline basin is represented by a semi-circular structure, which has been cut by left lateral strike-slip faults.

In the Isthmus Saline basin, salt structures are related with basement faults.

Chapter 7 Seismic Interpretation

7.1 Introduction

The regional tectonic evolution and salt tectonics within the Isthmus Saline Basin (ISB) have been interpreted using 2D seismic data together with 3D seismic survey.

The ISB is a NE-SW oriented asymmetric basin approximately 50 km long and 50 wide. It is dominated by a series of salt ridges and minibasins developed above a NW dipping Jurassic basement.

The aims of this chapter are to interpret a set of key 2D seismic lines that show major structures features within the basin and their relationship to the surrounding areas. The 3D seismic interpretation illustrates complex geometries of salt diapirs and associated salt withdrawal minibasins. These show a complex interaction of salt tectonics and sediment deposition.

In this thesis the 2D seismic data have been subdivided into three sets.

The first one was interpreted by PEMEX, 2008 but the author has reinterpreted, re-defining the structural domains.

The second and third set of data was interpreted by the author (Fig. 7.1).

- The first set of 2D seismic lines are represented by five regional seismic sections oriented NW-SE (R1 to R5 in green lines). These provide a regional vision of the South-eastern basins showing the domains and limits of the gravitational and compressional domain.

- The second set of 2D seismic lines, comprise three sections oriented NE-SW and show the salt structural features and salt geometry of the W and E sector of the ISB. D3 section shows the NW tip of Strike-slip Province (D1 to D3, blue lines).

- The third set of 2D is formed by fifteen sections (red lines), which cover most of the ISB. The lines are oriented NW-SE and NE-SW and show in detail the lateral variations of salt thickness and sedimentary sequences.

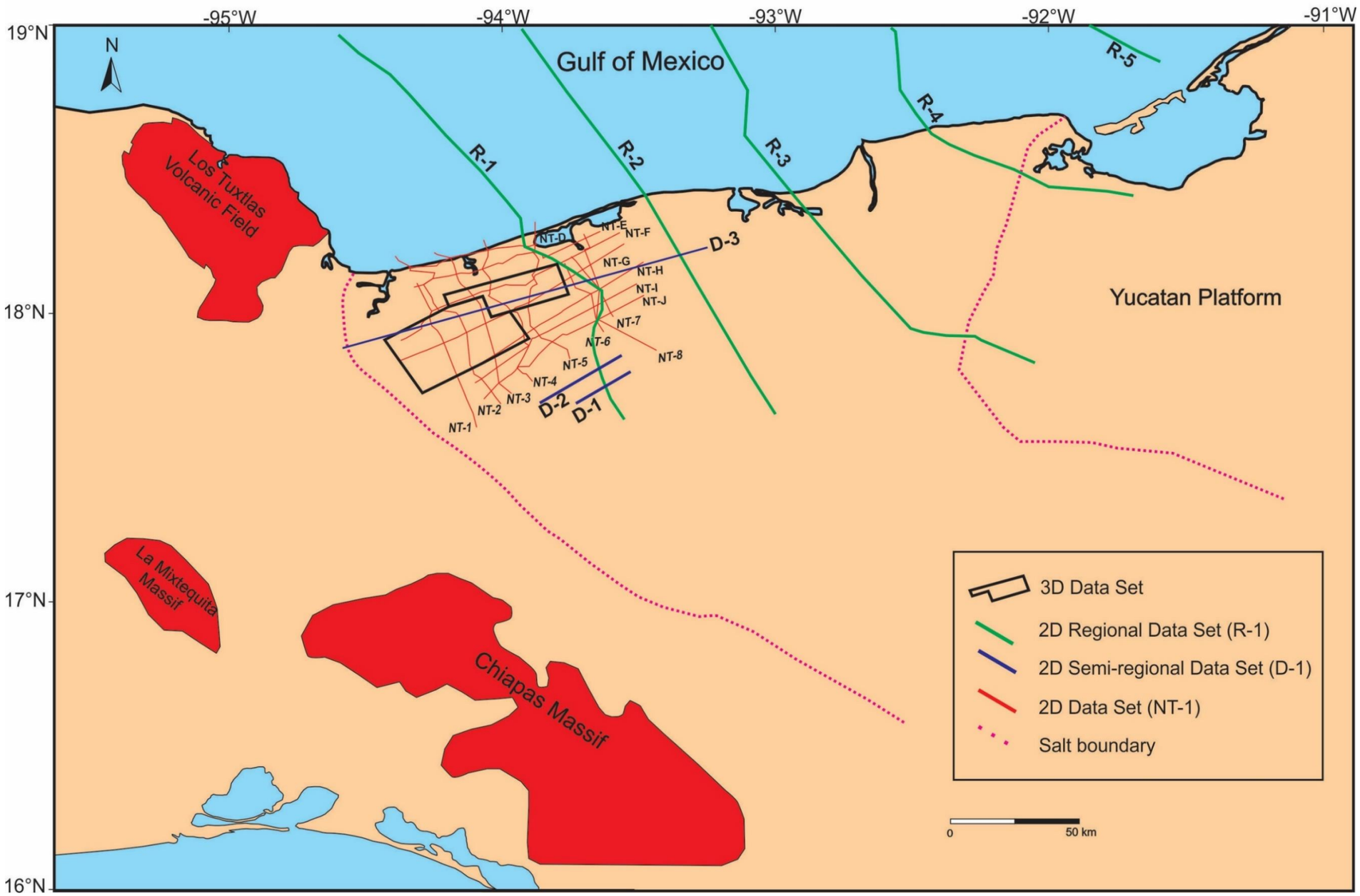

Fig.7.1 shows the location of 2D and 3D surveys used in this study.

3D seismic data illustrate the geometries of salt diapirs and associated salt withdrawal minibasins. These show complex interaction of salt tectonics and sediment deposition. The salt withdrawal basins are sub circular, encircle by narrow, elongated salt ridges.

7.2 Seismic 2D Interpretation

7.2.1 Regional structure: 2D seismic interpretation

The regional information is composed by five geological sections that have a length of 200 to 300 km and are spaced approximately 40 to 50 km. The sections cover the south-eastern basins from the tip of Chiapas Fold Belt to offshore along the salt province. The sections were built by PEMEX, 2008 and reinterpreted by the author (Fig. 7.2).

Section R1, is located to the west and is the closest to the study area. This section is the only one that passes through the strike-slip province and is characterized by a system of folds and thrusts that represent the contractional domain (Fig. 7.2.R1). It is considered that the detachment is represented by thin layers of salt which produces folds and thrust with high structural relief.

Isthmus Saline Basin is represented by a graben filled with Paleogene and Neogene sediments that reach up to 6 km thickness. Salt thickness is estimated to be 2 to 2.5 km (see chapter 8). The Paleogene sequence shows thickness variations, however, Neogene sequences has the highest thickness variations.

Toward the north salt structures are characterized by squeezed salt diapirs and allochthonous salt sheets. The individual allochthonous salt sheets are emplaced between the Miocene and Pliocene sequences.

Offshore, a series of salt-thrust structures detached on Jurassic salt, which thins northwestwards to a pinch out. The salt thinning represents the limit of the Salina del Istmo Province.

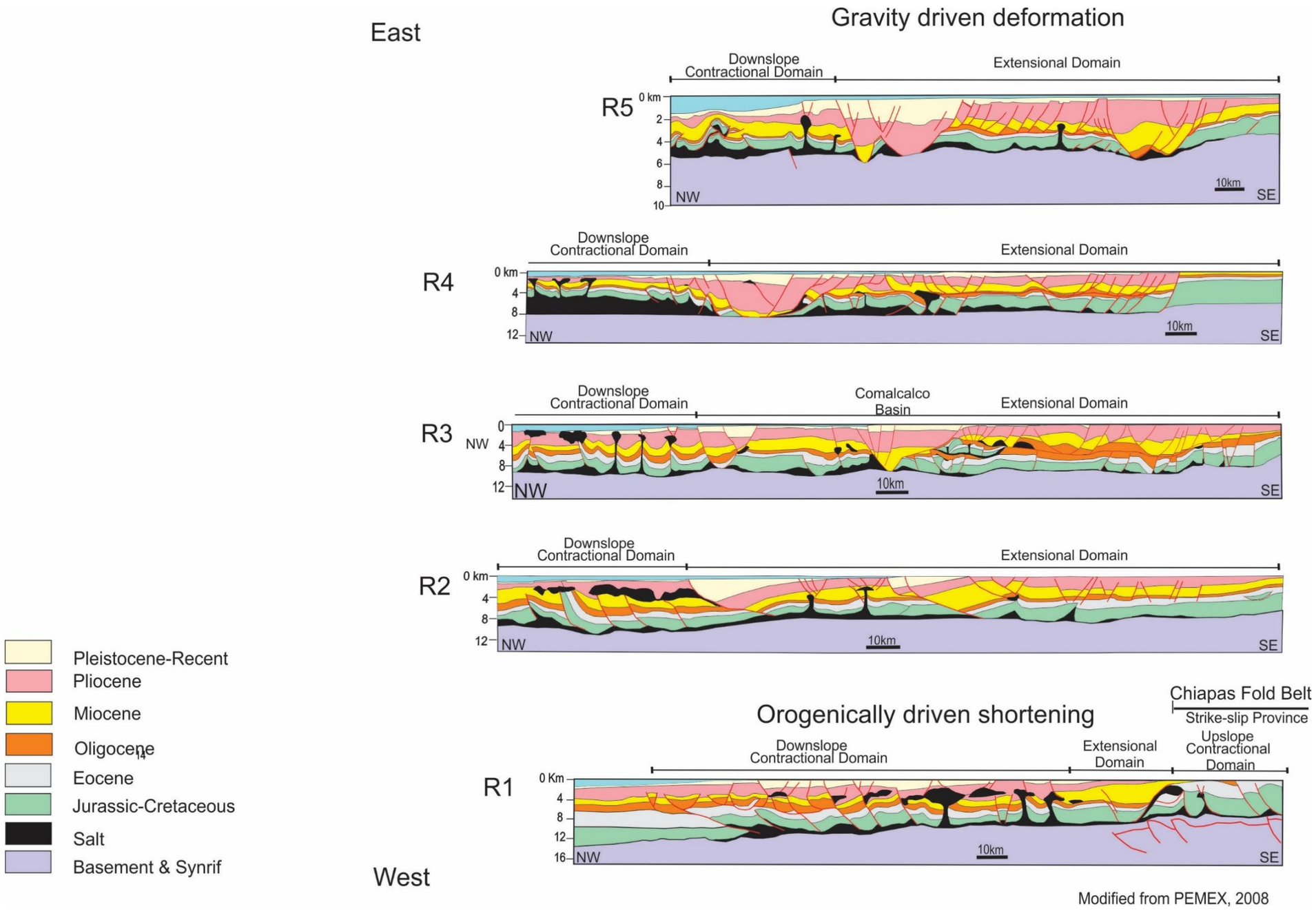

Fig. 7.2 Regional geologica sections of South-eastern of Gulf of Mexico (modified from PEMEX,2008)

Section R2 start onshore part on Cuenca del Sureste basins and ends offshore of Salina del Istmo Province, located 100 km to the east of R1 section .(Fig.7.2 R2).

In contrast with the section R1, section R2 is characterized by extensional domain structures. The normal faults system detached on Cretaceous top forming counter-regional structures during the Miocene. The development of regional listric and counter-regional structures are related to the high rate of sedimentation induced by the lifting of Sierra de Chiapas during the Neogene and the thick salt presence.

The compression zone is represented by squeezed diapirs, which started as passive diapirs during Mesozoic and later were compressed during Paleogene and Neogene. Conversely, other diapirs were not able to develop due to excessive sedimentation of the Upper Miocene and Pliocene.

At down slope, the salt structures show shortening, represented by salt thrusting and salt canopies located on the top of the Upper Miocene.

Section R3 shows a greater degree of structural complexity (Fig. 7.2 R3). The structural system is characterized by an extensional domain detaching on Jurassic salt. The extension system generates a system graben / rafts moving Mesozoic blocks during the Eocene. The orogenic compression during Paleogene cause over-thrusts of Mesozoic over Oligocene taking another detachment level (Oligocene top is characterized by shales). Continuous extension generates the development of another graben/ raft system during lower Pliocene (forming Comalcalco Basin). Down–slope, the compression zone is represented by squeezed salt diapir, which was compressed during Pliocene.

Section R4, starts with the extensional domain characterized by deep normal faults that detach on a thin Jurassic salt (Fig 7.2 R4). In this section the development of graben/ raft system is not developed but is characterized by Mesozoic rotated blocks developing salt diapirs, which reach the Oligocene surface. Over the top Oligocene detached surface a normal fault system and thrust structures are accommodated.

Towards the offshore a graben / raft system is developed during the Pliocene. The displaced block is represented by salt cored folds and compressed diapirs. On the diapir roof salt collapse generated minibasins.

Section R5, exhibits a system graben / raft during the Miocene. (Fig.7.2 R5). The high Miocene sedimentation rate possibly coming from the southwest to northeast generated the displacement of the Mesozoic and part of the Paleogene sequence to the northeast; that's mean, outside the section. That's why we do not observe thrusting in the section. The displaced blocks are affected by diapirs that cut the Miocene sequences. Oligocene sequence has been recognized as detachment surface where a series of normal faults are accommodated.

Offshore, another graben / raft were developed during the Pliocene-Pleistocene. The Mesozoic displaced block (raft) shows a series of squeezed diapirs, which are affected by reactivation during the Pliocene. Shortening is represented by salt thrust anticlines, which show a NW orientation.

Figure 7.3 summarizes the interpretation of the regional sections as well as gravity and magnetic data analysis. The south-west margin of the South-eastern Basin was affected by transpressive orogenic processes during the Middle-Late Miocene. The contractional trend correlated with the strike-slip province of the Chiapas Fold Belt (section R1). The progressive lifting of the Chiapas Massif generated a difference in the elevation that caused the collapse of the basin in NW-SE direction. The geometry semi-circular of the collapse coincides with the limit of the strike-slip province towards the southeast, while toward the east the collapse almost correlated with the subsurface Mesozoic platform margin (Fig. 7.3). The extension domain is represented by normal faults and graben /raft systems, which are clear in the regional sections. The contraction area is characterized by the development of diapirs that evolved in different stages and shortening, is characterized by salt core anticlines, squeezed salt diapirs; salt thrust anticlines and allochthonous salt sheets.

The contrasting structural architecture and the complex salt tectonic history are controlled by a combination of gravity-driven halokinetic processes, regional contractional tectonic processes and basement-involved strike-slip deformation as consequence of the plate convergence between the Caribbean (Chortis Block) and North American plates.

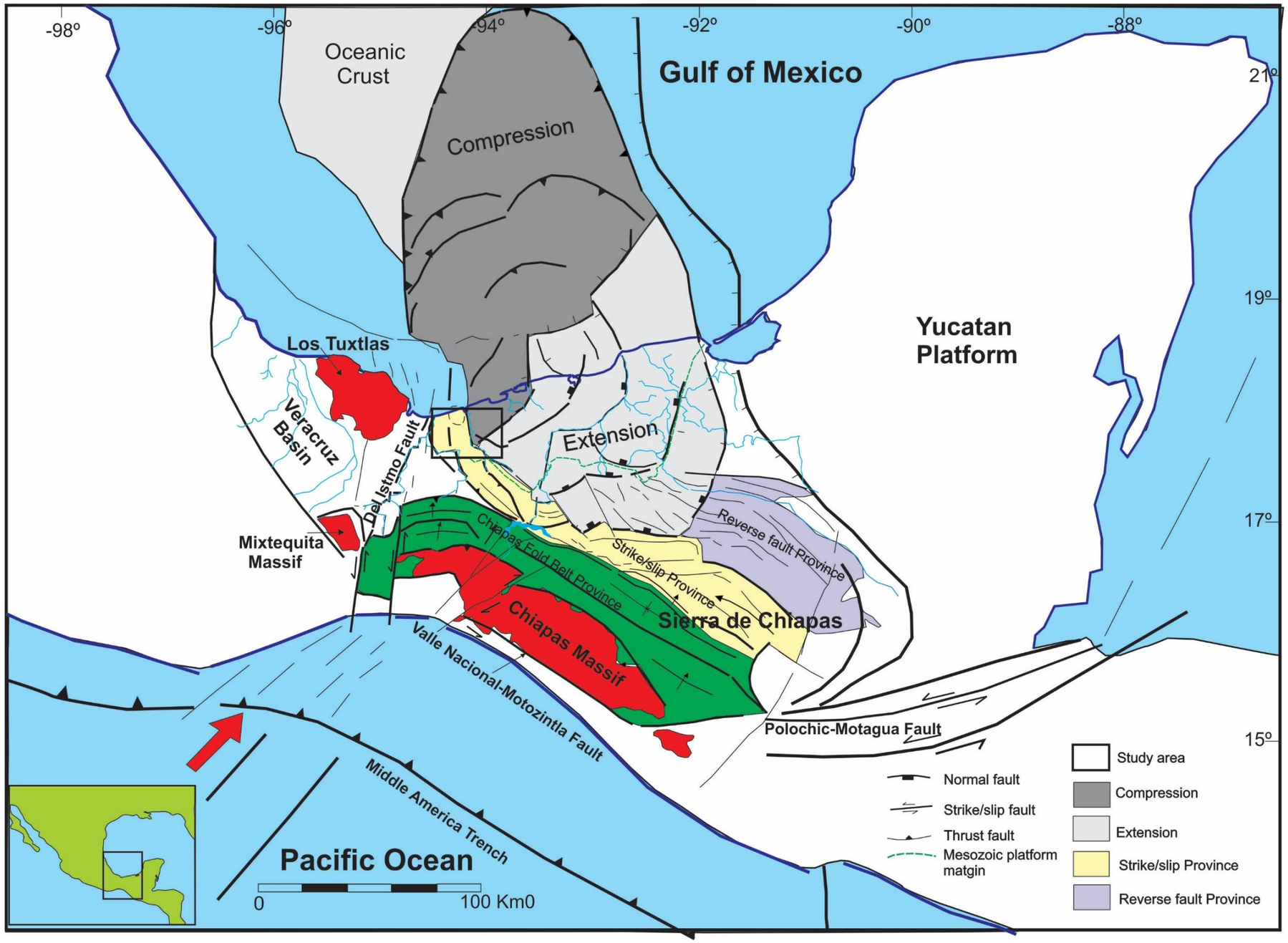

Fig.7.3Structural model of the SE of Mexico. The black rectangle represents the Isthmus Saline Basin.

7.2.2 Semi-regional Interpretation of the western sector of the ISB and the NW front of Sierra de Chiapas.

The semi-regional seismic data is composed by three TWT sections D1-D3 that have a length of 120 to 80 km and are spaced approximately 50 km apart. The sections are oriented SW-NE covering the western sector of the ISB and part of the SW tip of the Chiapas Fold Belt (Fig. 7.1). The quality of the seismic data is low (2D in time) and the stratigraphic control in the Isthmus Saline Basin has registered up to Lower Miocene. The set of seismic section were interpreted by the author.

D3 seismic section is represented by four structural blocks that regionally fall towards the north-east. The first block located to the west was controlled by a fault basement (A fault). The salt diapirs of this block are represented by squeezed salt diapirs, and salt canopies that were emplaces on Middle Miocene unconformity (Fig. 7.4). The second block to the east is characterized by squeezed salt diapirs. Salt diapirs show a high degree of contraction and developing normal faults by accommodation. The third block represent the Comalcalco Trough, is represented by a depocenter of almost 5.5 seconds thick of Neogene sediments. In this area deep seismic was not acquired, so the Mesozoic sequence is not observed. However, was interpreted a thin Mesozoic sequence and weld surface. The fourth block located to the east, is a higher block with respect to Comalcalco Trough. It is represented by a squeezed salt diapir and salt pillow on which detach a Neogene fault.

D2 seismic line shows a different pattern of salt structures. Figure 7.5 show that southward salt volume decreases. The structures are represented by salt pillow and squeezed diapirs flattened on top during Oligocene-Lower Miocene. These can be interpreted as: 1) the high rate of sedimentation during Middle - Late Miocene stopped the development of salt diapirs during Neogene; or 2) it could be the salt was already nearly welded by Neogene so diapir could not grow further. The eastern part of the section shows a strong shortening, it is characterized by a salt thrust structure.

D1 seismic line shows less salt thickness. The structural relief of SW of Strike-slip Province which is contrasting with the northwest and northeast. The structural style drastically changes with respect to previous sections. The SW tip margin of the Chiapas Fold Belt, is characterized by a strong shortening represented by squeezed salt structures and thrusting structure of Middle Miocene, Conversely, the north-east part of section show subtle salt core folds of Lower Miocene age (Fig. 7.6).

These set of seismic data shows the variation of salt thickness from south to north, structure style and age of deformation between the Oligocene in the South and Lower Pliocene in the north (Fig. 7.7). Toward Sierra de Chiapas, the orogenic deformation is represented by the structural relief and the strong contraction characterized by squeezed salt diapir and thrusting structures. Meanwhile, toward Isthmus Saline basin the orogenic deformation is represented by squeezed salt diapirs and thick salt canopies shallower to the northwest. This change in the deformation style from south to north is controlled by the relationship with salt thickness variation and probably basement geometry.

The Comalcalco Trough located to the east of the Isthmus Saline Basin represent one of the most interesting geological features in this area. The Neogene sediment thickness contrast with the isolated salt diapirs and sediment thickness of the ISB.

The Comalcalco Basin is characterized by being a Tertiary depression delimited by a NNE-SSW regional listric fault system (Fig.7.8).

The origin of the Comalcalco Basin is related with gravity-driven deformation often consists of thin-skinned linked systems, in which a body of sediments is translated basinward, accommodated by extension in its up dip portion, and contraction in the downdip region.

Figure 7.8 shows the NT-F and NT-8 sections with the purpose of demonstrating the geometry of the Comalcalco Basin and its regional structural relationship. The first oriented SW-NE shows the relationship between the isolated salt diapirs of the ISB and the Comalcalco Through. The NT-8 oriented NE-SW shows deformation of sedimentary sequence by gravity-driven extensional faults and rising of passive diapirs during the Paleogene. It is very likely that the Comalcalco Basin is the result of a transition from early systems

dominated by gravity gliding to younger systems dominated by gravity spreading as it has been proposed by Rowan (2000, 2004) in the northern margins of the Gulf of Mexico, but with the difference that southern margin is related to a convergent orogenic belt of Upper-Middle Miocene.

The thickness of the Upper Miocene depositional sequence increases drastically, which is associated with the evacuation of salt and the increase in the inclination of the basement, generating the development of normal listric and counter-regional faults. In some faults the displacement is transferred to depth through a series of ramps and minor detachments surfaces, until reaching a detachment in the autochthonous salt of the Middle Jurassic.

In some sectors of the Comalcalco Through, the stratigraphic units of the Mesozoic are absent, so Neogene sediments rest directly on welds produced by the evacuation of autochthonous salt. Theis concept of Mesozoic displaced blocks shows that the Reforma-Akal Uplift constitutes a mega-raft block limited to the SE and NW by two extensional evacuation basins.

Figure 7.9 shows a model to understand the structural relationship between the Reforma-Akal Uplift which constitutes a mega-raft block limited to the NW by Isthmus Saline Basin and Comalcalco Basin during Middle-Late Miocene and to the SE by Macuspana Basin. The model is related with gravity driven thin-skin movement from southeast to northwest. This model is characterized by extension generates a system graben / raft moving Mesozoic blocks during Miocene. The extensional development of the Macuspana Basin begins in Early Miocene towards NE. The extension generates a space which is filled by salt. This process displaces the Reforma - Akal block. Subsequently, during Middle Miocene take place the extension that generates the space of the Comalcalco Trough.

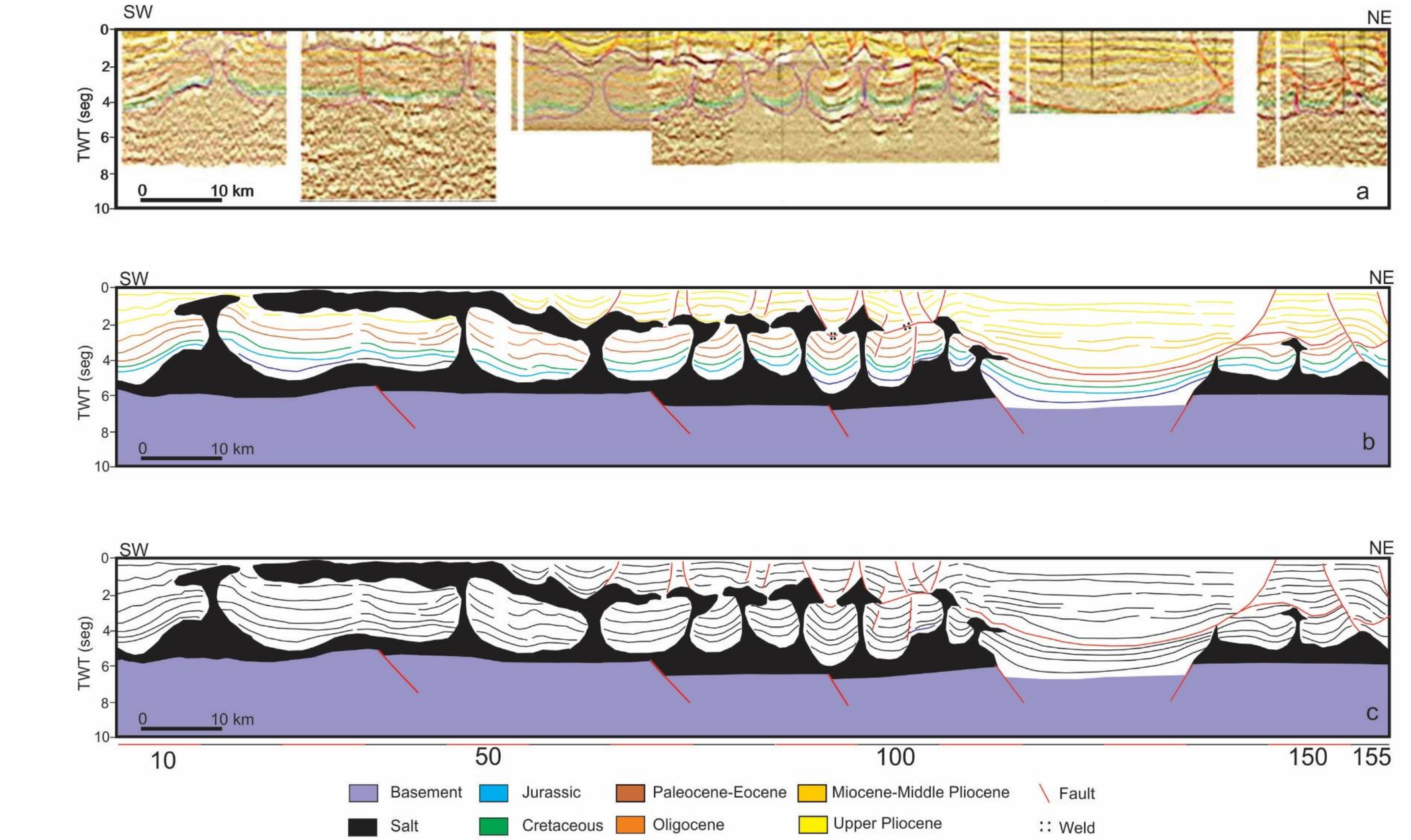

Fig. 7.4 Interpretation of TWT 2D seismic section. D3 section is oriented SW-NE of the Isthmus Saline Basin. a) Seismic section; b) seismic section with interpretation; c) line drawing.

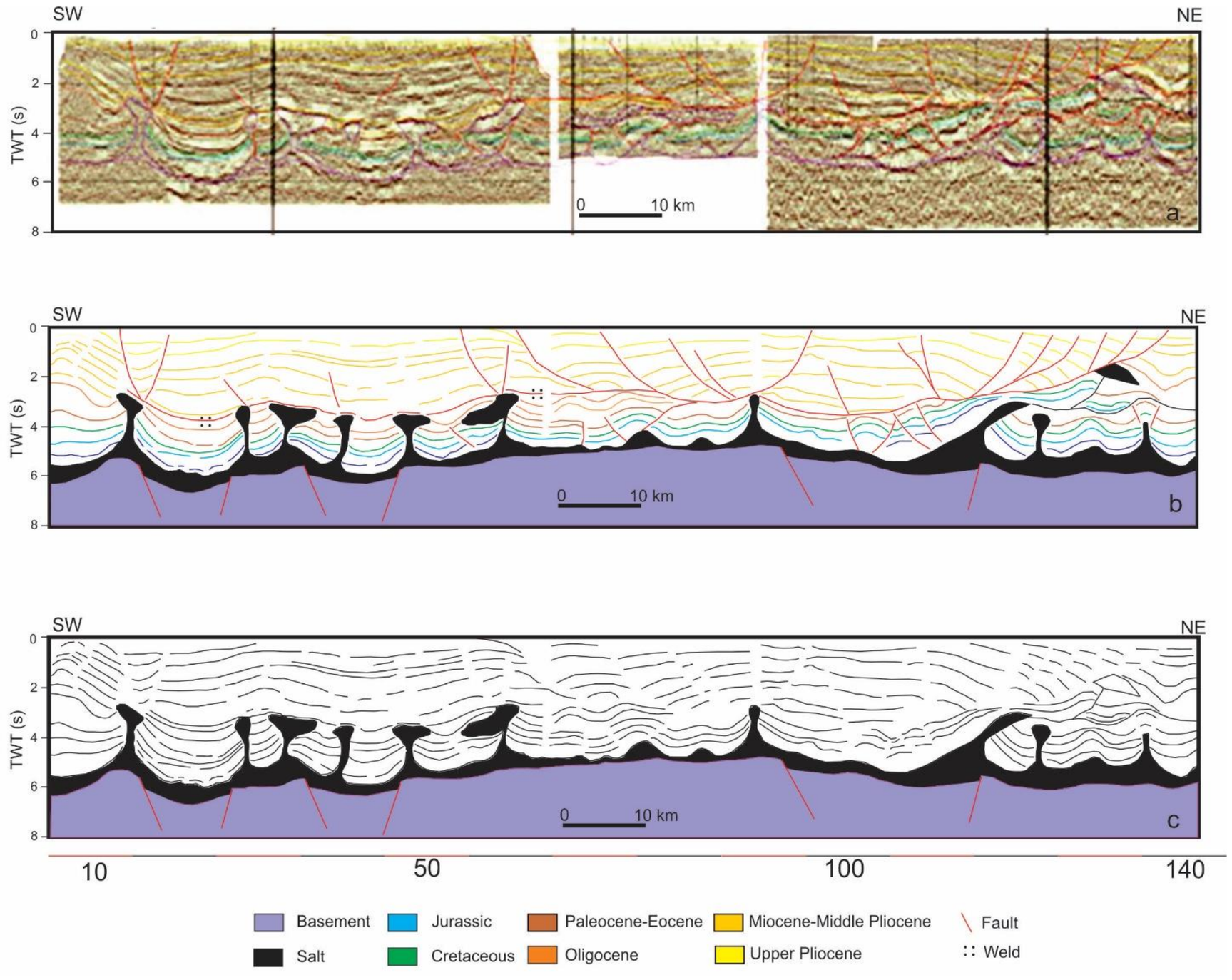

Fig. 7.5 Interpretation of TWT 2D seismic section. D2 section is oriented SW-NE of the Isthmus Saline Basin. a) Seismic section; b) seismic section with interpretation; c) line drawing.

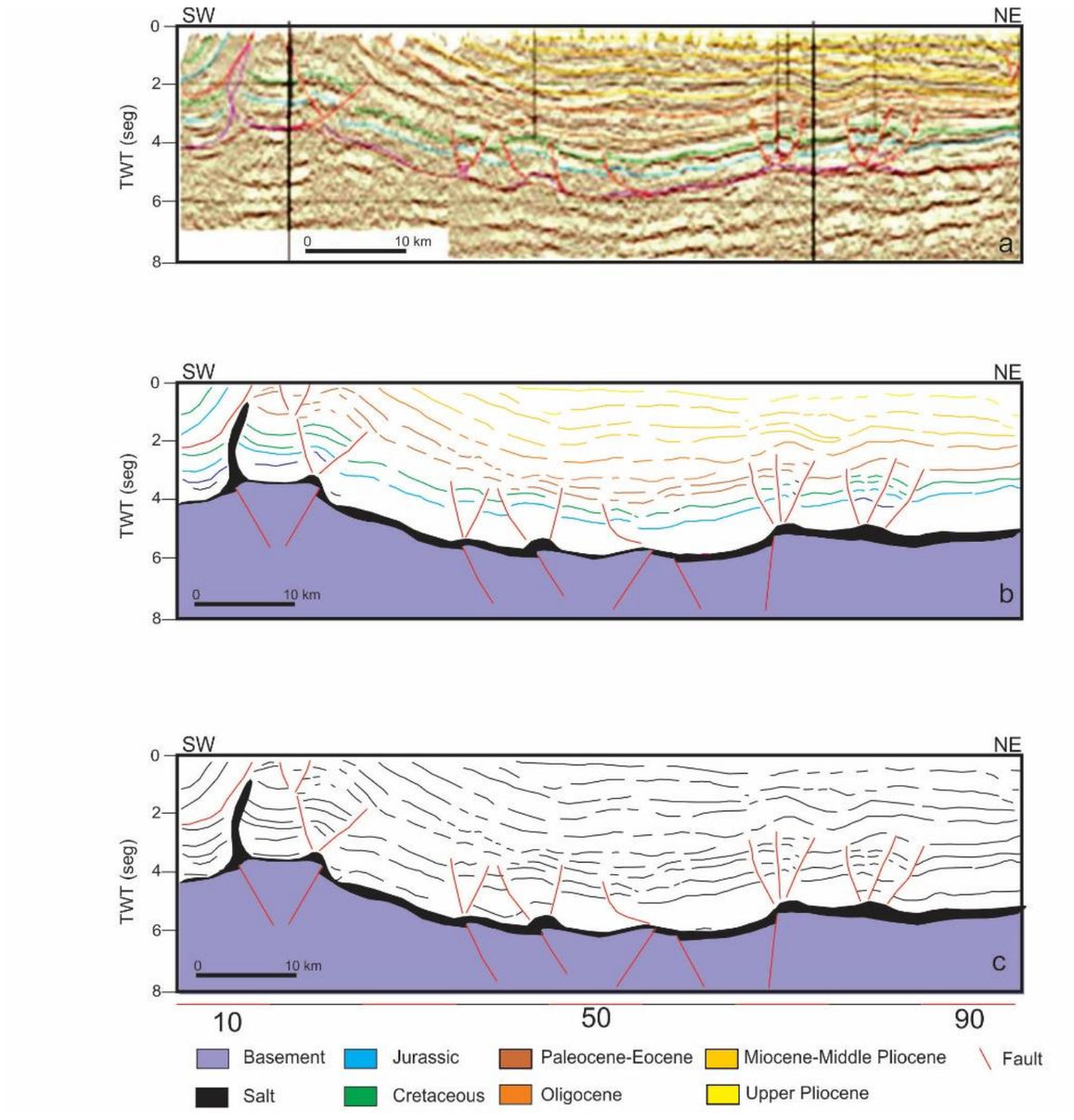

Fig. 7.6 Interpretation of TWT 2D seismic section. D1 section is oriented SW-NE of the Isthmus Saline Basin. a) Seismic section; b) seismic section with interpretation; c) line drawing.

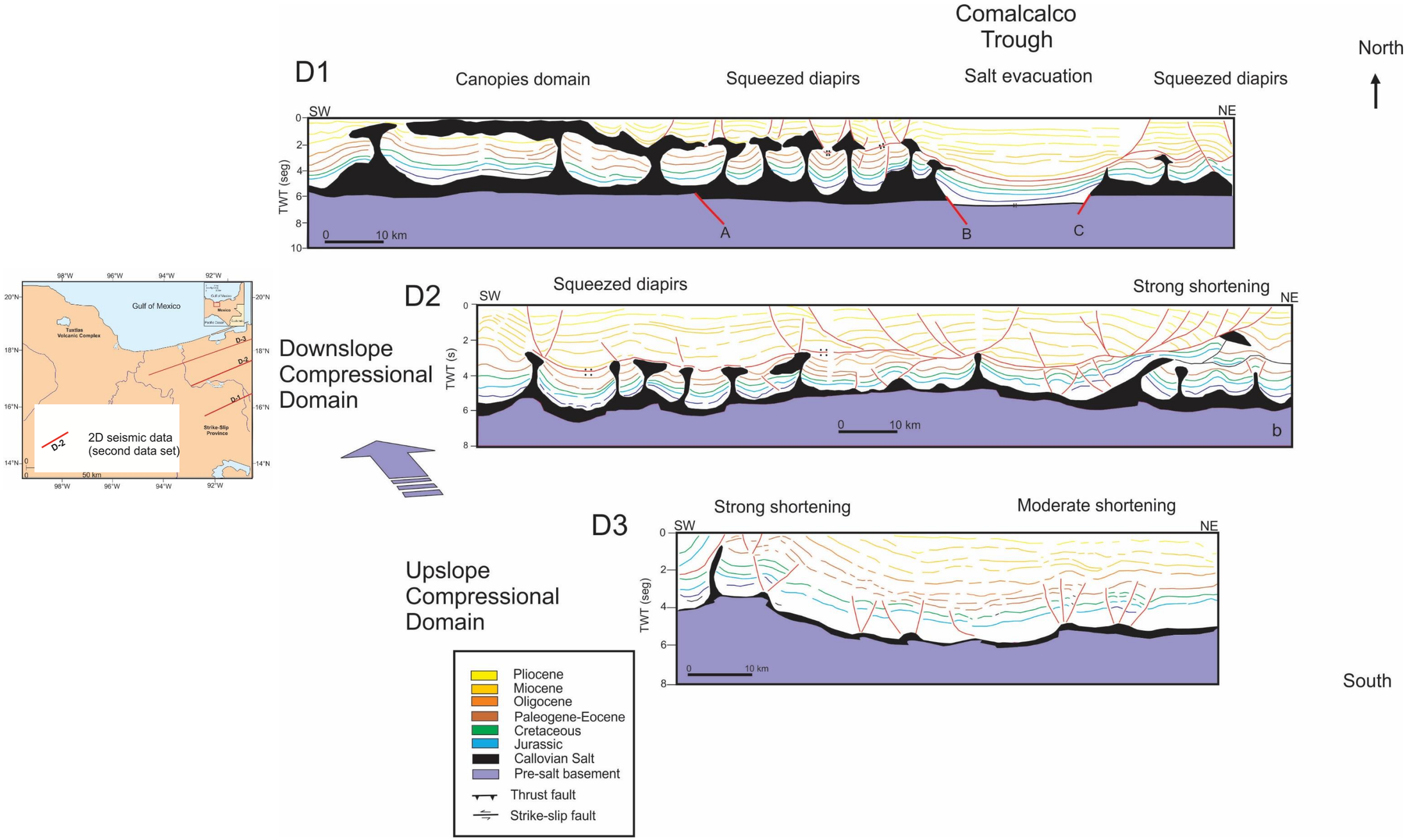

Fig. 7.7 Structural model of the Isthmus Saline Basin Interpretation of TWT 2D seismic section

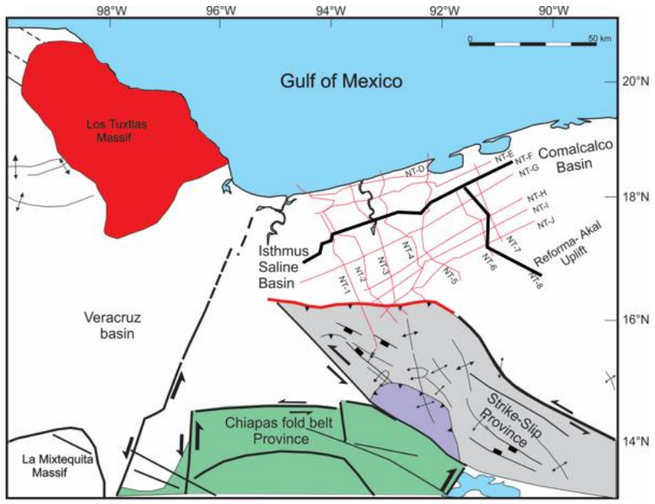

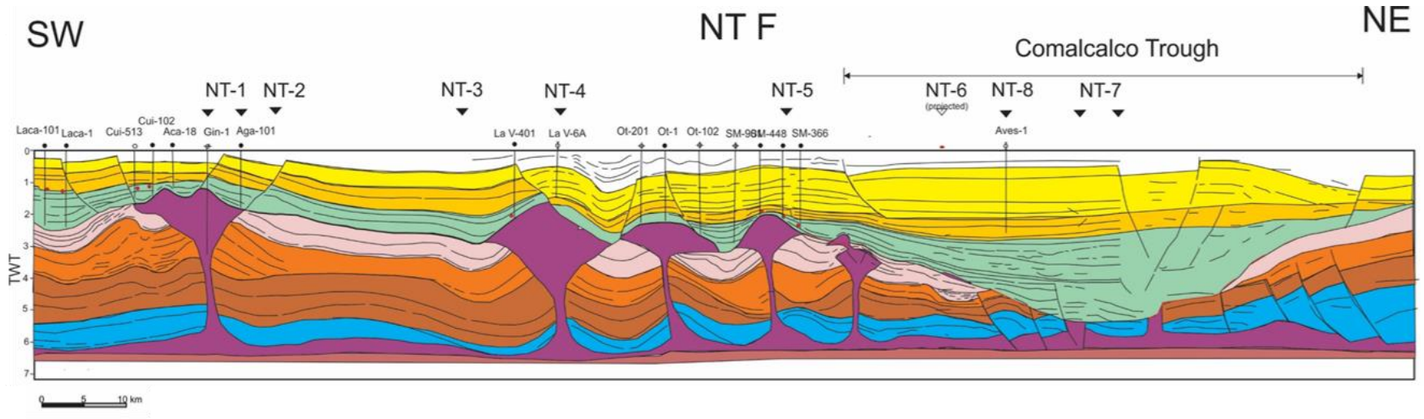

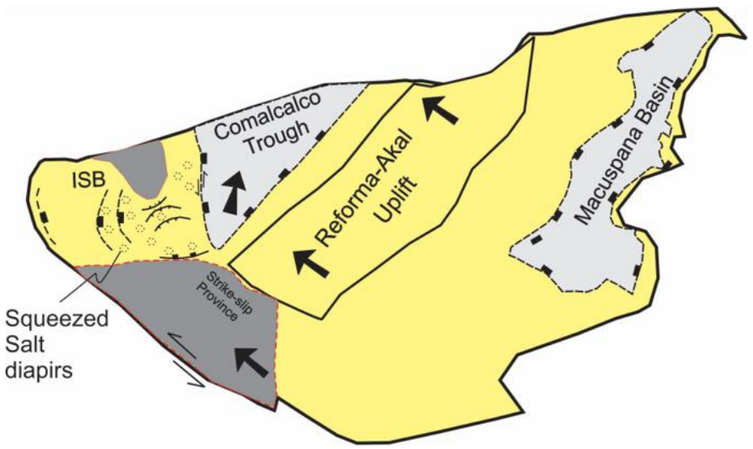

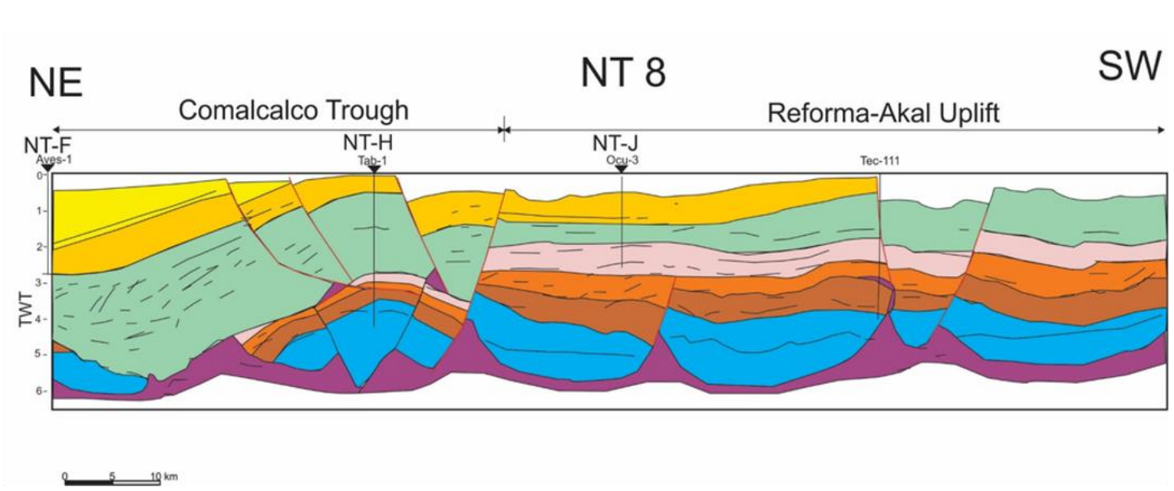

Fig. 7.8 Structural model of salt withdrawal basin of Comalcalco, Reforma-Akal Uplift and its relationship with salt diapirs of ISB. Interpretation of TWT 2D seismic section.

.

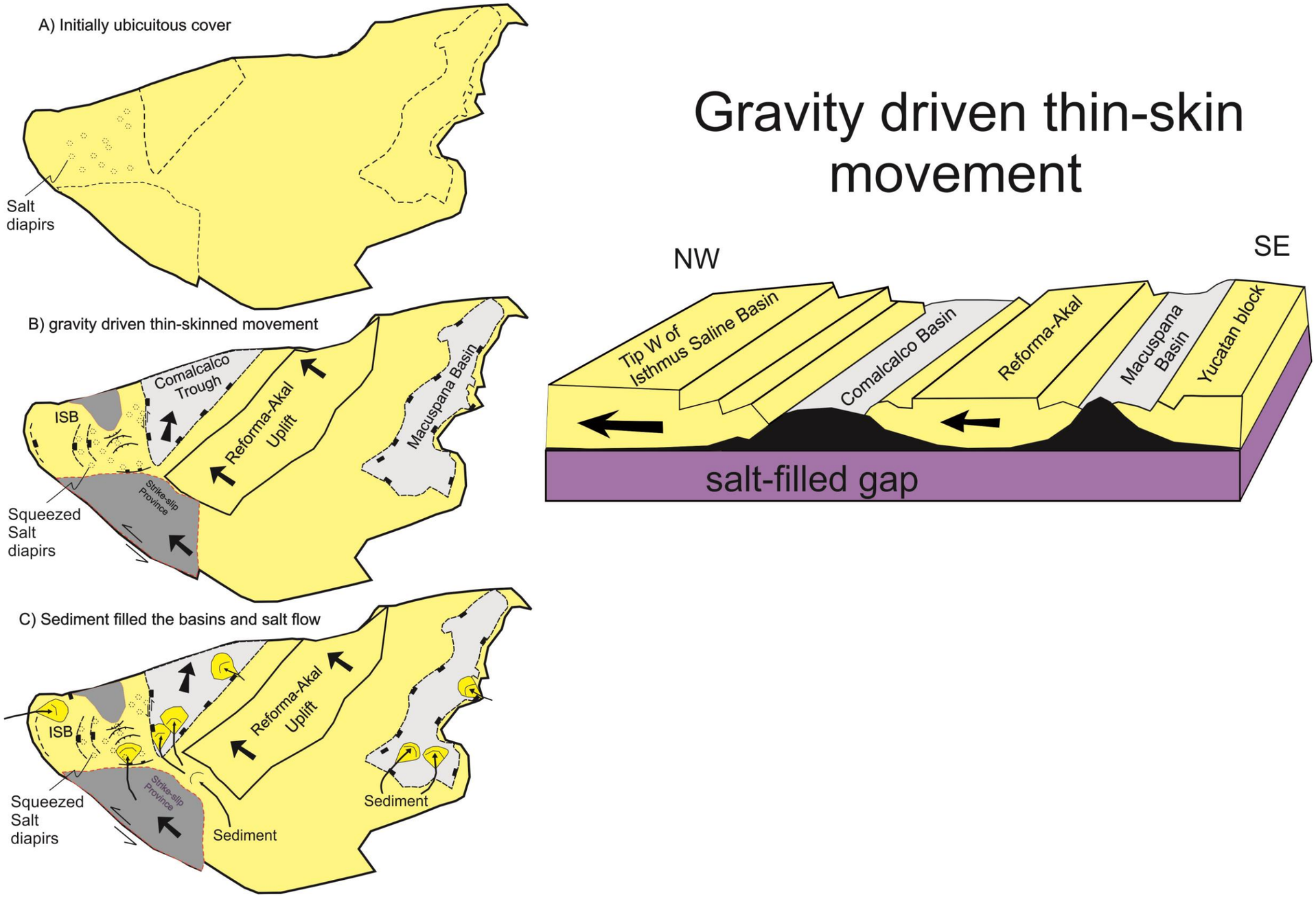

Fig. 7.9 Show a model that try to explain the structural relationship between Isthmus Saline basin and Comalcalco Basin during Middle-late Miocene.

Toward the southwest, orogenic processes lead to the uprising of the Chiapas Massif and the erosion and deposition of large volumes of sediment into the newly formed basin. The large volume of sediments transported toward Comalcalco trough generates flow of a large volume of salt towards the NNW. In the Isthmus Saline Basin the large volume of sediments that came from different directions gave way to deep minibasins and salt ridges flowing in different directions.

7.3 Interpretation 2D of Isthmus Saline Basin

The seismic interpretation was made with TWT 2D data and that the wells used just have reached rocks of the Upper Miocene. The wells drilled in the area have been on the saline diapirs, so when reaching the salt body, the drilling finished.

The interpretation of this data set allowed understanding the lateral variation of salt thickness, the deformation style as well as the variations in the rate of sedimentation in the Isthmus Saline basin. Figure 7.10 shows the distribution of the 15 sections covering almost entirely the ISB. The sections named with numbers run in NNW-SSE direction, these are oriented in the sense of sedimentation transport. The sections named with letters run in SSE-NNE direction, are oriented in the regional direction of the deformation. The description starts with the lines named with numbers from west to east.

The Figure 7.11 shows the Interpretation of TWT 2D seismic section. NT-1 section is oriented NNW-SSE of the Isthmus Saline Basin. This section shows thin salt thicknesses and very tight diapir. To the northwest, toward to the southeast, diapirs are welded. The thicknesses of the Neogene sedimentation are thin. In the southeast the Pliocene sedimentation is absent and towards the northwest is evident the development of small minibasins.

The NT-2 section is oriented NNW-SSE, this section shows more thickness of salt, the diapirs are wide and high towards the NW, while, to the southeast the diapirs are tighter and thinner. The variation in the thickness of the sedimentation is clear. To the southeast, the thickness of the Neogene sequence is greater than that of the northern part, where the Upper Miocene is considerably reduced (Fig. 7.12).

The NT-3 section is oriented NNW-SSE, it is characterized by folds and compressed diapirs. Towards the south-center part of the section the structures

are folds and compressed diapirs structures, while to the north the diapirs are wider and taller. The sedimentation variation of the Neogene sequence is greater in the south. The thickness of the Upper Miocene increases considerably while the northwest is reduced. The large volume of Neogene sediments is possibly occupied by the subsidence of the basement and the evacuation of large volumes of salt during Upper Miocene ((Fig. 7.13).

The NT-4 section is oriented NNW-SSE, it is characterized by compressed diapirs. In the southeast the diapirs are small and thin while towards the north-central part of the section there is a large diapir that deforms the Pliocene sequences. The thickness of the Neogene sequence to the east continues to be greater. The change of thickness of the Upper Miocene sequence in the southeast is evident, while to the north the growth of the salt diapirs reduces the thickness of this same sequence. In the northern part, almost at the end of the section, the collapse of the diapir roof and the formation of counter-regional fault form the development of mini-basins (Fig. 7.14).

The NT-5 section is oriented NNW-SSE, it is characterized by compressed diapirs. In the southeast the diapirs are small and thin while towards the northwest the diapirs are tall and thin and the salt extends through the Middle Miocene surface. In the southern part of the section, the first diapir controlled the development of listric faults that detached on the surface of the Middle Miocene. In the southern part of the section, the volume of sediments of the Upper Miocene and the diapir growth controlled the development of listric and counter-regional faults that detached on the surface of the Middle Miocene or on the top of the diapirs. The extensional system of the Neogene is clear and the thickness change of the Upper Pliocene sequences becomes more evident towards the north (Fig. 7.15).

. The NT-6 section is oriented NNW-SSE, it shows a thinning of salt thickness. Salt structures are represented by salt rollers. The compressive character of the diapirs is lost and the initial stages of the formation of roles and the incipient development of raft structures are interpreted. The Upper Miocene and Pliocene thickness is very large. This produces roll over and counter-regional faults, on the detached surfaces salt structure is characterized by salt pillow. (Fig. 7.16)

The NT-8 section is oriented NNW-SSE, it shows the structural arrangement from the Reforma - Akal Uplift to the Comalcalco Basin. The section is represented by salt rollers, starting gravity-driven extensional faults. The development of raft structures is represented by faults that reach the autochthonous evaporite units of the Middle Jurassic. The displacement of Mesozoic blocks causes those Neogene sediments to come into contact with autochthonous salt (Fig.7 17).

The NT-7 section is oriented NNW-SSE, it shows a thinning of salt thickness. Salt structures are represented by salt rollers and the incipient development of raft structures is interpreted. Toward the southeast Upper Miocene thickness is large and to the northwest Pliocene thickness becomes to be larger. This thickness variation produces roll over and counter-regional faults (Fig. 7.18).

In general, the seismic images are of very poor quality, however, the well data allows us to interpret that in the direction SSW-NNE is where the structural basement blocks is evident. These sections named with numbers are oriented in the regional direction of the deformation. The description of the sections will be from south to north.

The NT-J section is oriented SSW-NNE. The section shows at least two different structural levels of autochthonous salt which allows interpreting different levels of basement which fall from SSW to NNE. The section shows that salt thickness is thick and that salt diapirs may have initiated along extensional faults and evolved into diapirs in Middle Miocene. The seismic image does not allow seeing clearly the presence of primary rim synclines, indicating that the structures became diapir without going through a pillow phase. The geometry of salt diapirs is high and tight. The diapir located to the west of the section shows a younger deformation compared to the other diapirs which created at diapir crests in the Middle Miocene. The eastern sector of the section is characterized by fold of Middle Miocene which is related with the orogenic deformation of Chiapas Fold Belt (Fig. 7.19).

The NT-I section is oriented SSW-NNE, It shows two level of structural basement. Salt diapirs show thick salt thickness that evolved into diapirs into Middle Miocene. Salt diapirs are large and are compressed. Diapir growth ceased at the end of the Middle Miocene with burial by Upper Miocene and Pliocene strata. The presence of unconformities was locally developed above the diapirs during Middle -Upper Miocene (Fig 7.20).

The NT-H section is oriented SSW-NNE, It shows two level of structural basement. The section shows thick salt thicknesses, characterized by seven diapirs, which show a high degree of compression. Salt diapirs created at diapir crests in the Middle Miocene. Diapir growth ceased at the end of the Middle Miocene. The Upper Miocene and Pliocene present a subtle deformation that represents the continuous contractional deformation that the basin is subjected. The diapir located to the west of the section shows evidence of reactivation. This rejuvenation is interpreted to be caused during compression (Fig. 7.21).

The NT-G section is oriented SSW-NNE. Salt diapir present high degree of contraction, characterized by rejuvenated structures and collapse and development of normal faults. The western and central sector of the section compared with eastern sector show thickness variation. Toward the northeastern Upper Miocene and Pliocene sequences thickness becomes to be larger. Secondly, this section marks a change in thickness of the Neogene sequences to the north. To the north the Upper Miocene and Pliocene are thin, while to the south they are thicker. (Fig. 7.22).

The NT-F section is oriented SSW-NNE. The section shows different structural levels of autochthonous salt which allows interpreting different levels of basement. Salt diapirs are tall and thin compressed structures. Some structures show collapse of the roof of the structures and others show reactivation of the diapirs. Towards the west there are changes in thickness of the Neogene sequences (Fig. 23).

The NT-E section is oriented SSW-NNE. Salt diapirs are characterized by being tall and wide, compressed structures. Some diapirs show a conspicuous geometry where normal faults detached. The thickness of the Neogene sequences over diapirs is thinned, while to the northeast the thickness of the Pliocene grows considerably (Fig. 7.24).

The NT-D section is oriented SSW-NNE. This section shows the structural difference between blocks. Salt diapirs are characterized by being tall, wide and tight. The allochthonous salt tends to form allochthonous salt sutures thickness prevents having a good image below it. The thickness of the Neogene sequence is thin. Upper Miocene sediments fill the minibasins developed during salt evacuation. Neogene extensional faulting detached on salt allochthonous (Fig. 7.25).

Figures 7.26 and 7.27 integrate the geological sections within the basin with the purpose of having a clear vision about the show the geometry of the salt diapirs, basement geometry, and the possible control of the basement on the salt structures, the contraction and reactivation of the diapirs, the thickness variations of the stratigraphic sequences.

The geometry of the salt structures show variation from east to west. To the east salt structures are represented by salt rollers. Meanwhile, to the west the geometry changes to compressed diapirs controlled by the basement geometries. Salt diapirs various in shape and dimensions. Some diapirs show collapsed roofs while others show continuous rising produced by contraction.

In the east (NT7). Upper Miocene and Pliocene thickness is very large. This produces roll over and counter-regional faults, in this sector salt structure is characterized by salt pillow (NT'6, 7 and 8). To the west, the thickness tends to be lower but still develop counter-regional salt structures (NT-5). NT-4 and NT-2 sections show less thicknesses of overburden; in consequence salt diapirs tend to be more active. The uprisings that produce salt bodies generate development of fault that increases hydrocarbon migration to shallow levels.

The SW-NE direction shows clearly how thick sediment stopped salt movement. This is seen in the NT-H, I and J sections. Toward north thicknesses tend to be thinner so diapirs reactivation produces new space for hydrocarbon accumulation.

In the Isthmus Saline Basin salt diapirs may have initiated along extensional faults and evolved into diapirs in Middle Miocene-Upper Miocene times. Diapirs grew mainly by contraction. The salt diapirs have controlled the bathymetric relief created at diapir crests through to the Middle Miocene, Upper Miocene period. Sea-bed relief controlled the deposition of Miocene turbidite sandstones, and fluvio-deltaic sequences. These sequences represent the main reservoir rock in the ISB.

Figure 7.28 and 7.29 show the distribution of sedimentary facies in the SSW-NNE oriented section. The sections involved are NT-J, NT-I, NT-H, NT-G, NT-F, NT-E, NT-D. The representation is from south to north because variations of sedimentary facies represented by platform, deltaic and slope deposits can be visualized laterally and vertically.

This work initially was carried out by Varela-Santamaria et. al 2007 and the author has updated the sections during this research project. Due to poor

quality of seismic data, the understanding of distribution of the main sedimentary facies are useful for predicting of reservoir rocks, seal rocks in areas where these facies have not been explored.

The methodology used consisted in compiling the wells drilled from 2007 to 2016. Subsequently, with the well logs information, the paleontological description, the bathymetry and the lithological descriptions were loaded to the interpretation system (stratlog software). The information of approximately 15 wells helped to update the sections mentioned previously.

The importance of visualizing the sedimentary facies in a regional way, allows understanding how the sedimentary environments changed vertically and horizontally.

The basement geometry as well as sea-bed relief generated by salt diapirs controlled the deposition of Miocene and Pliocene turbidite sandstones, which are pinch out to the salt diapirs. However, highest-density turbidity currents flowed across diapir crests and good-quality channel sandstones were deposited across the tops of the diapirs. This deposit are represented in sections located mainly in centre and north of Isthmus Saline Basin represented in NT-G, NT-F, NT-E and NT-D sections (Fig. 7.28).

Platform sediments represented by deltaic and fluvio-deltaic deposits were mainly controlled by subsidence caused by: 1) sinking of the basement, 2) salt evacuation, and 3) siliciclastic platform progradation. These sedimentary facies constitute important hydrocarbon reservoirs, located towards the southern part of the Isthmus Saline Basin. The NT-J, NT-I and NT-H section lines show the Miocene and Pliocene platform sedimentary facies located south of the Isthmus Saline Basin (.(Fig. 7.29).

The Pliocene sedimentary facies in section NT-J are represented by platform facies. The sedimentary facies change lateral and vertically from coastal plains to fluvial deposits and to the west the facies are represented by lagoon facies.

The NT-I section is represented by wave dominated delta facies, deltaic plain and fluvial system sediments, laterally the facies change to coastal plain facies. These sedimentary facies are controlled by salt diapir structure.

The NT-H section is represented by a wave dominated delta facies but vertically it are dominated by coastal plain a fluvial sediments.

The NT-G section is represented by platform sedimentary facies. The section shows greater structural control, normal faults system represent the main lateral

change between blocks. The facies are mainly represented by wave dominated delta, coastal plain and fluvial facies.

The NT-F section is represented by platform facies. This line show structural control driven by saline diapirs. Normal faults represent the main migration routes toward the deltaic plain facies which represent one the main targets in Pliocene plays.

The NT-E section is represented by platform facies, the facies are characterized by wave dominated deltas and front delta facies. The vertical and lateral changes are delimitated by normal faults,

The NT-D section is represented by platform facies, the section shows a salt diapir controlling the fault system which connects with top of salt structures.

The analysis of sedimentary facies during Pliocene allows establishing that the Isthmus Saline Basin was dominated by platform conditions delimitated by normal fault systems. The faults system was controlled by salt diapir collapse and probably salt dissolution. These faults are very productive in delta plain reservoirs and some of them have been active from Pliocene.

The Upper Miocene sedimentary facies in section NT-J is represented by platform facies. These facies are controlled by salt diapir structure and a normal fault system. Toward east, facies change to slope facies, represented by turbidite sandstones. This section shows that Upper Miocene was controlled by coastal plain, lagoon facies and fluvial system deposits in the south of the basin.

The NT-I section shows the predominance of platform facies. The base of the sequence is represented by muddy shelf sediments with vertical variations of high energy deposit represented by wave dominated delta facies, deltaic and front delta sediments.

The NT-H section shows the vertical variation from relative deep water represented by muddy shelf sediments to shallower facies represented by deltaic sediments.

The NT-G section marks the deepening of the sedimentary facies represented by slope facies. The bathymetric relief modified by salt diapir controlled the distribution of turbidite sandstones. The turbidite sandstones facies characterizes the main reservoir rocks of the basin. The NT-F, E and D sections show the continuity of the slope facies, delimited by structural relief of the salt diapirs, as well as the normal fault system that favors the flow of hydrocarbons to the upper sequences.

Figure 7.30 and 7.31 show the structural configuration on time of Miocene and Pliocene which represent the main structural levels producers in the Isthmus Saline Basin.

The Miocene structural map shows an alignment of large salt diapirs oriented NNW-SSE dividing the west and east sector. This structural trend coincides with the structural step observed in the figure 7.24. The southern sector of the map shows an east-west listric system faults which represent the border of the basin. The west sector mainly is represented large structural lows oriented almost NNE-SSW. The western edge of the map shows a tight structural alignment oriented NNE-SSW, and to the north there is a semi-circular structure with some radial faults perpendicular to the structure. On the other hand, the eastern sector mainly is represented by listric faults and counter-regional faults developing roll-over structures (Fig.7.28).

The Pliocene structural map shows a subtle NNW-SSE alignment and represented by a couple of salt diapirs that divided the contractional domain to the west and extensional domain to the east. The contractional domain is represented by structural alignments oriented NNE-SSW and W-E. With large structural lows oriented SSW-NNE. The eastern sector is represented by listric and counter-regional faults (Fig.7.31).

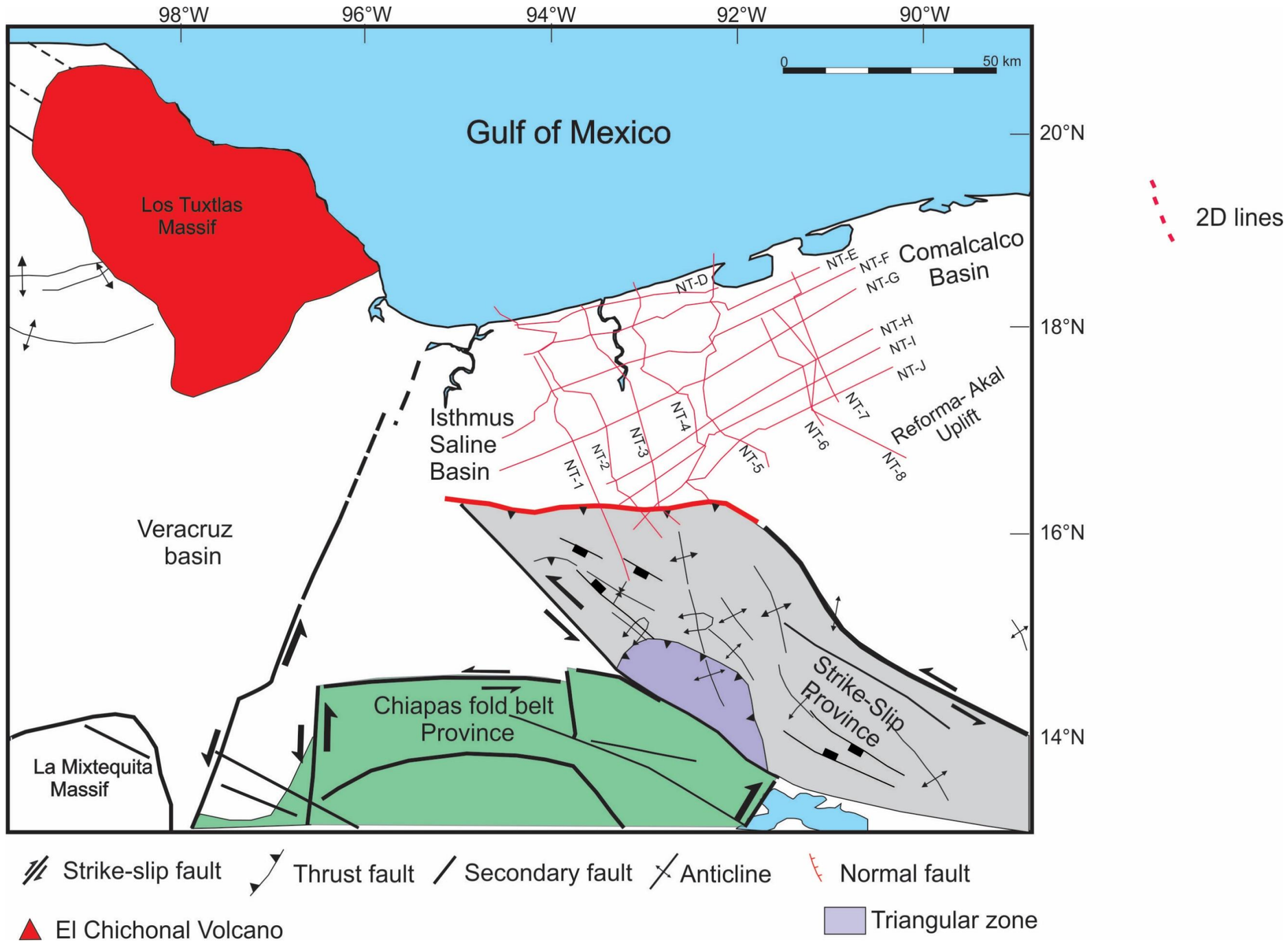

Fig. 7.10 shows location of 2D seismic section and 3D seismic surveys

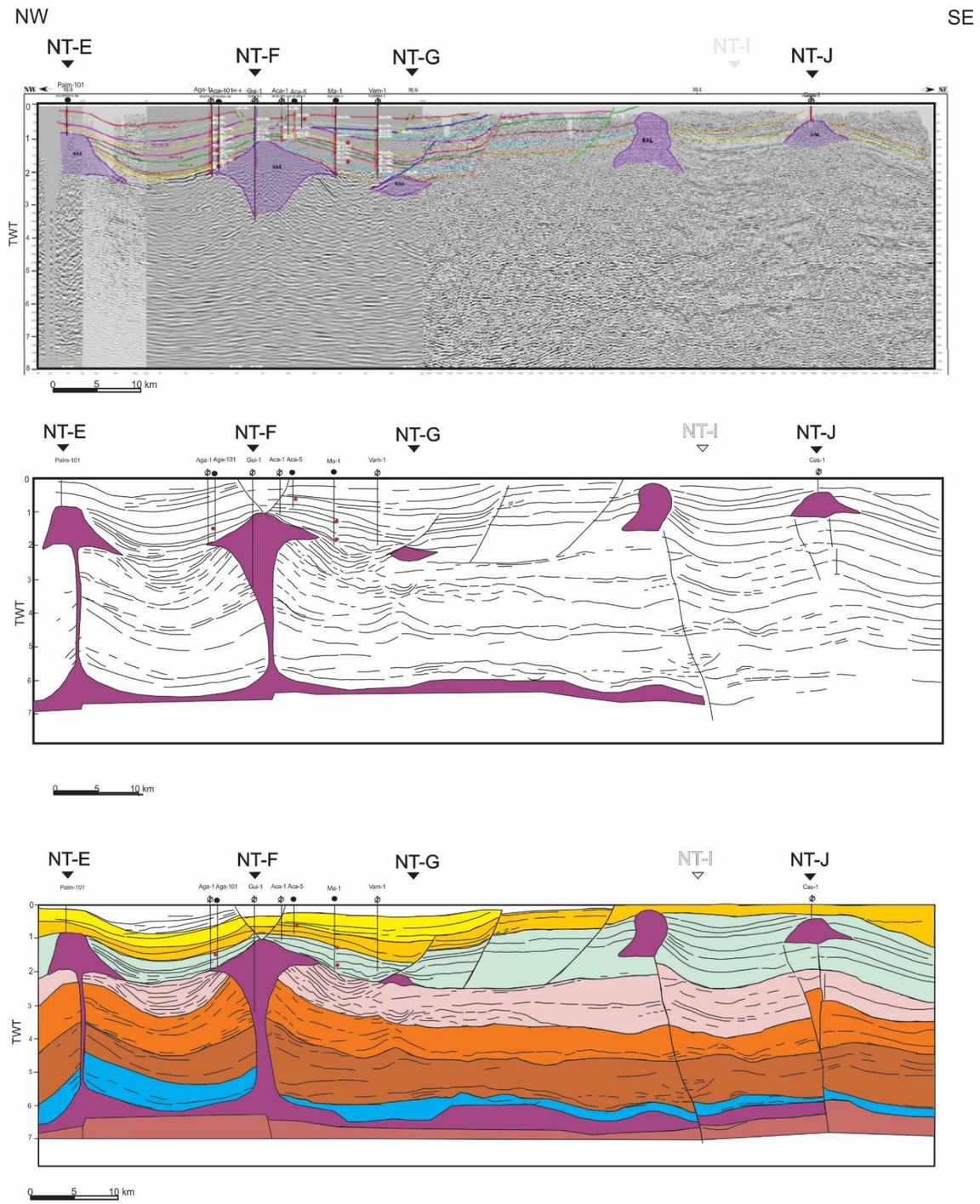

Fig. 7.11 Interpretation of TWT 2D seismic section. NT-1 section is oriented NNW-SSE of the Isthmus Saline Basin. a) Seismic section; b) line drawing; c) seismic section with interpretation

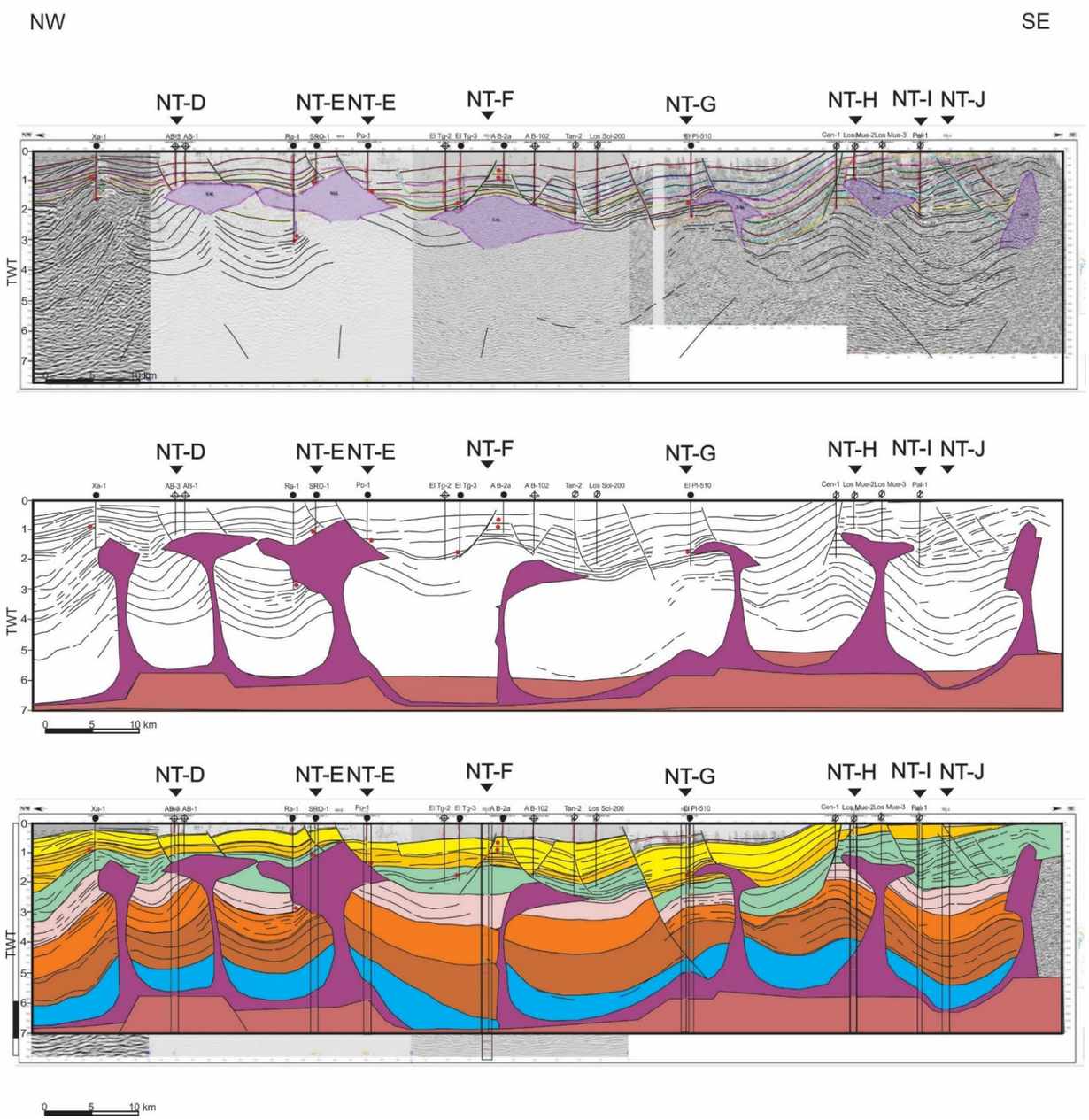

Fig. 7.12 Interpretation of TWT 2D seismic section. NT-2 section is oriented NNW-SSE of the Isthmus Saline Basin. a) Seismic section; b) line drawing; c) seismic section with interpretation.

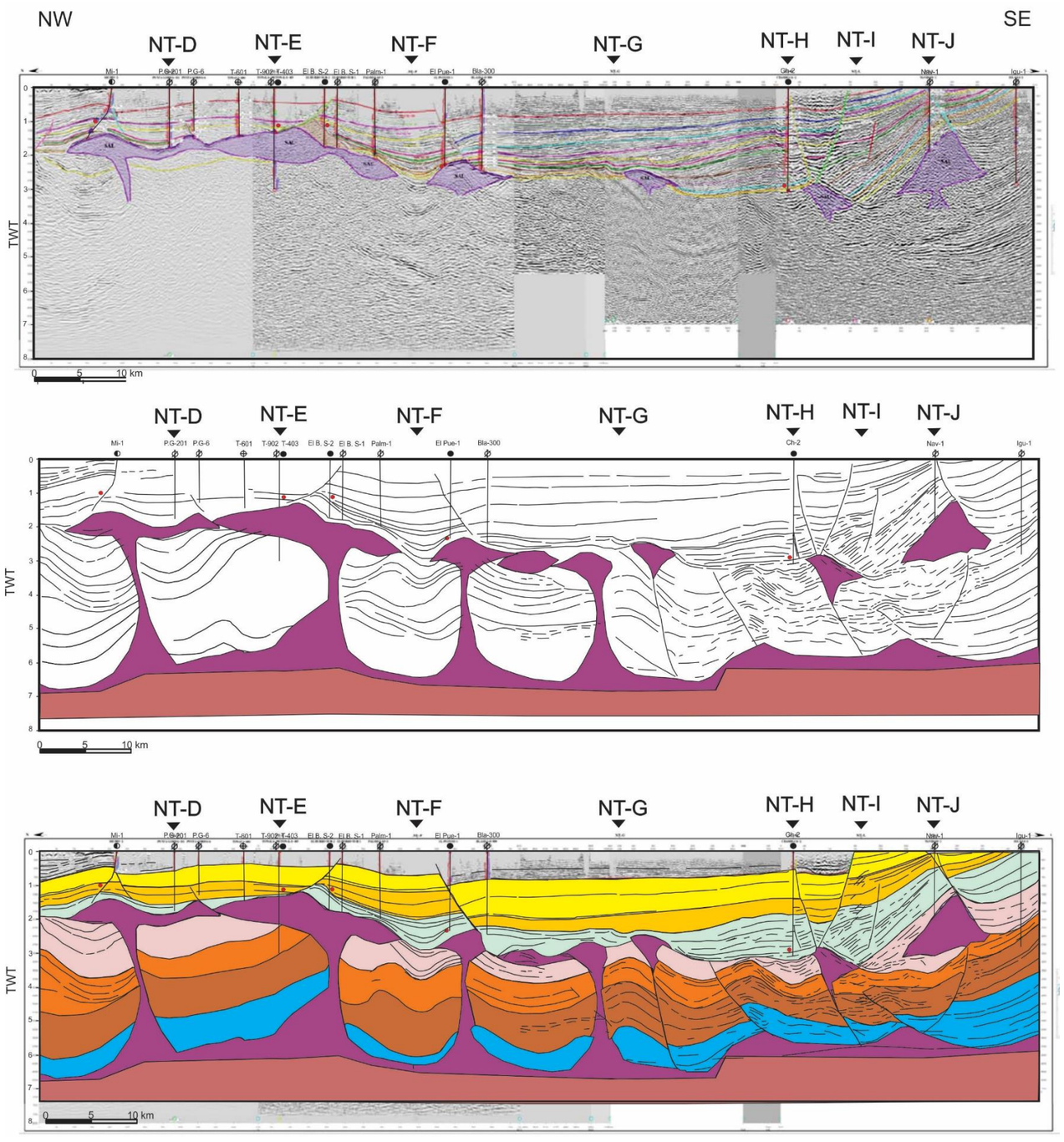

Fig. 7.13 Interpretation of TWT 2D seismic section. NT-3 section is oriented NNW-SSE of the Isthmus Saline Basin. a) Seismic section; b) line drawing; c) seismic section with interpretation.

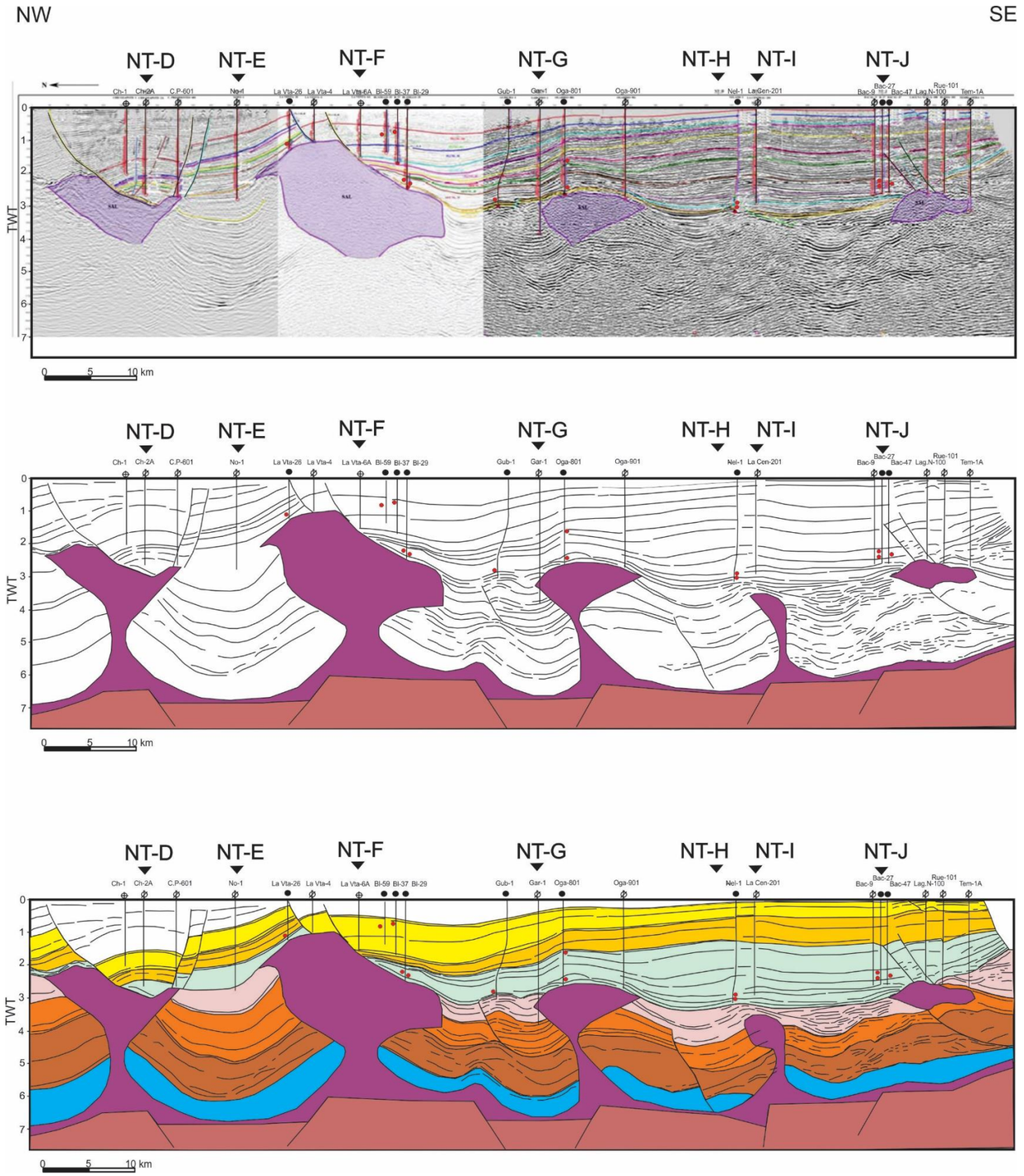

Fig. 7.14 Interpretation of TWT 2D seismic section. NT-4 section is oriented NNW-SSE of the Isthmus Saline Basin. a) Seismic section; b) line drawing; c) seismic section with interpretation.

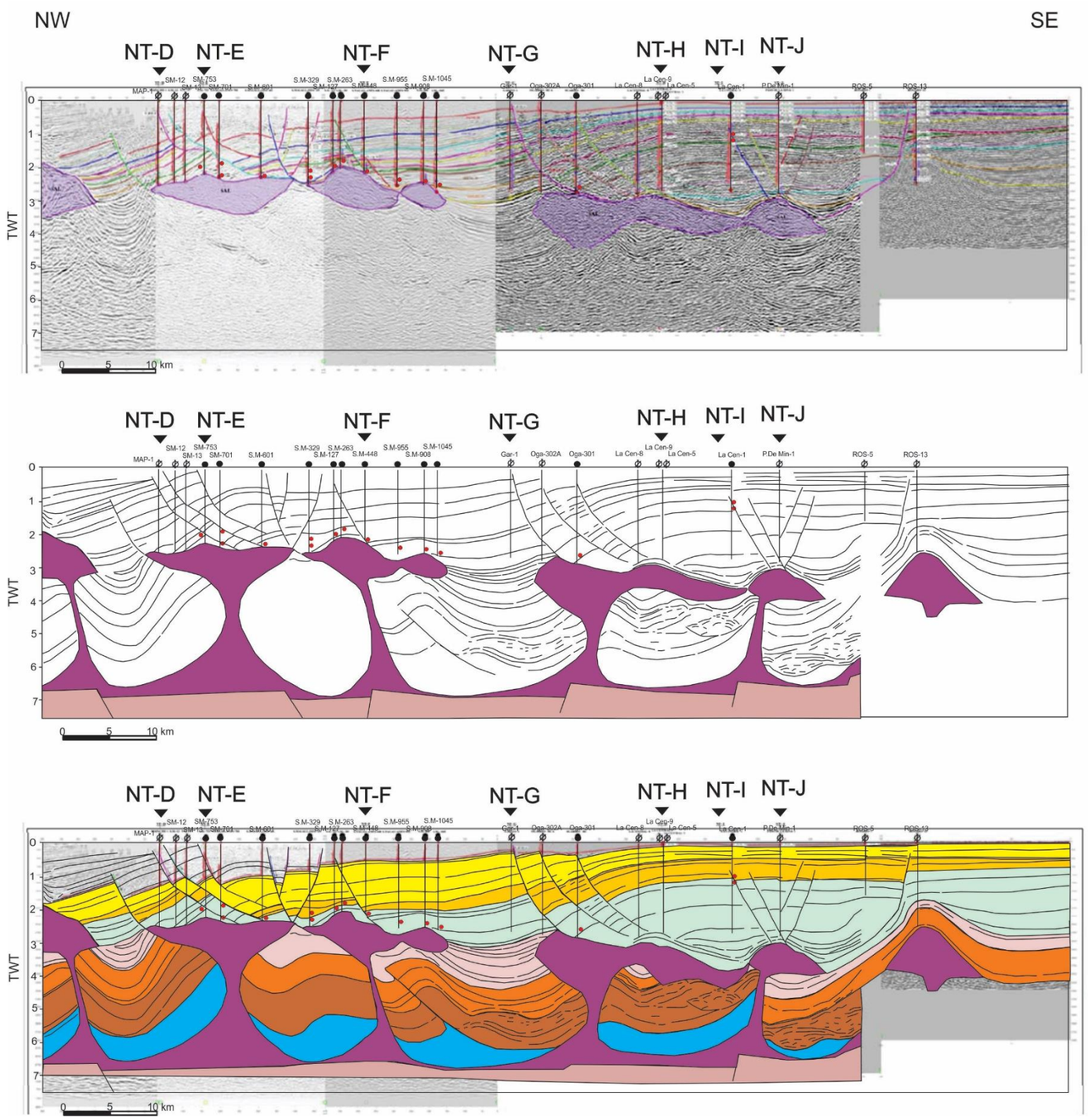

Fig. 7.15 Interpretation of TWT 2D seismic section. NT-5 section is oriented NNW-SSE of the Isthmus Saline Basin. a) Seismic section; b) line drawing; c) seismic section with interpretation.

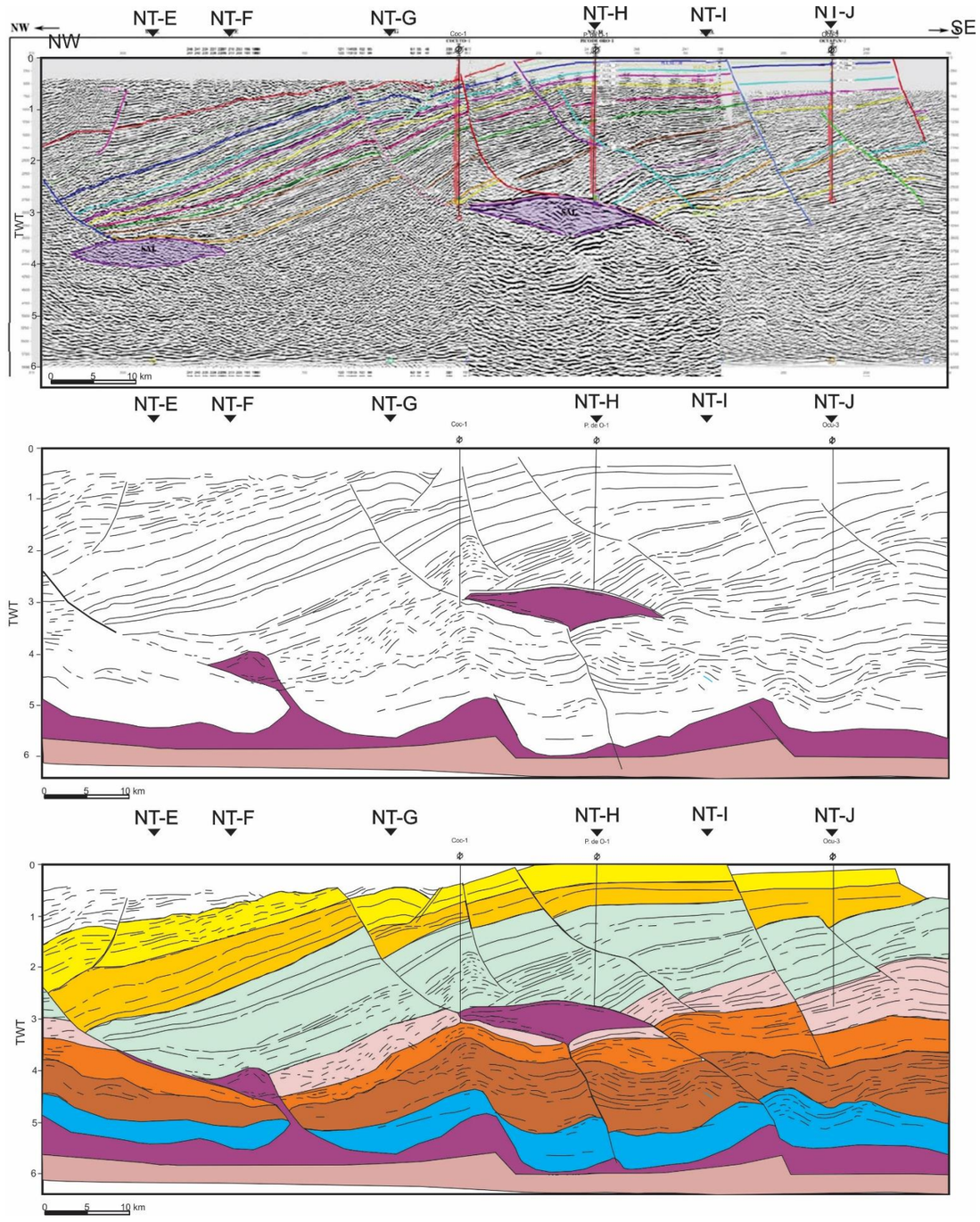

Fig. 7.16 Interpretation of TWT 2D seismic section. NT-6 section is oriented NNW-SSE of the Isthmus Saline Basin. a) Seismic section; b) line drawing; c) seismic section with interpretation.

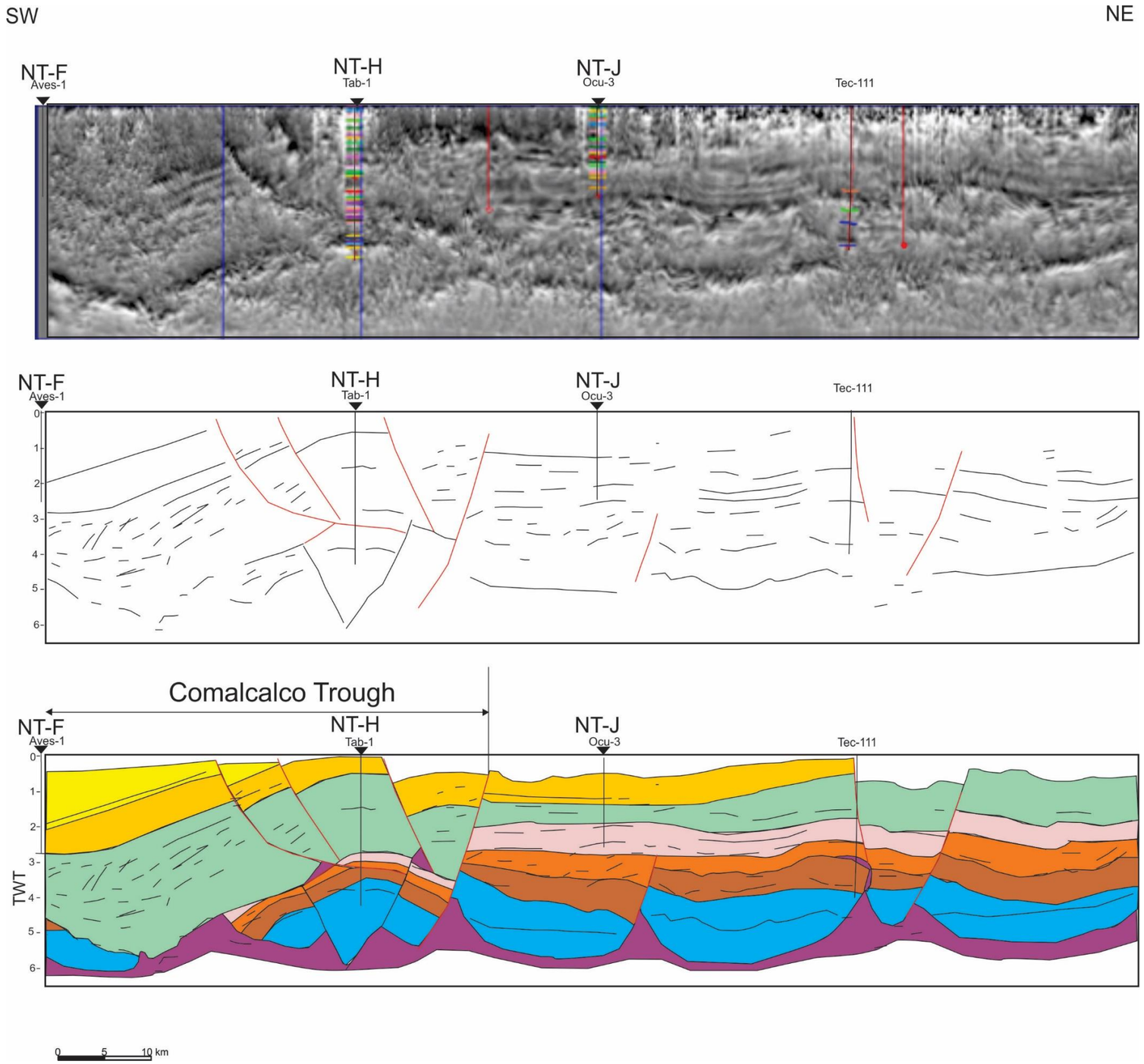

Fig. 7.17 Interpretation of TWT 2D seismic section. NT-8 section is oriented NNW-SSE of the Isthmus Saline Basin. a) Seismic section; b) line drawing; c) seismic section with interpretation.

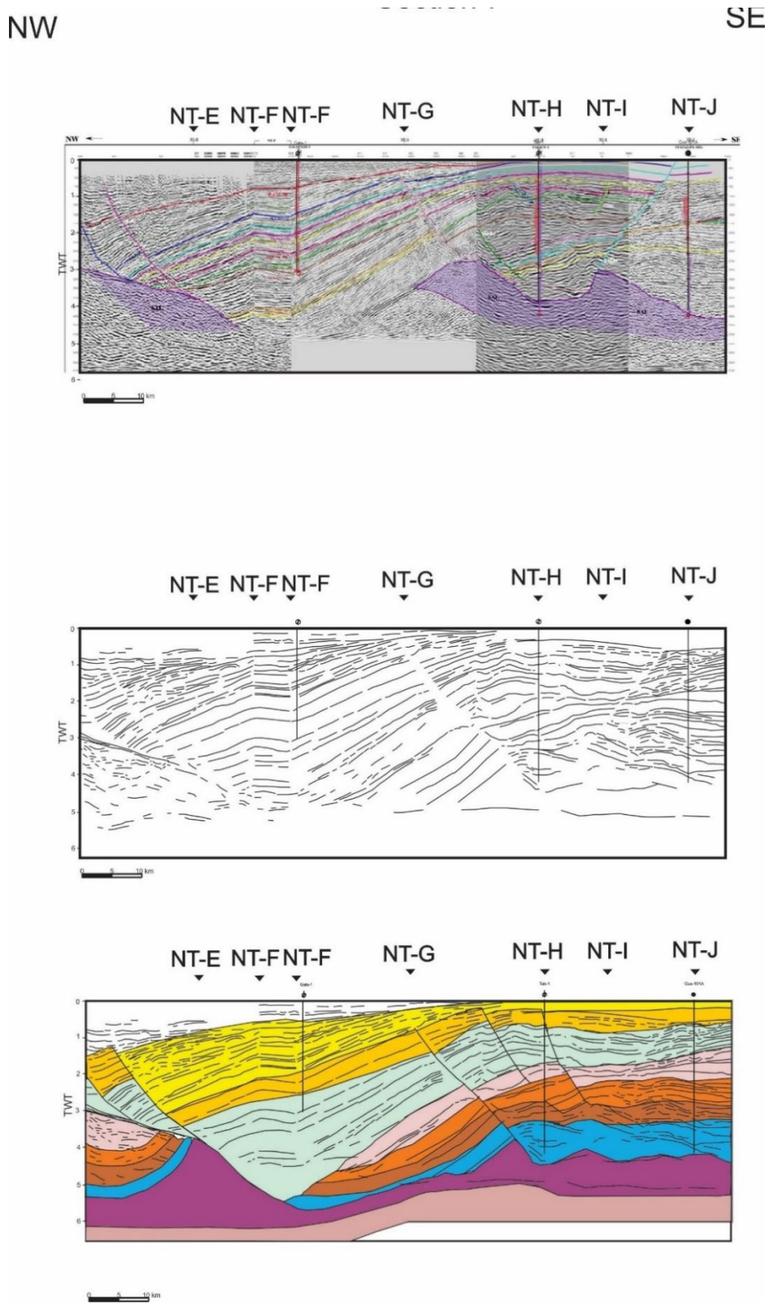

Fig. 7.18 Interpretation of TWT 2D seismic section. NT-7 section is oriented NNW-SSE of the Isthmus Saline Basin. a) Seismic section; b) line drawing; c) seismic section with interpretation.

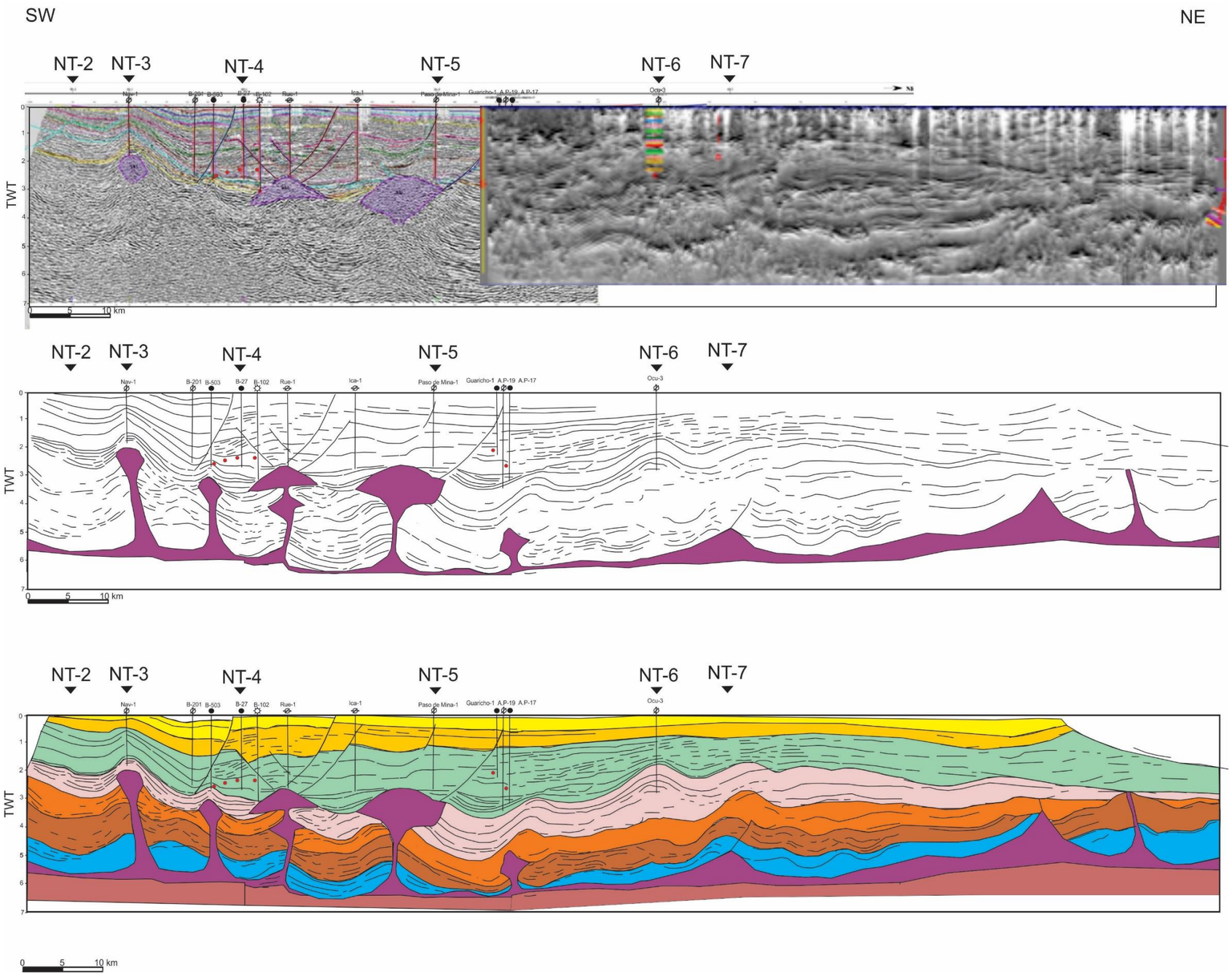

Fig. 7.19 Interpretation of TWT 2D seismic section. NT-J section is oriented SSW-NNE of the Isthmus Saline Basin. a) Seismic section; b) line drawing; c) seismic section with interpretation.

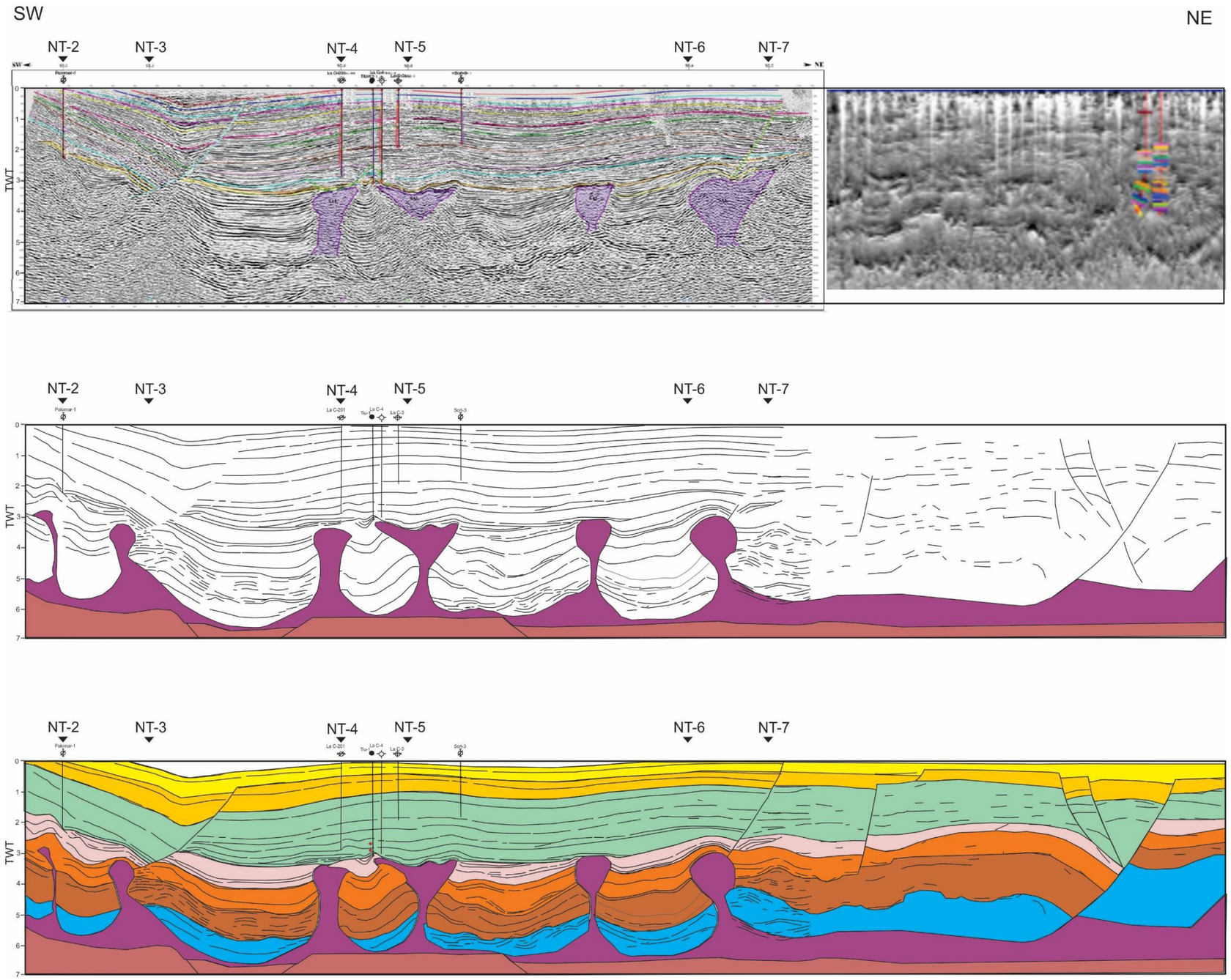

Fig. 7.20 Interpretation of TWT 2D seismic section. NT-I section is oriented SSW-NNE of the Isthmus Saline Basin. a) Seismic section; b) line drawing; c) seismic section with interpretation.

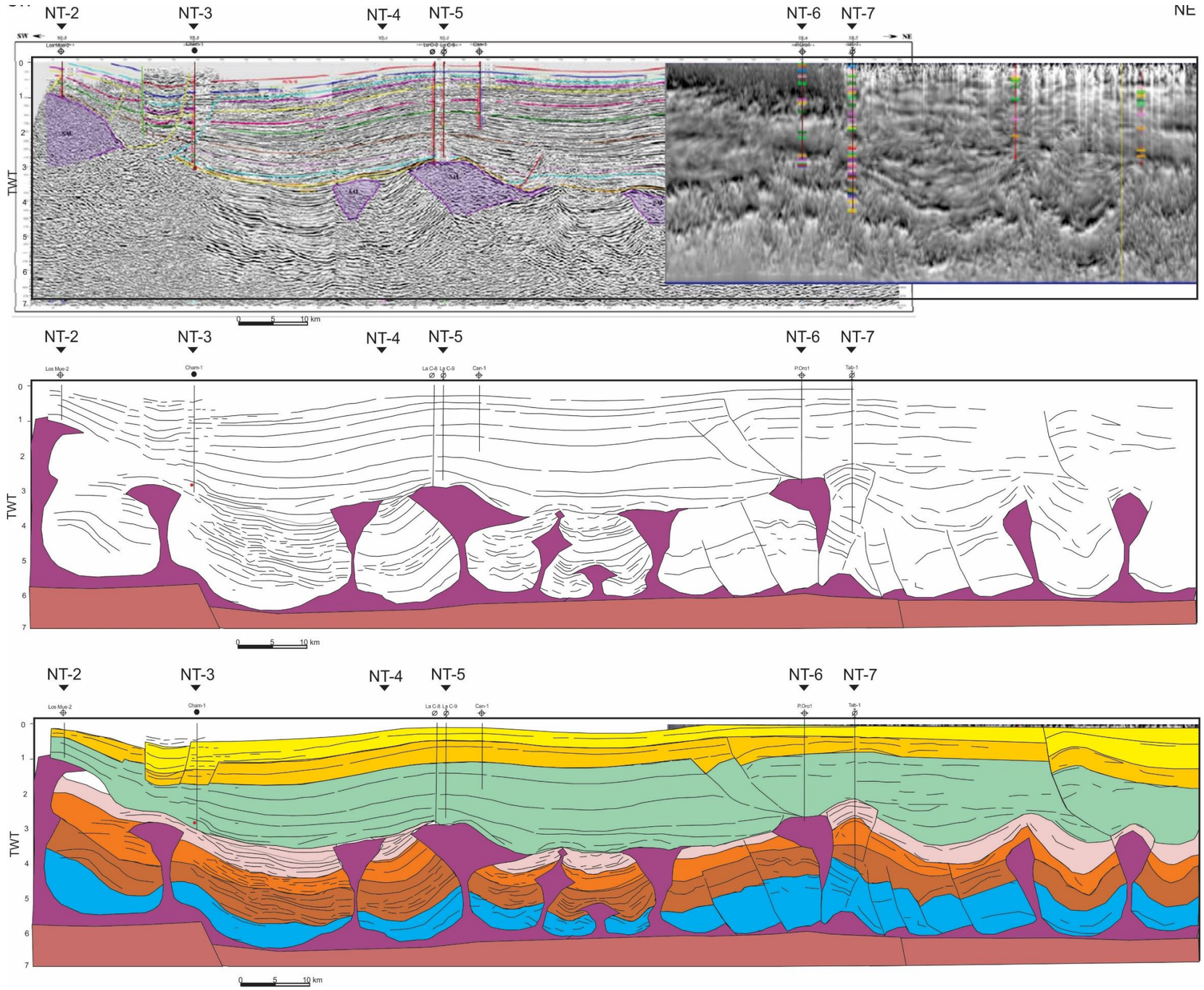

Fig. 7.21 Interpretation of TWT 2D seismic section. NT-H section is oriented SSW-NNE of the Isthmus Saline Basin. a) Seismic section; b) line drawing; c) seismic section with interpretation.

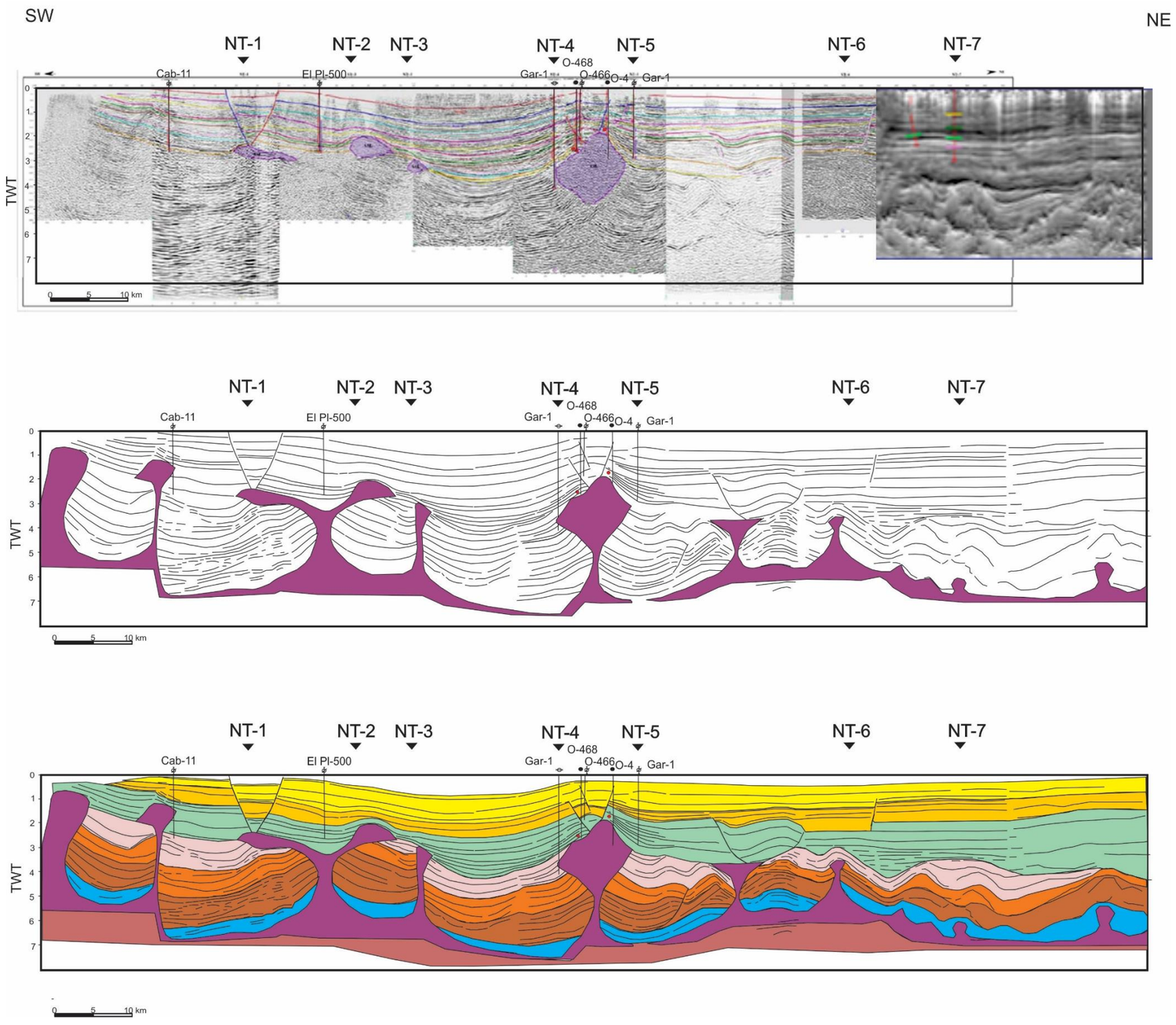

Fig. 7.22 Interpretation of TWT 2D seismic section. NT-G section is oriented SSW-NNE of the Isthmus Saline Basin. a) Seismic section; b) line drawing; c) seismic section with interpretation.

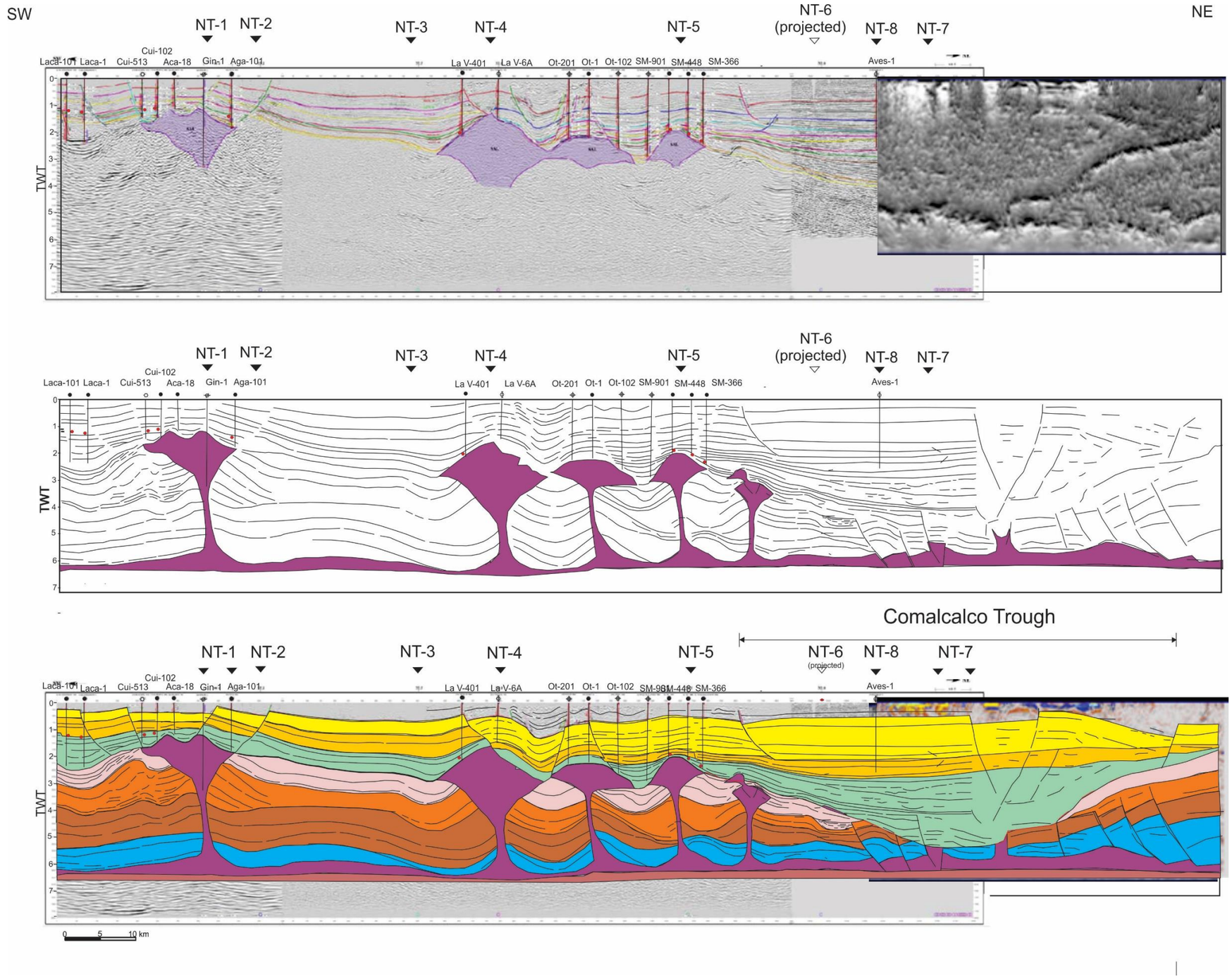

Fig. 7.23 Interpretation of TWT 2D seismic section. NT-F section is oriented SSW-NNE of the Isthmus Saline Basin. a) Seismic section; b) line drawing; c) seismic section with interpretation.

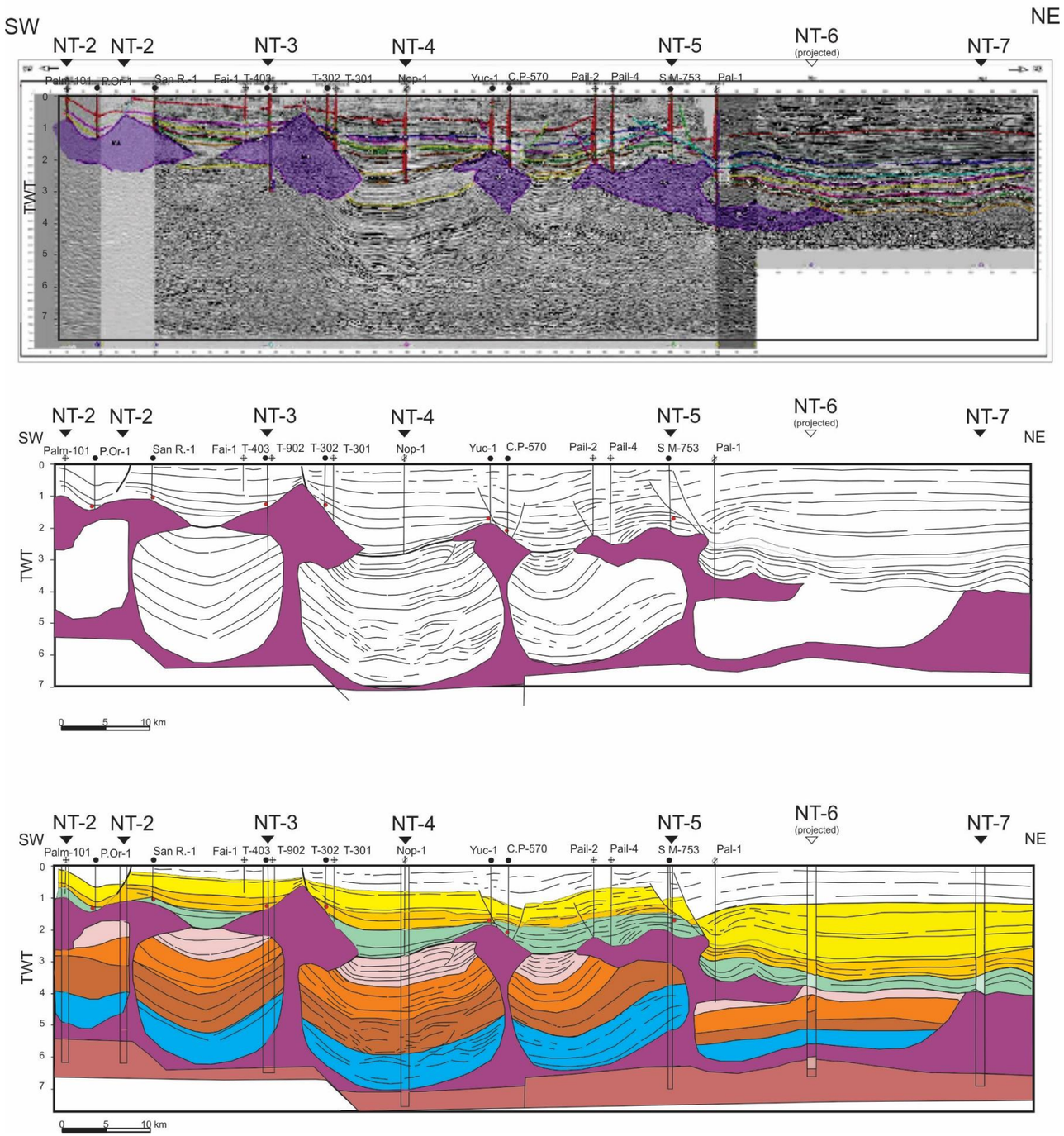

Fig. 7.24 Interpretation of TWT 2D seismic section. NT-E section is oriented SSW-NNE of the Isthmus Saline Basin. a) Seismic section; b) line drawing; c) seismic section with interpretation.

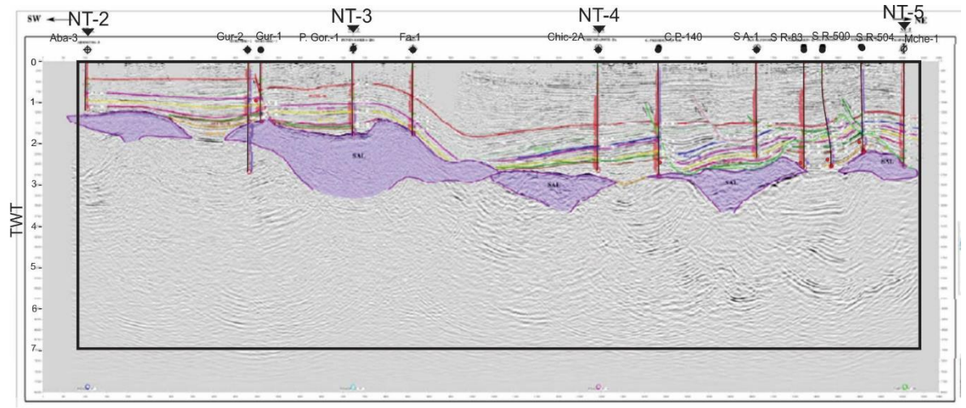

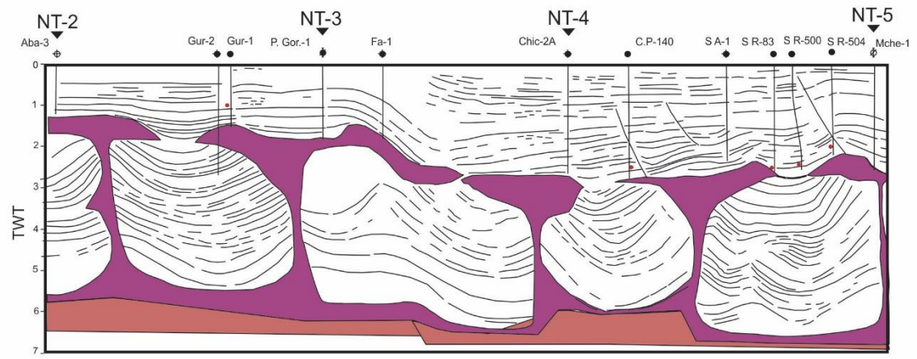

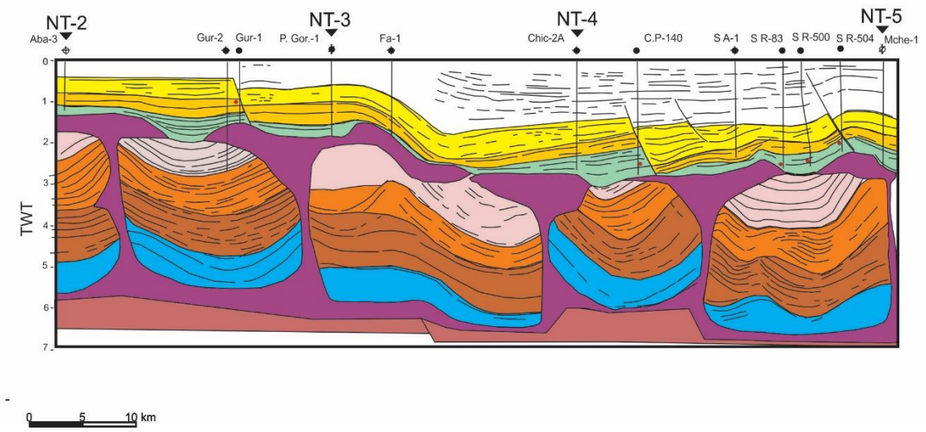

Fig. 7.25 Interpretation of TWT 2D seismic section. NT-D section is oriented SSW-NNE of the Isthmus Saline Basin. a) Seismic section; b) line drawing; c) seismic section with interpretation

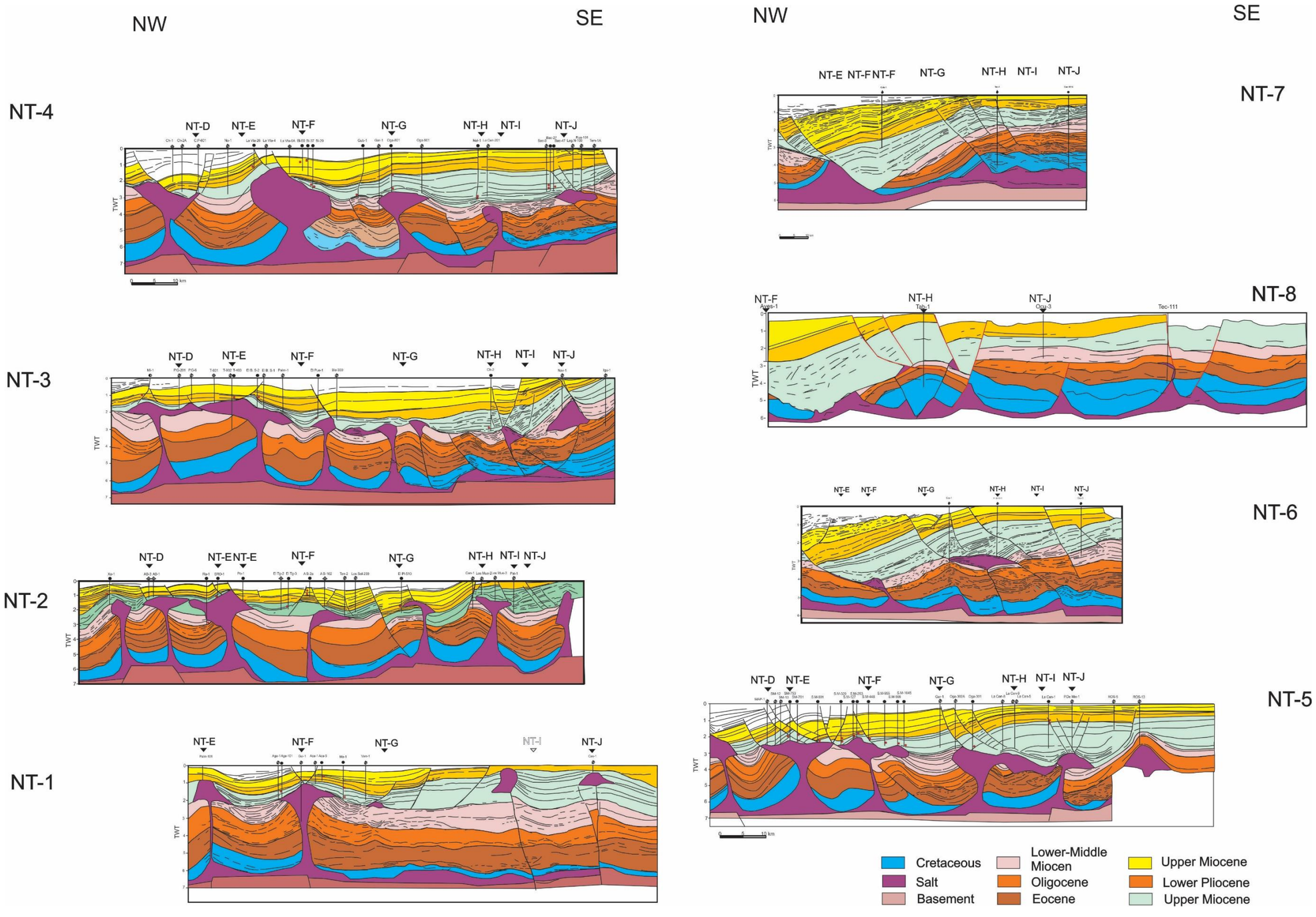

Fig. 7.26 Integration of geological sections oriented NNW-SSE of the Isthmus Saline Basin.

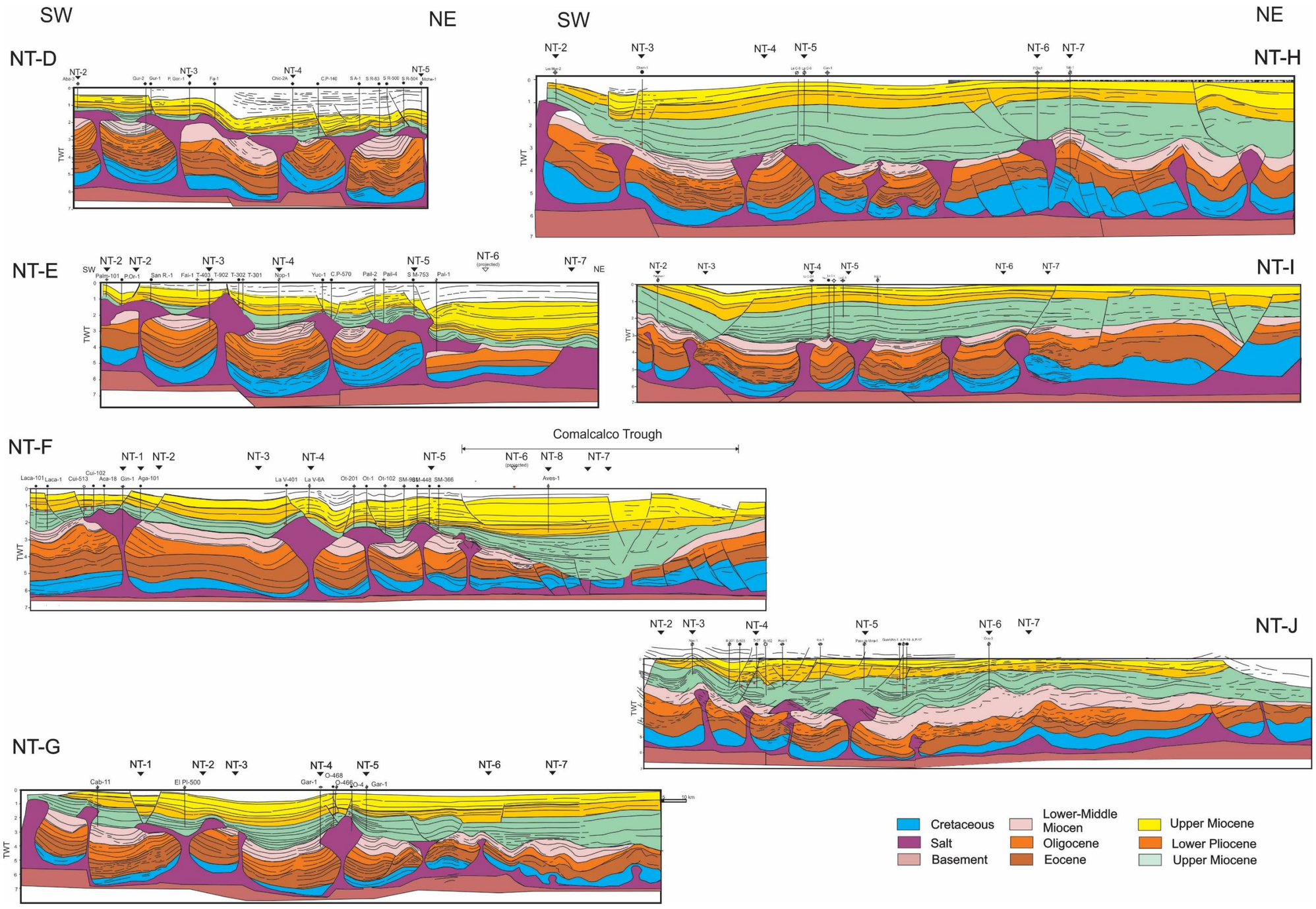

Fig. 7.27 Integration of geological sections oriented SSW-NNE of the Isthmus Saline Basin.

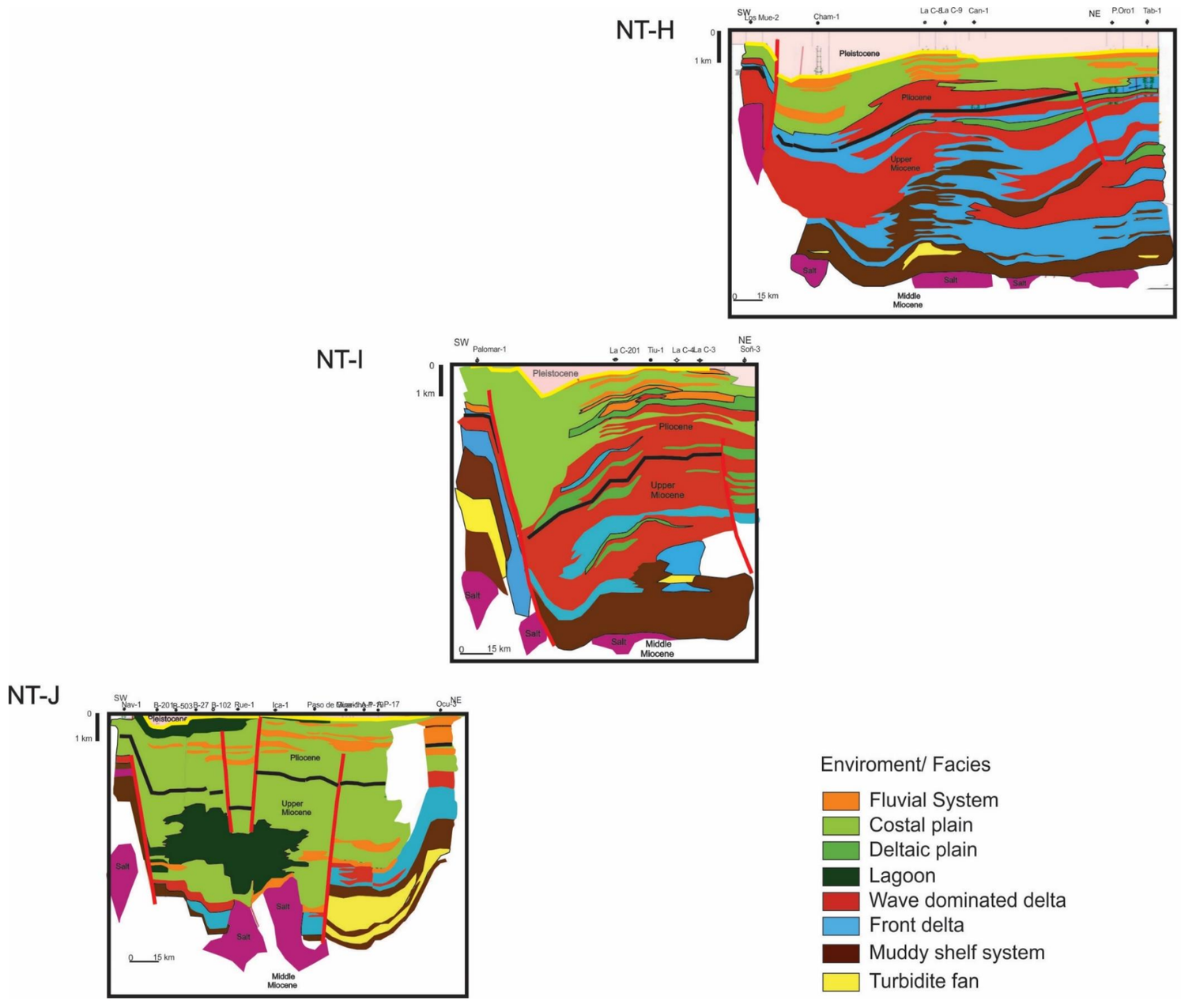

Fig. 7.28 Distribution of sedimentary facies controlled by salt diapirs in the section J, I, and H.

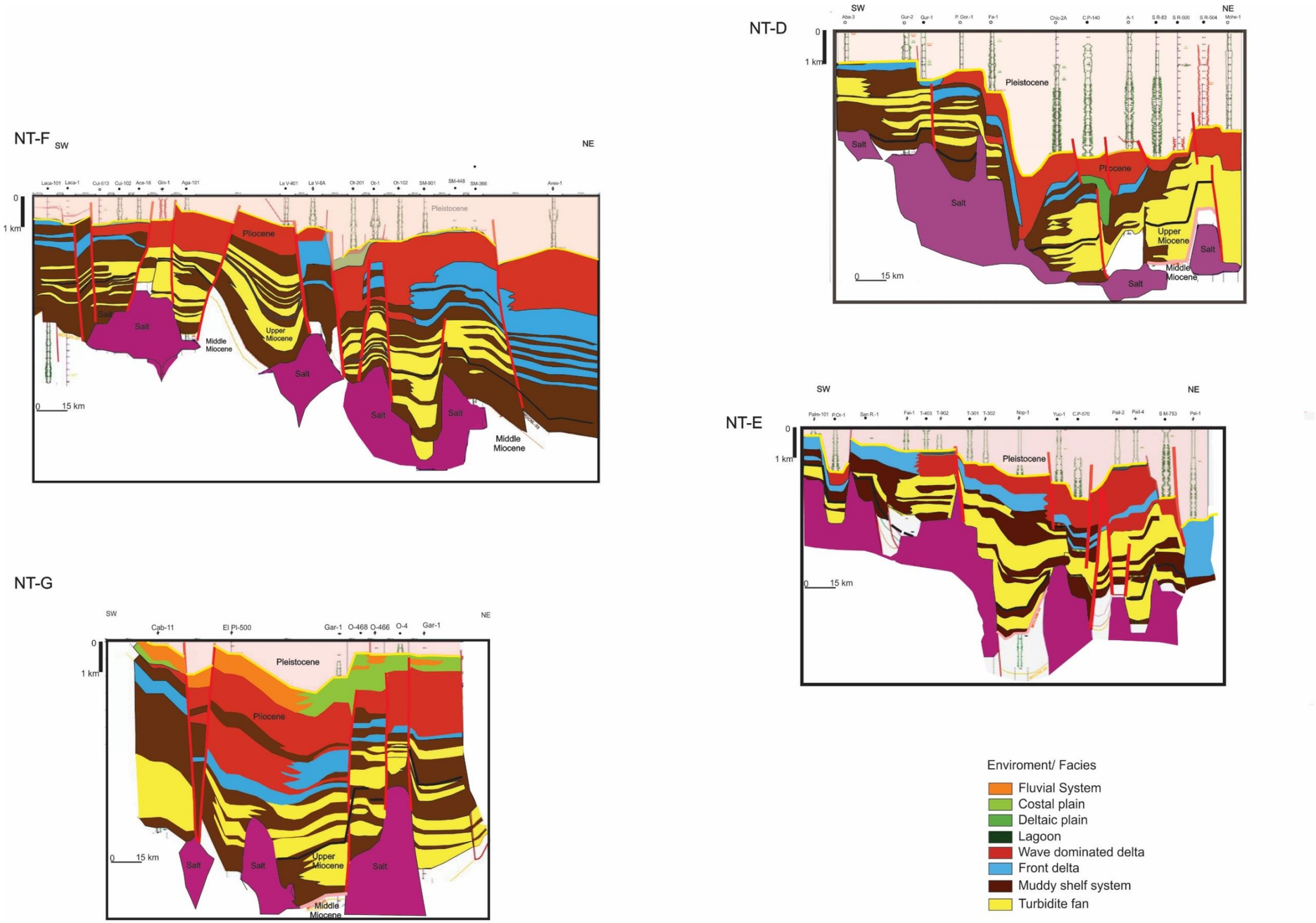

Fig. 7.29 Distribution of sedimentary facies controlled by salt diapirism in the section G, F, E and D.

7.4 Seismic 3D Interpretation

The 3D seismic data allowed define the structural style of the salt structures in the Isthmus Saline Basin. The structural style and geometry of the salt diapirs in the Isthmus Saline Basin can be subdivided in four salt sub-provinces. The subdivision is described from west to east (Fig. 7.32).

The western sector of the ISB is represented by a thick shallow salt canopy (fig 7.4 D3). This sub-province is characterized by 2000 m thick shallow allochthonous salt that was controlled by contraction. Although the seismic image is blurred by the thickness of allochthonous salt, it is considered that the deep-marine sediments are truncated or pinch out against the bodies of salt. In this area a sub-salt play is represented by deep-water sediments represented by turbidite sandstones (Fig. 7.28) which represent an important opportunity area.

At the central part of ISB, the structures are characterized by salt cored thrust structure and strike-slip structures (positive and negative flower structures) created an intra slope minibasin (Fig. 7.33, 34). In this area the transpression was intense that produced large and deep depocenter and vertical welds. The figures 7, 33 and 7.34 exemplify the structural style that characterizes this sub-province.

At the eastern sector of the basin is represented by two different styles of structures. The first is represented by squeezed salt diapirs associated to gravity-driven halokinetic processes and also tectonic compression (Fig. 7.35). This sub-province is located between the zone of compressive structures related to strike-slip faults to the west and the zone of structures for the evacuation of salt to the east. However, salt diapirs may have initiated with pillow phase and evolved into diapirs due to tectonic compression in Middle Miocene -Upper Miocene. The evidence of halokinetic processes are the rim synclines that indicates grew by downbuilding, but also there is evidence of tectonic compression. The second is associated with salt withdrawal basin where large thick sediments produced listric and counter-regional fault systems. (Fig. 7.34).

7.5 Summary

The ISB is a NE-SW oriented asymmetric basin approximately 50 km long and 50 wide. The structural analysis was carrying out with seismic data with different scales.

The analysis of regional seismic helped to understand that the Isthmus Saline Basin is being deformed by orogenic shortening while the rest of the basins show deformation styles related to gravitational deformation.

Regional model was established in which the Isthmus Saline Basin was divided by regional strike-slip faults. The division of the basin generated that the western sector of basin is characterized by compressive salt structures represented by compressed diapirs and the eastern sector is mainly characterized by extensive structures related to the evacuation of Comalcalco Basin.

The fifteen sections used to analyze the basin, allowed to know the geometry of the salt diapirs, the structural relationship between the basement and salt diapir, the vertical and lateral variations of the sedimentary facies.

The seismic sections oriented NNW-SSE showed the thickness variations of sediments from west to east. The distribution of the sedimentary sequences was controlled by the structural relief of the salt diapirs. The thickness variation of Neogene sediments is from 2.5 towards the west until 5.5 ms to the east.

The thin thickness of the Neogene sediments coincides with the province of salt canopies, which shows that salt canopies are extruded through thin roof and thicker roofs resist piercement as seen in sections NT4, NT-5, NT-6, NT-7 and NT-8

3D seismic data allowed sub-dividing the Isthmus Saline Basin into four structural sub-provinces:

The first sub-province is located to the west sector of the basin is characterized by allochthonous salt structures. The allochthonous salt can reach a thickness of up to 3000 m.

The second sub-province is characterized by contractional salt structures related with transpressive deformation. The shortened diapirs show different degrees of deformation due the relative mechanical weakness of the salt

diapirs. The contractional sub-province is characterized by a salient of diapirs that tend to nuclear folds and faults.

The third sub-province is represented by squeezed salt diapirs associated to gravity-driving halokinetic processes or due to tectonic compression or both.

The fourth sub-province is characterized by listric and counter-regional fault system associated with the salt withdrawal basin. This structural system is related to the evolution of the Comalcalco Basin which is linked to gravity extensional processes.

.

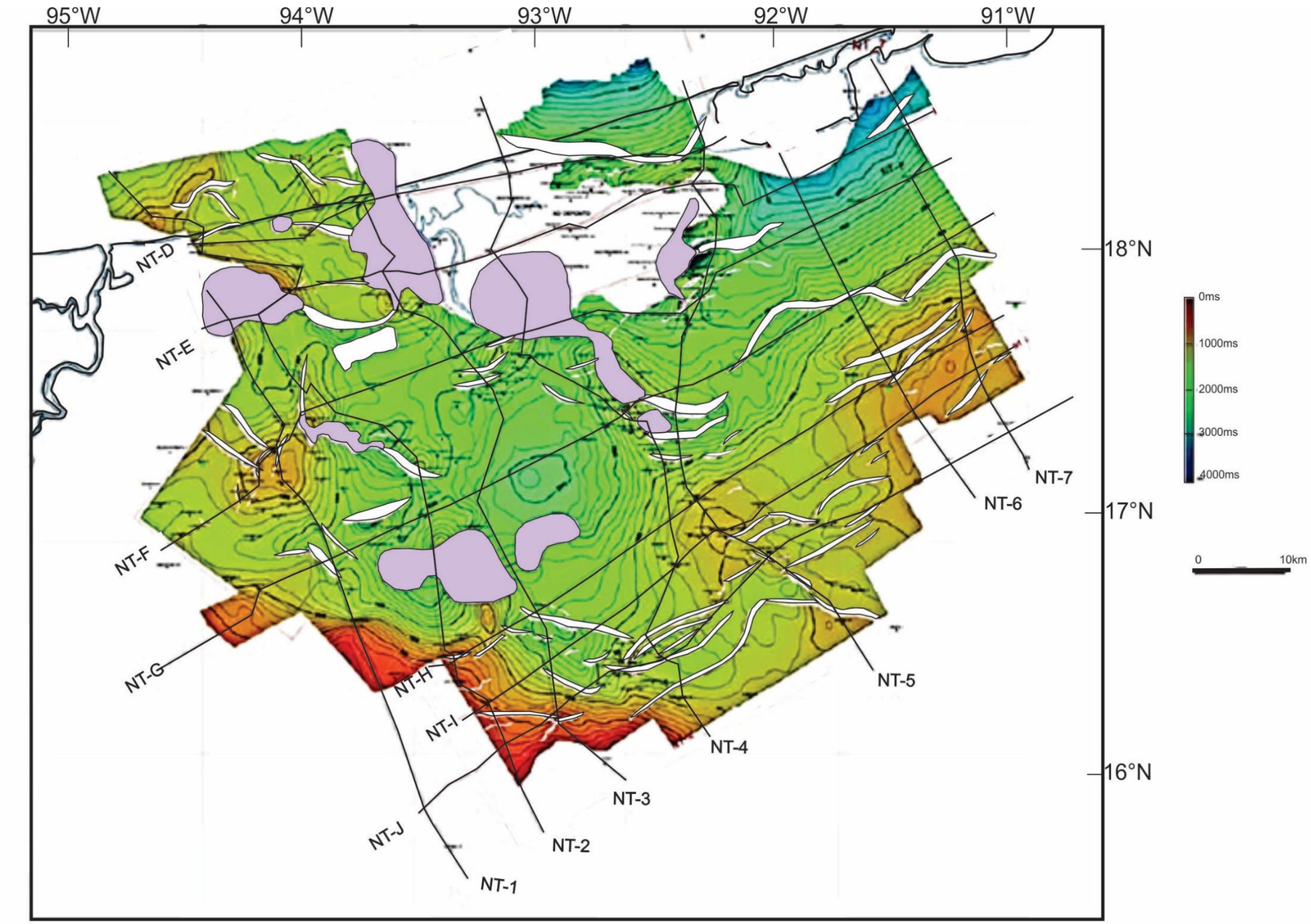

Fig. 7.30 Structural configuration on time (TWT) Miocene.

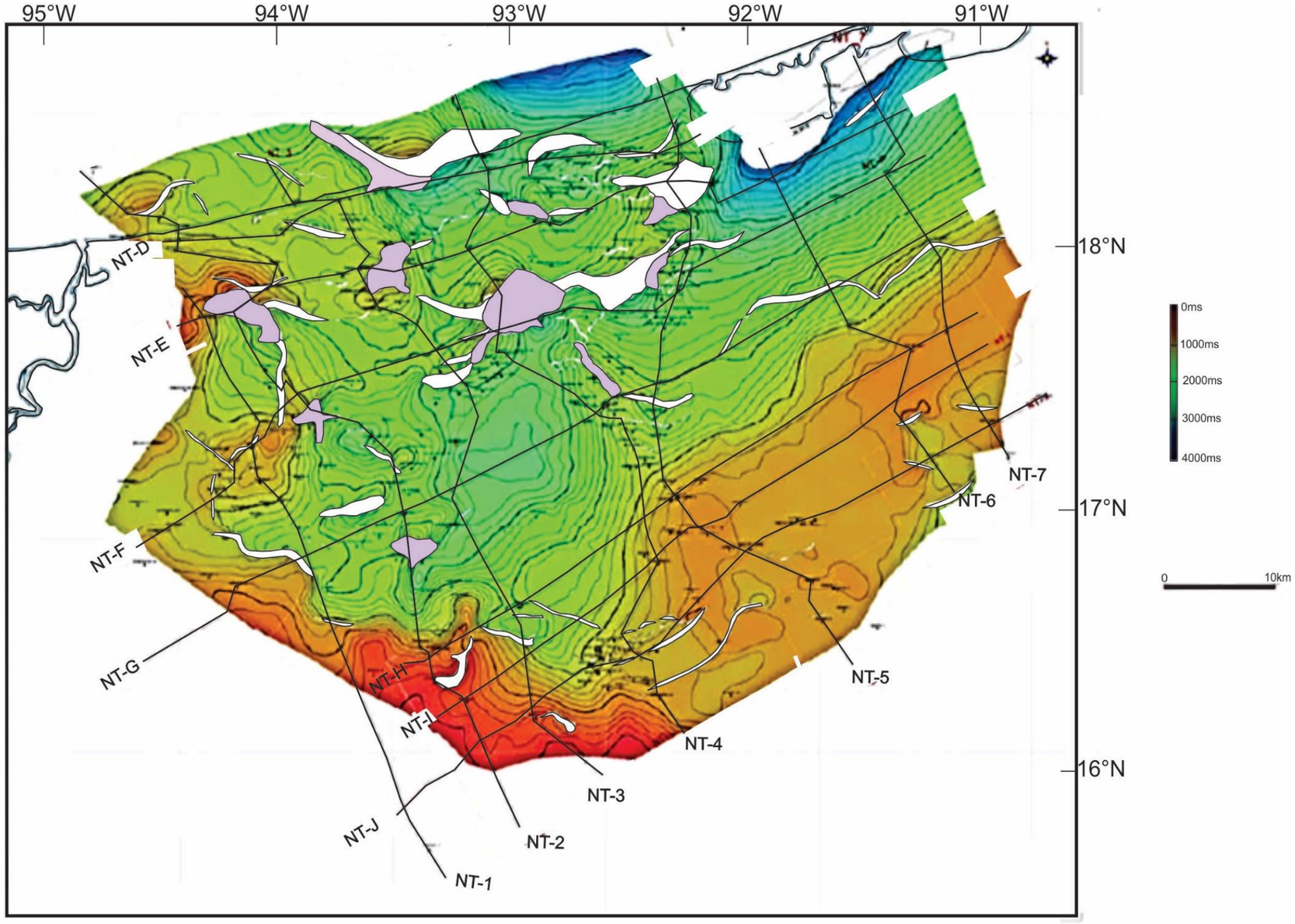

Fig. 7.31 Structural configuration on time (TWT) Pliocene.

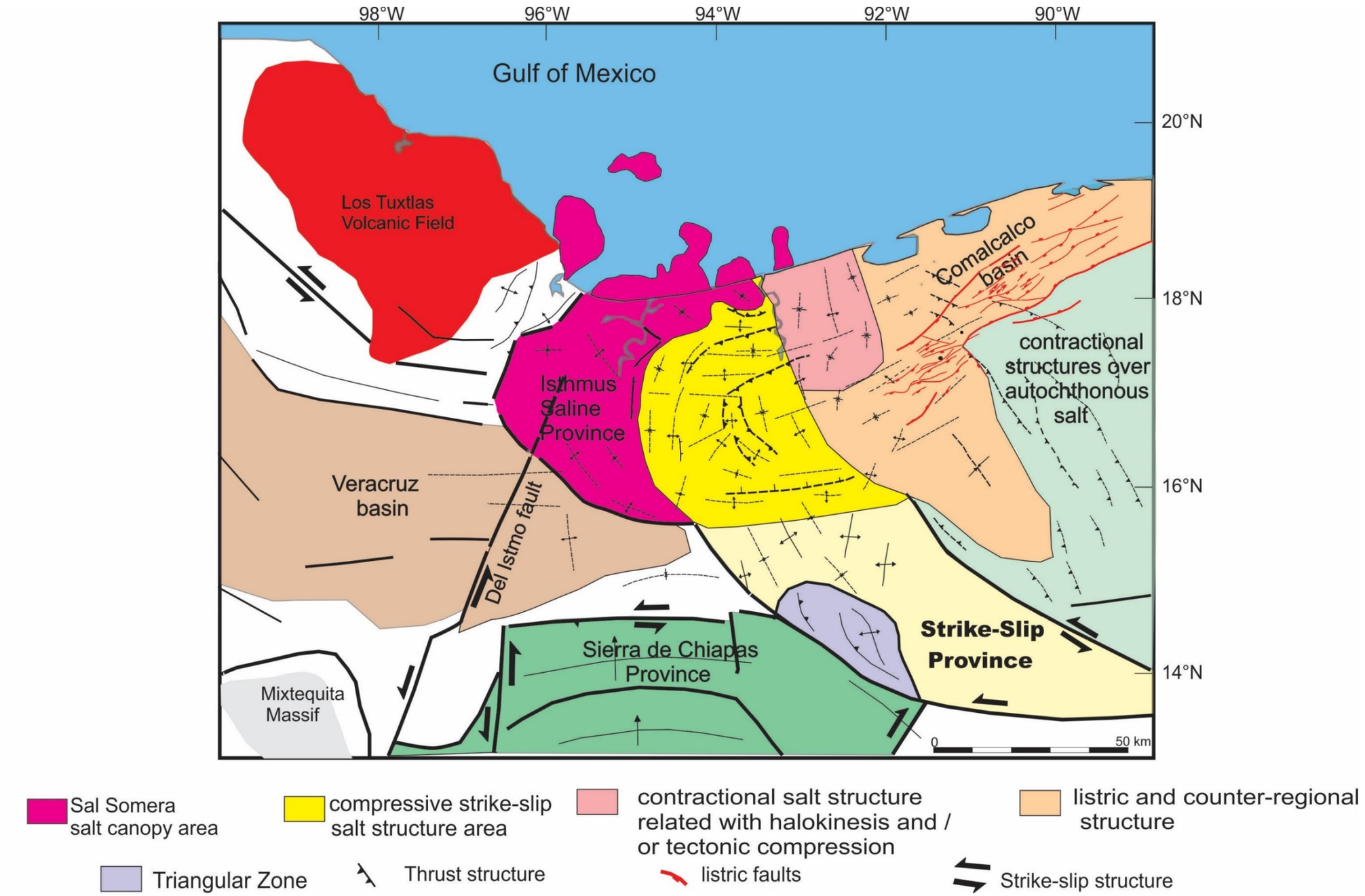

Fig. 7.32 Shows the Sub-provinces map of the Isthmus Saline Basin

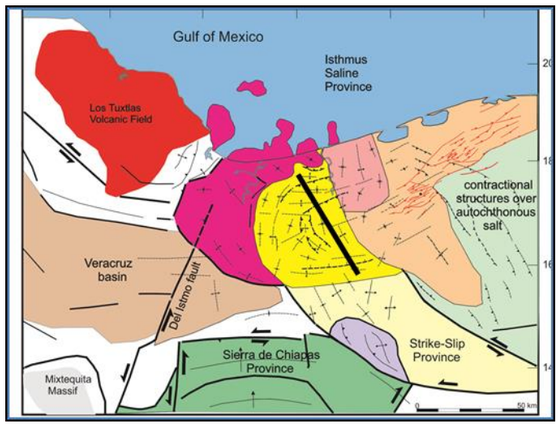

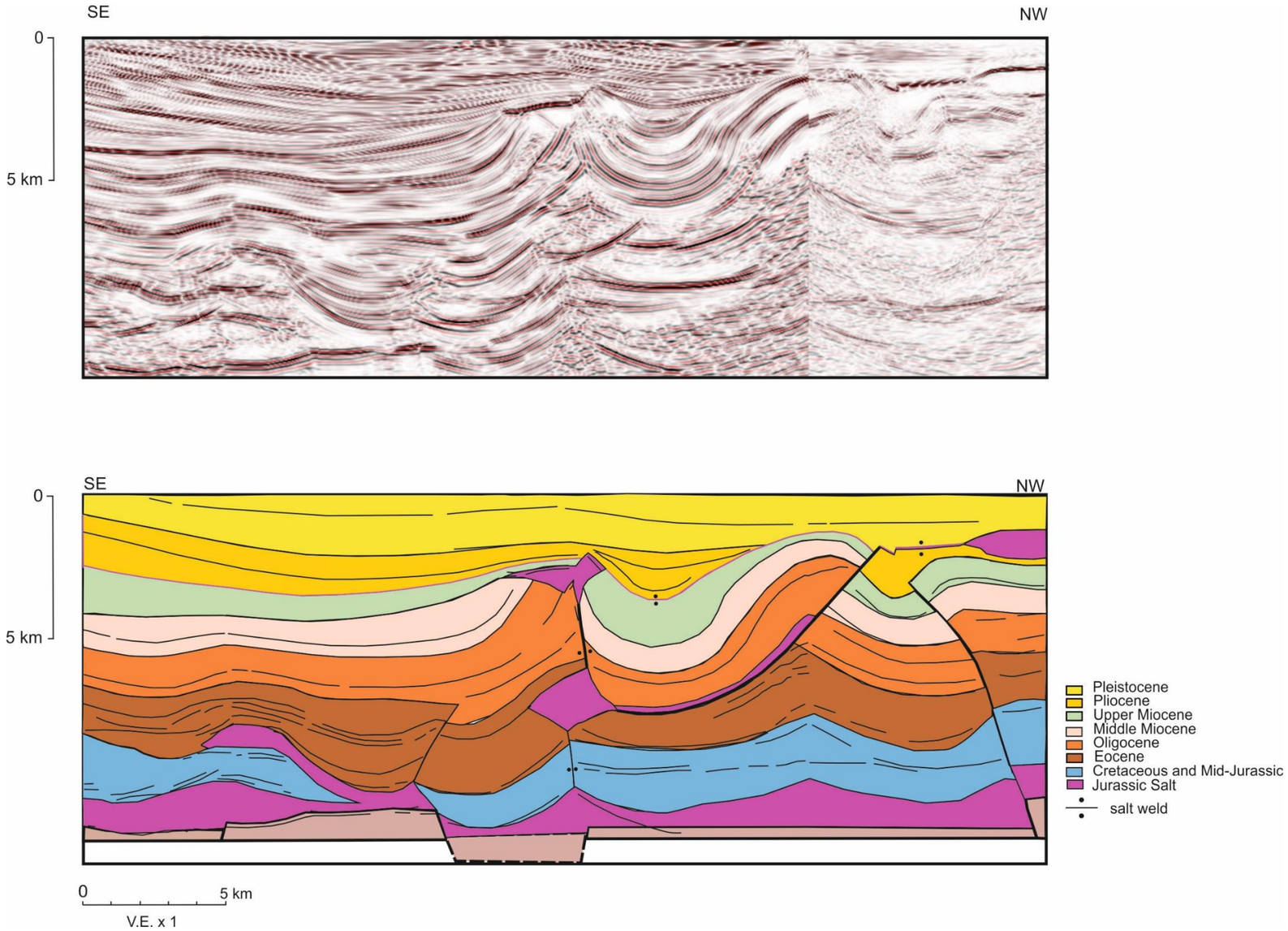

Fig. 7.33 Salt thrust structure represents the central sector of the Isthmus Saline Basin

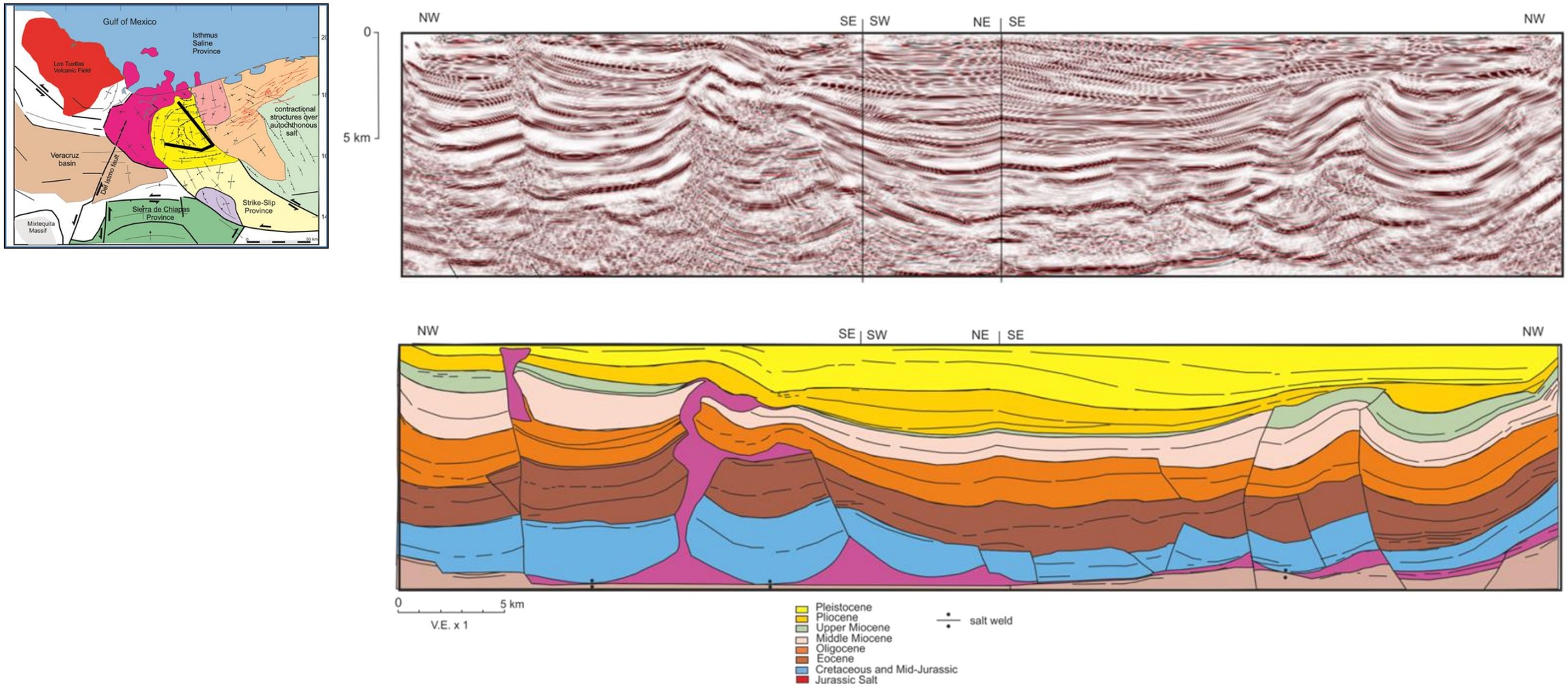

Fig. 7.34 Salt thrust structure related whit strike-slip fault system.

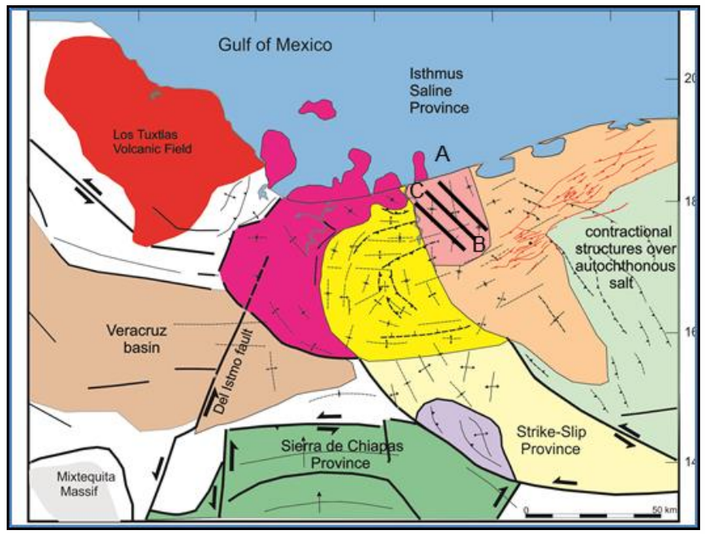

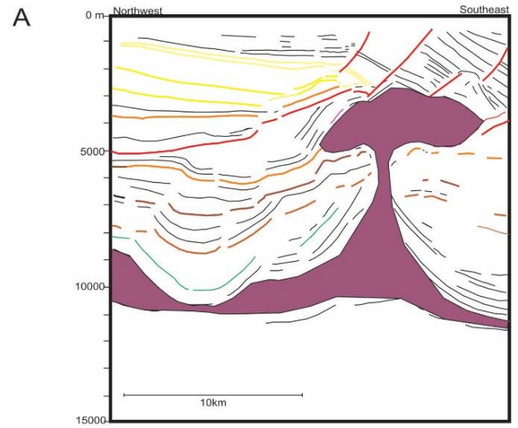

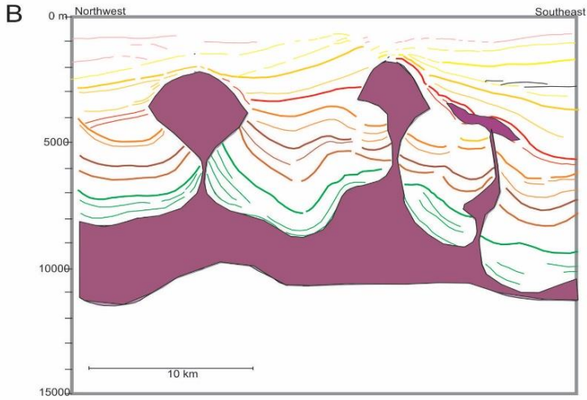

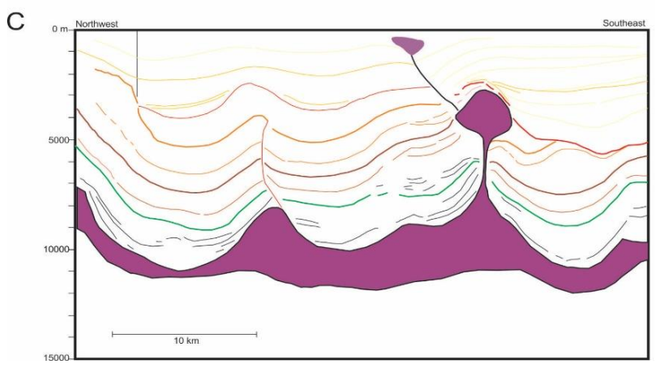

Fig. 7.35 Squeezed salt diapirs associated to gravity-driven halokinetic processes and / or tectonic compression.

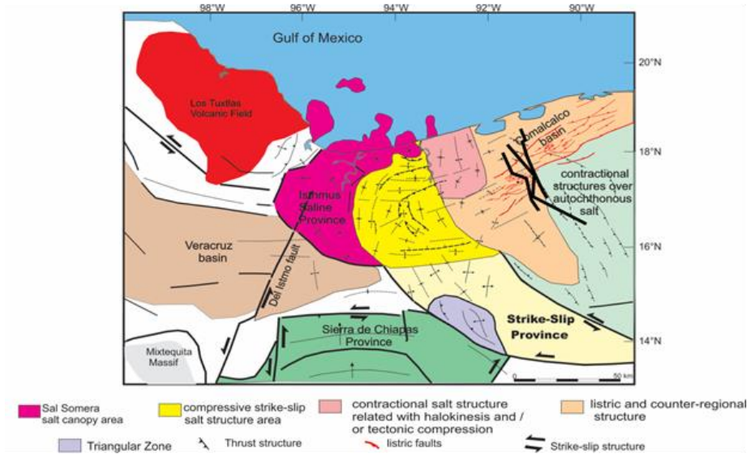

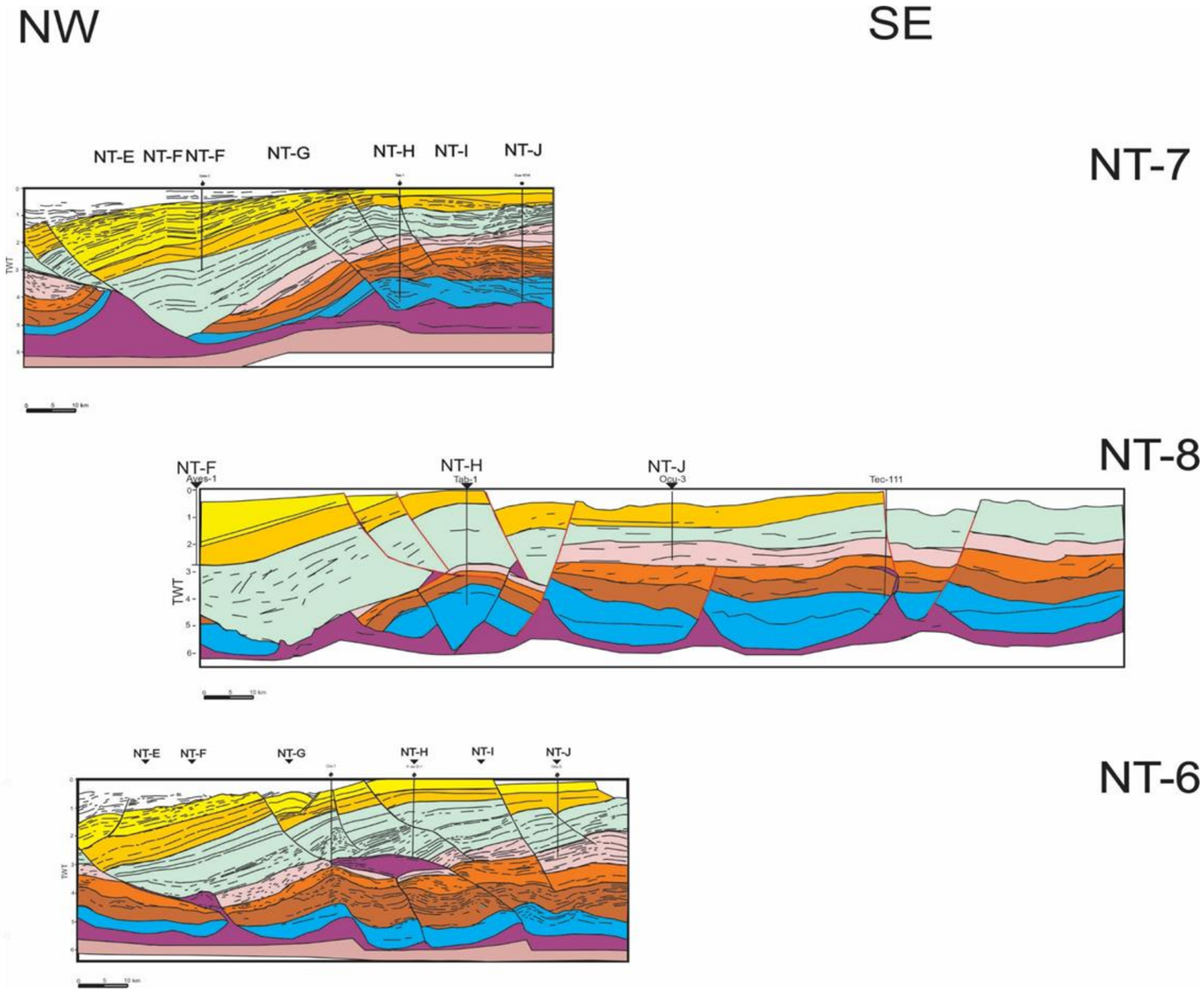

Fig. 7.36 Listric and counter-regional fault system associated with salt withdrawal basin of Comalcalco Basin.

Chapter 8 Kinematic analysis of the Tectonic Evolution of Isthmus Saline Basin

8.1 Introduction

The construction and restoration of cross-sections is a critical step in validating one's the structural interpretation. Furthermore they are a valuable tool to recreate the geometry of the kinematic analysis through geologic time (Hossak, 1995). Restoration techniques have been extensively used by the oil industry to reconstruct systematically the history of salt displacement and the changes associated with around it, aiding to predict new exploration areas. New concepts derived from structural reconstruction have lead researchers to understand the structural and sedimentological characteristics that helped them unravel of salt-related deformation. The flow properties of salt, together with its ability to dissolve make section balancing of salt structures complicated.

The practice method consists on restoring geological sections by assuming constant-area conditions for the sediment layers only and to leave the areas occupied by salt as gaps whose area may change through time (Dahlstrom, 1969; Hossack, 1995). A further factor to take into account when restoring geological sections is the reduction in volume of salt by dissolution. This reduction, up to 50%, results from assuming that salt structures have remained exposed or near the surface (Rowan, 1993).

The fundamental rules for the construction of balanced cross-sections were outlined by Dahlstrom (1969), and Elliott (1976) with further development and discussion by Geiser, (1988), Boyer and Elliot (1982), Marshak and Mitra (1986). More specifically the restoration of cross sections in salt basins has been developed by Rowan, & Kligfield, (1989), Rowan (1993), Rowan, Kligfield, Weimer,1993), Rowan (1995), Bishop, *et al* (1995), (McBride, *et al* (1998), Gottschalk, *et al* (2004), Trudgill (2011) and Rowan & Ratliff (2012). In general terms, when an interpretation cannot be restored successfully, the interpretation should be considered and developed.

This chapter addresses section restoration of four cross-sections, which have the purpose of systematically reconstruct the complex history of salt tectonics undergone by the Isthmus Saline Basin (ISB). In addition, these reconstructions intend to clarify

the role of salt deformation in the distribution of sedimentary facies (reservoirs), timing of trap formation, charge, migration and structural patterns above and below salt décollements. This information is fundamental for prediction of new exploration areas.

Four seismic lines (Fig. 8.1) were interpreted in depth and imported into Midland Valley's 2D Move section restoration and construction program (Midland Valley, 2013). The geo-seismic interpretations were validated using sequential restorations with iterative adjustments made where necessary to improve the deformed state geometries as well as the restored state structural geometries. This chapter presents an analysis of the four interpreted sections. Three of these sections are oriented NW-SE, with one of them going through a salt-cored fold system. The fourth section is oriented NE-SW. The fourth section was restored considering the contraction observed through several structural section oriented in that direction.

8.2 Results of Restored Sections

8.2.1 Introduction

Based on seismic interpretation results, four structurally balanced cross sections have been constructed and sequentially restored for the study area. Three of the restored sections were oriented perpendicular to the regional structural trend, which is parallel to the direction of tectonic transport (Fig. 8.1). Salt structures in the Isthmus Saline Basin can be interpreted in the context of a compressive strike-slip regime, in which three non-synchronous deformation systems can be identified from the shelf to the slope (further discussed in Chapter 7). Cross-sections were sequentially restored, through nine to eleven stages, from the Upper Cretaceous to present time. Total shortening and shortening rates for different stratigraphic intervals were plotted for all sections in order to illustrate the timing and amount of deformation. Additionally, a series of tables show the rate of shortening in millimetres per year for each restored section in the Isthmus Saline Basin since the Eocene.

8.2.2 Eastern Section basinward Dip Sections (NW-SE)

Section No.1 is a depth section and that represents a sector of the Isthmus Saline Basin. This section is oriented NW-SE and with a length of 30 km. The section passes through three closely spaced salt diapirs. In this region no salt-cored thrusts are identified. However, diapir geometries document intense shortening of to 23% which equivalent to 7 km (Fig. 8.2). Salt diapirs are interpreted to sit above basement faults that form the margins of half-grabens in the Isthmus Saline basin (further discussed in Chapter 7). Diapirs root down into the Callovian Salt mother salt layer, which extends through the entire southeast sub-basins becoming thinner towards the highs margins. Three diapirs have steep-sided flanks that penetrate up through Mesozoic and Tertiary stratigraphy, evidencing their long history of evolution. The end of diapirism is marked by the presence of a middle Miocene unconformity, which is associated to the formation of salt welds. The three diapirs have become inactive at different geological times: the first and second diapirs on the left and centre reach up almost to the Lower Pliocene, whereas the third diapir (on the right) has penetrated section as high as the Middle Miocene. The first, and second diapirs, are folded and inclined and stratigraphically sediments are thinned over diapir crest. Meanwhile, the third diapir shows salt welding caused by contraction.

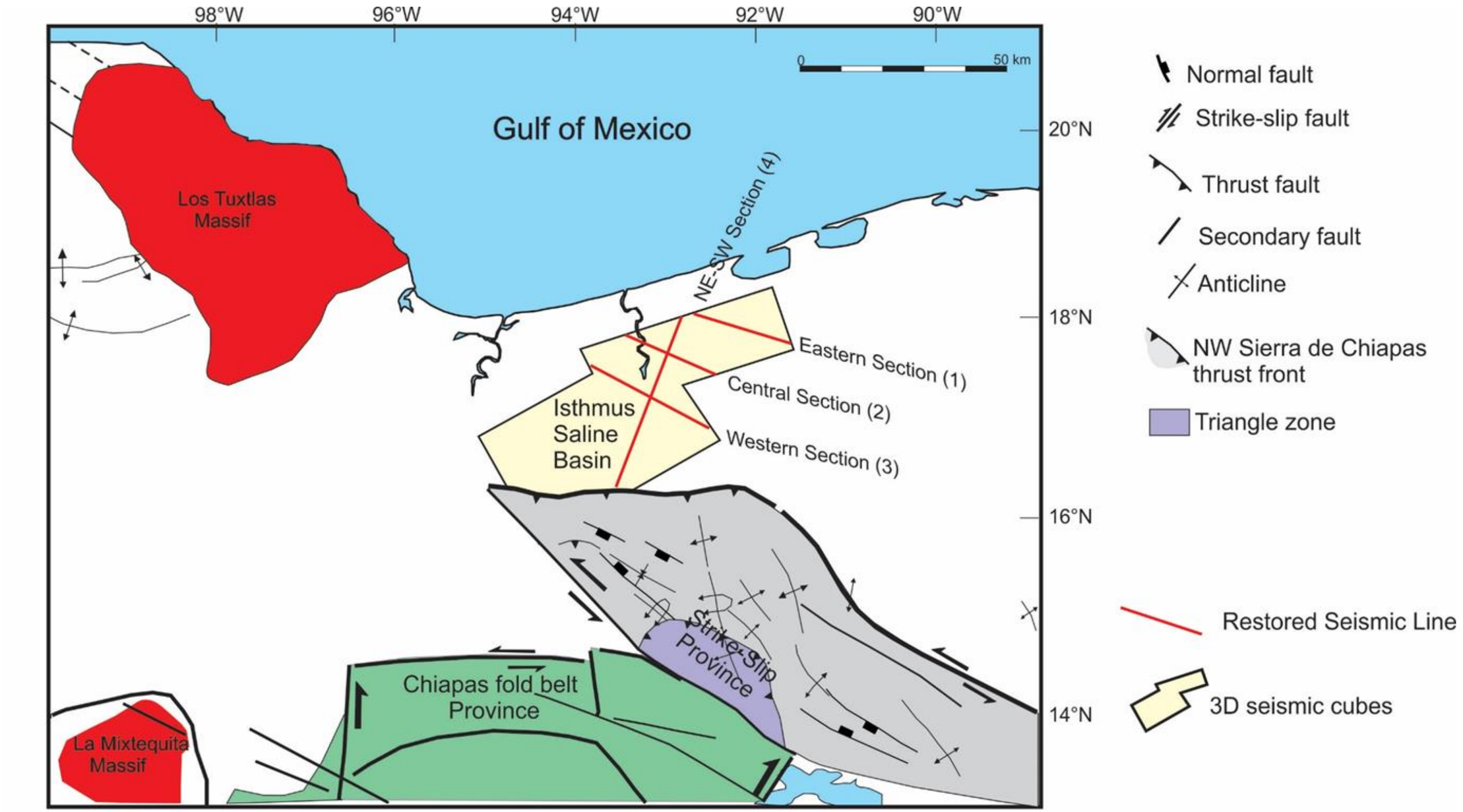

Figure 8.1 Map showing the location of sections used in the restoration and its relation with strike-slip province.

Restoration of the section No.1

In the Isthmus Saline Basin evidence has been found supporting the initiation of regional salt diapirism in the Middle - Late Jurassic. The restoration of the section one suggests that early reactive diapirism formed the salt walls that subsequently developed into diapirs and minibasins in Late Jurassic and Cretaceous times. By the end of the Late Cretaceous, diapirs were fully developed. Salt thickness or diapir high was estimated between 2.5 and 3 km (Fig. 8.3a).

During the Eocene, diapirs began to experience contraction. Salt diapirs show evidence of thinning of salt diapir neck and thrusting within the minibasin. The estimated shortening during Lower Eocene and Upper Eocene was 1.3 and 1.7 km respectively, and it was related with transpression and collision of Chortis block and Yucatán block during the Laramide Orogeny. The uplifting caused tectonic destabilization and resulted in the deposit of mass transport complex facies characterized by debris flows and conglomeratic sediments (Fig. 8.3 b, c).

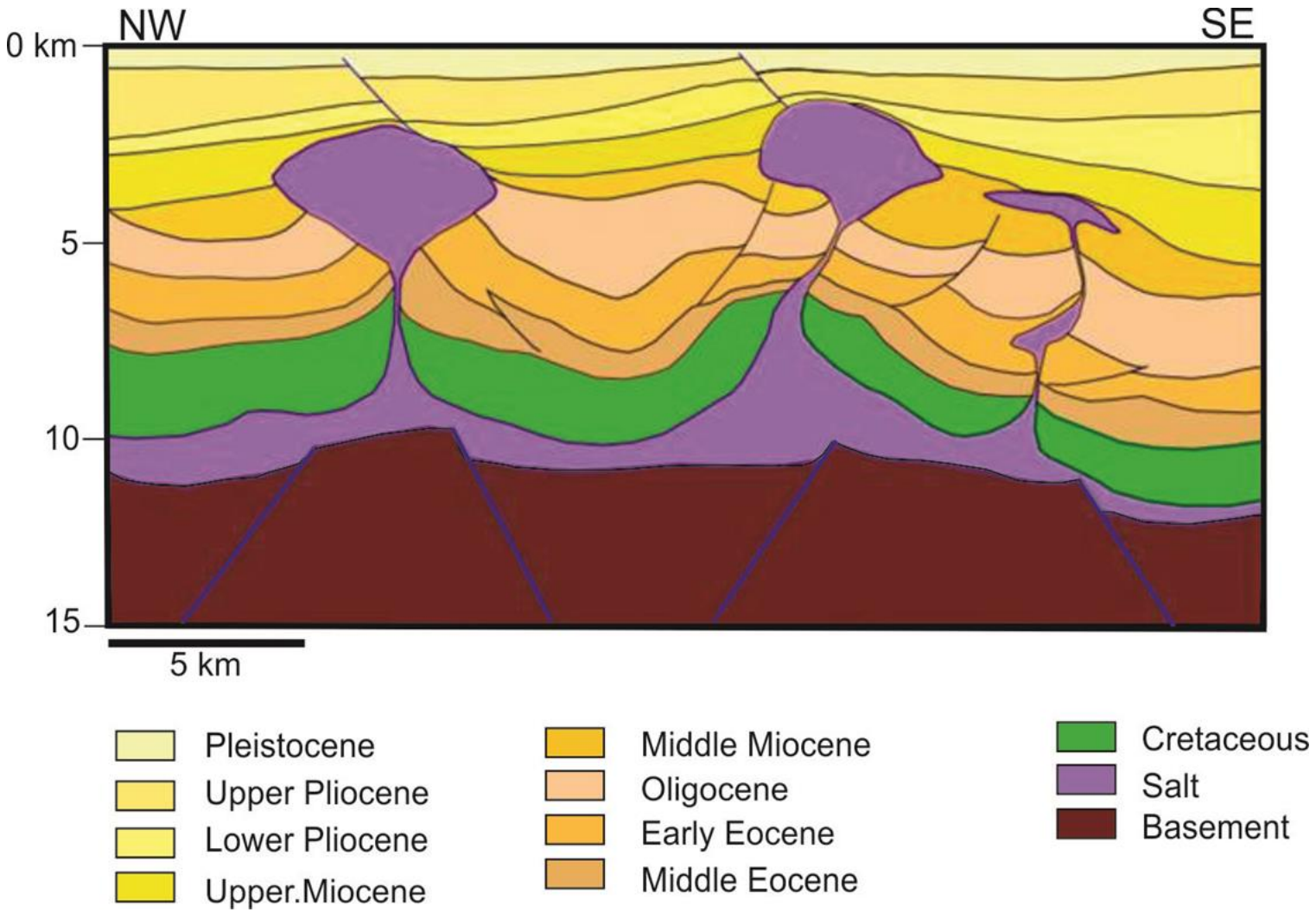

Figure 8.2 Depth-converted geologic section of the eastern sector (section 1)

continued during the Oligocene, producing a shortening of 1 km, and leading to fault thrusting (Fig. 8.3d). In this stage, the thickness of debris flows increased considerably due to the continue uplift of the Chiapas Massif. By the Middle - Late Miocene contraction related shortening had reached 2 Km (Fig. 8.3 e, f). Massive influx of clastic sediments derived from the newly-deformed mountain exposed to the south. The left and central diapirs continued to grow during this stage, but the right diapir was exhausted due to the depletion of the source layer overburden. The shortening diapir caused a large and deep depocenter between them.

Early and Late Pliocene show evidence of rejuvenation of salt. During this stage, section was shortened by 0.7 km and 0.21 km, respectively, leading to the uplift of the salt crest (Fig. 8.3 g, h). Salt diapir contraction caused salt roof uplift, leading to the development of extensional faults. This local extension balance local arching. The flow of turbidites and to a lesser extent deltaic sediments continued accumulating greater thickness in adjacent structural lows and thinning above diapir crest which has been mainly explored. At present day, both main diapirs have become completely inactive and are covered by fluvio-deltaic sediments (Fig. 8.3i).

The timing of basement faulting is uncertain. Assuming that rifting continued into Late Jurassic in the Gulf of Mexico (Salvador, 1987), restoration suggests that subsidence was thermal and isostatic to minimize the vertical thickness of salt in the section, the cover has been pinned at the left end of the section. Hence, the restorations provide an estimate of salt thicknesses.

8.3.3 Understanding Section No.2 (Central Section)

The central section (No.2) is a 40 km depth section oriented NW-SE. The geological section has a shortening of 59% which is equivalent to 24 km (Fig. 8.4). This section goes through three pre-existing salt diapirs spaced at approximately 10 km. Salt diapirs were interpreted to sit above basement faults, which represent the margins of half-grabens in the ISB. The diapirs root down into the Callovian Salt mother salt layer, which extends through the entire southeast sub-basins becoming thinner towards the margins highs. Three tall and squeezed diapirs have steep-sided

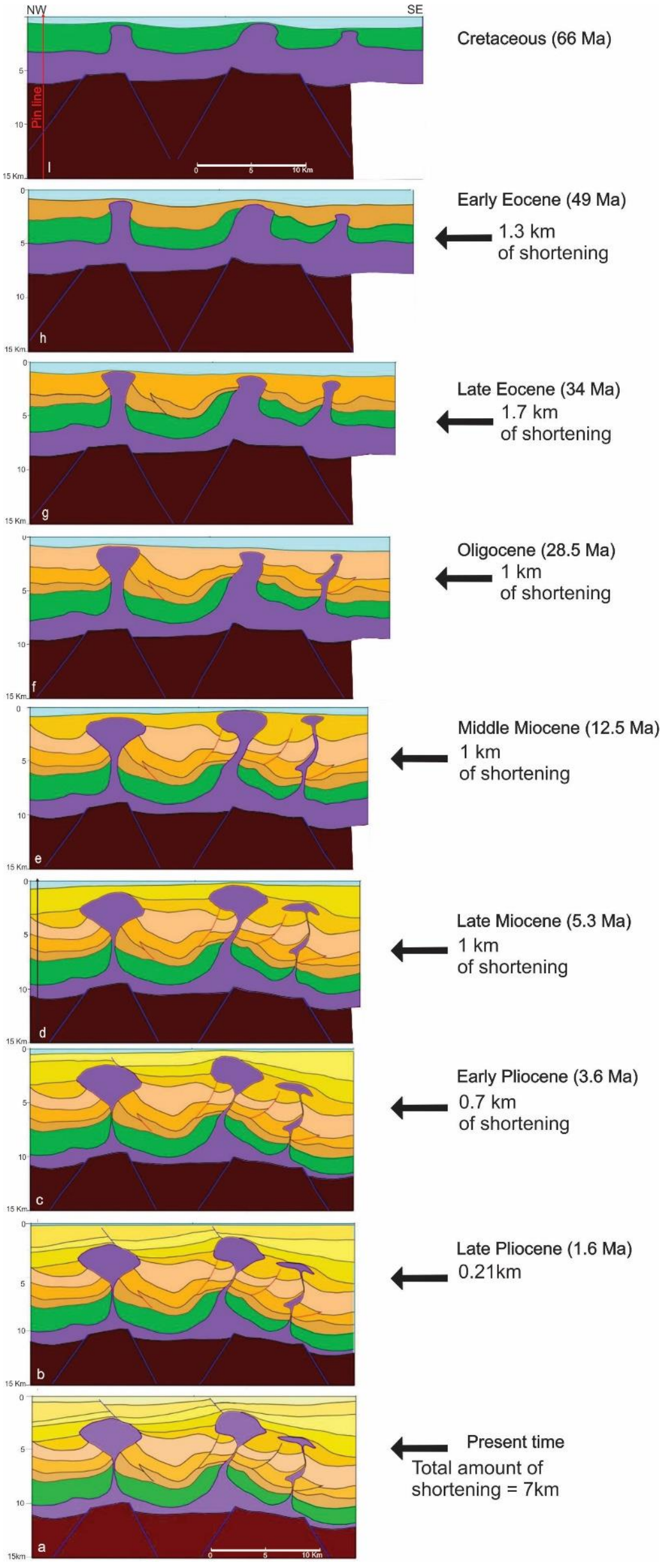

Figure 8.3 Progressive evolution of section No1 oriented NW-SE.

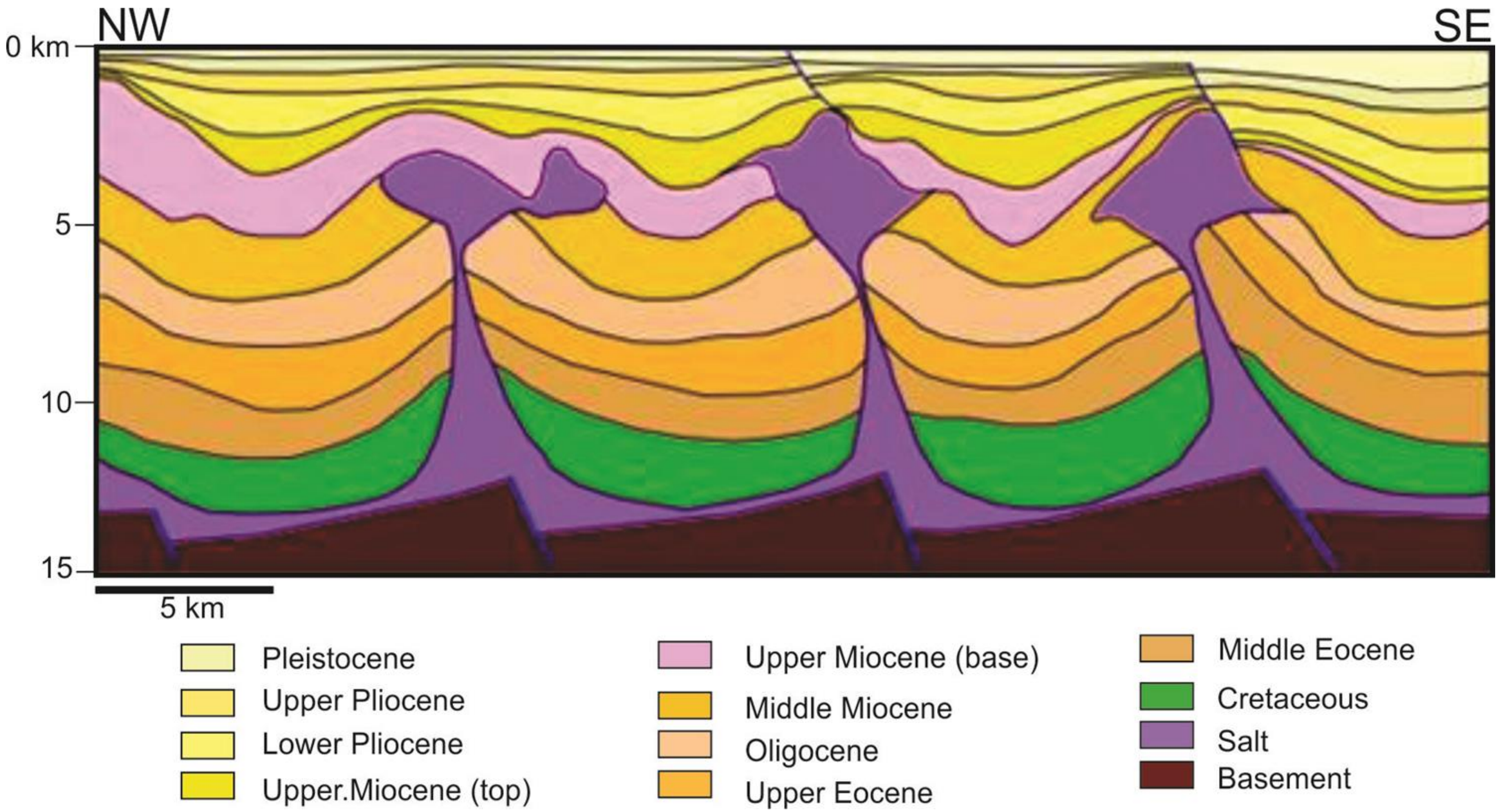

Figure 8.4 Depth-converted geological section of the central sector (section 2).

contacts that penetrate up through Mesozoic and Upper Miocene stratigraphy, evidencing the diapirs' long history of evolution. The three diapirs have become inactive at different geological times: the first, on the left, reaches up to the Middle Miocene; the second, on centre reaches up to near the Upper Miocene; the third diapir, on the right has penetrated section as high as Lower Pliocene. All diapirs were inclined and stratigraphically thinned above the diapir crest, although this feature is more pronounced in the right diapir, suggesting a gradual diapir rejuvenation induced by intense shortening. The end of diapirism is marked by roof uplift by inflation and extension balancing local arching.

Restoration of section No.2

The restoration carried out for this thesis suggests that early reactive diapirism formed the salt walls that subsequently developed into the diapirs and minibasin during Late Jurassic and Cretaceous. By the end of the Late Cretaceous, the diapirs were fully developed and reached the passive phase; original salt thickness was estimated between 2 and 2.5 km (Fig. 8.5). During Lower Eocene and Upper Eocene, diapirs were affected by intense compression, which yielded an estimated shortening of 1.4 and 7 km respectively. The shortening was a consequence of the oblique collision between Yucatán and the Chortis block. Compression increased the flow rate of salt and the inflation of salt diapirs rising at or near the sea floor. Additionally, this shortening yielded overturned adjacent strata which were filled by mass transport complex facies represented by debris flows and conglomeratic sediments (Fig.8.5, b, c).

Due to continued sinistral transform displacement of the Chortis block during the Oligocene, contraction caused an estimated shortening of 3.4 km. The lifting and erosion of the Chiapas Massif resulted in the deposition of considerable thickness of debris flows and turbidites. Sedimentary overload caused burial of one salt diapir (Fig. 8.5 d).

During the Middle Miocene, the Chiapas Massif was intensely compressed. This contraction caused an estimated shortening of 7 km, which are related with the Chiapas Massif uplift (Fig 8.5e). After an intense shortening of salt diapirs, large and

deep synclines were developed due to massive influx of turbiditic clastic sediments derived from the newly-deformed mountain exposed to the south. During this stage diapirs continued growing (Fig.8.5e). Subsequently, the Upper Miocene (base) sedimentary sequence was thinned towards the southeast. The cause of this thinning is likely to have been a salt-triggered displacement of source layer to the north-northwest yielding a minibasin to the north (Fig.8.5 f).

During the later stages of Late Miocene (Fig. 8.5 g), the basin started to experience a structural uplift towards the north. This event is evident in the restoration and is recorded by onlap against was represented by onlap again the base of Upper Miocene. Minibasins began to be filled by turbidites and deltaic sediments at this time.

During the Early Pliocene, the flow of turbidites and fluvial deltaic sediments resulted in minibasin formation, with greater accumulated thicknesses of sediments at the structural lows and thinning above diapir crests (Fig. 8.5 h).

The Upper Pliocene and Pleistocene were periods of salt rejuvenation, inflation and uplift of the right section's diapir roof, leading to the development of extensional faults. This local extension balanced local arching (Fig. 8.5 i, j). At present day, diapirs have become completely inactive and are covered by fluvial sediments (Fig. 8. 5 k).

8.3.4 Understanding Section No.3 (Western Section)

The western section (No.3) is a depth section imaging part of the Isthmus Saline Basin. It is oriented NW-SE and has a length of 33 km with a total shortening of 18%, (equivalent to 6 km) (Fig.8.6). This section is characterized by inclined weld (thrust weld) formed by the squeezing of salt diapir due to intense shortening in the Isthmus Saline Basin. Salt diapirs were interpreted to sit above the basement faults. the Isthmus Saline graben bounding basement faults. Diapirs root down into the Callovian Salt mother salt layer, which extends across the basin becoming thinner towards the margin highs. A salt thrust reaches the peak of deformation at the lower

of the upper Miocene boundary. This is evident in seismic data where stratigraphic thinning was observed against onlap surfaces

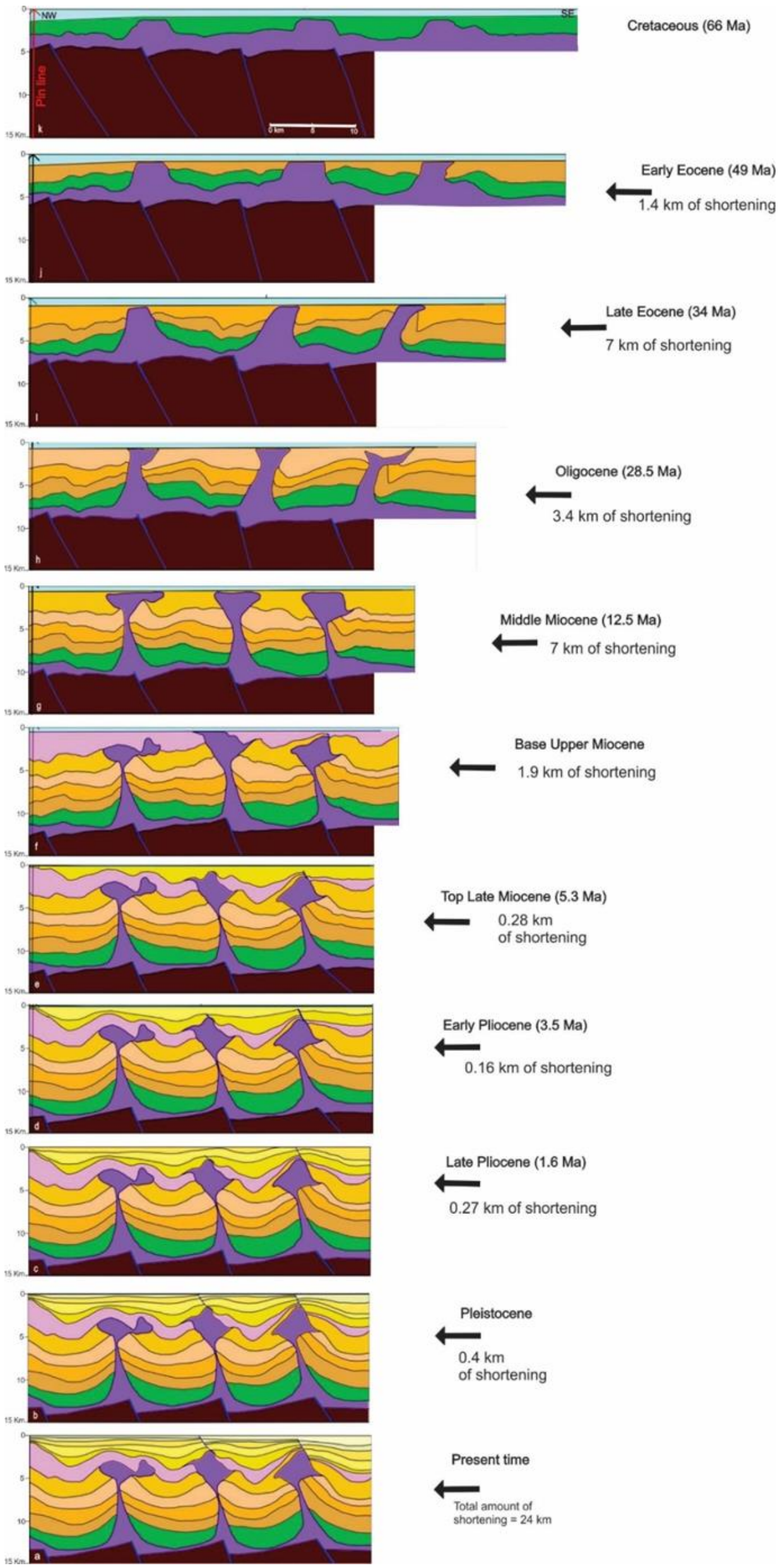

Figure 8.5 Progressive evolution of section No.2 oriented NW-SE.

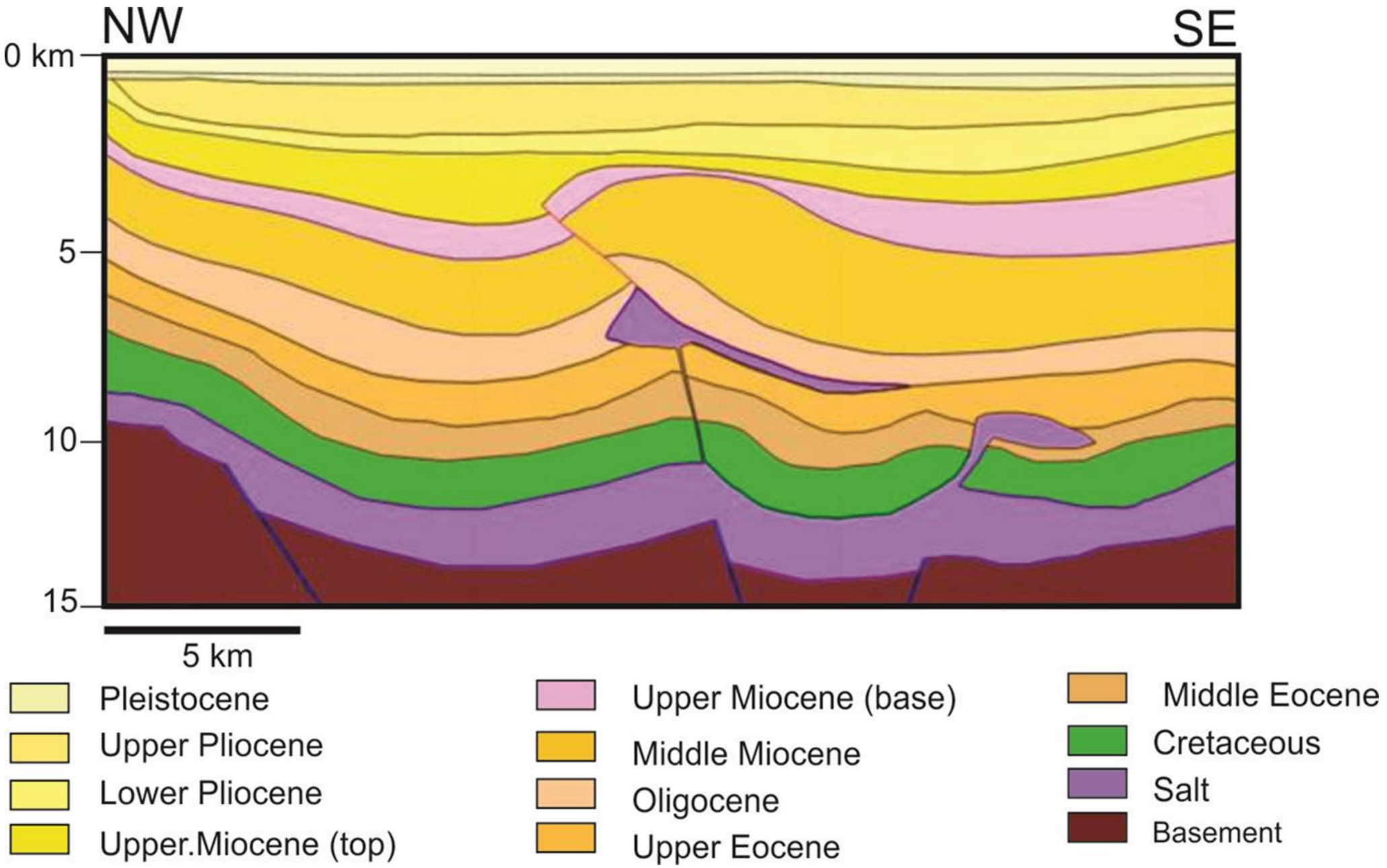

Figure 8.6 Geological section of western sector in depth (section 3).

The gradual decay of salt thrust related deformation is marked by the presence of an Upper Miocene unconformity above the salt thrust crest.

Restoration of section No.3

Restoration of this section suggests that early reactive diapirism formed the salt walls that subsequently developed into the diapirs and minibasin during the Cretaceous. By the end of the Late Cretaceous, a couple of passive diapirs had developed and reached the passive phase; original salt thickness was estimated between 2 and 1.5 km (Fig.8.7a). Lower Eocene and Upper Eocene diapirs were affected by intense compression, which yielded an estimated shortening of 1.2 and 1.6 km respectively. Contractional stresses were a consequence of the oblique collision between Yucatán and the Chortis Block. Tectonic uplift led to shortening and salt was extruded upwards from the diapir and toward the sea floor. Additionally, gravity-driven sedimentation yielded mass transport complex sediments such as debris flows and conglomeratic sediments (Fig.8.7, c).

The progressive transform displacement of the Chortis block during the Oligocene caused an estimated shortening of 0.9 km (Fig. 8.7d). Thickening of the sedimentary sequence towards the northwest evidences the ongoing process of lifting and inversion of the Chiapas Massif. Sedimentary overload caused burial of the right salt diapir (Fig. 8.7d).

The Middle Miocene and beginning of the Upper Miocene are a contraction period Regional shortening caused the exhumation of the Chiapas Massif and the beginning of contractional salt thrusting in the basin. Contraction causes a shortening of 1 and 0.44 km of shortening respectively. Contractional salt structures suggest that inversion tectonics affected the basin. This stage of shortening was characterized by a strong thickening of channelized turbidites sediments. (Fig. 8.7 f).

The top of the Late Miocene represents the end of contraction in this sector of the basin. In this contractional stage, the shortening was 0.54 km the flow of turbidites

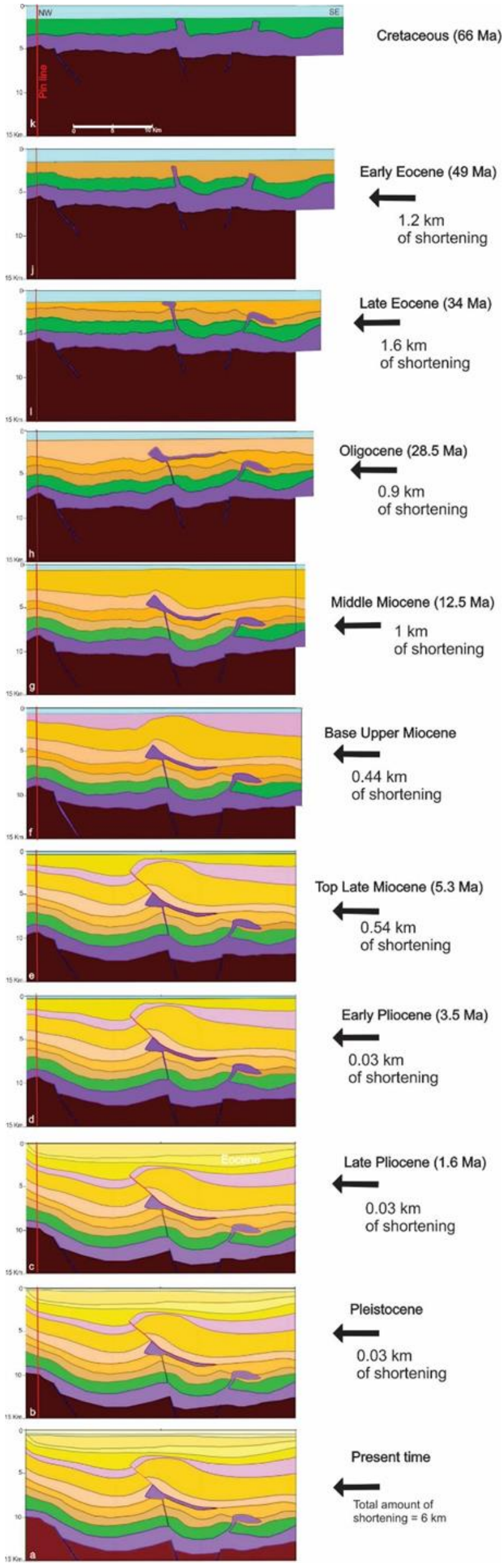

Figure 8.7a to k. Progressive evolution of section No3 oriented NW-SE.

and deltaic sediments continued accumulating greater thickness in adjacent structural lows and tapering above diapir crest (Fig.8.7g).

Tectonic stability during the Pliocene is evidenced by thick prograding fluvio–deltaic sediments which produced subsidence and minibasin development (Fig. 8.7h, i, j)

The timing of basement faulting is uncertain due to poor quality of seismic data. However, the restorations allow hypothesising about subsalt reverse faulting having been active from the Oligocene to the Late Miocene, facilitating and controlling the development of salt thrust structures.

8.3.5 Understanding Section No.4

The fourth section is a depth section oriented NE-SW and with a length of 39 km. This geological section has a shortening of 17%, which represent 7 km (Fig. 8.8). The section is characterised by diapirs that were affected by intense shortening. The diapir is characterized by a vertical pinch-off of with doming of a diapir roof due to shortening. Salt diapir is interpreted to sit above the basement faults, which formed a system of horst and grabens. Diapir root down into the Callovian salt mother layer, which becomes thinner towards the margins highs. Salt diapirs reach the peak of deformation at the beginning of the Upper Miocene. This episode is represented by stratigraphic thinning of the sequence. Salt diapirs were buried during the Lower Pliocene and subsequently rejuvenated during Upper Pliocene and Pleistocene.

Restoration of section No.4

Restoration of this section suggests that early reactive diapirism formed the salt walls that subsequently developed into the diapirs and minibasin in Cretaceous. By the end of the Late Cretaceous, passive diapirs and salt pillows were developed; salt thickness was estimated between 2 and 2.5 km (Fig 8.9 a).

Lower Eocene and Upper Eocene sequences show evidence of compression, resulting in an estimated shortening of 2.1 and 0.8 km, respectively. The salt diapir was shortened by regional contraction causing upward extrusion of the salt.

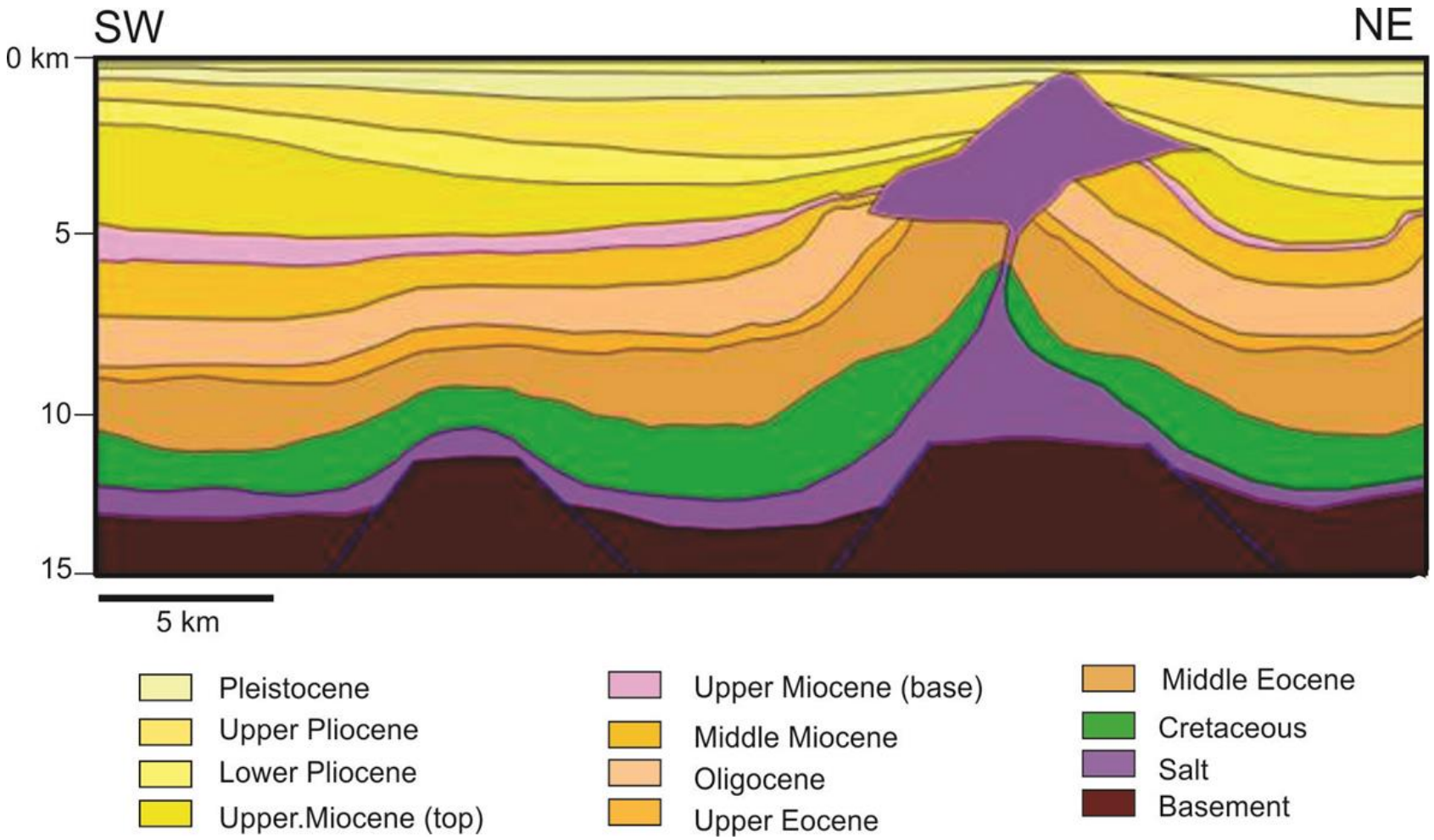

Figure 8.8 Geologic section No 4. The section is oriented SW-NE

structure. Contraction stresses resulted in the growth of salt pillows and subsequent folding of sedimentary sequences (debris flows and conglomerates) into a wide folding of sedimentary sequence yielding a width anticline at response of lateral forces. Sediments are represented by debris flows and conglomeratic sediments (Fig.8.9 b, c).

The progressive displacement of Chortis block in Oligocene caused an estimated shortening of 2.1 km (Fig. 8.9 d). In this period, thickness of debris flows and turbidites was increased. Shortening keep diapir growing up very close to the sea floor leaving salt roof flat. The width of diapir was contracted and flanking strata were upturned.

The Middle Miocene and beginning of the Upper Miocene were characterized by an estimated shortening of 0.5 and 1.1 km (Fig. 8.9e, f). Shortening, was reduced with respect to previous restored sections Strong thickening of deep water sediments is evidenced by the existence of channelized turbidites. The ongoing contraction triggered salt flow and upwards growth of salt diapirs, which have a flat salt roof. Toward northeast minibasin start the process of subsiding.

Shortening in the restored section decreased in the Pleistocene with respect to the Upper Miocene (Fig.8.9 g, h, i, j). A total shortening of 0.02 km was estimated. These stages were characterised by the continuous inflow of turbidites and fluvio-deltaic sediments derived from the Chiapas Massif, which was exposed to the south. Salt diapirs continued to grow upwards towards or near the sea floor. Minibasins were affected by active subsidence towards the southwest, with a predominantly northward flow of salt. At this time, salt diapirs were affected by rejuvenation.

The timing of basement faulting is not clear. However, restoration suggest that subsidence was controlled by thermal and isostatic effects. Additionally, it is very likely that shortening process causes deep faults reactivation. The structural evolution of salt and rejuvenation of salt diapirs were partly controlled by the configuration of horsts and grabens.

Figure 8.10 shows estimates of shortening rate in the restored section through geological time. The curves show large differences at different stages during shortening. Section number 2, stands out with respect to the other curves by the great peaks of shortening that this section experienced during the Eocene and Middle Miocene. It is evident that structural shortening was continuous between the Middle Eocene and Upper Miocene. The increase in shortening is related with the two main geologic contraction events observed in outcrops as unconformities or by lithological and thickness changes affecting the Southeast of Mexico. On the other hand, other sections show a similar structural behaviour, with rejuvenation episodes in section 1 evidenced by high peaks. In section three a decrease in the rate of shortening is observed, which suggest source layer depletion.

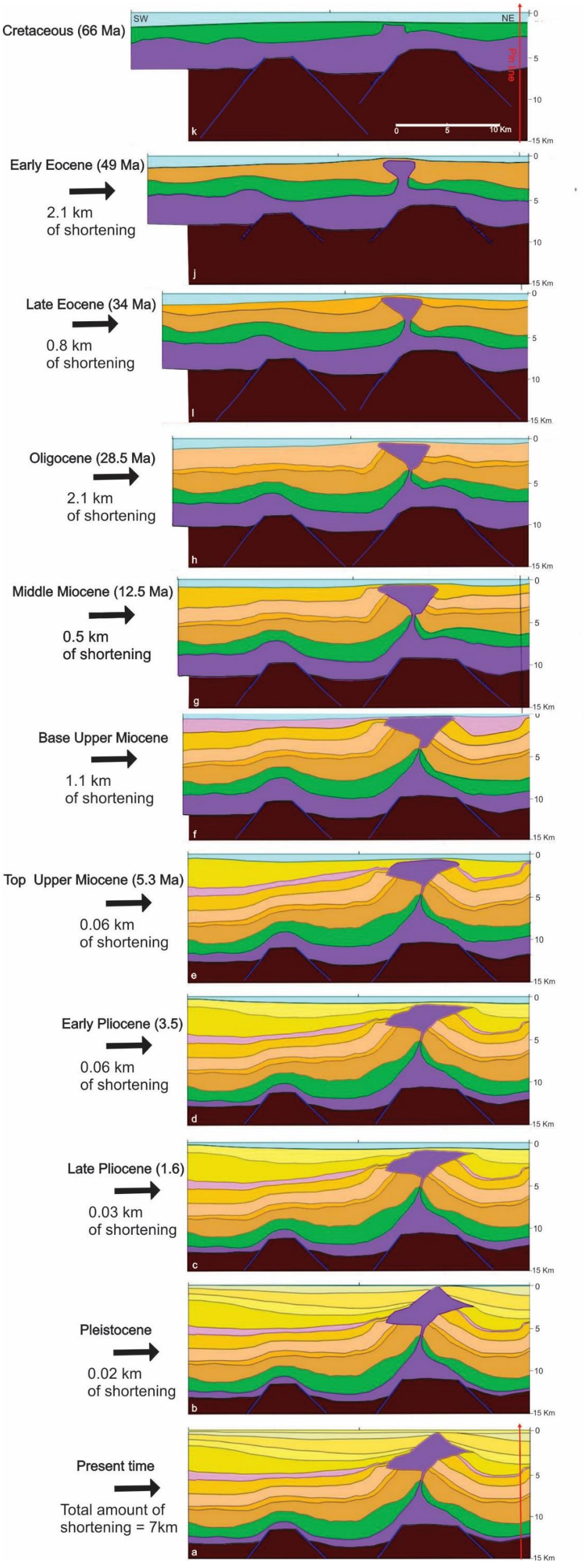

Figure 8.9 Progressive evolution of section No 4. The section is oriented SW-N

Figure 8.11, aims to explain the differences in shortening between all restored sections. Peel, et al., (1995) proposed that salt thickness is one of the main controls on structural style in contractional settings. This is in agreement with estimations of the salt source determined from the restored sections in the Isthmus Saline Basin (Fig. 8.12).

An analysis of shortening in (mm/ yr.) is shown in table 8.1 for each section restored in Isthmus Saline Basin. The table was constructed considering the total shortening (km) in relation with time of deformation (My) for each stage of contraction. Results are interpreted to indicate that salt tectonics in the Isthmus Saline Basin has been active since Eocene, with a recent decreased the ratio of shortening, despite the tectonic activity related to the subduction of the Pacific Plate. These tables also highlight the importance of strike-slip in the development of salt diapirs, such as that caused by compression tectonics in the Sierra de Chiapas fold belt.

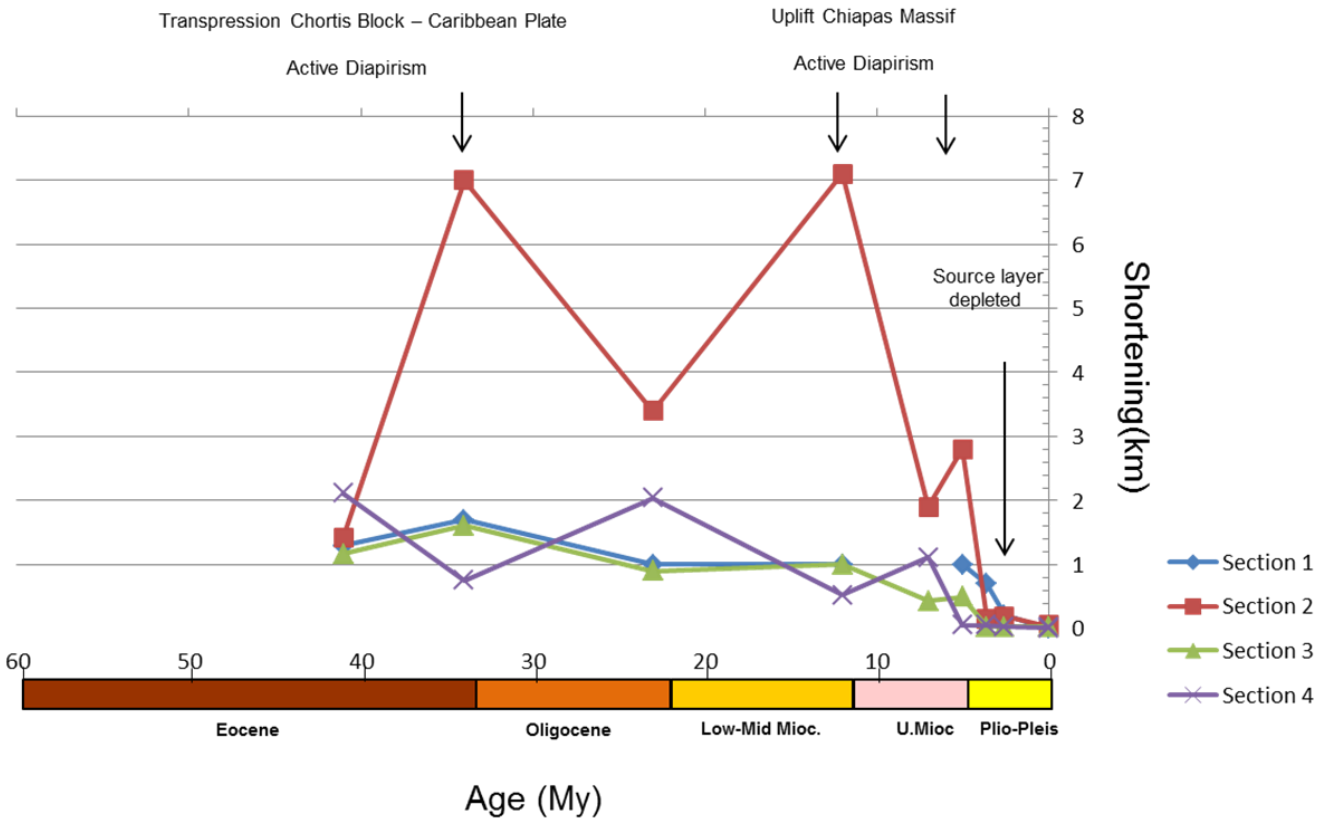

Figure 8.10 Estimation of shortening rates in restored section through time. Timing of the different stages of diapir development is Indicated.

.

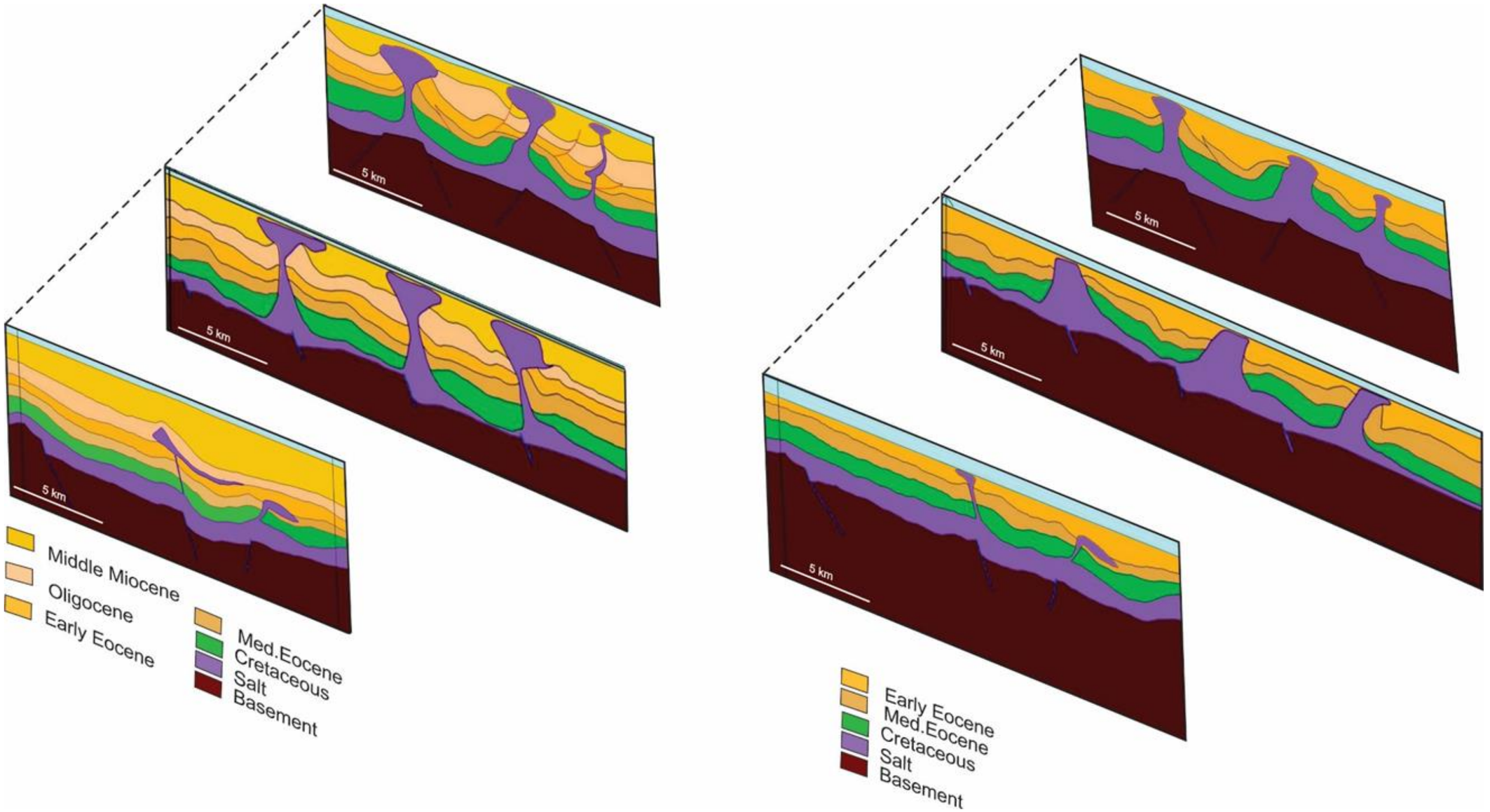

Figure 8.11 Comparison between two main stages of shortening controlled by salt thickness and high sedimentation rates.

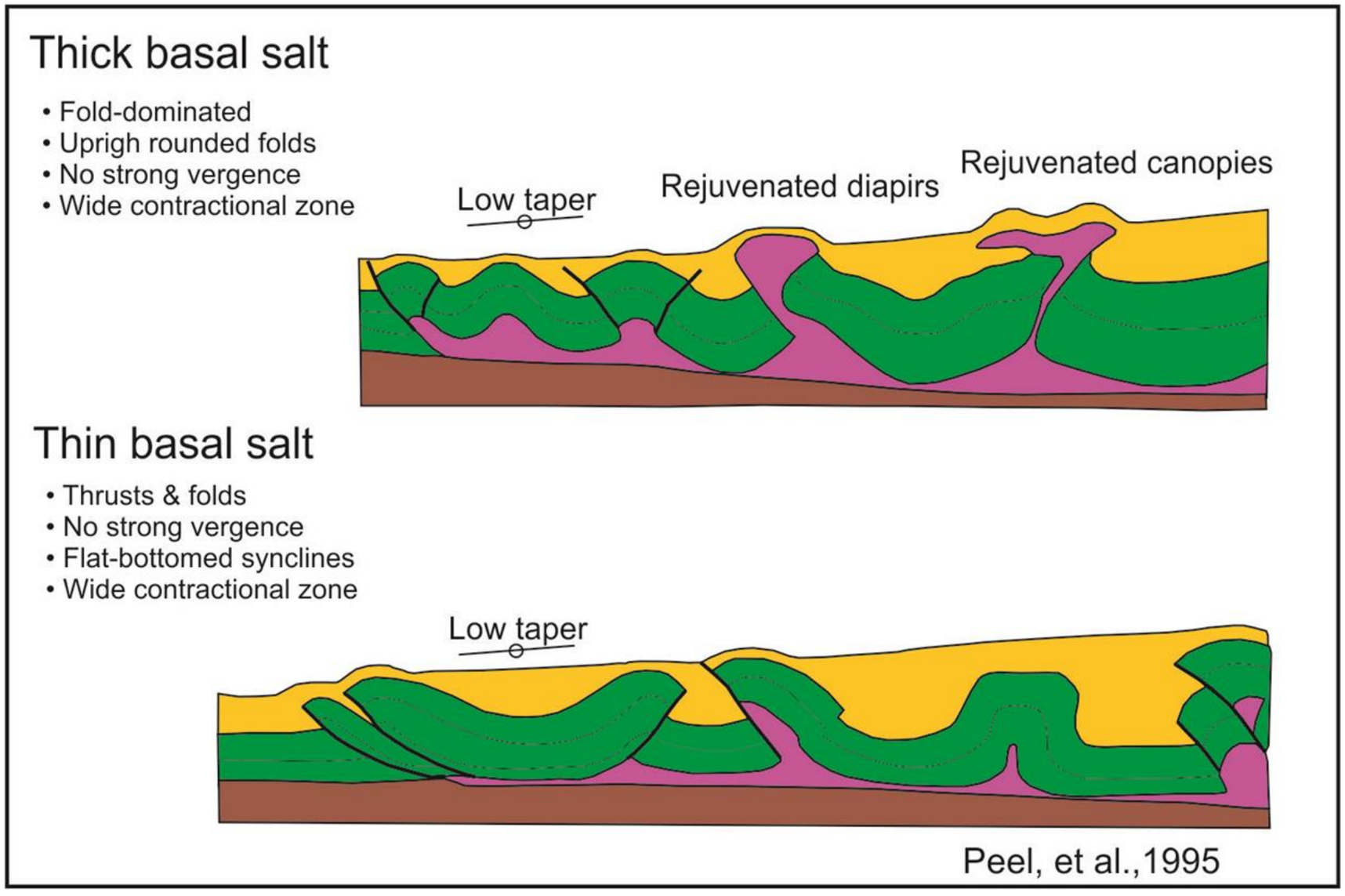

Figure 8.12 Effect of salt thickness on contractional structural styles (After Peel et al., 1995).

	Section 1	
Shortening (km)	Shortening rate (mm/yr)	Duration (My)
0.00	0.00	0.00
0.21	0.08	2.58
0.70	0.50	1.40
1.00	0.71	7.00
1.00	0.14	11.00
1.00	0.09	11.00
1.70	0.24	7.00
1.30	0.05	25.00

	Section 2	
Shortening (km)	Shortening rate (mm/yr)	Duration (My)
0.00	0.00	0.00
0.03	0.02	2.57
0.20	0.27	1.02
0.15	0.11	1.40
2.80	1.44	2.00
1.90	0.38	5.00
7.10	0.65	11.00
3.40	0.31	11.00
7.00	1.00	7.00
1.43	0.06	25.00

	Section 3	
Shortening (km)	Shortening rate (mm/yr)	Duration (My)
0.00	0.00	0.00
0.03	0.01	2.57
0.03	0.03	1.02
0.03	0.02	1.40
0.50	0.27	2.00
0.43	0.09	5.00
1.00	0.09	11.00
0.90	0.08	11.00
1.61	0.23	7.00
1.17	0.05	25.00

	Section 4	
Shortening (km)	Shortening rate (mm/yr)	Duration (My)
0.00	0.00	0.00
0.02	0.01	2.57
0.03	0.03	1.02
0.06	0.04	1.40
0.06	0.30	2.00
1.11	0.22	5.00
0.53	0.05	11.00
2.04	0.19	11.00
0.76	0.11	7.00
2.11	0.08	25.00

Table 8.1: Shortening rates in (mm/yr) in different stages of salt contraction for each restored section in the ISB

8.4 Summary

The restoration of four geological sections through salt structures in the Isthmus Saline Basin provided insights into the kinematic development of structures through time. The orientation of three of the restored sections was parallel to salt thrusting and salt diapir shortening. The structural restoration permitted estimations for first time of the shortening during Eocene and Oligocene in the basin, which has until now been masked by regional contraction of Middle Miocene.

The interpretation of triangular pedestal of salt in restored sections suggests that early salt diapirism originally formed as reactive diapirism during Early Jurassic, developing salt walls, which subsequently developed into diapirs during the Cretaceous.

Four distinct main detachment levels were recognised in the restored sections. From bottom to top, these are:

1 – Middle Jurassic (inferred as main detachment level)

2 – Top Cretaceous

3.- Middle- Top Eocene

3 - Middle Miocene (unconformity that is associated to salt weld).

The combination of the increased sediment loading at Eocene and Middle Miocene times increased the buoyancy forces in the salt source layer. Active compression resulting from the inversion of the Chiapas Massif was able to squeeze the diapir and lift its cover. Arching of the diapir's crest during Early-Late Pliocene has been interpreted as evidence for rejuvenation in some sectors of the basin. The rejuvenation coincides with several pulses of rapid regional sedimentation in the eastern side of the basin.

Chapter 9 Conclusions

9.1 Conclusions

The ISB is a NE-SW oriented asymmetric basin. The basin is approximately 50 km long and 50 km wide. It is bounds to the west by Los Tuxtla Volcanic Center and the Veracruz basin. To the east it is bounded by the Reforma-Akal horst, whereas in the south bounds by the Chiapas fold belt.

For the first time the Isthmus Saline Basin has been classified as an Inverted Foreland Basin.

The Neogene stratigraphy varies from deep-water to fluvial sediments.

The ISB is characterized by tall salt diapirs and minibasins with up to 6 km thick Paleogene-Miocene sediments.

The interior of the ISB is dominated by a series of isolated salt diapirs and minibasins developed above a NW dipping Precambrian basement.

The structural architecture and salt tectonic history are controlled by combination of gravity-driven halokinetic processes, regional contractional tectonic processes and basement-involved strike-slip deformation as consequence of the plate convergence between the Caribbean (Chortis Block and North America plate.

Isthmus Saline Basin is bounded to the north by a high basement. The block worked as buttress during compression.

Strike-slip fault system subdivide the Isthmus Saline basin into at least three blocks. These fault system were reactivated during later shortening in Upper Miocene.

Four distinct styles of salt structure are defined on the basis of their deformation style in the Isthmus Saline Basin: Salt canopy, Salt core thrust, Compressional salt diapirs and Listric and counter–regional faults systems.

Comalcalco Basin is the result of a transition from early systems dominated by gravity gliding to younger systems dominated by gravity spreading related to a convergent orogenic belt of Upper-Middle Miocene.

The thickness of the Upper Miocene depositional sequence change drastically, from 2.5 in the ISB until 5.5 ms in the Comalcalco Basin

In some sectors of the Comalcalco Through, the stratigraphic units of the Mesozoic are absent, so Neogene sediments rest directly on welds produced by the evacuation of autochthonous salt

This concept of Mesozoic displaced blocks shows that the Reforma-Akal Uplift constitutes a mega-raft block limited to the SE and NW by two extensional evacuation basins.

The contractional salt belt results from at least two episodes of basement-involved shortening. Their ages are poorly determined, but best estimates are (1) Early Eocene to Late Eocene, (2) Middle Miocene to Late Miocene.

Contractional deformation was caused by the lateral movement of the Chortís block. This transformed the salt anticlines into tall contractional diapirs and salt tongues and created a large intervening depocenter with sediment fill up to 6 km thick.

The sequential restoration showed that ISB has undergone intense active diapirism and sediment inflow due to progressive uplift of Chiapas Massif since the Middle Eocene to Pliocene.

Across the salt basin tectonic shortening varied from a minimum of 17% (7 km) to a maximum of 59% (24 Km). This variation of shortening is mainly controlled by the relationship between basement geometry and salt diapir thickness which greatly influenced the size and style of salt structures.

Restoration allowed estimating the distance of shortening: In the Middle Eocene-Eocene the shortening was from 2.5 to 8 km, and during the Middle Miocene-Upper Miocene was from 1.5 to 9 km.

The original thickness of the salt source layer could be only be approximated by kinematic restoration ranging between 2.5 to 3 km.

The reactivation of basement faults caused the developed reverse faults, thrust faults and positive flower structures which represent new potential migration routes.

REFERENCES

Anderson, T.H. & Schmidt, V.A. (1983). -The evolution of Middle America and the Gulf of Mexico-Caribean Sea region during Mesozoic time. *Bull.Geol. Soc. Am*., v.94, pp 941-966.

Andreáni, L., Le Pichon, X., Rangin, C., & Martínez-Reyes, J., (2008a). -The southern Mexico block: main boundaries and new estimation for its Quaternary motion. *Bulletin de la Societé Géologique de France*, 179, p. 209-223.

Andreáni, L., Rangin, C., Martínez-Reyes, J., Le Roy, C., Aranda-García, M., Le Pichon, X., Peterson-Rodríguez, R. (2008b). –Neogene left-lateral shearing along the Veracruz fault: the eastern boundary of the Southern Mexico Block. *Bulletin de la Societé Géologique de France*., 179, p. 195-208.

Angeles-Aquino, F. J., Reyes Nuñez, J., Quezada-Muñeton,J.M, (1992).- Evolución tectónica de la Sonda de Campeche, estilos estructurales resultantes y sus implicaciones en la generación y acumulación de hidrocarburos: II Simposio de Exploración Petrolera, IMP, México, D:F.

Badalini, G., Kneller, B., & Winker, C. D. (2000). - Architecture and processes in the late Pleistocene Brazos-Trinity turbidite system, Gulf of Mexico continental slope. In *Deep-Water Reservoirs of the World. GCSSEPM*, 20th Annual Research Conference. pp. 16-34

Barton, D.C. (1933). Mechanics of formation of salt domes with special reference to Gulf Coast salt domes of Texas and Lousiana. *AAPG Bulletin , 17* (9), p.1025-1083.

Beaubouef, R.T., & Friedmann, S.J. (2000). - High resolution seismic/sequence stratigraphic framework for the evolution of Pleistocene intraslope basins, western Gulf of Mexico: depositional models and reservoir analogs. In

Deep-water reservoirs of the world: GCSSEPM, 20th Annual Research Conference. pp. 40-60.

Benavides, G.L. (1950). –El anticlinal de Cerro Pelón, Mun. de Minatitlán, Ver. *AMGP*, Vol. II, No.10, p.49-65.

Bird, D.E., K. Burke, S.A. Hall, & J.F.Casey, (2005). – Gulf of Mexico tectonic history: Hotspots tracks, crustal boundaries, and early salt distribution: *AAPG Bulletin*, v.89, pp.311-328.

Bishop, D. J., Buchanan, P. G., & Bishop, C. J. (1995). -Gravity-driven thin-skinned extension above Zechstein Group evaporites in the western central North Sea: an application of computer-aided section restoration techniques. *Marine and Petroleum Geology , 12* (2), 115-135.

Bishop, R.S., & P.D. Snavely, (1994). -.Hydrocarbon systems in exploration, in: Revitalizacion de Provincias Petroliferas Maduras, Tercera Conferencia Internacional Conjunta AMGP/AAPG, Veracruz, México.

Blair, T.C. (1987). –Tectonic and Hydrologic Controls on Cyclic Alluvial Fan, Fluvial, and Lacustrine Rift-Basin Sedimentation, Jurassic-Lowermost Cretaceous Todos Santos Formation, Chiapas, Mexico, *Journal of Sedimentary Petrology*, Vol. 57, No. 5, p. 845-862.

Bouma, A. (1982). Intraslope basins in northwest Gulf of Mexico: A key to ancient submarine canyons and fans. In *Studies in continental margin geology*, *AAPG Memoir*, Vol. 34, p. 567-581.

Bouma.J., & Dekker, L. W. (1978). A case study on infiltratiion into dry clay soil l: Morphological observations. *Geoderma , 20* (1), 27-40.

Boyer, S. E. (1982). -Thrust systems. *AAPG Bulletin , 66* (9), 1196-1230.

Buffler, R.T., J.S. Watkins, F.L. Shaub, & J.L.Worzel, (1980). –Structure and early geologic history of the deep central Gulf of Mexico Basin, in R.H. Pilger Jr., ed., Proceeding of the Symposium on the Origin of the Gulf of Mexico and the Early Opening of the Central North Atlantic Ocean: Baton Rouge, Louisiana State University, p.3-16.

Buffler, R. T., F.J. Shaub, R. Huerta, A.B.K. Ibrahim, & J.S. Watkins, (1981). -A model for the early evolution of the Gulf of Mexico Basin: *Ocenologica Acta: Proceedings* of the 26th International Geological Congress, Geology of Continental Margins Symposium, Paris, France, July 7-17, 1980, p.129-136.

Buffler, R.T., & D.S.Sawyer, (1985). -Distribution of crust and early history, Gulf of Mexico basin, *GCAGS* Transactions, v.35, p.333-344.

Buffler, R.T., & W.A.Thomas, (1994). -Crustal structure and evolution of the southeaster margin of the North America and Gulf of Mexico Basin, *in* R.C.Speed, ed., Phanerozoic evolution of North America continent-ocean transitions: *Geological Society of America DNAG Continent-Ocean Transec* Volume, p.219-264.

Burkart, B., (1983). -Neogene North America-Caribbean plate boundary across norther Central America: Offset along the Polochic Fault: *Tectonophysics*, v.99, p.251-270

Burkart, B., & C.R. Scotese, (1990). -The Orizaba fault zone: Link between the Mexican Volcanic Belt and Strike-slip faults of Norther Central America: EOS, *American Geophysical Union Tran*s., v. 71, p.1159.

Capaul, W. A. (1987). Volcanoes of the Chiapas volcanic belt, Mexico. Unpubl. doctoral dissertation, Michigan Technological University, Hancock, Michigan, 169p.

Carfantan, J,C. (1976). El Prolongamiento del Sistema Polochic – Motagua en el Sureste de México, Una Frontera entre dos Provincias Geológicas. Congreso Latinoamericano de Geología 3, Acapulco, México. Resúmenes, p. 27.

Carfantan, J.C., (1986). -Du Système Cordillèrain Nord-Américain au Domaine Caraibe: Étdude Géologuique du Mexique Meridionale: Tesis de Doctorado de Estado, Université de Savoie Chambery, p. 555.

Carter, N.L., Horseman, S.T., Russel, J.E. & Handin, J. (1993). -Rheology of rocksalt. *Journal of Structural Geology, 15*, 125-136.

Cartwright, J., Stewart, S., & Clark, J. (2001). -Salt dissolution and salt-related deformation o the Forth Approaches Basin, UK North Sea. *Marine and Petroleum Geology, 18* (6), 757-778.

Castillo-Tejero,C. (1955). –Bosquejo estratigráfico de la Cuenca Salina del Istmo de Tehuantepec. *Bol. Asociación Mexicana de Geólogos Petroleros*, v.VIII,5-6, p.173-212.

Clark, J.A., Stewart, S.A.& Cartwright, J.A. (1999). -Mesozoic dissolution tectonics on the West Central Shelf, UK Central North Sea. *Marine and Petroleum Geology, 16*, 283-300.

Clara-Valdez, L. (2003). -Proyecto Sistemas Petroleros, (inédito). PEMEX Internal Publication, 45 figs, 20 tables.

Clemons, R.E., & Burkart, B. (1972). – Late Paleozoic orogeny in northwestern Guatemala, In Memorias 6. o Conferencia Geol 243_o. jpg (458 bytes) gica del Caribe, Margarita, Venezuela, p. 210-213.

Clemons, R.E., Anderson, T.H., Bohnenberger, O.H., & Burkart, B. (1974). -Stratigraphic nomenclature of recognized Paleozoic and Mesozoic rocks of western Guatemala: *AAPG Bulletin*, v. 58, p. 313–320.

Coney, P. J. (1976). -Plate tectonics and the Laramide Orogeny: New Mexico *Geological Society, Special Publication*, núm 6, p. 5-10.

Coney, P. J. (1979). -Tertiary evolution of cordilleran metamorphic core complexes, in Armentout, J.M.; Cole, MR.; and Fer Best, H., eds., Pacific Coast Paleogeography. Symposium 3. Pacific Section. *Society of Economic, Paleontologists and Mineralogists*, p. 14-28.

Coney, P.J., Crittenden, M.D. Jr., & Davis, G.H. (1980). – Cordilleran methamorphic core complex: An overview. *Geological Society of America Memoir* 153.

Coney, P. (1983). Un Modelo Tectónico de México y sus relaciones con América del Norte; *Revista del Instituto Mexicano del Petróleo*, v. 15(1), p. 6-15.

Coney, P.J. & Campa, M. F. (1983). - Tectono-stratigraphic terranes and mineral resource distributions in Mexico. *Canadian Journal of Earth Sciences*, 20(6) p. 1040-1051, https://doi.org/10.1139/e83-094

Contreras, V. H., & Castillon, M. B. (1968). - Domes of the Isthmus of Tehuantepec: *AAPG Memoir* 8, p. 244-260

Colletta, B., J. Letouzey, R. Pinedo, J. F. Ballard, P. Balé. (1991). -Computerized X-ray tomography analysis of sand-box experiments: Examples of thin-skinned thrust systems. *Geology, 19*, 1063-1067.

Concit, 1981. Informe Geológico del Prospecto Figueroa, I.G.Z.S. 635. Petróleos Mexicanos, Superintendencia General, Distrito de Exploración Zona Sur, (unpublished).

Concit, (1982). -Prospecto Puerta del Uzpanapa. PEMEX, Z. S., I. G. Núm. 662,

79p, (unpublished)

Cramez, C. and M.P.A. Jackson, (2000). -Superposed deformation straddling the continental-oceanic transition in deep-water Angola; *Marine and Petroleum Geology*, v.17, p.1095-1109.

Cruz, H.P., Verdugo, V.R., & Barcenas, P.R., (1977). –Origin and distribution of Tertiary conglomerates, Veracruz Basin, Mexico, *AAPG*, v.61, p.207-226.

Damon, P. & E. Montesinos. (1978). -Late Cenozoic volcanism and metallogenesis over an active Benioff zone in Chiapas, Mexico. *Arizona Geological Society Digest , 11*, 155-168.

Davis, D. M., & Engelder, T. (1985). -The role of salt in fold-and-thrust belts. *Tectonophysics , 119* (1), 67-88.

Davison, I., Alsop. G. I., & Blundell, D.J. (1996a). -Salt tectonics: some aspects of deformation mechanics. In – Alsop, G. I., Blundell, D.J., and Davison, I. (eds). Salt Tectonics. *Geological Society of London, Special Publication* 100, 1-10.

Davison, I., Bosence, D., Alsop, G.I. and Blundell, D.J. 1996b. -Deformation and sedimentation around active Miocene salt diapirs on the Tihama Plain, Northwest Yemen. In: Alsop, G. I., Blundell, D.J., and Davison, I. (eds). Salt Tectonics. *Geological Society of London Special Publication*, 100, 23-39.

Dahlstrom, C. D. (1969). -Balanced cross sections. *Canadian Journal of Earth Sciences, 6* (4), 743-757.

Davis, D.M., Engelder, T. (1985). –The role of salt in fold-and-thrust belts. *Tectonophysics* 119, p. 67-88.

De la Cruz –Servando, R & Martin -Del Pozzo, A. L. (2009) -The 1982 eruption of el Chichón Volcano, Mexico: eye-witness perspecives of the disaster. *Geof Internacional*. 48, 1, p.21-31.

DeMets, C.and Dixon, T., 1999. New kinematic models for Pacific – North America motion from 3 Ma to present, 1: Evidence for steady motion and biases in the NUVEL-1A model, *Geophys. Res. Lett*., v 26, pp 1921-1924.

DeMets, C. (1993). – Earthquake slip vectors and estimate of present-day plate motion. J. *Geophys.Res.,* 98, p. 6703-6714.

DeMets, C., Gordon, R.G., Argus, D.F., Stein, S. (1990). – Current plate motion. *Geophysical journal International* 101, p. 425-478.

DeMets, C., Jansma, P.E., Mattioli, G.S., Dixon, T.H., Farina, F., Bilham, R., Calais, E., & Mann, P. -(2000). GPS geodetic constraints on Caribbean-North America plate motion, *Geophys. Res. Lett*., v 27, p. 437-440.

DeMets, C., Gordon, R.G., Argus, D.F., Stein, S. (2010). –Geologically current plate motion*. Geophysical journal International* 181, p. 1-80.

Dengo, G., 1968. -Estructura geológica, historia tectónica y morfología de América Central, Centro Regional de Ayuda Técnica, México, D.F., 50 p.

Dobson, L.M., & R.T. Buffler, 1997. -Seismic Stratigraphy and geologic history of Jurassic rocks, northeastern Gulf of Mexico: *AAPG Bulletin*, v.81, p.100-120.

Draper, G., G. Gutierrez, & J.F. Lewis. (1996). –Thrust emplacement of the Hispaniola peridotite belt: Orogenic expression of the mid-Cretaceous Caribbean arc polarity reversal? *Geology*, v.24, n.12, p.1143-1146.

Edgell, H. (1996). -Salt tectonism in the Persian Salt Basin. In Alsop, G. I., Blundell, D.J., and Davison, I. (eds). Salt Tectonics, *Geological Society of London, Special Publication*,100, pp.129-151.

Edwards, M.B., (1980). -The Live Oak delta complex: An unstable shelf-edge delta in the deep Wilcox trend of south Texas. *Gulf Coast Association of Geological Societies Transactions*, v. 30, pp 611-622.

Elliott, D. (1976). -The energy balance and deformation mechanisms of thrust sheets. *Philosophical Transactions of the Royal Society of London A: Mathematical, Physical and Engineering Sciences, 283* (1312), 289-312.

Estavillo, G. C. F. y M. Herrera S. (1988). -Estudio Estratigráfico Sedimentológico de los lechos rojos de la Formación Todos Santos del Prospecto Pueblo Viejo, Chis. IMP, Subdir. Tec. Explor., Proy. C-3035. 67 p. (unpublished).

Ewing, T.E. (1991). -Structural framework, in Salvador A., Ed., *The Gulf of Mexico Basin*. Boulder, Colorado, *Geological Society of America*. The Geology of North America, v.J. p.150-180.

Farhoudi, G. (1978). A comparison of Zagros geology to island arcs. *Journal of Geology* , v.85, 3, 323-334.

Ferrari, L., Valencia-Moreno, M., & Bryan, S. (2007). Geology of México: Celebrating the centenary of the Geological Society of México. p.1-39.

Ferrari, L., Valencia-Moreno, M., & Bryan, S. (2007). Magmatism and tectonics of the Sierra Madre Occidental and its relation with the evolution of the western margin of North America. *Geological Society of America Special Papers*, 422, p.1-39.

Figueroa, J., 1963. Historia sísmica y estadística de temblores de la costa occidental de México. *Bol. Bibliogr. Geofís. Oceanogr. Am* 3, p.107-134

Garcia-Molina, G. (1994). -Structural evolution of SE Mexico (Chiapas-Tabasco-Campeche) offshore and onshore: Rice University, PhD. Dissertation, p.161.

García- Palomares, J. M. (1981a). -Prospecto Nizandá (Oaxaca). PEMEX, Z. S., I. G. Núm. 796, 39 p. (unpublished).

Garcia-Palomo, A., Macias, J.L., Espindola, J.M. (2004). – Strike-slip faults and K-alcaline volcanism at El Chichon volcano, southeastern Mexico. *Journal of Volcanology and Geothermal Research* 136, p.247-268.

Ge, H., & Jackson, M.P.A. (1998). -Physical modelling of structures formed by salt withdrawal: implications for deformation caused by salt dissolution. *AAPG Bulletin, 82* (2), p. 228-250.

Ge, H., Jackson, M.P.A. & Vendeville, B.C. (1997). -Kinematics and dynamics of salt tectonics driven by progradation. *AAPG*, p. 398-423.

Geiser, P. A. (1988). -Mechanisms of thrust propagation: some examples and implications for the analysis of overthrust terranes. *Journal of Structural Geology, 10* (8), p. 829-845.

Giles, K. A., & Rowan, M. G. (2012). -Concepts in halokinetic-sequence deformation and stratigraphy. *Geological Society, London, Special Publications , 363* (1), p. 7-31.

Godinez-Urban, A. Lawton, T., Molina, R., Iriondo, A., Weber, B., and Lopez, M. (2009). -Jurassic volcanic and sedimentary rocks of the La Silla and Todos Santos Formation, Chiapas: Record of Nazas arc magmatism and rift-basin formation prior to opening of Gulf of Mexico, *Geosphera*, v.7; no.1; p.121-144.

Goldhammer, R.K. (1999). -Mesozoic sequence stratigraphy and paleogeographic evolution of northeast Mexico: in C. Bartolini, J.L. Wilson, and T.F. Lawton, eds., Mesozoic sedimentary and tectonic history of north-central Mexico: *Geological Society of America Special Paper* 340, p.1-58

Goldhammer, R.K., & C.A. Johnson. (2001). -Middle Jurassic - Upper Cretaceous Paleogeographic evolution and sequence stratigraphic framework of the northwest Gulf of Mexico rim: in C. Bartolini, T. Buffler, and A. Cantú-Chapa, eds., The western Gulf of Mexico Basin: Tectonics, sedimentary basins and petroleum systems: *AAPG Memoir* 75, p.45-81.

Gómez-Cabrera, P.T. & Jackson, M.P.A. (2009). – Regional Salt Tectonics in the Offshore Salina del Istmo Basin, Southeastern Mexico . In Petroleum System in the Southern Gulf of Mexico. (ed) Bartolini, C. and Román-Ramos, J.R. *AAPG Memoir* 90, p.1-28.

González-Alvarado, J. (1963). -Exploración geológica del Área Tumbalá-Chilón, Chiapas. I.G.Z.S. 490. Petróleos Mexicanos, Superindencia General, Distrito de Exploración Zona Sur, p. 21-32, inédito.

Gonzáles-Alvarado, J. (1967). –Informe Geológico del área Teopisca-Chiapa de Corzo, Chiapas: Petróleos Mexicanos, Zona Sur, Informe geológico num. 518, s/p. (inédito).

González-Garcia, R., & Q. N. Holguín. (1992). Geology of the source rocks of Mexico: 13th World Petrol. Congr., Proceed., v. XLI, p. 37-50

Gose, W. A., & Sanchez-*Barreda*, L. A. (1981). -Paleomagnetic results from southern Mexico. *Geofisica Internacional*, 20(3).

Guzmán-Speziale M & J.J. Meneses-Rocha. (2000). -The North America-Caribbean plate boundary west of the Motagua-Polochic fault system: a fault jog in southeastern Mexico. *J. South Amer.Sci*., **13**, p. 459-468.

Gottschalk, R. R., Anderson, A. V., Walker, J. D., & Da Silva, J. C. (2004). Modes of contractional salt tectonics in Angola Block 33, Lower Congo basin, west Africa. In *Salt-sediment interactions and hydrocarbon prospectivity: 24th Annual Research Conference*, *GCSSEPM* Foundation, p. 705-734

Grajales-Nishimura,J.M., Cedillo-Pardo,E., Rosales-Domínguez, C., Morán-Zenteno, D.J., Alvarez, W., Claeys, P., Ruíz-Morales, J., García-Hernández, J., Padilla-Avila, P. & Sánchez-Ríos, M.A. (2000). - Chicxulub impact: The origin of reservoir and seal facies in the southeastern Mexico oil fields. *Geology*; v. 28; no. 4; p. 307–310; 4 figures

Hall, D.J., T.D. Cavanaugh, J.S. Watkins, & K.J McMillen. (1982). -The rotation origin of the Gulf of Mexico based on regional gravity data, in J.S. Watkins and C.L. Drake, eds., Studies in continental margin geology: *AAPG Memoir* 34, p.115-126.

Ham-Wong, J. M. (1979). Prospecto Nazareth Chiapas Informe Geológico No. 745. Petroleos Mexicanos, Zona Sur, 8-18. (unplublished)

Handschy, J.W., G.R.Keller, & K.J. Smith. (1987). -The Ouachita system in northern Mexico, *Tectonics*, v.6, n.7, p.323-330.

Hayward, A. B., & Graham, R. H. (1989). -Some geometrical characteristics of inversion. *Geological Society, London, Special Publications , 44* (1), p.17-39.

Herrera-Soto, M.E., and Estavillo-González, C.F. (1991). -Análisis estratigráfico y modelo de sedimentación en la Formación Todos Santos en el área del alto Uzpanapa- Matías Romero, Oaxaca*: Revista del Instituto Mexicano del Petróleo*, v. 22, p. 5–42.

Hildebrand, A. R., Penfield, G. T., Kring, D. A., Pilkington, M., Camargo Z, A., Jacobsen, S. B., & Boynton, W. V. (1991). - Chicxulub crater: a possible Cretaceous/Tertiary boundary impact crater on the Yucatan Peninsula, Mexico. *Geology*, 19(9), 867-871.

Holguín-Quiñonez, N. (1985). -Evaluación geoquímica del sureste de México: *Bol. Asoc. Mex. Geol. Petrol*., v. 37, p. 3-48.

Holman, W. E., & Robertson, S. S. (1994). -Field development, depositional model and production performance of the turbiditic ‘‘J’’sands at prospect Bullwinkle, Green Canyon 65 field, outer-shelf Gulf of Mexico. In *Submarine Fans and Turbidite Systems*. Submarine Fans and Turbidite Systems: *GCSSEPM* Foundation,15th Annual Bob Perkins Research Conference, p. 425-437

Herrera-Soto, M., Estavillo-Garcia, C.F., y Brito-Arias, M. (1990). Estudio estratigráfico de los lechos rojos de la Formación Todos Santos en el área de Valle Nacional, Oaxaca. México, D.F., Instituto Mexicano del Petróleo, Subdirección de Tecnología de Exploración, Proyecto C-3048, s/p., 144p. (unpublished).

Hudec, M. R., & Jackson, M. P. A. (2006). Advance of allochthonous salt sheets in passive margins and orogens. *AAPG Bulletin , 90* (10), 1535-1564.

Hudec, M. R. & Jackson, M. P. A. (2007). Terra infirma: Understanding salt tectonics. *Earth-Science Reviews , 82* (1), 1-28.

Hudec, M. R., Jackson, M. P. & Schultz-Ela, D. D. (2009). -The paradox of minibasin subsidence into salt: Clues to the evolution of crustal basins. *Geological Society of America Bulletin , 121* (1-2), 201-221.

Hudec, M., and Jackson, M.P.A. (2011). *Salt mine: a digital atlas of salt tectonics.* Bureau of Economic Geology Udden Book Series No.5 and *AAPG Memoir*, 99.

Hudec, M., I. O. Norton, M.P.A. Jackson, & F. J. Peel. (2013). -Jurassic evolution of the Gulf of Mexico salt basin: *AAPG Bulletin*, v.97, No.10, p.1683-1710.

Humphris, C.C. Jr. (1978). -Salt movement on continental slope, norther Gulf of Mexico, in A.H. Bouma, G.T. Moore, and J.M. Coleman, eds., Framework,

facies and oil-trapping characteristics of upper continental margin: *AAPG Studies in Geology* 7, p 69- 85.

Jackson, M. P. A., & Vendeville, B. C. (1994). -Regional extension as a geologic trigger for diapirism. *Geological Society of America Bulletin, 106* (1), 57-73.

Jackson, M. P. A., Cramez, C., & Fonck, J. M. (2000). -Role of subaerial volcanic rocks and mantle plumes in creation of South Atlantic margins: implications for salt tectonics and source rocks. *Marine and Petroleum Geology, 17* (4), 477-498.

Jackson, M.P.A., & Vendeville, B.C. (1994). -Regional extension as a geological trigger for diapirism. *Geological Society of America Bulletin, 106*, 57-73.

Jackson, M.P.A., and Talbot, C.J. (1991). -A glossary of salt tectonics. In *Geological Circular 91-4* (p. 44). Bureau of Economic Geology, University of Texas at Austin.

Jackson, M.P.A., and Talbot, C.J. (1994). -Advances in salt tectonics. In P. Hancock (Ed.), *Continental deformation* (pp. 259-280). Oxford, UK: Pergamon Press and International Union of Geological Sciences .

Jackson, M.P.A., and Talbot, C.J. (1986). -External shapes, strain rates, and dynamics of salt structures. *Geological Survey of America Bulletin , 97*, p.305-323.

Jackson, M.P.A., and Talbot,C.J. (1994).- Advances in Salt tectonics. In P. Hancock (Ed.), *Continental Deformation* (pp. 150-180). Oxford, U.K, Pergamon Press and International Union of Geological Science.

Jackson, M.P.A., Vendeville, B.C., & Schultz-Ela, D.D. (1994). Structural Dynamics of Salt Systems. *Annual Review of Earth Sciences and Planetary Sciences , 22*, p.93-117.

Jacobo-Albarran, J. (1997). -Studio geologico e petrologico del complesso vulcanico di Los Tuxtlas, Stato di Veracruz, Messico. -PhD Thesis, University degli Studi di Pisa, Italy, 147p.

Jacobo, A. J. y Murillo, M. G. (1989). -Carta del basamento de México. IMP, Subdir. Tec. Explor. Proy. C-2017. (inédito).

Jacobo-Albarran, J.; Valencia, I.J.J.; Moreno, L. M., Suarez, R.G., Rosales, R. J., Cerrillo, C.J., Alor, O.I., Castillo, Z.H., Diaz, A. J.L., Guzman, L. N., Lopez, P. H., Martinez, M.J.A., Moreno, G. M., Pastrana, V. E., Soni, M.,O. (2003). -Interpretacion Tectonica del Basamento en el Area Reforma-Comalcalco. Informe Geologico, Istituto Mexicano del Petroleo y Petroleos Mexicanos, Exploracion y Produccion, Villahermosa, Tab. (unplublished).

Jennette, D., T.Wawrzyniec, K.Fouad, D.B. Dunlap, J. Meneses-Rocha, F. Grimaldo, R. Munoz, D. Barrera, C.T. Williams-Rojas & A. Escamilla. (2003). –Traps and turbidite reservoir characteristics from a complex and evolving tectonic setting, Veracruz Basin, southeastern Mexico. *AAPG Bulletin*, v.87, No.10, p.1599-1622.

Jenyon, M. (1988). -Seismic expression of salt dissolution-related features in the North Sea. *Bulletin of Canadian Petroleum Geology, 36* (3), p.274-283.

Jenyon, M. (1984). -Seismic response to collapse structures in the Southern North Sea. *Marine and Petroleum Geology , 1* (1), p. 27-36.

Jenyon, M. (1986). Some consequences of faulting in the presence of a salt rock interval. *Journal of Petroleum Geology , 9* (1), p. 29-52.

Johnson, C.A & C.G.A. Harrison. (1990). -Neotectonics in central Mexico. *Phys. Earth Planet. Int.*, 64, p. 187-210

Johnson, C.A., and Barros, J.A. (1993). Tertiary tectonics and margin truncation in southern Mexico, *in*: Pindell, J.L., and B.F. Perkins (eds.), Mesozoic and

Early Cenozoic Development of the Gulf of Mexico and Caribbean Region, A contex for Hydrocarbon Exploration, *GCSSEPM* Foundation 13th Annual Reseach Conference Proceedings, p.181-191.

Johnson, C.A., Goldhammer, R.K. & Meneses-Rocha, J. (1999). -Tectonic, Stratigraphy, and Hydrocarbon System Development of the Southern Gulf Rim, México and Guatemala: A Synthesis, unpublished Internal report, 49 pp.

Jones, I.A., and I.Davison. (2014). Seismic imaging in and around salt bodies. *Interpretation , 2* (4), p. 1-20.

Keppie, J.D., & Moran-Zenteno,D.J. (2005). –Tectonic implications of alternative Cenozoic reconstructions for southern Mexico and the Chortis block. *International Geology Review* 47, p. 473-491.

Koyi, H. (1991). Gravity overturns, extension, and basement fault activation. *Journal of Petroleum Geology , 14* (2), p.117-142.

Koyi, H. (1993). The effect of basement faulting on diapirism. *Journal of Petroleum Geology , 16* (3), p. 285-312.

Le Roy, C., C. Rangin X. Le Pichon, H. Thi Ngoc, L. Andreani, & M. Aranda-Garcia. (2007). -Neogene crustal shear zone along the western Gulf of Mexico margin and its implications for gravity slinding processes: Evidences from 2D and 3D multichannel seismic data. *Bull. Soc geol. Fr., 178, No 2, p.175-185.*

Letouzey, J., B. Colletta, Vially R., & Chermette, J.C. (1995). -Evolution of salt related structure in a compressive setting. In M. D. Jackson (Ed.), *Salt tectonics: a global perpective*. *AAPG Memoir* 65, p. 41-60.

López-Infanzón, M. (1991). –Petrologic study of volcanic rocks from the Chiconquiaco-Palma Sola área, Central Veracruz, Mexico. MS Thesis, Tulane University, New Orleans, La.

López-Ramos, E. (1983). -Geologia de Mexico, v.3, 3rd edition, 453 pp.

López-Vega, J. (1980). -Evaluación económica petrolera del área Comitán-Pedregal, Estado de Chiapas: *Bol. Asoc. Mex. Geol. Petrol*., v.32, p. 57-77

Malfait, B. T. & Dinkelman, M.G. (1972). -Circum-Caribbean tectonic and igneous activity, and the evolution of the Caribbean Plate: *Geological Society of America*, v.83, p. 25 1-272

Mandujano-Velázquez, J.J., & J.D. Keppie. (2009). -Middle Miocene Chiapas fold and thrust belt of Mexico: a result of collision of the Tehuantepec Transform/Ridge with the Middle America Trench. *Geological Society, London,* Special Publications, 327, p. 55-69.

Mandujano-Velázquez,J.J.& Vázquez-Meneses, M.E. (1996). -Reseña bibliográfica y análisis estratigráfico de la Sierra de Chiapas. *Boletín de la Asociación Mexicana de Geólogos Petroleros*, v.45 (1), p. 31-41.

Marshak, S., & Mitra, G. (1988). -*Basic methods of structural geology.* Prentice Hall

Mart, Y., & D. A. Ross. (1987). -Post Miocene rifting and diapirism in the northern Red Sea. *Marine Geology , 74* (3-4), 173-190.

Marton, G., & R.T. Buffler. (1993b). -The southeastern Gulf of Mexico in the framework of the opening of the Gulf of Mexico Basin, *in*: Pindell, J.L., and B.F.Perkins (eds.), *Mesozoic and Early Cenozoic Development of the Gulf of Mexico and Caribbean Region, A Contexfor Hidrocarbon Exploration*, *GCSSEPM* Foundation 13th Annual Reseach Conference Proceedings, p. 51-67

Marton, G., & R.T. Buffler. (1994). -Jurassic reconstruction of the Gulf of Mexico Basin: *International Geology Review*, v.36, p. 545-586, doi: 10.1080/00206819409465475.

McBride, B. C., Rowan, M. G., & Weimer, P. (1998). -The evolution of allochthonous salt systems, northern Green Canyon and Ewing Bank (offshore Louisiana), northern Gulf of Mexico. *AAPG Bulletin, 82* (5), 1013-1036.

Meneses-Rocha J.J. (1985). -Tectonic evolution of the Strike-Slip fault province of Chiapas, Mexico. – MA Thesis, University of Texas, Austin, Texas.

Meneses-Rocha J. J. (1987). -Marco tectónico y paleogeográfico del Triásico Tardío Jurásico en el Sureste de México: *Boletín de la Asociación Mexicana de Geólogos Petroleros*, v. 39, no. 2, p. 3–69.

Meneses-Rocha. J.J., M. I. Gutierrez, & Ch. J. Gómez. (1987). -Evaluación geológica regional de la Sierra de Chiapas: Informe Geológico No. 1031, Z. SE: Petróleos Mexicanos (unpublished), PEMEX Internal Publication, 44 figs.,17 tables, 69 appendices, 395 p.

Meneses-Rocha J.J. (1991). -Tectonic development of the Ixtapa graben, Chiapas, Mexico.- PhD Dissertation, University of Texas, Austin, Texas. 270 p.

Meneses-Rocha J.J. (2001). -Tectonic evolution of the Ixtapa graben, an example of a strike-slip basin of southeastern Mexico: Implications for regional petroleum system. *In*: C. BARTOLINI, R.T. BUFFLER & A. CANTU-CHAPA, Eds., The western Gulf of Mexico Basin: tectonics, sedimentary basin and petroleum system. *AAPG Mem*., **75**, 183-21

Michaud, F. (1987). -Stratigraphie et paleogeographie du Mesozoique du Chiapas, sud-est du Mexique: These du Doctorat, Université Paris 6, 301 p.

Mora-Oropeza, G., Iparrea, A., Oviedo, A. (2001). –Petroleum Geology of the Salina del Istmo Basin, AAPG Convention, Denver, Colorado. Search and Discovery Article # 90906,

Mosser, F. (1972). -The Mexican volcanic belt. Structure and tectonics. *Geofisica Internacional*, v.12, p.55-70.

Múgica, M.R., 1987. Estudio petrogenético de las rocas ígneas y metamórficas en el Macizo de Chiapas. *Instituto Mexicano del Petróleo*, Proyecto C-2009, inédito.

Nalpas, T., & Brun, J.P. (1993). Salt flow and diapirism related to extension at a crustal scale. *Tectonophysics, 229*, p.349-362.

Nixon, G.T. (1982). The relationship between Quaternary volcanism and the seismic structure of the subducted ocean lithosphere. *Bull. Geol. Soc. Am*. 93, p.514-523

Ortega-Gutiérrez, F., Mitre-Salazar, L. M., & Roldán-Quintana, J. (1992). Carta geológica de la República Mexicana. Consejo de Recursos Minerales y en el Instituto de Geología de la UNAM.

Oviedo-Perez, A. E. (1997). -Estrategía para añadir reservas, caracterizar e incrementar la producción de los campos Terciarios y evaluar el potencial petrolero subsalino de Agua Dulce, Veracruz., in *AIMP*, *Memorias de Trabajos Técnicos*, XXXV Congreso Nacional, Tomo II, Exploración y Yacimientos , 19p

Padilla y Sanchez, R.J. (1986). -Post-Paleozoic tectonics of Northeast Mexico and its role In the evolution of the Gulf Of Mexico: *Geofísica Internacional*, v. 25, No. 1, p. 157-206

Pantoja-Alor, J., Fries, C., Jr., Rincón-Orta, C., Silver, L. y Solorio-Munguía,G.J., 1974. Contribuciones a la Geocronología del Estado de Chiapas. Boletín de

la *Asociación Mexicana de Geólogos Petroleros*, v. 26 (4-6, Publicación Especial), p. 205-223.

Parker, T. J., & McDowell, A. N. (1955). -Model studies of salt-dome tectonics. *AAPG Bulletin , 39* (12), p.2384-2470.

Parker, T. J., & McDowell, A. N. (1955). -Model studies of salt-dome tectonics. *AAPG Bulletin , 39* (12), 2384-2470.

Peel, F.J., C.J.Travis, & J.R.Hossack. (1995). -Genetic structural provinces and salt tectonics of the Cenozoic offshore U.S. Gulf of Mexico: a preliminary analysis, in M.P.A. Jackson, D.G. Roberts, and S. Snelson, eds., Salt tectonics: a global perpective: *AAPG Memoir* 65, p.153-175.

Pemex Exploración y Producción-Informe Final. (2000). -Estudio Interregional *"Tectonica Salina y sus Implicaciones en la Exploración Petrolera*,. PEMEX Internal publication, 70 figs, 20 tables. (unpublished).

Philippe, Y. I. (1994). -Transfer zone in the Southern Jura thrust belt (Eastern France): Geometry, development, and comparison with analogue modeling experiments. In *Hydrocarbon and petroleum geology of France*, p.327-346. Springer Berlin Heidelberg.

Pilcher, R. S., Kilsdonk, B., & Trude, J. (2011). -Primary basins and their boundaries in the deep-water northern Gulf of Mexico: Origin, trap types, and petroleum system implications. *AAPG Bulletin*, 95(2), 219-240.

Pindell, J., & J .F. Dewey. (1982). -Permo-Triassic reconstruction of western Pangea and the evolution of the evolution of the Gulf of Mexico/Caribbean region, *Tectonics*, v.1 p.179-212.

Pindell, J. (1985). -Alleghenian reconstruction and the subsequent evolution of the Gulf of Mexico, Bahamas and Proto-Caribbean Sea, *Tectonics*, v.4, p.1-39.

Pindell, J. (1993). -Regional Synopsis of Gulf of Mexico and Caribbean Evolution, in: Pindell, J.L. and B.F. Perkins (eds.), Mesozoic and Early Cenozoic Development of the Gulf of Mexico and Caribbean Region, A Context for Hydrocarbon Exploration, *GCSSEPM* Foundation 13th Annual Research Conference Proceeding, p.251-274.

Pindell, J. L., & L. Kennan. (2003). -Mexico and Gulf of Mexico, in: Exploration Framework Atlas Series: Volume 4: Tectonic Analysis, Ltd., unpublished non-exclusive commercial exploration atlas in CD-ROM

Poliakov, A.N.B., Podladchicov, Y., & Talbot, C. (1993). Initiation of salt diapirs with frictional overburdens: numerical experiments. *Tectonophysics , 228* (3-4), p.199-210.

Prather, B.E., Booth, J.R., Steffens, G.S., & Craig, P.A. (1988). Classification, lithology calibration, and stratigraphic succession of seismic facies of intraslope basin, deep water Gulf of Mexico. *AAPG Bulletin , 82* (5), 701-728.

Prost, G. & M. Aranda. (2001). -Tectonics and hydrocarbon system of the Veracruz Basin, Mexico. *In*: C. BARTOLINI, R.T. BUFFLER & A. CANTU-CHAPA, Eds., The western Gulf of Mexico Basin: tectonics, sedimentary basin and petroleum system. *AAPG Mem*., 75, 271-291.

Quezada-Muñetón, J.M. (1987). -El Cretácico Medio-Superior-Terciario Inferior en la Sierra de Chiapas: *Bol. Asoc. Mex. Geol. Petrol*., v. 39, p. 3-98.

Quezada-Muñetón, J.M. y Ferrusquía-Villafranca, I. (2013). – Gloria Alencaster y su influjo en la investigación geológica de Chipas: Las discontinuidades geológicas Mesozoicas de la Sierra de Chiapas y su significación regional, Un ejemplo, *Paleontología Mexicana* 63, p. 90-115.

Renne, P.R., Deino, A.L., Hilgen, F.J., Kuiper, K. F., Mark, D.F., Mitchell III, W.S., Morgan, L.E., Smit, J. (2013). –Time scale of critical events around the Cretaceous-Paleogene boundary. *Science*, 339, p.684-687.

Richard, P. D., Naylor, M. A., & Koopman, A. (1995). Experimental models of strike-slip tectonics. *Petroleum Geoscience , 1* (1), p.71-80.

Richard, P. (1991). -Experiments on faulting in a two-layer cover sequence overlying a reactivated basement fault with oblique-slip. *Journal of Structural Geology , 13* (4), p.459-469.

Robin, C. (1982). Relations volcanologic-magmatologie-geodynamique:application au passage entre volcanisms alcalin et andésitique dans le Sud Mexican (axe trans-mexicain et province alkaline orientale).– Ph.D Thesis, Annales Scientifiques de l'Universite de Clermont-Ferrand II, France, 503p.

Robles-Nolasco, J., Obispo, G. D., Sanchez, F. L. B., Zaldivar, R. J., Ruiz, M. J., Monroy, S. F., De Anda, G. M. A., De La Cruz, E. D., Villa, G. L. (2011). –Regional study of fractures in Cretaceous Rocks of the Campeche Sound, Southern Gulf of Mexico. *GCAGS Transactions*, p. 363-372.

Rodríguez-Correa, A., 1979. Estudio radiométrico y distribución de las rocas extrusivas de la Unidad Pueblo Viejo en el borde occidental del Macizo de Chiapas. *Instituto Mexicano del Petróleo*, Proyecto C-1051, (unplublished).

Rosales-Domínguez, M.C., Bermúdez-Santana, J.C., Aguilar-Piña, M. y González, V. (1993). –Aplicación bioestratigráfica de los foraminíferos bentónicos de una secuencia carbonatada del Cretácico Medio-Superior de la Sierra de Chiapas (parte III). México, D.F., *Instituto Mexicano del Petróleo*, Gerencia de Exploración, Proyecto CAC-3102, 129 p., 26 láms., y anexos (unplublished).

Rosales Domínguez, M.C., Grajales Nishimura, J. M., & Carreño, A. L. (2005). Foraminíferos planctónicos en diques clásticos inyectados en la secuencia miocénica del borde occidental de la Cuenca Salina del Istmo. *Revista Mexicana de Ciencias Geológicas*, 22(3).

Ross, M.I., & C.R. Scotese. (1988). -A hierarchical tectonic model of the Gulf of Mexico and Caribbean Region: *Tectonophysics*, v. 155, p.139-168.

Rowan, M. G. (1993). A systematic technique for the sequential restoration of salt structures. *Tectonophysics , 22* (3), p. 331-348.

Rowan, M. G. (1995). Structural styles and evolution of allochthonous salt, central Louisiana outer shelf and upper slope. In M. R. Jackson (Ed.), *Salt Tectonics: A Global Perspective,* AAPG Memoir 65, p. 199-228.

Rowan, M. G., & Kligfield, R. (1989). -Cross section restoration and balancing as aid to seismic interpretation in extensional terranes. *AAPG Bulletin, 73* (8), p.955-966.

Rowan, M.G., Kligfield, R., & Weimer, P. (1993). -Processes and rates of deformation. in J. B. Armentrout (Ed.), *Rates of Geological Processes* Fourteenth Annual Research Conference, *GCSSEPM*, p. 209-218.

Rowan, M.G., Trudgill, B.D., Fiduk, J.C., 2000. Deepwater, salt-cored fold belts: lessons from the Mississippi Fan and Perdido fold belts, northern Gulf of Mexico. In: Mohriak, W.,Talwani, M. (Eds.), Atlantic Rifts and Continental Margins: American Geophysical Union Geophysical Monograph, 115, pp. 173–191.

Rowan,M.G., Peel, F.J., Vendeville, B.C., 2004. Gravity-driven fold belts on passive margins.In: McClay, K.R. (Ed.), Thrust Tectonics and Hydrocarbon Systems: AAPG Mem., 82,pp. 157–182.

Rowan, M. G., & Ratliff, R. A. (2012). -Cross-section restoration of salt-related deformation: Best practices and potential pitfalls. *Journal of Structural Geology , 41*, p. 24-37.

Rowan, M.G., & P.Weimer. (1998). Salt-sediment interaction, northern Green Canyon and Ewing bank (offshore Louisiana), northern Gulf of Mexico. *AAPG Bulletin, 82* (5), 1055-1082.

Ruiz-Osorio, A.S. (2008). – Uso de la evaluación genética de cuencas en un transecto de la subcuenca petrolera del Sureste de Mexico. MS. Thesis Universidad Nacional Autónoma de México, México, D.F. p. 235

Ruiz-Osorio, A.S. (2009). – Sedimentación terrígena del Eoceno en el Sureste de México y sus implicaciones en la busqueda de yacimientos en turbiditas. III Congreso y Exposicion Internacional del Petróleo en México, Ver.

Salvador, A. (1987). -Late Triassic–Jurassic paleogeography and origin of Gulf of Mexico basin: *A APG Bulletin*, v. 71, p. 419–451

Salvador, A. (1991a). -The Gulf of Mexico Basin: *Geological Society of America*, The Geology of North America, v. J, p.

Sánchez-Hernández, H. (2013). -*Stratigraphic characterization and evolution of a Mid-Tertiary age deep water system, Holok area, SW Gulf of Mexico.* PhD Thesis , University of Aberdeen, Aberdeen, Scotland, 250p.

Sánchez- Montes de Oca, R. (1979). -Geología petrolera de la Sierra de Chiapas: *Boletín de la Asociación Mexicana de Geólogos Petroleros*, v. 31, no. 1–2, p. 67–97.

Sánchez-Montes de Oca, R. (1980). -Geología petrolera de la Sierra de Chiapas: *Bol. Asoc. Mex. Geol. Petrol*., v. 31, Nos. 1-2, p. 67-77.

Sánchez-Montes de Oca, R., (1969). -Estratigrafía y paleogeografía del Mesozoico de Chiapas: Seminario sobre exploración petrolera, *Instituto Mexicano del Petróleo*, México, v. 3, 31 p.

Sánchez-Rios, M.A., & Salmerón-Ureña, P. (1995). –El Paleogeno en Mexico. *Asoc. Paleont. Arg., Publ. Espec*. No3, Resumen.

Sandwell, D.T., Müller, R.D., Smith, W.H.F., Garcia, E. & Francis, R. (2014). –New marine gravity model from CtyoSat-2 and Jason-1 reveals buried tectonic structure, *Science*, 346, p.65-67.

Sans, M., & Koyi, H. A. (2001). -Modeling the role of erosion in diapir development in contractional settings. *Geological Society of America Memories*, 111-112.

Sawyer, D.S., R.T. Buffler, & R.H. Pilger Jr. (1991). -The crust under the Gulf of Mexico Basin, in A . Salvador, ed., The Gulf of Mexico: *Geological Society of America*, The Geology of North America, v.J, p.53-72

Sawyer, D. E., Flemings, P. B., Shipp, R. C., & Winker, C. D. (2007). -Seismic geomorphology, lithology, and evolution of the late Pleistocene Mars-Ursa turbidite region, Mississippi Canyon area, northern Gulf of Mexico. *AAPG Bulletin , 91* (2), 215-234.

Schlaepfer, J.C., Mora, J. C., & Rodríguez, E. M. (1972). Stratigraphy and Microfacies of the Sierra Madre del Sur Mesozoic, Chiapas. Boletin de la *Asociación Mexicana de Geólogos Petroleros*, v.XXVII, No. 1-3, p.1.95

Schaaf, P., Morán-Zenteno, D., and Hernández-Bernal, M. del S. (1995).-Paleogene continental margin truncation in southwestern Mexico: Geochronological evidence. *Tectonics,* v.14, No. 5, p, 1339-1350.

Sheriff, R.E., & Geldart, L.P. (1995). *Exploration Seismology.* Cambridge University Press, 2nd ed.

Stephan, J.F., Mercier de Lepinay, B., Calais, E., Tardy, M., Beck, C., & Carfantan, J.C.(1990). -Paleogeodynamic maps of the Caribbean: 14 steps from Lias to Present: *Bull. Soc. Geol. France, 8em Ser*., v. VI, no. 6, p. 915-919.

Stewart, S. A., Harvey, M. J., Otto, S. C., & Weston, P. J. (1996). Influence of salt on fault geometry: examples from the UK salt basins. *Geological Society, London, Special Publications , 100* (1), 175-202.

Stewart, S. A., Ruffell, A. H., & Harvey, M. J. (1997). Relationship between basement-linked and gravity-driven fault systems in the UKCS salt basins. *Marine and Petroleum Geology , 14* (5), 581-604.

Stewart, S.A. & J.A. Clark. (1999). Impact of salt on the structure of the Central North Sea hydrocarbon fairways. In A. Fleet (Ed.), *Petroleum Geology of Northwest Europe: Proceedings of the 5th conference*, p. 179-200.

Sosa-Patrón, A. A., J. G. Cárdenas-López, C. Cárdenas-Lara, O. Pinto-Gómez, M. E. Guzzy-Arredondo, M. E. Monroy-Audelo, & R. Castellanos-Calvo. (2009). Integrated geological interpretation and impact on the definition of Neogene plays in the Isthmus Saline Basin, Mexico, in C. Bartolini and J. R. Román-Ramos,eds., Petroleum systems in the southern Gulf of Mexico: *AAPG Memoir* 90, p. 29 –47.

Soto-Cuervo, A., Ortega-Gonzalez, V. & Mora-Oropeza, G. (2009).- Present and Future of the Salina del Istmo Basin and its offshore extensión into the Gulf of Mexico. In Petroleum System in the Southern Gulf of Mexico. (ed) Bartolini, C. and Román-Ramos, J.R. *AAPG Memoir* 90, p.465-470.

Suárez, G. (2000). Reverse faulting in the Isthmus of Tehuantepec: Backarc deformation induced by the subduction of the Tehuantepec ridge. *Special Papers-Geological Society of America*, p. 263-268.

Suárez, G., & López, A. (2015). Seismicity in the southwestern Gulf of Mexico: evidence of active back arc deformation. *Revista Mexicana de Ciencias Geológicas,* 32(1).

Talbot, C.J. (1978). -Halokinesis and thermal convection. *Natura , 273*, p.739-741.

Talbot, C. J. (1998). -Extrusions of Hormuz salt in Iran. *Geological Society, London, Special Publications , 143* (1), p.315-334.

Talbot, C. J., & Jarvis, R. J. (1984). -Age, budget and dynamics of an active salt extrusion in Iran. *Journal of Structural Geology , 6* (5), p.521-533.

Talbot, C.J., Medvedev, S., Alavi, M., Shahrivar, H. & Heidadri, E. (2000). Salt extrusion at Kuh-e-Jahani, Iran, from June 1994 to November 1997. *Geological Society of London, Special Publication , 174* (1), 93-110.

Tankard, A. J., & Balkwill, H. R. (1989). Extensional tectonics and stratigraphy of the North Atlantic margins: Introduction. *AAPG Memoir* vol. 46. 54. ;175-195.

Tari. G., J. Molnar & P. Ashton. (2003). -Examples of salt tectonics from West Africa: a comparative approach, in Arthurt, T.J., MacGregor, D.S. & Cameron, N.R. eds., Petroleum Geology of Africa: New Themes and Developing Technologies, *Geological Society, London, Special Publication*, v 2007, p.85-104.

Toniolo, H., Parker, G., Voller, V., & Beaubouef, R. T. (2006). Depositional turbidity currents in diapiric minibasins on the continental slope: experiments—numerical simulation and upscaling. *Journal of Sedimentary Research , 76* (5), p.798-818.

Trudgill, B.D., Rowan, M..G., Fidduk, J.C., Weimer, P., Gale, P. E., Korn, B. E., Phair, R. L., Gafford, W. T., Roberts, G. R., & Dobbs, S. W. (1999). -The Perdido fold belt, northwestern deep Gulf of Mexico: part 1; structural

geometry, evolution, and regional implications: *AAPG Bulletin*, v.83, p.88-113.

Trudgill, B. D. (2011). -Evolution of salt structures in the northern Paradox Basin: Controls on evaporite deposition, salt wall growth and supra-salt stratigraphic architecture. *Basin Research, 23* (2), 208-238.

Trudgill, B. D., & Rowan, M. G. (2004). -Integrating 3D seismic data with structural restorations to elucidate the evolution of a stepped counter-regional salt system, Eastern Louisiana Shelf, Northern Gulf of Mexico. *Geological Society, London, Memoirs , 29* (1), 165-176.

Trusheim, F. (1960). -Mechanisms of salt migration in northern Germany. *American AAPG Bulletin , 44*, p.1510-1540.

Turcotte, D.L, & Schubert, G. (1982). -*Geodynamics, applications of continuum physics to geological problems.* John Wiles & Sons Inc. publications, 450 p.

Urai, J.L., Spiers, C.J., Peach, C., Zwart, H. J. & Lister, G.S. (1986). Weakening of rock salt by water during long-term creep. *Nature , 324*, p. 554-557.

Van Keken, P.E., Spiers, C.J. van den Berg, & Muyzert, E.J. (1993). -The effective viscosity of rock salt: implications of steady stage creep laws in numerical models of salt diapirsm. *Tectonophysics , 225*, p. 457-476.

Varela-Santa Maria, M., Granados-Molina, O., Guerrero-Tristan, M., Pinto-Gomez, O., Reyna-Martinez, G., Marin-Sosa, C., Martinez-Mendez, J.A., Zuniga-Barrios, I., Alonso-Gomez, J. and Lopez-Valdivieso, H. (2007). –Proyecto La Central-Rodador. PEMEX Internal publication, 120 figs, 25 tables. (unpublished).

Vendeville, B. C. (1991). -Mechanisms generating normal fault curvature: a review illustrated by physical models. *Geological Society, London, Special Publications, 56* (1), p.241-249.

Vendeville, B.C., and Jackson, M.P.A. (1992a). -The rise of diapirs during thin-skinned extension. *Marine and Petroleum Geology, 9*, 331-353.

Vendeville, B.C., B.G. Hangxing and Jackson, M.P.A. (1995). -Scale Models of salt tectonics during basement-involved extension. *Petroleum Geosiences, 1*, p.179-183.

Vendeville, B.C., Jackson, M.P.A. (1992b). -The fall of diapirs during thin-skinned extension. *Marine and Petroleum Geology, 9*, 331-353.

Vendeville, B.C., Jackson, M.P.A, & Weijermars, R. (1993). -Rates of salt flow in passive diapirs and their source layers. In *Rates of geological processes*, *GCSSEPM* 14th Annual Research Conference, p. 269-276.

Verduzco, B., Fairhead, J. D., Green, C. M. (2004). - New insights into magnetic derivatives for structural mapping. *The Leading Edge* February: p.116-119.

Viniegra-Osorio, F. (1971). -Age and Evolution of Salt Basins of Southeastern Mexico, *AAPG Bulletin*, v.55, no.3, p. 478-494.

Waltham, D. (1997). -Why does salt start to move. *Tectonophysics*, v282, (1-4), p.117-128.

Warren, J. (1997). -Evaporites, brines and base metals: fluids, flow and the evaporite that was. *Australian Journal of the Earth Sciences , 44*, 149-183.

Warren, J. (2006). *Evaporites: sediments, resources and hydrocarbons.* Springer Science & Business Media.

Watkins, J.S., G. MacRae & G.R. Simmons. (1995). Bipolar simple shear rifting responsible for distribution of megasalt basins in Gulf of Mexico?, in C.J. Travis, B.C.Vendeville, H. Harrison, F.J. Peel, M.R. Hudec, & B.F. Perkins, eds., Salt, sediment and hydrocarbons: 16th Annual *GCSSEMP Foundation* Reseach Conference, Houston, Texas, p.297-305.

Weijermars, R., Jackson, M.P.A., & Vendeville, B.C. (1993). -Rheological and tectonics of salt provinces. *Tectonophysics*, v.217, (1-2), p.143.174.

Winker, C.D, & R.T.Buffler, 1988. -Paleogeographic Evolution of Early Deep-Water Gulf of Mexico and Margins, Jurassic to Middle Cretaceous (Comanchean): *AAPG Bulletin*, v. 72, p. 318-346

Winker, C. D., & Booth, J. R. (2000). -Sedimentary dynamics of the salt-dominated continental slope, Gulf of Mexico: integration of observations from the seafloor, near-surface, and deep subsurface. In *Deep-Water Reservoirs of the World* Proc. *GCSSEPM* 20th Annu. Res. Conf., p. 1059-1086.

Withjack, M. O., & Callaway, S. (2000). Active normal faulting beneath a salt layer: an experimental study of deformation patterns in the cover sequence. *AAPG Bulletin, 84* (5), p. 627-651.

Witt, C., Rangin, C., Andreani, L, Olaez, N., & Martinez, J. (2012). The transpressive left-lateral Sierra Madre de Chiapas and its buried front in the Tabasco plain (southern Mexico). *Journal of the Geological of Society, London*, v.169, p.143.155.

Wu, S., Bally, A.W., & Cramez, C. (1990). -Allochthonous salt, structure and stratigraphy of the north-eastern Gulf of Mexico. Part II: Structure, *Marine and Petroleum Geology*, v 7, p 334-370.

Wu, S. & Bally, A.W. (2000). -Slope tectonics-comparisons and contrast of structural styles of salt and shale tectonics of the northern Gulf of Mexico with shale tectonics of offshore Nigeria in Gulf of Guinea, in W. MOHRIAK AND M. TALWANI, (eds), Atlantic Rifts and Continental Margins: *American Geophysical Union, Geophysical Monograph* 115, p. 151-172.

Zoback, M.L., & Zoback, M. D. (1986). –Tectonic stress field of the continental United States. *Submmited for publication in* Pakiser, L. and W. Mooney

(eds.), Geophysical Framework of the Continental United States, *Geological Society of America Memoir*.